

RICE UNIVERSITY

Synthesis and Applications of Dirhodium Metallopeptides

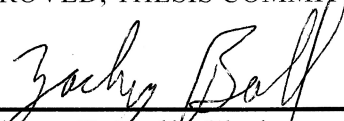
by

Alexander Nikolaevich Zaykov

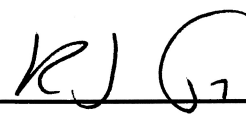
A THESIS SUBMITTED
IN PARTIAL FULFILLMENT OF THE
REQUIREMENTS FOR THE DEGREE

Doctor of Philosophy

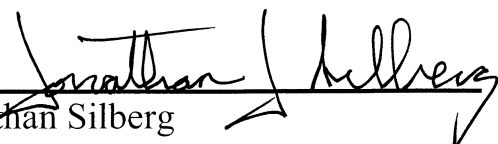
APPROVED, THESIS COMMITTEE




Zachary T. Ball, Chair
Assistant Professor of Chemistry



Ronald J. Parry
Professor of Chemistry and
Professor of Biochemistry and Cell
Biology



Jonathan Silberg
Assistant Professor of Biochemistry
and Cell Biology



Daniel G. Cohen
Associate Professor of History

HOUSTON, TEXAS
MARCH 2012

Abstract

Synthesis and Applications of Dirhodium Metallopeptides

by

Alexander Nikolaevich Zaykov

The work describes the development of a new class of synthetic metallopeptides that features a dirhodium metal center. Combination of peptide and dirhodium properties leads to unique effects on peptide structure, peptide-protein interactions, and metal catalytic activity aimed at small molecule as well as protein substrates. Dirhodium is directly bound to carboxylate side chains of aspartate or glutamate yielding kinetically inert coordination complexes. This improves stability, allows purification and provides enhanced biocompatibility. Bridging of two side chains in the same sequence enables control of the peptide secondary structure. Dirhodium metallopeptides are applied to regulate coiled coil dimerization, stabilize and induce helical secondary structure, catalyze enantioselective organometallic transformation, and serve as ligands for proteins. These results lead to the development of hybrid organic-inorganic therapeutic agents, biological probes for study of protein-protein interactions, and enantioselective metallopeptide catalysis.

Acknowledgments

I am exceedingly grateful for the experiences during my graduate career at Rice University. First, I would like to extend my sincere thanks to my advisor Zach Ball for his guidance, patience and friendship. Being one of his first students, I was lucky to share the challenges and successes of his early career as a professor. He shared much of his knowledge and experience throughout these years and instilled high standards for research, publishing and public presentation. Certainly, his mentorship and encouragement of innovative thinking were invaluable in my training as a scientist. I would like to think that I managed to teach him a lesson or two as well.

My progress would be impossible without much help I received from other professors and scientists at Rice. I would like to especially thank Prof. Jeffrey Hartgerink and Prof. Joff Silberg for allowing me to invade their labs. Most of my research would not be possible without the instrumentation and the expertise they were willing to provide. A very special thanks to Sean Moran for sharing his expertise of 2D NMR, to Kevin MacKenzie for patiently working with me on NMR structure determination, and to Michael Vu for teaching me recombinant protein expression and molecular biology techniques. Thanks to Sandy Yates, Tan Guo and Chris Pennington for taking care of the Mass Spec facility, to Prof. Yousif Shamoo and Milya Davlieva for the assistance with protein crystallization, to Larry Alemany for all the help with NMR experiments, and to Prof. Angel Marti for the help with the fluorescence polarization experiments.

I am grateful for all my friends who provided the encouragement, the help and the place to complain. The grad school experience would not be the same without Jessica Herron (a.k.a. “sister”) who has been a labmate and my partner in crime since the very start. Since coming to Rice, I gained a great friend Chris Jones with whom I shared many adventures. Brian Popp, who was a postdoc in the lab and now a professor at WVU, has been a tremendous help in every aspect. A very special thanks to all of my other co-workers: Ramya Sambasivan, Ritu Kundu, Zhen Chen, Farrukh Vohidov, Cara Bovet, and Vincenzo Russo. I want to particularly acknowledge the place where I found many other friends and the place that helped to relieve the stress of the graduate school – Valhalla.

I want to thank my family, that though is far away, had faith in me and gave me the support and love when needed.

Lastly, but certainly not least, I want to thank Emily for simply being the love of my life. You are the best thing that happened to me in these years and I am looking forward to many more years we share together.

Alexander Zaykov

Content

Chapter 1. Thesis overview	1
Chapter 2. Design of functional metallopeptides	5
2.1. Introduction	5
2.2. Metallopeptide design.....	7
2.3. Functional metallopeptides	14
2.3.1. Electron transfer	14
2.3.2. Luminescent metallopeptides	17
2.3.3. Catalysis	20
2.4. References	25
Chapter 3. Structure, synthesis and properties of dirhodium complexes	36
3.1. Structure and synthesis of dirhodium complexes	37
3.2. Catalysis.....	40
3.3. Bioorthogonal reactivity	49
3.4. Antitumor properties.....	52
3.5. References	54
Chapter 4. Synthesis of dirhodium metallopeptides	59
4.1. Introduction	61
4.2. Development of metalation conditions	63
4.3. Synthesis of the “zinc finger” (ZF) dirhodium metallopeptide	67
4.4. Synthesis of metallopeptides with free carboxylates	69
4.5. Solution structure and stability of zinc-finger metallopeptide	72
4.6. Conclusion	75
4.7. Experimental section	76

4.7.1. General information.....	76
4.7.2. Synthetic procedures	78
4.7.3. NMR study and structure calculation.....	82
4.7.4. Experimental data	83
4.8. References	90
Chapter 5. Dirhodium based control of peptide folding and assembly	90
5.1. Introduction	92
5.2. Control of coiled coil heterodimerization.....	96
5.3. Stabilization of helical conformation with dirhodium linker.	98
5.4. Induction of helical conformation with dirhodium linker.	102
5.5. <i>Bis</i> -peptide and trans-complexes with dirhodium	104
5.6. Conclusions	107
5.7. Experimental section	109
5.7.1. General information.....	109
5.7.2. Analytical data.....	115
5.8. References	132
Chapter 6. Kinetic and stereoselectivity effects of phosphite ligands in dirhodium catalysis	137
6.1. Introduction	139
6.2. Phosphite additives and enantioselectivity	143
6.3. Kinetics	143
6.4. Discussion.....	146
6.5. Conclusion	150
6.6. Experimental Section.....	151
6.6.1. General information.....	151
6.6.2. Synthetic procedures	152
6.6.3. Analytical data.....	153

6.6.4. Ligand screening	155
6.6.5. Equilibrium constants.....	155
6.6.6. Rate measurements.....	158
6.7. References	161
Chapter 7. Dirhodium metallopeptides as MDM2 ligands.....	162
7.1. Introduction	162
7.2. MDM2 protein	165
7.3. Dirhodium metallopeptide design	167
7.4. Fluorescence polarization affinity measurements	170
7.5. Conclusions	172
7.6. Experimental section	173
7.6.1. General considerations	173
7.6.2. Experimental Procedures.....	174
7.6.3. Analytical data.....	177
7.7. References	191

List of Figures

Figure 2-1.	Structure of an α -helix.....	9
Figure 2-2.	Helical peptide with metal coordinated to histidine positioned four residues apart ($i, i+4$)	9
Figure 2-3.	Examples of β -hairpin metalloptides with bipyridyl group on the side chain and the turn of the hairpin	10
Figure 2-4.	Packing of hydrophobic residues at coiled-coil interface and helical wheel diagram of a parallel coiled coil	11
Figure 2-5.	Coiled coil assembly mediated by cadmium(II) – cysteine complex, an electron-transfer system based on coiled-coil assembly and a helix-turn-helix metalloptide featuring iron cluster $[\text{Fe}_4\text{S}_4]$ and nickel(II) metal centers	12
Figure 2-6.	Four-helix bundle metalloptides with dizinc center and iron-porphyrin centers.....	13
Figure 2-7.	Electron transfer across electrostatic dimer composed of coiled-coil ruthenium metalloptides	16
Figure 2-8.	Four-helix bundle heme-metalloptide mimicking cytochrome <i>c</i> protein	16
Figure 2-9.	A model of the chimera metalloptide generated from the homeodomain <i>engrailed</i> and the EF-hand of calmodulin	18
Figure 2-10.	High affinity lanthanide-binding tag peptide with terbium(III)	19
Figure 2-11.	Functional group similarity between amino-acid side chains and common chiral ligands.....	21

Figure 2-12. Synthesis of Ru(I) metallopeptide with unnatural phosphine side chains	22
Figure 2-13. β -turn phosphine peptide, model structure of its palladium(II) complex and asymmetric allylic substitution reaction catalyzed by the metallopeptide complex	23
Figure 3-1. Structure of dirhodium tetraacetate complex	38
Figure 3-2. General methods for synthesis of dirhodium complexes	40
Figure 3-3. Examples of dirhodium catalyzed diazo-reaction	43
Figure 3-4. Symmetry and transition state of chiral carboxylates and amidate catalysts in cyclopropanation and C-H insertion reactions	44
Figure 3-5. Examples of chiral dirhodium carboxylate and amidate catalysts	46
Figure 3-6. Three different classes of diazo substrates	47
Figure 3-7. Chemoselectivity of dirhodium catalysts	47
Figure 3-8. Examples of dirhodium catalysis in total synthesis	48
Figure 3-9. Dirhodium catalyzed insertion reaction with 3-methyl indole and styryl-diazo reagent in aqueous solution	50
Figure 3-10. Selective labeling of myoglobin at the exposed tryptophan residues with styryl-diazo substrate and dirhodium catalyst	51
Figure 3-11. pH range improvement of the dirhodium-catalyzed protein labeling	51
Figure 3-12. Overlay of diguanidine adducts of dirhodium and cisplatin	53
Figure 3-13. Examples of diimine dirhodium complexes for DNA photocleavage and cancer treatment	54

Figure 4-1. Synthesis of dirhodium complexes with dirhodium tetracarboxylate precursor	62
Figure 4-2. Synthesis of dirhodium complexes from dirhodium precursor with acetonitrile ligands	62
Figure 4-3. Synthesis of dirhodium complexes from dirhodium precursor with trifluoroacetate ligands	63
Figure 4-4. Dirhodium precursors used in developing peptide metalation conditions.....	63
Figure 4-5. Synthesis of acetylated aspartame	64
Figure 4-6. HPLC of crude ligand exchange reaction between Amac and $\text{Rh}_2(\text{OAc})_4$ via the sealed vial procedure	65
Figure 4-7. HPLC of crude ligand exchange reaction between Amac and $\text{Rh}_2(\text{OAc})_4$ via Soxhlet extraction procedure.....	65
Figure 4-8. HPLC of crude ligand exchange reaction between phenylacetic acid and $[\text{Rh}_2(\text{OAc})_2(\text{MeCN})_6](\text{BF}_4)_2$ precursor.....	65
Figure 4-9. HPLC of crude ligand exchange reaction between Amac and <i>cis</i> - $\text{Rh}_2(\text{tfa})_2(\text{OAc})_2$ in THF	66
Figure 4-10. HPLC trace of metalation reaction between acetylated aspartame and $\text{Rh}_2(\text{OAc})_2(\text{tfa})_2$ in MES buffer.....	66
Figure 4-11. HPLC trace of metalation reaction between acetylated aspartame and $\text{Rh}_2(\text{OAc})_3(\text{tfa})_1$ in MES buffer	67
Figure 4-12. HPLC of crude ligand exchange reaction between Amac and 1:1 mixture of $\text{Rh}_2(\text{tfa})_3(\text{OAc})_1$ and $\text{Rh}_2(\text{tfa})_4$ under aqueous reaction conditions.....	67
Figure 4-13. Synthesis of a dirhodium metallopeptide ZF- $\text{Rh}_2(\text{OAc})_2$	68
Figure 4-14. HPLC of crude metalation reaction in synthesis of metallopeptide ZF- $\text{Rh}_2(\text{OAc})_2$	68

Figure 4-15. CD spectra of the free peptide ZF and metallopeptide ZF-Rh ₂ (OAc) ₂	72
Figure 4-16. Overlay of 16 representative conformations of ZF-Rh ₂ (OAc) ₂ metallopeptide from simulated annealing molecular dynamics calculations.....	74
Figure 4-17. HPLC analysis of reversible dirhodium metalation of peptide ZF	75
Figure 4-18. HPLC and MALDI-TOF MS of the peptide ZF.....	83
Figure 4-19. HPLC of the crude coupling reaction and of the isolated complex ZF-Rh ₂ (OAc) ₂ , ESI-MS of the isolated complex ZF-Rh ₂ (OAc) ₂	84
Figure 4-20. HPLC trace and MS data for isolated P4 ^{PG} peptide.....	84
Figure 4-21. HPLC trace and MS data of purified metallopeptide P4-Rh ₂ (OAc) ₂	85
Figure 4-22. HPLC trace and MS data of purified fluorescein-labeled metallopeptide F-P4-Rh ₂ (OAc) ₂	85
Figure 4-23. HPLC trace of crudes of metallation reaction, in-situ palladium deprotection and fluorescein labelling with FITC for P4 metallopeptide synthesis.....	86
Figure 4-24. ¹ H-NMR peptide ZF and metallopeptide ZF-Rh ₂ (OAc) ₂	86
Figure 4-25. Representative region of the ROESY spectrum for ZF-Rh ₂ (OAc) ₂ metallopeptide.....	87
Figure 5-1. E3/K3 heterodimeric coiled coil.....	93
Figure 5-2. CD spectra of peptide coiled coil systems.....	97
Figure 5-3. Cleavage of the dirhodium-peptide adduct re-establishes coiled-coil structure.....	98

Figure 5-4. CD spectra demonstrating the effect of dirhodium binding on the secondary structure of <i>bis</i> -carboxylate peptides.....	101
Figure 5-5. A model structure of the EE4-Rh ₂ (OAc) ₂ metallopeptide	101
Figure 5-6. ³ J _{HN-HA} coupling constants and NOE connectivity for the metal-binding region of the EE3G-Rh ₂ (OAc) ₂ complex	103
Figure 5-7. CD spectra of <i>bis</i> -peptide–dirhodium complexes and a model structure of the antiparallel (EE4) ₂ Rh ₂ metallopeptide.....	105
Figure 5-8. CD spectra of <i>trans</i> -dirhodium-peptide complexes.	106
Figure 5-9. NH-Hα region of the ROESY spectrum of the EE4G-Rh ₂ (OAc) ₂ complex	115
Figure 5-10. HPLC and CD spectroscopy of a mixture of E3 and K3-Rh ₂ (OAc) ₂ demonstrating the time course of dirhodium cleavage in KOAc solution	116
Figure 5-11. HPLC and MALDI-TOF MS of the peptide K3	117
Figure 5-12. HPLC and MALDI-TOF MS of the peptide E3	117
Figure 5-13. HPLC of the crude coupling reaction and of the isolated complex K3-Rh ₂ (OAc) ₂ , and ESI-MS of the isolated complex K3-Rh ₂ (OAc) ₂	118
Figure 5-14. HPLC and MALDI-TOF MS of the peptide EE3	118
Figure 5-15. HPLC and MALDI-TOF MS of the peptide DD3.....	119
Figure 5-16. HPLC and MALDI-TOF MS of the peptide DE3	119
Figure 5-17. HPLC and MALDI-TOF MS of the peptide ED3	119
Figure 5-18. HPLC and MALDI-TOF MS of the peptide EE4	120
Figure 5-19. HPLC and MALDI-TOF MS of the peptide DD4.....	120
Figure 5-20. HPLC and MALDI-TOF MS of the peptide DD4G.....	120

Figure 5-21. HPLC and MALDI-TOF MS of the peptide EE4G.....	121
Figure 5-22. HPLC and MALDI-TOF MS of the peptide ED4G	121
Figure 5-23. HPLC and MALDI-TOF MS of the peptide sED4	121
Figure 5-24. HPLC and MALDI-TOF MS of the peptide EE3G.....	122
Figure 5-25. HPLC of the crude coupling reaction and of the isolated complex EE3-Rh ₂ (OAc) ₂ , and ESI-MS of the isolated complex EE3-Rh ₂ (OAc) ₂	122
Figure 5-26. HPLC of the crude coupling reaction and of the isolated complexes EE3-Rh ₂ (pyrr) ₂ <i>iso-A</i> and EE3-Rh ₂ (pyrr) ₂ <i>iso-B</i>	123
Figure 5-27. ESI-MS of the isolated complexes EE3-Rh ₂ (pyrr) ₂ <i>iso-A</i> , EE3-Rh ₂ (pyrr) ₂ <i>iso-B</i>	123
Figure 5-28. HPLC of the crude coupling reaction and of the isolated complexes (EE3) ₂ Rh ₂ <i>iso-A</i> and (EE3) ₂ Rh ₂ <i>iso-B</i>	124
Figure 5-29. ESI-MS of the isolated complexes (EE3) ₂ Rh ₂ <i>iso-A</i> and (EE3) ₂ Rh ₂ <i>iso-B</i>	124
Figure 5-30. HPLC of the crude coupling reaction and of the isolated complex DD3-Rh ₂ (OAc) ₂ , and ESI-MS of the isolated complex DD3-Rh ₂ (OAc) ₂	125
Figure 5-31. HPLC of the crude coupling reaction and of the isolated complex DE3-Rh ₂ (OAc) ₂ , and ESI-MS of the isolated complex DE3-Rh ₂ (OAc) ₂	125
Figure 5-32. HPLC of the crude coupling reaction and of the isolated complex ED3-Rh ₂ (OAc) ₂ , and ESI-MS of the isolated complex ED3-Rh ₂ (OAc) ₂	126
Figure 5-33. HPLC of the crude coupling reaction and of the isolated complex EE4-Rh ₂ (OAc) ₂ , and ESI-MS of the isolated complex EE4-Rh ₂ (OAc) ₂	126

Figure 5-34. HPLC of the crude coupling reaction and of the isolated complex <i>trans</i> -EE4-Rh ₂ (OAc) ₂ , and ESI-MS of the isolated complex <i>trans</i> -EE4-Rh ₂ (OAc) ₂	127
Figure 5-35. HPLC of the crude coupling reaction and of the isolated complexes (EE4) ₂ Rh ₂ <i>iso-A</i> and (EE4) ₂ Rh ₂ <i>iso-B</i>	127
Figure 5-36. ESI-MS of the isolated complex complexes (EE4) ₂ Rh ₂ <i>iso-A</i> and (EE4) ₂ Rh ₂ <i>iso-B</i>	128
Figure 5-37. HPLC of the crude coupling reaction and of the isolated complex DD4-Rh ₂ (OAc) ₂ , and ESI-MS of the isolated complex DD4-Rh ₂ (OAc) ₂	128
Figure 5-38. HPLC of the crude coupling reaction and of the isolated complex DD4G-Rh ₂ (OAc) ₂ , and ESI-MS of the isolated complex DD4G-Rh ₂ (OAc) ₂	129
Figure 5-39. HPLC of the crude coupling reaction and of the isolated complex EE4G-Rh ₂ (OAc) ₂ , and ESI-MS of the isolated complex EE4G-Rh ₂ (OAc) ₂	129
Figure 5-40. HPLC of the crude coupling reaction and of the isolated complex <i>trans</i> -EE4G-Rh ₂ (OAc) ₂ , and ESI-MS of the isolated complex <i>trans</i> -EE4G-Rh ₂ (OAc) ₂	130
Figure 5-41. HPLC of the crude coupling reaction and of the isolated complex ED4G-Rh ₂ (OAc) ₂ , and ESI-MS of the isolated complex ED4G-Rh ₂ (OAc) ₂	130
Figure 5-42. HPLC of the crude coupling reaction and of the isolated complex sED4-Rh ₂ (OAc) ₂ , and ESI-MS of the isolated complex sED4-Rh ₂ (OAc) ₂	131

Figure 5-43. HPLC of the crude coupling reaction and of the isolated complex EE3G-Rh ₂ (OAc) ₂ , and ESI-MS of the isolated complex EE3G-Rh ₂ (OAc) ₂	131
Figure 6-1. X-H insertion of dirhodium metallocarbene intermediates	141
Figure 6-2. Fitting of UV-vis data for (L1)Rh ₂ (OAc) ₂	144
Figure 6-3. Fitting of UV-vis data for Rh ₂ (OAc) ₄	144
Figure 6-4. Mechanism of dual-path enantioselective catalysis.	146
Figure 6-5. Plot of kinetic data and fit for the reactivity ratio, γ	147
Figure 6-6. Experimental measurement of partitioning between phosphite-bound and unligated catalyst for the two steps of the reaction, diazo decomposition and silane insertion	148
Figure 6-7. HPLC trace and ESI-MS of the (L1)Rh ₂ (OAc) ₂ metallopeptide	153
Figure 6-8. HPLC trace and ESI-MS of the (L2)Rh ₂ (OAc) ₂ metallopeptide.	153
Figure 6-9. HPLC trace and ESI-MS of the (L3)Rh ₂ (OAc) ₂ metallopeptide.	154
Figure 6-10. HPLC trace and ESI-MS of the (L4)Rh ₂ (OAc) ₂ metallopeptide	154
Figure 6-11. Raw UV-vis data for (L1)Rh ₂ (OAc) ₂	157
Figure 6-12. Raw UV-vis data for Rh ₂ (OAc) ₄	157
Figure 6-13. Concentrations of the dirhodium species and the ligand.....	158
Figure 6-14. Linear relationship between $-\log([diazo]/[diazo]_0)$ and time at various concentrations of triphenyl phosphite.....	159
Figure 6-15. ¹ H NMR of (L1)Rh ₂ (OAc) ₂ compared with ¹ H NMR of (L1)Rh ₂ (OAc) ₂ with 1 equiv of triphenylphosphite	160

Figure 6-16. ^1H NMR of $(\text{L1})\text{Rh}_2(\text{OAc})_2$ in the region 2.3-5.2 ppm	160
Figure 6-17. ^1H NMR of $(\text{L1})\text{Rh}_2(\text{OAc})_2$ in the region 0.7-2.3 ppm.	161
Figure 7-1. Conceptual scheme depicting cooperative interaction of a peptide and a dirhodium center with a protein's binding pocket and site-specific labeling of a protein catalyzed by the proximal dirhodium ...	166
Figure 7-2. Defense function of the p53 protein and its regulation by the MDM2	168
Figure 7-3. Examples peptide and small molecule inhibitors of the MDM2	168
Figure 7-4. Structure of MDM2 protein with bound p53 helical peptide and a model of the metallopeptide $\text{P7-Rh}_2(\text{OAc})_2$ bound to the MDM2	169
Figure 7-5. Fluorescence polarization assays with FITC-dirhodium peptides and MDM2 [5-109] protein.....	171
Figure 7-6. HPLC trace and MS data for isolated P1 peptide.....	177
Figure 7-7. HPLC trace of crudes of metalation reaction and fluorescein labeling with FITC for $\text{P1-Rh}_2(\text{OAc})_2$	177
Figure 7-8. HPLC trace and MS data of purified product for $\text{P1-Rh}_2(\text{OAc})_2$ metallopeptide synthesis before and after fluorescein labeling with FITC.....	178
Figure 7-9. HPLC trace and MS data for isolated P2 peptide.....	179
Figure 7-10. HPLC trace of crudes of metalation reaction, in-situ palladium deprotection and fluorescein labeling with FITC (bottom) for $\text{P2-Rh}_2(\text{OAc})_2$ metallopeptide synthesis	179

Figure 7-11. HPLC trace and MS data of purified product for P2- Rh ₂ (OAc) ₂ metallopeptide synthesis before and after fluorescein labeling with FITC.....	180
Figure 7-12. HPLC trace and MS data for isolated P3 peptide.....	181
Figure 7-13. HPLC trace of crudes of metalation reaction and fluorescein labeling with FITC for P3-Rh ₂ (OAc) ₂ metallopeptide synthesis	181
Figure 7-14. HPLC trace and MS data of purified product for P3- Rh ₂ (OAc) ₂ metallopeptide synthesis before and after fluorescein labeling with FITC.....	182
Figure 7-15. HPLC trace and MS data for isolated P4 peptide.....	183
Figure 7-16. HPLC trace of crudes of metalation reaction , in-situ palladium deprotection and fluorescein labeling with FITC for P4- Rh ₂ (OAc) ₂ metallopeptide synthesis	183
Figure 7-17. HPLC trace and MS data of purified product for P4- Rh ₂ (OAc) ₂ metallopeptide synthesis before and after fluorescein labeling with FITC.....	184
Figure 7-18. HPLC trace and MS data for isolated P6 peptide.....	185
Figure 7-19. HPLC trace of crudes of metalation reaction and fluorescein labeling with FITC for P6-Rh ₂ (OAc) ₂ metallopeptide synthesis	185
Figure 7-20. HPLC trace and MS data of purified product for P6- Rh ₂ (OAc) ₂ metallopeptide synthesis before and after fluorescein labeling with FITC.....	186
Figure 7-21. HPLC trace and MS data for isolated P7 peptide.....	187

Figure 7-22. HPLC trace of crudes of metalation reaction and fluorescein labeling with FITC for P7-Rh ₂ (OAc) ₂ metallopeptide synthesis	187
Figure 7-23. HPLC trace and MS data of purified product for P7-Rh ₂ (OAc) ₂ metallopeptide synthesis before and after fluorescein labeling with FITC.....	188
Figure 7-24. HPLC trace and MS data for isolated fluorescein-p53-WT peptide	189
Figure 7-25. HPLC trace and MS data for isolated fluorescein-P5 peptide	189
Figure 7-26. SDS-page gel of MDM2 protein purification by Ni-NTA affinity column with gradient concentration of imidazole	190
Figure 7-27. MALDI and SDS-page gel for TEV protease cleavage of the His-tag and auxiliary peptide from the MDM2 protein.	190

List of Tables

Table 2-1. General structure of Hoveyda's peptide ligands and examples of the enantioselective reactions catalyzed by their metal complexes	24
Table 4-1. Statistics for 16 representative solution structures of the ZF-Rh ₂ (OAc) ₂ from molecular dynamics simulations.....	73
Table 4-2. Chemical shifts of ZF-Rh ₂ (OAc) ₂ metallopeptide	88
Table 5-1. Helicity of free peptides and dirhodium metallopeptide complexes	100
Table 5-2. Yields of the metallopeptides obtained from <i>cis</i> -Rh ₂ (tfa) ₂ (OAc) ₂ precursor using general procedure.....	114
Table 6-1. Screen of additives for increased enantioselectivity.	142
Table 6-2. Triphenylphosphite as an additive for enantioselective dirhodium reactions	145
Table 6-3. Experimentally determined kinetic and thermodynamic parameters	145
Table 7-1. Peptide sequences and MDM2 affinity (K_d) obtained by a fluorescence polarization assay.	170

Abbreviations

Instrumentation:

CD	Circular Dichroism
CNS	Crystallography and NMR System
COSY	(Two-dimensional NMR) Correlation Spectroscopy
ESI	ElectroSpray Ionization
FP	Fluorescence Polarization
FRET	Förster Resonance Energy Transfer
HPLC	High-Performance Liquid Chromatography
HSQC	(Two-dimensional NMR) Heteronuclear Single Quantum Coherence Spectroscopy
MALDI	Matrix-Assisted Laser Desorption/Ionization
MRI	Magnetic Resonance Imaging
MS	Mass Spectrometry
MS/MS	Tandem Mass Spectrometry
NMR	Nuclear Magnetic Resonance Spectroscopy
NOESY	(Two-dimensional NMR) Nuclear Overhauser Effect Spectroscopy
ROESY	(Two-dimensional NMR) Rotating frame Overhauser Effect Spectroscopy
UV-vis	Ultraviolet-visible Spectroscopy

Materials:

Amac	Acetylaspartame
BINOL	1,1'-Bi-2-naphthol
Bipy	2,2'-Bipyridine
CHCA	α -Cyano-4-hydroxycinnamic Acid
DCM	Dichloromethane
DIEA	Diisopropyl Ethyl Amine
DMF	Dimethylformamide
DMSO	Dimethyl Sulfoxide
MES	2-(N-morpholino)ethanesulfonic Acid
NBD	Norbornadiene
NHC	N-Heterocyclic Carbene
PEG	Polyethylene Glycol
TADDOL	$\alpha, \alpha, \alpha', \alpha'$ -Tetraaryl-1,3-dioxolan-4,5-dimethanol
TBHA	N-tert-butyl Hydroxylamine
TFA	Trifluoroacetic Acid
TFE	Trifluoroethanol
THF	Tetrahydrofuran
TIS	Triisopropyl Silane

Other:

PDB	Protein Data Bank
ET	Electron Transfer
rt	Room Temperature

Chapter 1

Thesis overview

Chapter 2 provides a brief overview of the design principles and peptide structural elements that are utilized in the engineering of metallopeptides and covers important functional applications that have been developed with metallopeptides structures. Examples are presented of the well-folded, metal-containing architectures with peptide structures spanning from the simple α -helix or β -hairpin motifs to the more complex multi-peptide assemblies. Bringing a metal complex and a peptide into a single structure results in functions that can both be analogous and entirely unique to the functions of natural metalloproteins. The incorporation of redox-active metalcenters into a peptide scaffold was used to create systems capable of the electron transfer; short peptide tags that can bind luminescent lanthanide ions were utilized for imaging applications and protein structure characterization; and the selectivity of the catalytic metal centers was altered with peptides serving as the chiral ligands.

Chapter 3 introduces dirhodium metal complexes, their structure, synthesis and applications. The catalytic properties of dirhodium are of particular interest because of their efficiency in the chemistry of diazo-compounds. A number of synthetically useful transformations can be accomplished, such as C–H and X–H insertion ($X =$ heteroatom), cycloaddition to the unsaturated bonds and ylide formation with electron rich atoms. The development of chiral dirhodium complexes ensured their utility in asymmetric organic synthesis. Dirhodium reactivity was also applied in the site-selective modification of protein substrates, selectively

targeting exposed tryptophan residues on the protein surface. In addition to the applications of catalytic function, dirhodium complexes have shown the potential to be used as antitumor agents. The antitumor activity of dirhodium is similar to the cisplatin drug, proceeding through metal binding to a DNA strand. A series of intercalating dirhodium complexes were also developed that are capable of cleaving DNA upon photoexcitation.

The development of techniques allowing the attachment of a dirhodium metallocenter to peptide side-chain carboxylates is described in Chapter 4.¹ Because typical methods for the synthesis of dirhodium complexes require high temperatures and organic solvents, a new approach had to be developed to be more compatible with peptide chemistry. Metallopeptides can be synthesized in mild aqueous conditions and high yields, employing dirhodium complexes with trifluoroacetate ligands as precursors. To eliminate the problem of multiple reactive centers with polycarboxylate peptides, a strategy utilizing orthogonally protected carboxylic amino acids was applied. Dirhodium metalation is generally robust, although it can be reversed through prolonged treatment with acetates at neutral pH. A metallopeptide, the sequence of which was derived from a β -hairpin motif of a “zinc finger” protein, was synthesized and structurally characterized by NMR, demonstrating the capability of bridging two carboxylic residues on the same peptide chain to form a well-defined metal macrocycle.

Chapter 5 explores the capacity of dirhodium bridging metalation to enforce a peptide secondary structure.² First, the heterodimerization of a coiled coil could be controlled through linking two distant residues on one of the peptides. Metalation results in the inability of this peptide to form a

coiled-coil assembly. The formation a coiled-coil structure can be initiated upon de-metalation by an acetate treatment. Second, dirhodium bridging of carboxylic residues positioned three and four residues apart constrains the peptide in an α -helical conformation. The geometry of dirhodium ligands is important; only *cis*-orientation of ligated amino-acid carboxylates produces improvement in peptide helicity, while *trans*-ligation is both unfavorable and helix-breaking. Furthermore, helical metallopeptides with two peptide chains ligated to the same dirhodium core can be produced.

The development of helical dirhodium metallopeptides was most beneficial in the designing of enantioselective catalysts for diazo transformation. Chapter 6 focuses on the study of catalytic activity of dirhodium metallopeptides and the effect of axial coordination on their selectivity. For the first time, reactivity towards diazo compounds was recorded for dirhodium complexes with an axial ligand. The addition of triphenylphosphite ligands to the Si–H insertion reaction resulted in improved enantioselectivity for the reaction catalyzed by dirhodium complexes with a single peptide ligand.

In Chapter 7, dirhodium metallopeptides are evaluated as ligands for MDM2 protein.⁴ A study was performed with a series of metallopeptides based on the sequence of the wild type p53 protein and a peptide ligand with an enhanced affinity to MDM2. A multistep synthesis was executed, involving an orthogonal protection of carboxylate residues as allyl esters and an installation of fluorescein dye at the N-terminus. Affinities of the metallopeptides for MDM2 were measured with a fluorescence polarization assay and were found to be similar to the parent peptide sequences.

- (1) Zaykov, A. N.; MacKenzie, K. R.; Ball, Z. T. *Chem. Eur. J.* **2009**, *15*, 8961.
- (2) Zaykov, A. N.; Popp, B. V.; Ball, Z. T. *Chem. Eur. J.* **2010**, *16*, 6651.
- (3) Zaykov, A. N.; Ball, Z. T. *Tetrahedron* **2011**, *67*, 4397.
- (4) Zaykov, A. N.; Ball, Z. T. *Chem. Comm.* **2011**, *47*, 10927.

Chapter 2

Design of functional metallopeptides

2.1. Introduction

Metals are an essential part of biological systems. They play a role in protein folding, oxygen transport and signal transduction. Metalloproteins can catalyze transformations unfeasible with purely biopolymer structures, placing them in a central role of metabolism. The unique functions of metals originate from their fundamental properties.¹ Lewis acidity and high coordination number of metal ions define their role in protein folding. An electronic configuration of an open d-shell grants them multiple oxidation states and catalytic activity. The role of protein environments, however, cannot be underestimated. A protein scaffold organizes metals in multicenter enzymes, creates a unique environment around the catalytic metal center, provides high specificity and selectivity toward substrates, and activates metals by imposing a high-energy entatic state.²

Not surprisingly, a number of research groups work on designing and mimicking the structure and function of natural systems, as well as attempting to produce unnatural ones.³ One approach to install a novel function is to combine a biomolecule with a non-native transition metal complex.⁴ The advancements of inorganic and organometallic chemistry in the last few decades offer a great variety of metal catalysts, electron-transfer (ET) systems and luminescent complexes, utilizing almost every metal of the periodic table. Incorporating unnatural metals and metal complexes within a

protein has the potential for improving their properties and creating metalloproteins with functions unprecedented in nature.

A protein scaffold offers the ability to control first and second coordination spheres around the metal center.^{5,6} The environment around a metal can be tuned by altering a protein sequence via mutagenesis or by directly varying a peptide sequence in the solid-phase synthesis. Identifying functional systems can be accomplished by high-throughput screening of combinatorial libraries.³ In comparison to small-molecule ligands, changing the structure of protein ligands can be easier since it only requires the substitution of its building blocks—amino acids. Also, proteins possess intrinsic chirality that can be utilized to engineer catalysts for enantioselective reactions. Designing a chiral small molecule ligand is a costly and time-consuming endeavor. On the other hand, the modular structure and intrinsic chirality of polypeptides makes them potentially promising ligands for enantioselective synthesis. The size of proteins contributes to better regio- and stereo- specificity since more distal groups on the substrate can act as directing groups. Enhanced specificity would be a great advantage in the synthesis of complex molecules with multiple reactive functionalities that typically require intricate protecting schemes. Certainly, several issues are yet to be resolved for proteins to be utilized as widely as small molecule ligands. The solubility and activity in organic solvents, the ability to coordinate metals in a specific manner, or the necessity of unnatural ligands for catalytic function (phosphines or NHC for example) are just a few challenges that need to be addressed.

Aside from catalysis, electron transfer (ET) and fluorescent properties can be incorporated into designed metalloproteins. Both the nano-scale size of proteins and their ability to form larger assemblies allow for the

incorporation of ET complexes into functional arrays or for blending them with natural ET systems. Light-harvesting and photo-catalytic systems can be developed with this approach.⁵ A fusion of lanthanide binding peptide sequences to natural proteins has found applications for in-vivo imaging and protein structure determination.⁶

Though there is no well-accepted distinction between proteins and peptides, the latter are typically defined as less than 40-50 residues in length. For the purpose of this introduction I will mainly focus on the design and development of functional metallopeptides. Various examples of metallopeptides with catalytic, electron-transfer and imaging properties are presented.

2.2. Metallopeptide design

When it comes to designing a novel metalloprotein, two general approaches have emerged: remodeling a natural protein or designing a metalloprotein from *de novo* principles.⁷ Starting with a native protein, one may consider several approaches to engineer a new metalloprotein: reconstitution of metal cofactor (covalent modification of heme for example), modification of a binding pocket to adopt alternative prosthetic groups or metals, covalent and potentially site-specific modification of protein to incorporate metal-binding ligands, or the use of small-molecule protein ligands as an anchor for non-covalent attachment of a metal complex.^{3,4} More recently, the incorporation of unnatural amino acids via an amber stop codon has become available, offering the capability to install metal ligands in the protein of interest at the defined position.^{8,9} All these methods take advantage of the unique structural composition of natural proteins and therefore require information about their structure. The *de novo*

approach first emerged as a tool to test our understanding of protein structure and ability first to reproduce metal-binding sites and later, to construct new functional systems.¹⁰ The design of metallopeptides (as smaller entities) thus served both as the testing ground and as the way to create small functional metalloproteins.

In the *de novo* design approach metals are utilized for two common purposes. Similar to nature, metal-protein interactions can drive protein folding or inherent properties of the metal can define the function of metalloprotein. Designed peptides often require sequences that have a high propensity to form secondary structural elements, as their smaller size compared to proteins removes additional stabilization provided by the protein tertiary structure. Metallopeptide design is closely related to *de novo* design of proteins in general and DeGrado provides a nice outline of the principles as well as the various folds that can be utilized for this purpose.¹¹ Installation of metal binding sites can be used to stabilize the structure of designed peptide or to induce the formation of secondary superstructures and peptide assemblies.¹⁰

The most common secondary structural element in *de novo* design is an alpha helix due to its high stability provided by a rich hydrogen bond network spanning across the helix (Figure 2-1). After years of research, α -helicity is well understood and extensively reviewed.¹²⁻¹⁴ Early examples of helical metallopeptides were produced in the Ghadiri group. In a helical structure, the side chains of amino acids four residues apart ($i, i+4$) are projected into close proximity to each other. Placing two electron-donor histidine residues in these positions was demonstrated to be suitable for bidentate binding of copper(II), zinc(II), nickel(II), and cadmium(II) metal ions (Figure 2-2),¹⁵ as well as ruthenium (III) complexes.¹⁶ Similar results

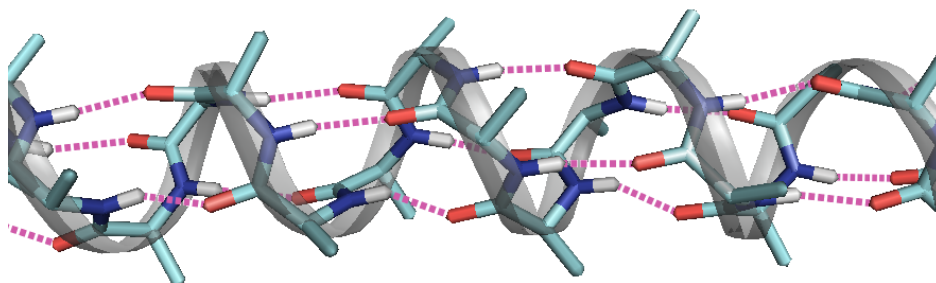


Figure 2-1. Structure of an α -helix demonstrating rich hydrogen bond network (created in PyMol).

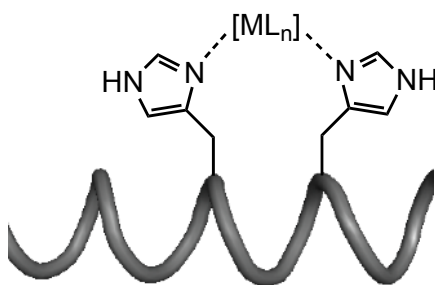


Figure 2-2. Helical peptide with metal coordinated to histidine positioned four residues apart ($i, i+4$).¹⁵

were achieved by Hopkins et al. utilizing unnatural amino-diacetic side chains in $i, i+4$ or $i, i+3$ arrangements.^{17,18} More recently, the same concept of bridging $i, i+4$ positions was used by Fairlie to induce helicity in very short peptides via metalation with ruthenium(III) and palladium(II) complexes.¹⁹⁻²²

Though β -sheets are widely found in native proteins, designing stable peptide systems with this structure is quite a challenging task.^{23,24} As a result, few examples of metallopeptides that employ this secondary structure element are found in the literature. β -hairpins capable of binding zinc(II) ions were developed initially by the Imperiali group.²⁵ Searle later utilized a similar design for the stabilization of β -sheet conformation.²⁶ In both cases, metal binding is mediated by two histidine residues placed on opposite strands of the hairpin. More stable folds can be achieved by recruiting amino

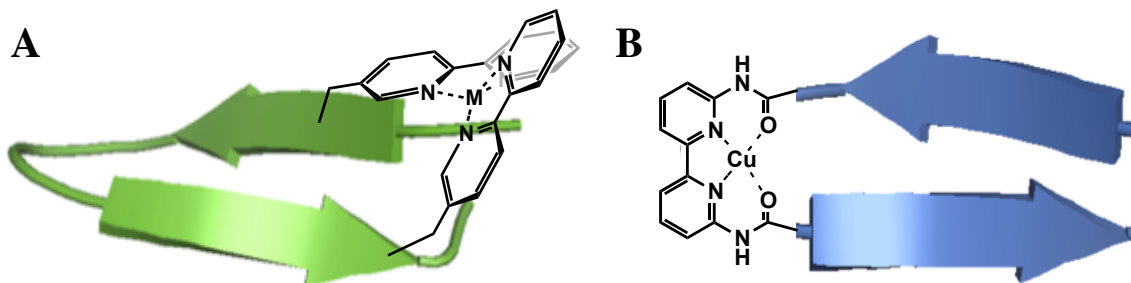


Figure 2-3. Examples of β -hairpin metallopeptides with bipyridyl group on the side chain (image A) and the turn (image B) of the hairpin.^{27,28}

acids with unnatural side-chain ligands that have higher affinities for a metal ion. Strong nitrogen donor ligands—bipyridyl or phenanthrolyl groups—were employed to induce folding of the β -hairpin in the presence of metal (Figure 2-3, A).²⁸ Schneider and Kelly demonstrated that a bipyridyl structure could also be used as a mimic of the β -turn. A unique structure was designed with two strands of the hairpin connected via bipyridyl functionality (Figure 2-3, B) and was shown to exhibit copper(II)-dependent reversible folding.²⁷

A coiled coil structure is assembled from well-defined helical elements and allows construction of more complex systems, avoiding the need to synthesize long-chain peptides.^{29,30} It is considered to be a secondary superstructure rather than a quaternary structure, which is typically attributed to the assembly of two or more polypeptide chains. Because of the propensity to form higher order structures, it is a very common structural motif in proteins.³¹ Assembly of α -helices into a coiled coil is driven by hydrophobic interactions and is associated with the localization of hydrophobic residues on one side of a helix (Figure 2-4).

Metals have been used to stabilize a coiled coil assembly by providing metal-ligand interactions in addition to the hydrophobic packing.

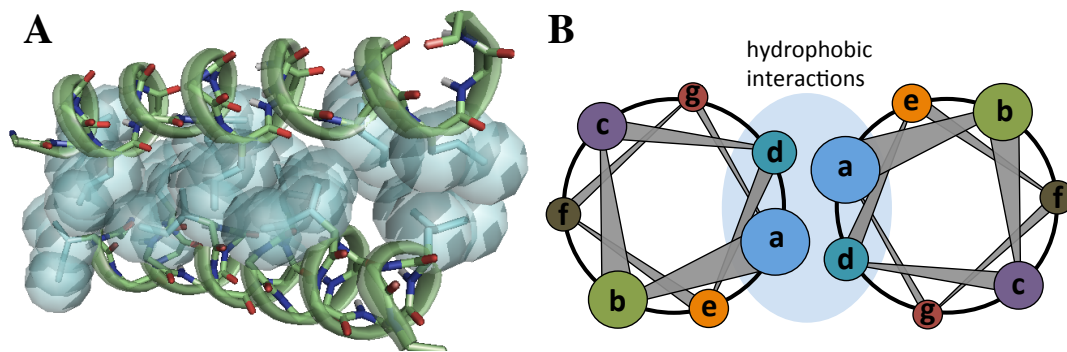


Figure 2-4. (A) Packing of hydrophobic residues at coiled-coil interface (created in PyMol from PDB entry 1U0I) (B) Helical wheel diagram of a parallel coiled coil, hydrophobic residues in the positions *a* and *d*.

For instance, coiled coil formation can be triggered with lanthanide ions, driven by ligation of the side-chain carboxylates positioned on the periphery of the helices.³² Cysteine residues are preferred ligands for metals and are often used for engineering metal binding pockets. Four cysteine residues, installed inside the hydrophobic interface of a coiled coil structure, favor folding via formation of a cadmium(II) thiolate complex (Figure 2-5, A).³³ Coiled-coil heterodimers composed of two distinct α -helices were utilized by Ogawa and colleagues to engineer an electron transfer system where two helices were decorated with different ruthenium complexes (Figure 2-5, B).⁵ A secondary superstructure with two directly connected helices is defined as a helix-turn-helix motif. A remarkable example of a designed metalloprotein that simultaneously accommodates an iron cluster $[\text{Fe}_4\text{S}_4]$ and a nickel(II) metal center was developed by Holm et al. (Figure 2-5, C).^{34,35} Helix-turn-helix, however, is not limited to the formation of a coiled coil. A subclass— α - α corners—have two helices overlapping at an angle and is a quite abundant motif.³⁶ Lanthanide metalloproteins featuring this structural element were engineered in the Franklin group (see section 2.3.2).^{37,38}

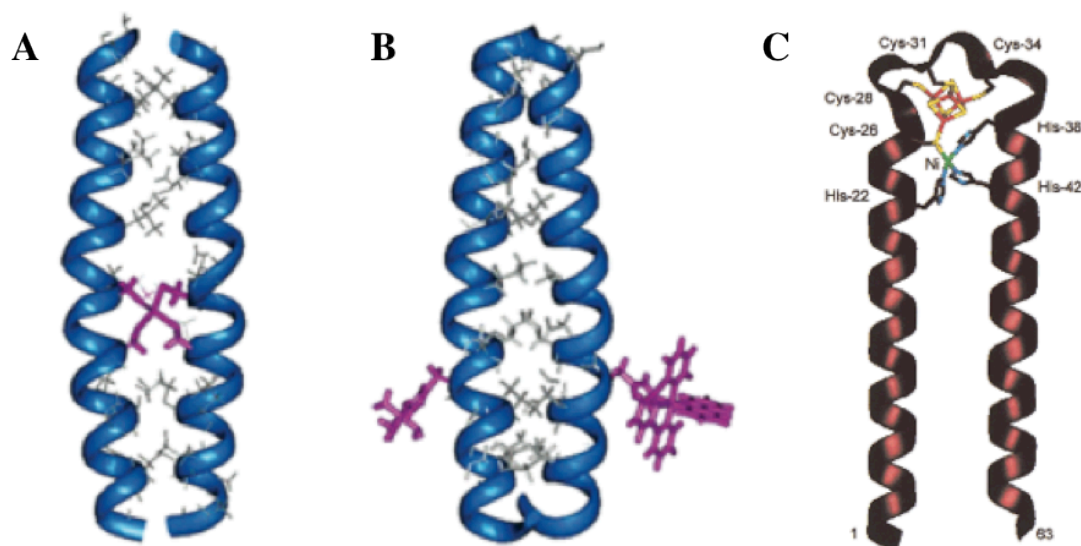


Figure 2-5. (A) Coiled coil assembly mediated by cadmium(II) – cysteine complex⁵ (B) Electron-transfer system based on coiled-coil assembly⁵ (C) Helix-turn-helix metalloprotein featuring metal centers: iron cluster [Fe₄S₄] and nickel(II).³⁴

Structures containing several helices in assembly—helix bundles—are directly related to coiled coils and rely on the same principle of hydrophobic packing.³⁹ Installation of metal binding sites in the core of the bundles yields structures with a metal buried inside the assembly and isolated from the solvent. This attribute is valuable for the creation of metalloproteins with functions that would otherwise be compromised by exposure to the aqueous environment.

The interaction between a metal and peptide side chains can be used as a driving force for the assembly of helix bundles. Significant contributions to the development of metalloproteins with three-helix bundle structures have been presented by Pecoraro and co-workers.^{10,40-44} Four-helix bundles are of particular interest as their size approaches that of small proteins. In the synthesis of diiron metalloproteins, DeGrado and colleagues

demonstrated a prime example of the retrostructural approach that encompasses identifying structural similarities in the natural systems and

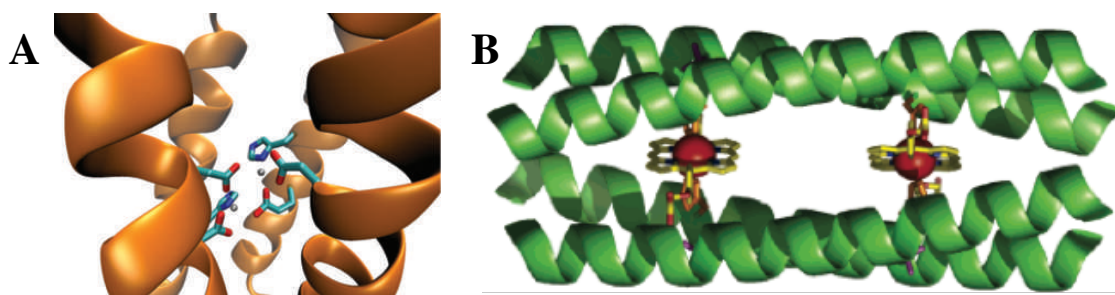


Figure 2-6. Four-helix bundle metalloproteins with (A) dizinc center and (B) iron-porphyrin centers.^{7,49}

applying the knowledge in engineering a *de novo* protein.⁴⁵ The metal-binding sites of diiron proteins share a common structure; they were used to deduce and construct a four-helix bundle mimic that assembles into a well-ordered miniprotein (Figure 2-6, A). A four-helix bundle model was also utilized to produce metalloproteins with porphyrin cofactors, therefore mimicking natural heme systems (Figure 2-6, B).⁴⁶⁻⁵⁰

A beta-hairpin-loop-helix is one other motif that is accessible via solid-phase peptide synthesis and is a potential candidate for synthesis of metalloproteins. Though a β -hairpin is typically not very stable as a stand-alone structure, association with a helix can somewhat favor its formation. This motif is typical in zinc finger proteins and can be isolated as a free metalloprotein. Other metals have been incorporated in place of zinc to produce metalloproteins retaining DNA-binding ability.⁵¹⁻⁵³

Though methods of designing new metalloprotein and metalloprotein structures have advanced significantly in recent years, the number of functionally useful structures remains limited. Simply combining polypeptide structures with a metal does not always lead to metalloproteins with desired properties. Progress in this area, however, provides a

foundation for the next step of metallopeptide design focused on the engineering of practically valuable systems.

2.3. Functional metallopeptides

2.3.1. Electron transfer

Electron transfer (ET) is a focus of many research groups because of its importance in energy transmission inside biological systems.⁵⁴ ET is central to photosynthesis, respiration, regulatory mechanisms and biochemical synthesis.⁵⁴⁻⁵⁶ Due to the challenges associated with natural ET systems that are typically integrated into cell membranes,^{57,58} alternative ways to study them have emerged.^{5,59} Modeling natural systems with de-novo designed metallopeptides has been a productive approach.⁵ Initial models focused on a simple attachment of two chromophores to polypeptide chains.⁶⁰ Natural ETs, however, more often proceed intermolecularly, occurring between separate species. In pursuit of a design that better represents a real system, more interesting examples have appeared such as metallopeptides that have a well-defined secondary structure and are capable of supramolecular organization.^{59,61}

Redesigned ET systems often feature the same metals and cofactors as encountered in native proteins: most commonly hemes, copper(I), and iron-sulfur clusters.⁵⁸ Their activity however is highly dependent on the coordination environment, making the design of functional ET metallopeptides quite challenging. Among unnatural metals, ruthenium complexes are particularly favored due to their range of electropotential, the minimal structural changes during oxidation or reduction, and a strong affinity for histidine residues.⁵⁴

A significant effort to study ET processes with *de novo* metalloptides was made by Ogawa and colleagues. Various systems with ruthenium complexes were produced to evaluate ET along the polypeptide chain as well as across supramolecular assemblies.^{5,60} Especially interesting results were obtained in the systems that had been constructed based on the coiled coil structure. In an early example, they demonstrated that electron transfer can occur across a non-covalent assembly of two homologous helices that are ligated with [Ru(trpy)(bpy)](His) and [Ru(NH₃)₅](His) complexes at the histidine residues (Figure 2-5, B).^{59,61} In the following ET experiments, coiled coil assemblies were used to assess the effects of the helix dipole moment that results from alignment of backbone carbonyls,⁶² and of the dipoles produced by the charged residues in the electrostatic protein complexes (Figure 2-7).⁶³ Ogawa's group had also designed a unique four-helix metalloptide with a multinuclear copper(I) thiolate cluster that is active in photoinduced ET with various ruthenium complexes via intermolecular collisional mechanism.⁶⁴

Electrostatic forces were also put in use to study ET within the electrostatic assembly of cytochrome *c* protein with a simple ruthenium metalloptide that features a polyglutamate sequence.^{65,66} Two parallel electron transfer pathways were observed from emission lifetime

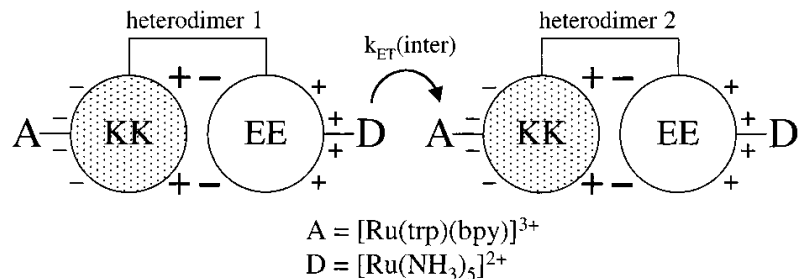


Figure 2-7. Electron transfer across electrostatic dimer composed of coiled-coil ruthenium metallopeptides.^{59,63} (KK and EE are lysine- and glutamate- rich peptides that assemble into a heterodimeric coiled coil)

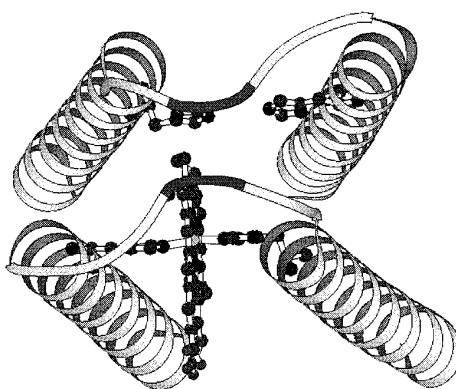


Figure 2-8. Four-helix bundle heme-metallopeptide mimicking cytochrome *c* protein.⁵⁰

measurements. Double exponential decay kinetics was attributed to simultaneous ET in a transient complex of photoexcited metallopeptide with the protein and in an equilibrium complex between a metallopeptide with the protein. The concept of using non-covalent interactions to construct ET systems with natural proteins had also been rewarding with non-peptide systems.^{67,68}

A metallopeptide that mimics natural systems provides a model that can be used to understand natural processes. One such metallopeptide with a four-helix bundle architecture was designed by Dutton and co-workers (Figure 2-8) to study redox chemistry of *c*-type cytochromes.⁵⁰ Specifically, this model has allowed them to look into the coupling of heme redox

processes with heme protonation/deprotonation that is often observed in natural cytochromes. An unexpected role of carboxylic residues and consequent dependence on pH was determined, motivating a search for similar structures in natural metalloproteins.

Dutton further probed proton-coupled redox chemistry with the mimic metallopeptide immobilized on gold surface.⁶⁹ The observed dependence of redox potential on pH in this system was consistent with the previous study. An inquiry into the binding of carbon monoxide (CO) in this model revealed that CO absorption could be modulated by the electro-potential of the surface. Electroreduction of the heme iron(III) to iron(II) gives the preference for CO ligation proceeding with the histidine displacement from the heme axial site. Re-oxidation of the system results in the release of the CO and reconstruction of the bis-histidine metal site. The authors suggest that designed metallopeptide films could be used for engineering sensors. Natural ET metalloproteins, however, are usually integrated inside lipid membranes. To examine ET occurring across a hydrophobic–hydrophilic interface, Dutton designed amphiphilic metallopeptides that can be successfully incorporated into the micelle bilayer.⁷⁰⁻⁷² Aside from the examples described here, many other metallopeptides with ET capabilities have been designed, demonstrating the importance of this topic and its potential applications.⁷³⁻⁸³

2.3.2. Luminescent metallopeptides

The photophysical properties of some metal complexes make them attractive for incorporation into a protein scaffold for imaging applications. Lanthanide ions terbium(III) and europium(III) are of particular interest, because of their long-lived fluorescence lifetimes, narrow emission profile,

and large Stokes shifts (difference between the wavelengths of absorption and emission maxima).^{6,84,85} The similarity between lanthanides and calcium ions allows their integration into calcium-binding proteins.^{86,87} A short peptide modeled after a Ca^{2+} -binding loop was successfully used to produce a terbium metallopeptide exhibiting luminescence upon energy transfer from the attached salicylic acid donor.⁸⁸ Various other examples of lanthanide-binding peptides were published as well.⁸⁹⁻⁹⁵

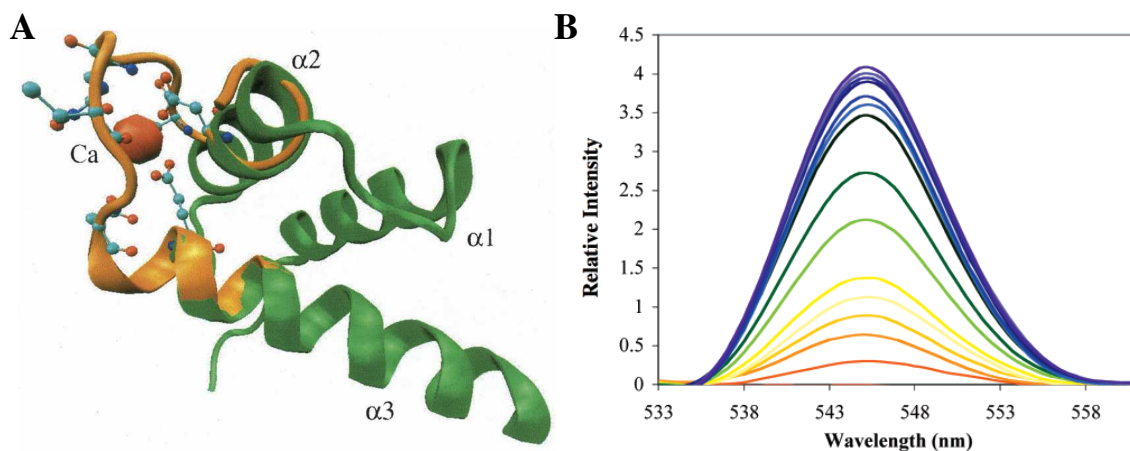


Figure 2-9. (A) A model of the chimera metallopeptide generated from the homeodomain *engrailed* (green, PDB: 2HDD) and the EF-hand of calmodulin (orange, PDB: 1OSA). (B) Increase in the Tb(III) fluorescence intensity upon titration of the designed peptide with TbCl_3 .⁹⁶

Franklin and co-workers remodeled the helix-turn-helix motif of the DNA-binding protein homeodomain *engrailed* (PDB: 2HDD) to incorporate the metal-binding site of *calmodulin* (Figure 2-9).^{37,38} Subsequent metalation with europium(III) or terbium(III) produces luminescent metallopeptides that retain DNA-binding capability.^{97,98} Intense terbium fluorescence was observed at 545 nm upon FRET from the proximal tryptophan excited at 290 nm (Figure 2-9, B). The same peptide was utilized to bind a gadolinium(III) ion for the potential application as an MRI contrast agent.⁹⁹

Imperiali has further developed small lanthanide binding sequences with improved affinity to the lanthanide metals as well as enhanced fluorescence intensity. Initial optimizations yielded a peptide with $K_d = 220$ nM, a 10-fold improvement over previous examples.¹⁰⁰ Further combinatorial screening resulted in a peptide with $K_d = 57$ nM, which is lowered to 2 nM affinity upon constraining the peptide with a disulfide bond.^{101,102} Structural characterization of the optimized peptide demonstrates

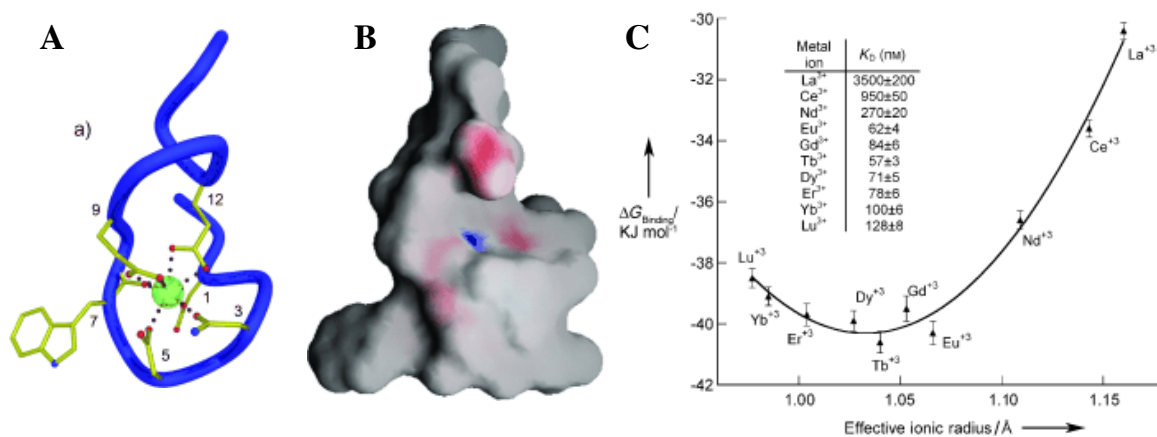


Figure 2-10. (A) Structure of high affinity lanthanide-binding tag peptide and terbium(III) ion (LBT-Tb³⁺) (B) Electrostatic surface potential of LBT metalloprotein (C) Dependence of binding free energy with the LBT on the effective ionic radii of rare-earth metals.¹⁰³

that terbium(III) ion is isolated from the aqueous environment and results in enhanced fluorescence (Figure 2-10, A and B).¹⁰³ It is also quite selective for terbium(III) ion when compared with other rare-earth metals. The lanthanide-binding tag was utilized to study protein-protein interactions,¹⁰⁴ modified to display other sensitizing groups,⁸⁵ and incorporated into proteins to act as a handle for NMR and X-ray structure determination.^{6,105-107}

2.3.3. Catalysis

Metallopeptides with catalytic function are attractive targets and are gaining interest in scientific circles.^{108,109} The benefits of peptides arise from their modular structure allowing construction of a ligand from easily accessible building blocks. Though polypeptide ligands can potentially alter catalyst reactivity, the capability of controlling the spatial environment around the catalytic center is more valuable. Specifically, enantioselectivity of the catalyst can be coupled to the chirality of a peptide and amino acids, or regioselectivity can be attained via control of the secondary coordination sphere and non-covalent interactions between a peptide ligand and a substrate.^{110,111} In comparison to small molecule ligands, the size of a peptide offers the prospect of designing ligands that can direct selectivity with respect to the distal functionalities on a substrate.

Amino acids by themselves were recognized as a convenient source of chirality and have been widely explored as ligands to transition metal complexes and auxiliaries in organic synthesis.¹¹²⁻¹¹⁵ Combining amino acids into peptides can also provide stereocontrol around the catalytic center¹¹⁶ as a defined secondary structure of peptides brings additional structural information and symmetry elements. Enantio- and regio- selectivity of catalysts with peptide ligands is a function of its primary structure that can be tuned via optimization of peptide sequence.¹¹⁷⁻¹¹⁹ Screening libraries of peptide ligands allows discovery of promising catalysts whereas intelligent design can be complex. The intrinsic chirality of amino acids determines chirality of the secondary structures. Thus inversion of reaction selectivity can be achieved utilizing enantiomers of amino acids, i.e. using D or L

isomers.¹²⁰ D-amino acids, however, are expensive, again making sequence optimization a more reasonable approach.

Transition metal catalysts often have functional groups that are distinct from natural amino-acid side chains, such as phosphine, carbene, oxazoline, pyridyl, dienyl, cyclopentadienyl or alkenyl functionalities.¹²¹ At the same time, certain ligands resemble the functional groups found in peptides. Examples include a phenolic hydroxyl group present in both the tyrosine side chain and series of BINOL ligands or nitrogen heterocycles represented in the histidine side chain and pyridyl-type ligands (Figure 2-11).

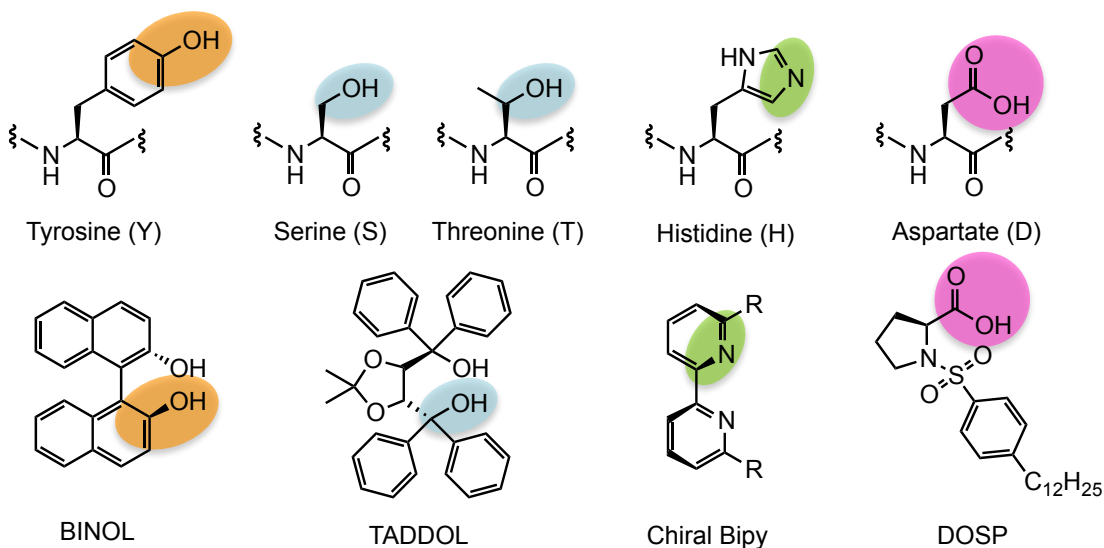


Figure 2-11. Functional group similarity between amino-acid side chains and common chiral ligands.

Surprisingly though, most of the efforts were focused on the incorporation of amino acids that display unnatural functional groups. This is partially due to stronger affinities of non-native ligands as well as wider ranges of their electronic properties. Also, peptide ligands are not always optimal for metal catalysis because of potential issues that come with peptide structures. The acidity of an amide backbone may be unsuitable for

catalysis of a reaction requiring strongly basic conditions where a proton source can quench the reaction. Due to the insolubility of peptides in most organic solvents, catalysis is often limited to polar and protic solvents (water, alcohols, DMSO or DMF), therefore methods that can address this problem are highly beneficial.

Gilbertson and co-workers developed procedures for the synthesis of peptides with amino acids containing a phosphine side chain and utilized them to produce catalytic metallopeptides with transition metal centers.¹²²

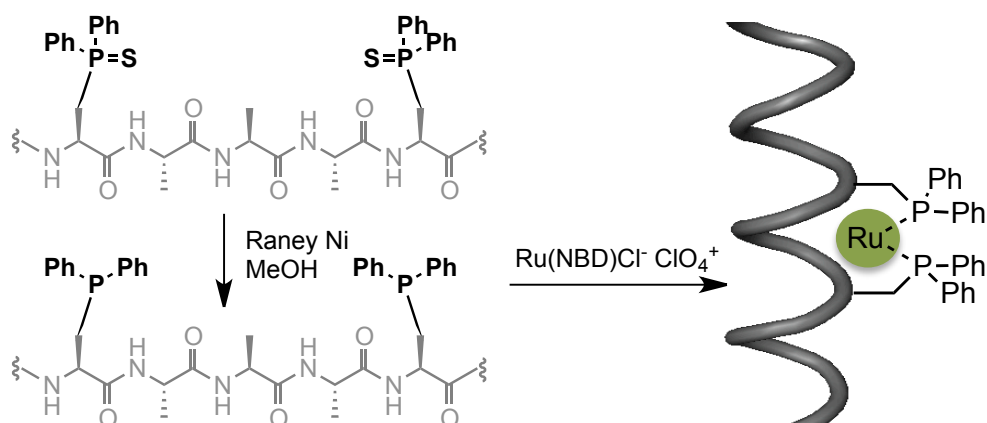


Figure 2-12. Gilbertson's synthesis of Ru(I) metallopeptide with unnatural phosphine side chains.

The phosphine functionality is not suitable for solid support peptide synthesis as it is readily oxidized under these conditions. To circumvent this problem, the synthesis was carried out with a phosphosulfide derivative. The sulfide analogue of phosphoalanine (also referred as phosphoserine) was successfully used to synthesize unnatural peptides using standard Fmoc procedures. A free phosphine can be produced by reduction with Raney nickel and metallated with rhodium(I) (Figure 2-12).¹²³⁻¹²⁵ Alternatively, a phosphine group can be installed in postsynthetic modification of tyrosine.¹²⁶

Two phosphine amino acids spaced four residues apart in the 12 amino-acid helical peptide ligate to rhodium(I) forming a catalytically active

metallopeptide with a well-defined secondary structure (Figure 2-12).^{124,125} These rhodium metallopeptides do not lose their catalytic activity if immobilized on a solid support.¹²⁷ To demonstrate the utility of peptide sequence optimization in search for an enantioselective catalyst, libraries of metallopeptides were created and screened for enantioselective reduction of methyl 2-acetamidoacrylate.^{118,119} Though only low enantioselectivity values were obtained, the validity of library screening was demonstrated.

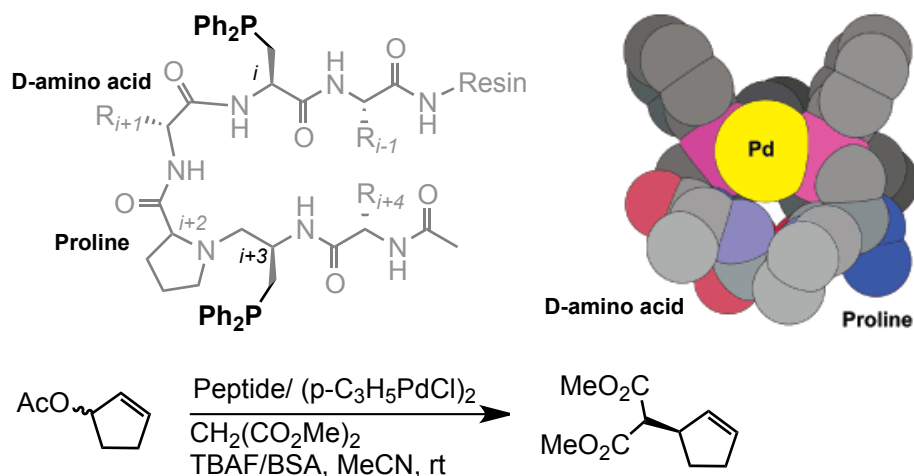


Figure 2-13. (top) Gilbertson's β -turn phosphine peptide and model structure of its palladium(II) complex and (bottom) asymmetric allylic substitution reaction catalyzed by the metallopeptide complex.^{128,129}

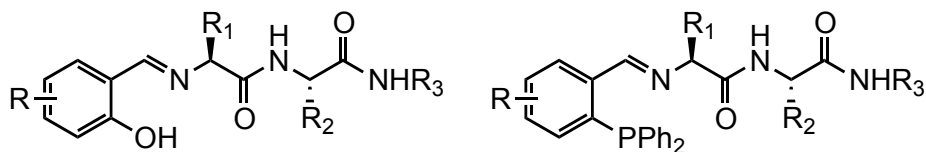
To improve selectivity of phosphine-peptide ligands, the second generation of ligands was developed based on the β -turn motif. Phosphine amino acids were placed in i , $i+3$ positions on both sides of the Pro–X turn, where X is a variable D-amino acid.¹²⁸ This time, a palladium(II) metallopeptide was produced and tested as an asymmetric catalyst for asymmetric allylic substitution. Even the initial hits gave 60% ee in the model reaction between dimethyl malonate and cyclopentenyl acetate (Figure 2-13) and selectivity was improved up to 75% ee with a ligand identified from a 96-member library.¹²⁸ Further optimization of peptide

sequence and reaction conditions yielded catalyst with 95% ee.^{129,130} The study also shows that selectivity is uniquely linked to the chirality of β -turn secondary structure and not chirality of individual residues. The substitution of turn-stabilizing residues or an increase in the spacing between the phosphines results in significantly lower ee values.^{122,131} Meldal and colleagues also utilized peptide-phosphine ligands to synthesize palladium metallopeptides for the same asymmetric allylic substitution reaction.^{132,133}

Aside from phosphine-containing peptides, some work was published on the inclusion of amino acids with N-heterocyclic carbene (NHC) functionality¹³⁴ as well as the synthesis of NHC metallopeptides.¹³⁵⁻¹³⁷ However, only preliminary catalytic results are available.¹³⁵

Along with oligopeptides, various groups assessed shorter di- and tri-peptides in enantioselective catalysis. Hoveyda's group has been developing a series of ligands that have a short peptide backbone and are drastically modified at the side chains and termini. Phosphine, pyridyl or phenolic groups at the N-terminus provide the metal binding and the unnatural side chains of the peptide establish stereoselectivity (Table 2-1). Using the combinatorial library approach, they were able to achieve highly

Table 2-1. General structure of Hoveyda's peptide ligands¹⁴⁹ and examples of the enantioselective reactions catalyzed by their metal complexes.



Metal	Ligand class	Transformation	References
Zr, Hf	OH	Imine alkylation with alkylzinc reagents	143,146,151, 152
Al	OH	Alkylation of α -ketoesters with dialkylzinc reagents	158
Ti	OH	Cyanide addition to epoxides	138,142,150
Ti	OH	Cyanide addition to imines	139-141
Cu	PPh ₂	Conjugate addition of alkylzinc reagents to nitroalkenes	144,159
Cu	PPh ₂	Allylic alkylation with alkylzinc reagents	160
Cu	PPh ₂	Conjugate addition of alkylzinc reagents	145,147,148, 153,154

enantioselective ligands for a number of metals and a large variety of transformations.^{117,138-154} Similar examples include alkene epoxidation by Francis et al.,¹⁵⁵ conjugate addition by Breit et al.,¹⁵⁶ and Heck reaction by Jayasinghe et al.¹⁵⁷ In comparison to Gilbertson's work, these systems directly rely on the chirality of the amino acids and not the secondary structure of the peptide ligand.

2.4. References

- (1) Anfinsen, C. B. *Metalloproteins: structural aspects*, 1991.
- (2) Holm, R. H.; Kennepohl, P.; Solomon, E. I. *Chem. Rev.* **1996**, 96, 2239.
- (3) Lu, Y. In *Encyclopedia of Inorganic Chemistry*; John Wiley & Sons, Ltd: 2006.

- (4) Lu, Y. *Curr. Opin. Chem. Biol.* **2005**, *9*, 118.
- (5) Hong, J.; Kharenko, O. A.; Ogawa, M. Y. *Inorg. Chem.* **2006**, *45*, 9974.
- (6) Allen, K. N.; Imperiali, B. *Curr. Opin. Chem. Biol.* **2010**, *14*, 247.
- (7) Lu, Y.; Yeung, N.; Sieracki, N.; Marshall, N. M. *Nature* **2009**, *460*, 855.
- (8) Link, A. J.; Mock, M. L.; Tirrell, D. A. *Curr. Opin. Biotechnol.* **2003**, *14*, 603.
- (9) Wang, L.; Schultz, P. G. *Chem. Comm.* **2002**, 1.
- (10) Ghosh, D.; Pecoraro, V. L. *Inorg. Chem.* **2004**, *43*, 7902.
- (11) DeGrado, W. F.; Summa, C. M.; Pavone, V.; Nastri, F.; Lombardi, A. *Annual Review of Biochemistry* **1999**, *68*, 779.
- (12) Scholtz, J. M.; Baldwin, R. L. **1995**.
- (13) Munoz, V.; Serrano, L. *Curr. Opin. Biotechnol.* **1995**, *6*, 382.
- (14) Aurora, R.; Creamer, T. P.; Srinivasan, R.; Rose, G. D. *J. Biol. Chem.* **1997**, *272*, 1413.
- (15) Ghadiri, M. R.; Choi, C. *J. Am. Chem. Soc.* **1990**, *112*, 1630.
- (16) Ghadiri, M. R.; Fernholz, A. K. *J. Am. Chem. Soc.* **1990**, *112*, 9633.
- (17) Ruan, F.; Chen, Y.; Hopkins, P. B. *J. Am. Chem. Soc.* **1990**, *112*, 9403.
- (18) Ruan, F.; Chen, Y.; Itoh, K.; Sasaki, T.; Hopkins, P. B. *J. Org. Chem.* **1991**, *56*, 4347.
- (19) Ma, M. T.; Hoang, H. N.; Scully, C. C. G.; Appleton, T. G.; Fairlie, D. P. *J. Am. Chem. Soc.* **2009**, *131*, 4505.
- (20) Kelso, M. J.; Beyer, R. L.; Hoang, H. N.; Lakdawala, A. S.; Snyder, J. P.; Oliver, W. V.; Robertson, T. A.; Appleton, T. G.; Fairlie, D. P. *J. Am. Chem. Soc.* **2004**, *126*, 4828.

- (21) Kelso, M. J.; Hoang, H. N.; Appleton, T. G.; Fairlie, D. P. *J. Am. Chem. Soc.* **2000**, *122*, 10488.
- (22) Kelso, M. J.; Hoang, H. N.; Oliver, W.; Sokolenko, N.; March, D. R.; Appleton, T. G.; Fairlie, D. P. *Angew. Chem.* **2003**, *115*, 437.
- (23) Mayo, K. H.; Ilyina, E.; Park, H. *Prot. Sci.* **1996**, *5*, 1301.
- (24) Guerois, R.; Paz, M. L. *Protein design: methods and applications*; Humana Press, 2006.
- (25) Imperiali, B.; Kapoor, T. M. *Tetrahedron* **1993**, *49*, 3501.
- (26) Platt, G.; Chung, C.-W.; Searle, M. S. *Chem. Comm.* **2001**, 1162.
- (27) Schneider, J. P.; Kelly, J. W. *J. Am. Chem. Soc.* **1995**, *117*, 2533.
- (28) Cheng, R. P.; Fisher, S. L.; Imperiali, B. *J. Am. Chem. Soc.* **1996**, *118*, 11349.
- (29) Litowski, J. R.; Hodges, R. S. *J. Biol. Chem.* **2002**, *277*, 37272.
- (30) Hodges, R. S. *Biochem. Cell Biol.* **1996**, *74*, 133.
- (31) Kohn, W. D.; Mant, C. T.; Hodges, R. S. *J. Biol. Chem.* **1997**, *272*, 2583.
- (32) Kohn, W. D.; Kay, C. M.; Sykes, B. D.; Hodges, R. S. *J. Am. Chem. Soc.* **1998**, *120*, 1124.
- (33) Kharenko, O. A.; Ogawa, M. Y. *J. Inorg. Biochem.* **2004**, *98*, 1971.
- (34) Laplaza, C. E.; Holm, R. H. *J. Am. Chem. Soc.* **2001**, *123*, 10255.
- (35) Musgrave, K. B.; Laplaza, C. E.; Holm, R. H.; Hedman, B.; Hodgson, K. O. *J. Am. Chem. Soc.* **2002**, *124*, 3083.
- (36) Aravind, L.; Anantharaman, V.; Balaji, S.; Babu, M. M.; Iyer, L. M. *FEMS Microbiol. Rev.* **2005**, *29*, 231.
- (37) Welch, J. T.; Kearney, W. R.; Franklin, S. J. *Proc. Natl. Acad. Sci. USA* **2003**, *100*, 3725.

- (38) Kim, Y.; Welch, J. T.; Lindstrom, K. M.; Franklin, S. J. *J. Biol. Inorg. Chem.* **2001**, *6*, 173.
- (39) Lovejoy, B.; Choe, S.; Cascio, D.; McRorie, D. K.; DeGrado, W. F.; Eisenberg, D. *Science* **1993**, *259*, 1288.
- (40) Farrer, B. T.; Harris, N. P.; Balchus, K. E.; Pecoraro, V. L. *Biochemistry* **2001**, *40*, 14696.
- (41) Dieckmann, G. R.; McRorie, D. K.; Tierney, D. L.; Utschig, L. M.; Singer, C. P.; O'Halloran, T. V.; Penner-Hahn, J. E.; DeGrado, W. F.; Pecoraro, V. L. *J. Am. Chem. Soc.* **1997**, *119*, 6195.
- (42) Iranzo, O.; Chakraborty, S.; Hemmingsen, L.; Pecoraro, V. L. *J. Am. Chem. Soc.* **2010**, *133*, 239.
- (43) Chakraborty, S.; Touw, D. S.; Peacock, A. F. A.; Stuckey, J.; Pecoraro, V. L. *J. Am. Chem. Soc.* **2010**, *132*, 13240.
- (44) Suzuki, K.; Hiroaki, H.; Kohda, D.; Nakamura, H.; Tanaka, T. *J. Am. Chem. Soc.* **1998**, *120*, 13008.
- (45) Lombardi, A.; Summa, C. M.; Geremia, S.; Randaccio, L.; Pavone, V.; DeGrado, W. F. *Proc. Natl. Acad. Sci. U. S. A.* **2000**, *97*, 6298.
- (46) Bender, G. M.; Lehmann, A.; Zou, H.; Cheng, H.; Fry, H. C.; Engel, D.; Therien, M. J.; Blasie, J. K.; Roder, H.; Saven, J. G.; DeGrado, W. F. *J. Am. Chem. Soc.* **2007**, *129*, 10732.
- (47) Robertson, D. E.; Farid, R. S.; Moser, C. C.; Urbauer, J. L.; Mulholland, S. E.; Pidikiti, R.; Lear, J. D.; Wand, A. J.; DeGrado, W. F.; Dutton, P. L. *Nature* **1994**, *368*, 425.
- (48) Ghirlanda, G.; Osyczka, A.; Liu, W.; Antolovich, M.; Smith, K. M.; Dutton, P. L.; Wand, A. J.; DeGrado, W. F. *J. Am. Chem. Soc.* **2004**, *126*, 8141.

- (49) Cochran, F. V.; Wu, S. P.; Wang, W.; Nanda, V.; Saven, J. G.; Therien, M. J.; DeGrado, W. F. *J. Am. Chem. Soc.* **2005**, *127*, 1346.
- (50) Shifman, J. M.; Moser, C. C.; Kalsbeck, W. A.; Bocian, D. F.; Dutton, P. L. *Biochemistry* **1998**, *37*, 16815.
- (51) Predki, P. F.; Sarkar, B. *Metal replacement in "zinc finger" and its effect on DNA binding*, 1994; Vol. 102 Suppl 3.
- (52) Krizek, B. A.; Merkle, D. L.; Berg, J. M. *Inorg. Chem.* **1993**, *32*, 937.
- (53) Bertini, I. *Biological inorganic chemistry: structure and reactivity*; University Science Books, 2007.
- (54) Gray, H. B.; Winkler, J. R. *Annu. Rev. Biochem.* **1996**, *65*, 537.
- (55) Moser, C. C.; Keske, J. M.; Warncke, K.; Farid, R. S.; Dutton, P. L. *Nature* **1992**, *355*, 796.
- (56) Mayo, S. L.; Ellis, W. R.; Crutchley, R. J.; Gray, H. B. *Science* **1986**, *233*, 948.
- (57) Verkhovskaya, M. L.; Belevich, N.; Euro, L.; Wikström, M.; Verkhovsky, M. I. *Proc. Natl. Acad. Sci. USA* **2008**, *105*, 3763.
- (58) Page, C. C.; Moser, C. C.; Dutton, P. L. *Curr. Opin. Chem. Biol.* **2003**, *7*, 551.
- (59) Kornilova, A. Y.; Wishart, J. F.; Xiao, W.; Lasey, R. C.; Fedorova, A.; Shin, Y.-K.; Ogawa, M. Y. *J. Am. Chem. Soc.* **2000**, *122*, 7999.
- (60) Ogawa, M. Y. *In Molecular and Supramolecular Photochemistry*; Marcel Dekker: New York, 1999; Vol. 4.
- (61) Kozlov, G. V.; Ogawa, M. Y. *J. Am. Chem. Soc.* **1997**, *119*, 8377.
- (62) Fedorova, A.; Chaudhari, A.; Ogawa, M. Y. *J. Am. Chem. Soc.* **2002**, *125*, 357.
- (63) Kornilova, A. Y.; Wishart, J. F.; Ogawa, M. Y. *Biochemistry* **2001**, *40*, 12186.

- (64) Hong, J.; Kharenko, O. A.; Fan, J.; Xie, F.; Petros, A. K.; Gibney, B. R.; Ogawa, M. Y. *Angew. Chem. Int. Ed.* **2006**, *45*, 6137.
- (65) Liu; Hong, J.; Ogawa, M. Y. *J. Am. Chem. Soc.* **2003**, *126*, 50.
- (66) Lasey, R. C.; Liu; Zang, L.; Ogawa, M. Y. *Biochemistry* **2003**, *42*, 3904.
- (67) Hayashi, T.; Hisaeda, Y. *Acc. Chem. Res.* **2001**, *35*, 35.
- (68) Dunn, A. R.; Dmochowski, I. J.; Winkler, J. R.; Gray, H. B. *J. Am. Chem. Soc.* **2003**, *125*, 12450.
- (69) Chen, X.; Discher, B. M.; Pilloud, D. L.; Gibney, B. R.; Moser, C. C.; Dutton, P. L. *J. Phys. Chem. B.* **2001**, *106*, 617.
- (70) Discher, B. M.; Noy, D.; Strzalka, J.; Ye, S.; Moser, C. C.; Lear, J. D.; Blasie, J. K.; Dutton, P. L. *Biochemistry* **2005**, *44*, 12329.
- (71) Ye, S.; Discher, B. M.; Strzalka, J.; Xu, T.; Wu, S. P.; Noy, D.; Kuzmenko, I.; Gog, T.; Therien, M. J.; Dutton, P. L.; Blasie, J. K. *Nano Lett.* **2005**, *5*, 1658.
- (72) Noy, D.; Discher, B. M.; Rubtsov, I. V.; Hochstrasser, R. M.; Dutton, P. L. *Biochemistry* **2005**, *44*, 12344.
- (73) Case, M. A.; McLendon, G. L. *Acc. Chem. Res.* **2004**, *37*, 754.
- (74) Zheng, Y.; Case, M. A.; Wishart, J. F.; McLendon, G. L. *J. Phys. Chem. B.* **2003**, *107*, 7288.
- (75) Mutz, M. W.; Case, M. A.; Wishart, J. F.; Ghadiri, M. R.; McLendon, G. L. *J. Am. Chem. Soc.* **1999**, *121*, 858.
- (76) Mutz, M. W.; McLendon, G. L.; Wishart, J. F.; Gaillard, E. R.; Corin, A. F. *Proc. Natl. Acad. Sci. USA* **1996**, *93*, 9521.
- (77) Mihara, H.; Nishino, N.; Hasegawa, R.; Fujimoto, T.; Usui, S.; Ishida, H.; Ohkubo, K. *Chem. Lett.* **1992**, *21*, 1813.

- (78) Fahnenschmidt, M.; Bittl, R.; Schlodder, E.; Haehnel, W.; Lubitz, W. *Phys. Chem. Chem. Phys.* **2001**, *3*, 4082.
- (79) Rau, H. K.; Snigula, H.; Struck, A.; Robert, B.; Scheer, H.; Haehnel, W. *Eur. J. Biochem.* **2001**, *268*, 3284.
- (80) Rau, H. K.; DeJonge, N.; Haehnel, W. *Proc. Natl. Acad. Sci. USA* **1998**, *95*, 11526.
- (81) Cristian, L.; Piotrowiak, P.; Farid, R. S. *J. Am. Chem. Soc.* **2003**, *125*, 11814.
- (82) Nanda, V.; Rosenblatt, M. M.; Osyczka, A.; Kono, H.; Getahun, Z.; Dutton, P. L.; Saven, J. G.; DeGrado, W. F. *J. Am. Chem. Soc.* **2005**, *127*, 5804.
- (83) Schnepf, R.; Haehnel, W.; Wieghardt, K.; Hildebrandt, P. *J. Am. Chem. Soc.* **2004**, *126*, 14389.
- (84) Richardson, F. S. *Chem. Rev.* **1982**, *82*, 541.
- (85) Reynolds, A. M.; Sculimbrene, B. R.; Imperiali, B. *Bioconjugate Chem.* **2008**, *19*, 588.
- (86) Hogue, C. W.; MacManus, J. P.; Banville, D.; Szabo, A. G. *J. Biol. Chem.* **1992**, *267*, 13340.
- (87) MacKenzie, C. R.; Clark, I. D.; Evans, S. V.; Hill, I. E.; MacManus, J. P.; Dubuc, G.; Bundle, D. R.; Narang, S. A.; Young, N. M.; Szabo, A. G. *Immunotechnology* **1995**, *1*, 139.
- (88) Clark, I. D.; Hill, I.; Sikorska-Walker, M.; MacManus, J. P.; Szabo, A. G. *FEBS Lett.* **1993**, *333*, 96.
- (89) Kanellis, P.; Yang, J.; Cheung, H. C.; Lenkinski, R. E. *Arch. Biochem. Biophys.* **1983**, *220*, 530.
- (90) Procyshyn, R. M.; Reid, R. E. *J. Biol. Chem.* **1994**, *269*, 1641.

- (91) Siedlecka, M.; Goch, G.; Ejchart, A.; Sticht, H.; Bierzynski, A. *Proc. Natl. Acad. Sci. USA* **1999**, *96*, 903.
- (92) Bemquerer, M. P.; Bloch Jr, C.; Brito, H. F.; Teotonio, E. E. S.; Miranda, M. T. s. M. *J. Inorg. Biochem.* **2002**, *91*, 363.
- (93) Marsden, B. J.; Hodges, R. S.; Sykes, B. D. *Biochemistry* **1988**, *27*, 4198.
- (94) Malik, N. A.; Anantharamaiah, G. M.; Gawish, A.; Cheung, H. C. *Biochim. Biophys. Acta Protein Struct. Mol. Enzymol.* **1987**, *911*, 221.
- (95) MacManus, J. P.; Hogue, C. W.; Marsden, B. J.; Sikorska, M.; Szabo, A. G. *J. Biol. Chem.* **1990**, *265*, 10358.
- (96) Lim, S.; Franklin, S. J. *Prot. Sci.* **2006**, *15*, 2159.
- (97) Harris, K. L.; Lim, S.; Franklin, S. J. *Inorg. Chem.* **2006**, *45*, 10002.
- (98) Jain, S.; Welch, J. T.; Horrocks, W. D.; Franklin, S. J. *Inorg. Chem.* **2003**, *42*, 8098.
- (99) Caravan, P.; Greenwood, J. M.; Welch, J. T.; Franklin, S. J. *Chem. Comm.* **2003**, 2574.
- (100) Franz, K. J.; Nitz, M.; Imperiali, B. *ChemBioChem* **2003**, *4*, 265.
- (101) Nitz, M.; Franz, K. J.; Maglathlin, R. L.; Imperiali, B. *ChemBioChem* **2003**, *4*, 272.
- (102) Martin, L. J.; Sculimbrene, B. R.; Nitz, M.; Imperiali, B. *QSAR Comb. Sci.* **2005**, *24*, 1149.
- (103) Nitz, M.; Sherawat, M.; Franz, K. J.; Peisach, E.; Allen, K. N.; Imperiali, B. *Angew. Chem.* **2004**, *116*, 3768.
- (104) Sculimbrene, B. R.; Imperiali, B. *J. Am. Chem. Soc.* **2006**, *128*, 7346.
- (105) Silvaggi, N. R.; Martin, L. J.; Schwalbe, H.; Imperiali, B.; Allen, K. N. *J. Am. Chem. Soc.* **2007**, *129*, 7114.

- (106) Martin, L. J.; Hähnke, M. J.; Nitz, M.; Wöhnert, J.; Silvaggi, N. R.; Allen, K. N.; Schwalbe, H.; Imperiali, B. *J. Am. Chem. Soc.* **2007**, *129*, 7106.
- (107) Barthelmes, K.; Reynolds, A. M.; Peisach, E.; Jonker, H. R. A.; DeNunzio, N. J.; Allen, K. N.; Imperiali, B.; Schwalbe, H. *J. Am. Chem. Soc.* **2010**, *133*, 808.
- (108) Deuss, P. J.; den Heeten, R.; Laan, W.; Kamer, P. C. J. *Chem. Eur. J.* **2011**, *17*, 4680.
- (109) Rosati, F.; Roelfes, G. *ChemCatChem* **2010**, *2*, 916.
- (110) Letondor, C.; Ward, T. R. *ChemBioChem* **2006**, *7*, 1845.
- (111) Thomas, C. M.; Ward, T. R. *Chem. Soc. Rev.* **2005**, *34*, 337.
- (112) Jarvo, E. R.; Miller, S. J. *Tetrahedron* **2002**, *58*, 2481.
- (113) Gnass, Y.; Glorius, F. *Synthesis* **2006**, 1899.
- (114) Studer, A. *Synthesis* **1996**, 1996, 793.
- (115) Jose, L. V.; Dolores, B.; Luisa, C.; Efraim, R.; Juan, E. *Curr. Org. Chem.* **2005**, *9*, 219.
- (116) Miller, S. J. *Acc. Chem. Res.* **2004**, *37*, 601.
- (117) Amir H, H. *Chem. Biol.* **1998**, *5*, R187.
- (118) Gilbertson, S. R.; Wang, X. *Tetrahedron Lett.* **1996**, *37*, 6475.
- (119) Gilbertson, S. R.; Wang, X. *Tetrahedron* **1999**, *55*, 11609.
- (120) Konno, R.; Brockner, H.; D'Aniello, A.; Fisher, G. H.; Fujii, N.; Homma, H. *D-Amino Acids: Practical Methods and Protocols: Free D-Amino Acids*; Nova Science, 2009.
- (121) Zhou, Q.-L. *Privileged Chiral Ligands and Catalysts*; Wiley-VCH, Weinheim, 2011.
- (122) Agarkov, A.; Greenfield, S.; Xie, D.; Pawlick, R.; Starkey, G.; Gilbertson, S. R. *J. Pept. Sci.* **2006**, *84*, 48.

- (123) Gilbertson, S. R.; Chen, G.; McLoughlin, M. *J. Am. Chem. Soc.* **1994**, *116*, 4481.
- (124) Gilbertson, S. R.; Wang, X. *J. Org. Chem.* **1996**, *61*, 434.
- (125) Gilbertson, S. R.; Chen, G.; Kao, J.; Beatty, A.; Campana, C. F. *J. Org. Chem.* **1997**, *62*, 5557.
- (126) Gilbertson, S. R.; Starkey, G. W. *J. Org. Chem.* **1996**, *61*, 2922.
- (127) Gilbertson, S. R.; Wang, X.; Hoge, G. S.; Klug, C. A.; Schaefer, J. *Organometallics* **1996**, *15*, 4678.
- (128) Gilbertson, S. R.; Pawlick, R. V. *Angew. Chem. Int. Ed.* **1996**, *35*, 902.
- (129) Greenfield, S. J.; Agarkov, A.; Gilbertson, S. R. *Org. Lett.* **2003**, *5*, 3069.
- (130) Agarkov, A.; Greenfield, S. J.; Ohishi, T.; Collibee, S. E.; Gilbertson, S. R. *J. Org. Chem.* **2004**, *69*, 8077.
- (131) Agarkov, A.; Uffman, E. W.; Gilbertson, S. R. *Org. Lett.* **2003**, *5*, 2091.
- (132) Christensen, C. A.; Meldal, M. *Chem. Eur. J.* **2005**, *11*, 4121.
- (133) Christensen, C. A.; Meldal, M. *J. Comb. Chem.* **2006**, *9*, 79.
- (134) Xu, G.; Gilbertson, S. R. *Org. Lett.* **2005**, *7*, 4605.
- (135) Worm-Leonhard, K.; Meldal, M. *Eur. J. Org. Chem.* **2008**, *2008*, 5244.
- (136) Lemke, J.; Metzler-Nolte, N. *Eur. J. Inorg. Chem.* **2008**, *2008*, 3359.
- (137) Lemke, J.; Metzler-Nolte, N. *J. Organomet. Chem.* **2011**, *696*, 1018.
- (138) Shimizu, K. D.; Cole, B. M.; Krueger, C. A.; Kuntz, K. W.; Snapper, M. L.; Hoveyda, A. H. *Angew. Chem. Int. Ed.* **1997**, *36*, 1704.

- (139) Krueger, C. A.; Kuntz, K. W.; Dzierba, C. D.; Wirschun, W. G.; Gleason, J. D.; Snapper, M. L.; Hoveyda, A. H. *J. Am. Chem. Soc.* **1999**, *121*, 4284.
- (140) Porter, J. R.; Wirschun, W. G.; Kuntz, K. W.; Snapper, M. L.; Hoveyda, A. H. *J. Am. Chem. Soc.* **2000**, *122*, 2657.
- (141) Porter, J. R.; Traverse, J. F.; Hoveyda, A. H.; Snapper, M. L. *J. Am. Chem. Soc.* **2001**, *123*, 984.
- (142) Deng, H.; Isler, M. P.; Snapper, M. L.; Hoveyda, A. H. *Angew. Chem. Int. Ed.* **2002**, *41*, 1009.
- (143) Akullian, L. C.; Snapper, M. L.; Hoveyda, A. H. *Angew. Chem. Int. Ed.* **2003**, *42*, 4244.
- (144) Luchaco-Cullis, C. A.; Hoveyda, A. H. *J. Am. Chem. Soc.* **2002**, *124*, 8192.
- (145) Hird, A. W.; Hoveyda, A. H. *Angew. Chem.* **2003**, *115*, 1314.
- (146) Traverse, J. F.; Hoveyda, A. H.; Snapper, M. L. *Org. Lett.* **2003**, *5*, 3273.
- (147) Degrado, S. J.; Mizutani, H.; Hoveyda, A. H. *J. Am. Chem. Soc.* **2001**, *123*, 755.
- (148) Degrado, S. J.; Mizutani, H.; Hoveyda, A. H. *J. Am. Chem. Soc.* **2002**, *124*, 13362.
- (149) Josephsohn, N. S.; Kuntz, K. W.; Snapper, M. L.; Hoveyda, A. H. *J. Am. Chem. Soc.* **2001**, *123*, 11594.
- (150) Cole, B. M.; Shimizu, K. D.; Krueger, C. A.; Harrity, J. P. A.; Snapper, M. L.; Hoveyda, A. H. *Angew. Chem. Int. Ed.* **1996**, *35*, 1668.
- (151) Fu, P.; Snapper, M. L.; Hoveyda, A. H. *J. Am. Chem. Soc.* **2008**, *130*, 5530.

- (152) Akullian, L. C.; Porter, J. R.; Traverse, J. F.; Snapper, M. L.; Hoveyda, A. H. *Adv. Synth. Catal.* **2005**, *347*, 417.
- (153) Mizutani, H.; Degrado, S. J.; Hoveyda, A. H. *J. Am. Chem. Soc.* **2002**, *124*, 779.
- (154) Brown, M. K.; Degrado, S. J.; Hoveyda, A. H. *Angew. Chem. Int. Ed.* **2005**, *44*, 5306.
- (155) Francis, M. B.; Jacobsen, E. N. *Angew. Chem. Int. Ed.* **1999**, *38*, 937.
- (156) Breit, B.; Laungani, A. C. *Tetrahedron Asymm.* **2003**, *14*, 3823.
- (157) Jayasinghe, D.; Kraatz, H.-B. *Inorg. Chim. Acta* **2006**, *359*, 3054.

Chapter 3

3.1. Structure and synthesis of dirhodium complexes

The first records of dirhodium complexes date back to the early 1960's when a dirhodium tetraacetate complex was first isolated from the reaction of a rhodium(III) salt and acetic acid in ethanol.^{1,2} An elemental analysis provided the composition of the product to be $\text{Rh}(\text{O}_2\text{CCH}_3)_2$ and its crystal structure was determined, establishing a distinctive paddle-wheel structure with two rhodium(II) atoms bridged by four carboxylate ligands (Figure 3-1).^{2,3} The distance of only 2.4 Å between the rhodium atoms corresponds to a direct bond between the two and explains the unique properties of these binuclear complexes.⁴ Since this discovery, various other complexes were produced featuring a number of bridging ligands largely dominated by carboxylates and carboxyamidates.⁵ The coordination of equatorial ligands is typically strong and irreversible, requiring high temperatures for ligand exchange to occur.^{6,7} On the contrary, ligation to the axial dirhodium sites is labile, showing preference for soft Lewis bases such as phosphines and N-heterocyclic carbenes.⁷ The properties of the dirhodium complexes vary considerably depending on the ligand environment; this inspired a number of research groups to undertake ligand optimization to produce dirhodium complexes with diverse applications as described below.

A thorough review of various dirhodium complexes can be found in the "Multiple Bonds Between Atoms" book,⁵ which covers the diversity of the available complexes. It is necessary to emphasize the importance of

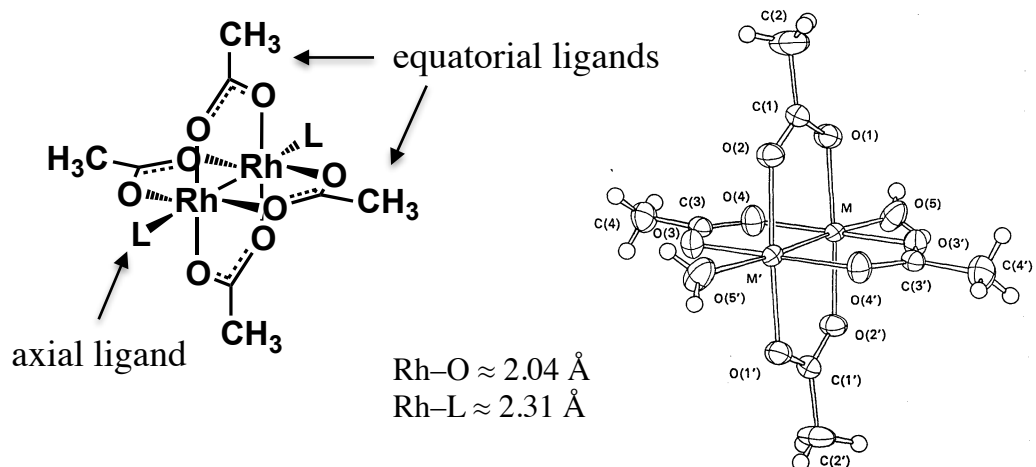


Figure 3-1. Structure of dirhodium tetraacetate complex.⁴

equatorial ligands that are typically anionic in character and provide κ^2 coordination via a delocalized negative charge. The assortment of the bridging ligands can be classified by the atoms bound to the dirhodium: κ^2 -O,O' dioxygen ligands such as carboxylates, thiocarboxylates, carbonates and sulfates; κ^2 -O,X oxygen-heteroatom(X) ligands such as amidates and phosphates; κ^2 -N,N' dinitrogen ligands such as amidinates and triazenaides; and other complexes with rhodium ligated to phosphorus and carbon atoms. Though bridging does stabilize the dirhodium core, the complexes with non-bridging equatorial ligands were also prepared, such as simple complexes with monochelating aqua and nitrile ligands or unique diimine and porphyrin complexes.^{5,8-11}

Axial sites of dirhodium complexes are usually occupied by solvent molecules unless stronger ligands are present. The scope of axial ligands is enormous with examples representing most of the electron-donor functionalities.⁵ Dirhodium complexes have been reported with electron-rich nitrogen ligands such as nitriles and nitrogen heterocycles, oxygen-donors like water, alcohols and DMSO, and various adducts with phosphines and carbenes. The unique structural geometry of the complexes was utilized to

prepare oligomeric and polymeric constructs using multidentate ligands coordinated to the opposite axial sites.^{13,14} The axial dirhodium sites are central in catalysis and as the result, strong axial ligands are usually avoided as they can interfere with reactivity both via competitive inhibition and via the *trans*-effect between the axial sites.¹² The *trans*-effect is an effect of a coordinated ligand on the affinity of the ligand in the *trans*-position. In this case, the decrease in Lewis acidity of the axial dirhodium site affects both binding of a substrate and reactivity of the dirhodium center.

Dirhodium complexes are synthesized via three general methods: the reduction of rhodium(III), the oxidation of rhodium(I) compounds in the presence of equatorial ligands, or ligand substitution on a dirhodium precursor (Figure 3-2). The reduction method is usually employed to produce simple tetracarboxylates complexes,^{1,2,15-18} while the oxidation method is only utilized for the synthesis of amidinate complexes.¹⁹ Most of the dirhodium complexes are prepared from the generic dirhodium tetraacetate. Carboxylate exchange can be performed either by heating the precursor with neat ligand or by using excess ligand at reflux in a high-boiling solvent like chlorobenzene.⁵ This method is efficient for the synthesis of a large number of complexes, yet is not suitable under circumstances in which the amount of ligand is limited or the ligand is unstable at high temperatures. A reduced amount of ligand in the second procedure is achieved using Soxhlet extraction allowing the ligand exchange reaction to be driven to completion by absorbing evolved acetic acid (Figure 3-2).²⁰ Typically, ligand substitution is pushed until all four ligands are replaced, although it can be stopped at the partial exchange, yielding mixed-

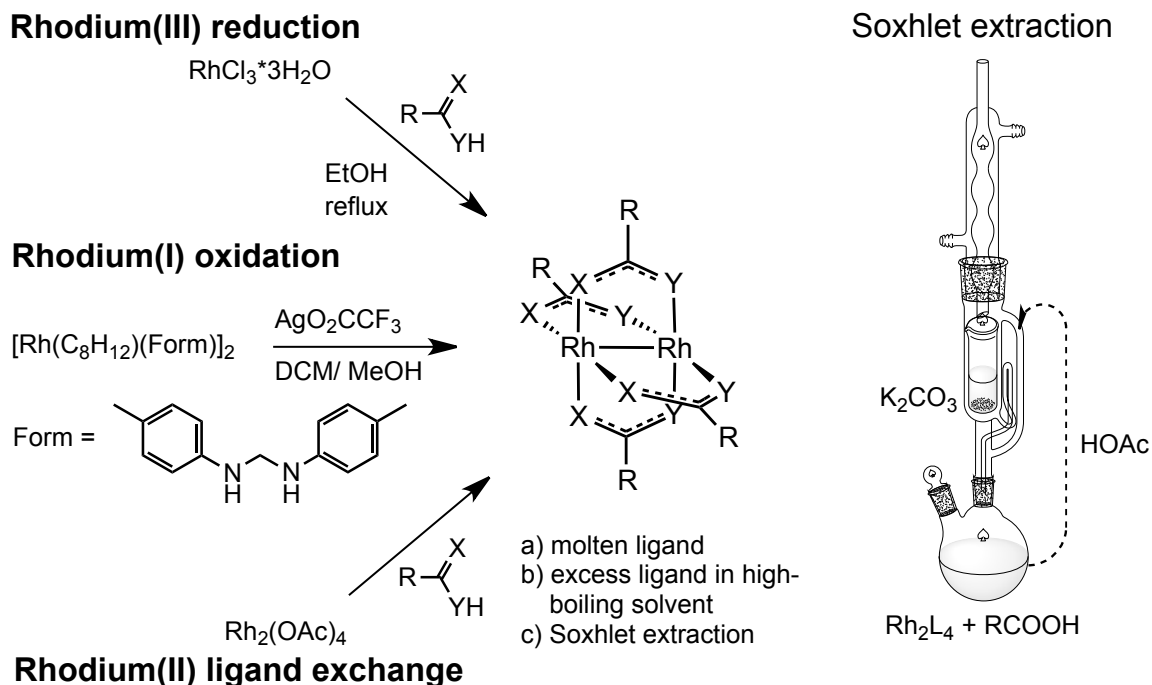


Figure 3-2. General methods for synthesis of dirhodium complexes (left) and Soxhlet extraction set-up for driving ligand exchange by absorbing volatile acetic acid (right).^{15,17,19,20}

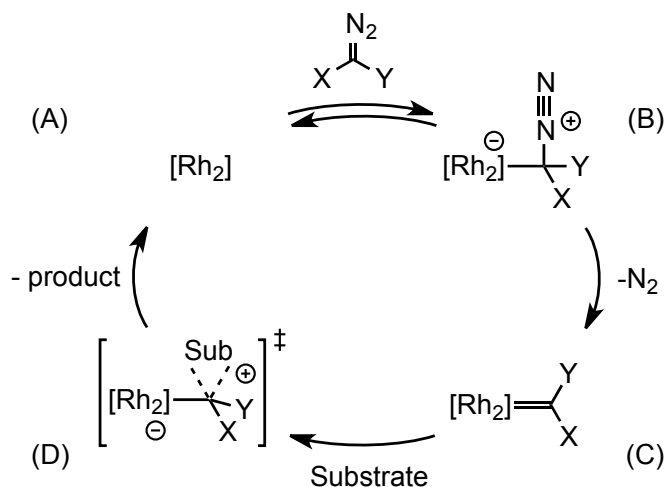
ligand complexes. Kinetic analysis of the exchange of acetates to trifluoroacetate ligands demonstrates the preference for formation of the *cis*-disubstituted product due to the *trans*-equatorial effect.⁷ *Cis*-geometry complexes are also favored with ligands other than carboxylates, indicating generality of this trend,^{19,21-24} with a few exceptions in case of amidates.^{25,26}

3.2. Catalysis

Dirhodium complexes are efficient at catalytic decomposition of diazo compounds to form highly reactive intermediates that can further undergo a variety of transformations, such as insertion into the bonds with hydrogen atoms, cycloaddition to unsaturated bonds and ylide formation with electron rich atoms. These reactions can be performed enantioselectively, employing

one of many chiral equatorial ligands that were developed over the last couple decades, therefore making dirhodium a commercially valuable catalytic system. Aside from the diazo chemistry, dirhodium had also been applied as a catalyst in allylic oxidation, Diels-Alder, silylformylation, hydrosilylation, silane alcoholysis and hydroboration.²⁷⁻³⁶

Catalytic activity of the dirhodium complexes is attributed to the Lewis acidity of the axial coordination sites. In the case of diazo chemistry, an electrophilic attack on the diazo-carbon proceeds to the formation of a diazonium intermediate (Scheme 3-1, B) that, after expulsion of dinitrogen, yields a dirhodium metallocarbene intermediate (Scheme 3-1, C).^{37,38} The slow step of the reaction has been suggested to be the formation of the metallocarbene with the preceding step existing as an equilibrium between the free diazo substrate and the substrate bound in the diazonium intermediate.³⁸ No direct observation of a dirhodium metallocarbene intermediate, however, has been reported as the result of its high reactivity. The metallocarbene undergoes an immediate attack on an electron-rich center of the substrate (Scheme 3-1), or proceeds to the formation of a dimer.³⁹



Scheme 3-1. Catalytic cycle of the dirhodium in diazo-chemistry.

A diversity of transformations available with this chemistry can be categorized in 3 groups: the insertion of carbene across C–H or X–H bond (X = N, O, S, Si, etc), the carbene addition to unsaturated bonds with the formation of various size rings (cyclopropanation, cyclopropenation, aromatic cycloaddition, etc.), and the attack on an electron lone pair of heteroatom proceeding with an ylide formation (O, N, P, S ylides).^{40,41} Figure 3-3 provides just some of the typical examples while in-depth literature is available for a more broad overview.^{40,42-46} Dirhodium catalysis of cyclopropanation and C–H insertion reactions are by far the most developed and have found widest application in organic synthesis. These reactions can be accomplished in a highly enantioselective manner using chiral carboxylate and amidate ligands (Figure 3-3, a-d).^{5,20,40,45}

Models of reaction transition states help to rationalize enantioselectivity and to design new chiral catalysts. In the case of cyclopropanation, the π -orbital of the double bond attacks an electrophilic carbon at the rhodium center and proceeds to form the product via a three-centered transition state and simultaneous dissociation of the metal (Figure 3-1).⁴⁷⁻⁴⁹ A four-centered transition state, on the other hand, was suggested in case of the cyclopropenation reaction with an alkyne taking over the coordination site at the equatorial position (Figure 3-4).⁵⁰ Both three-center and four-center transition states were proposed to occur in the C–H insertion reaction, though the non-dissociative three-centered path is generally more accepted.^{43,44,48,51,52} Enantioselectivity of these transformations is the result of steric congestion around the dirhodium active site created by chiral ligands. The two major classes of the characteristic dirhodium chiral complexes differ in symmetry: D₂ in the case of carboxylate complexes with steric bulk positioned on the opposing quadrants of the model (Figure 3-4) and C₂ in

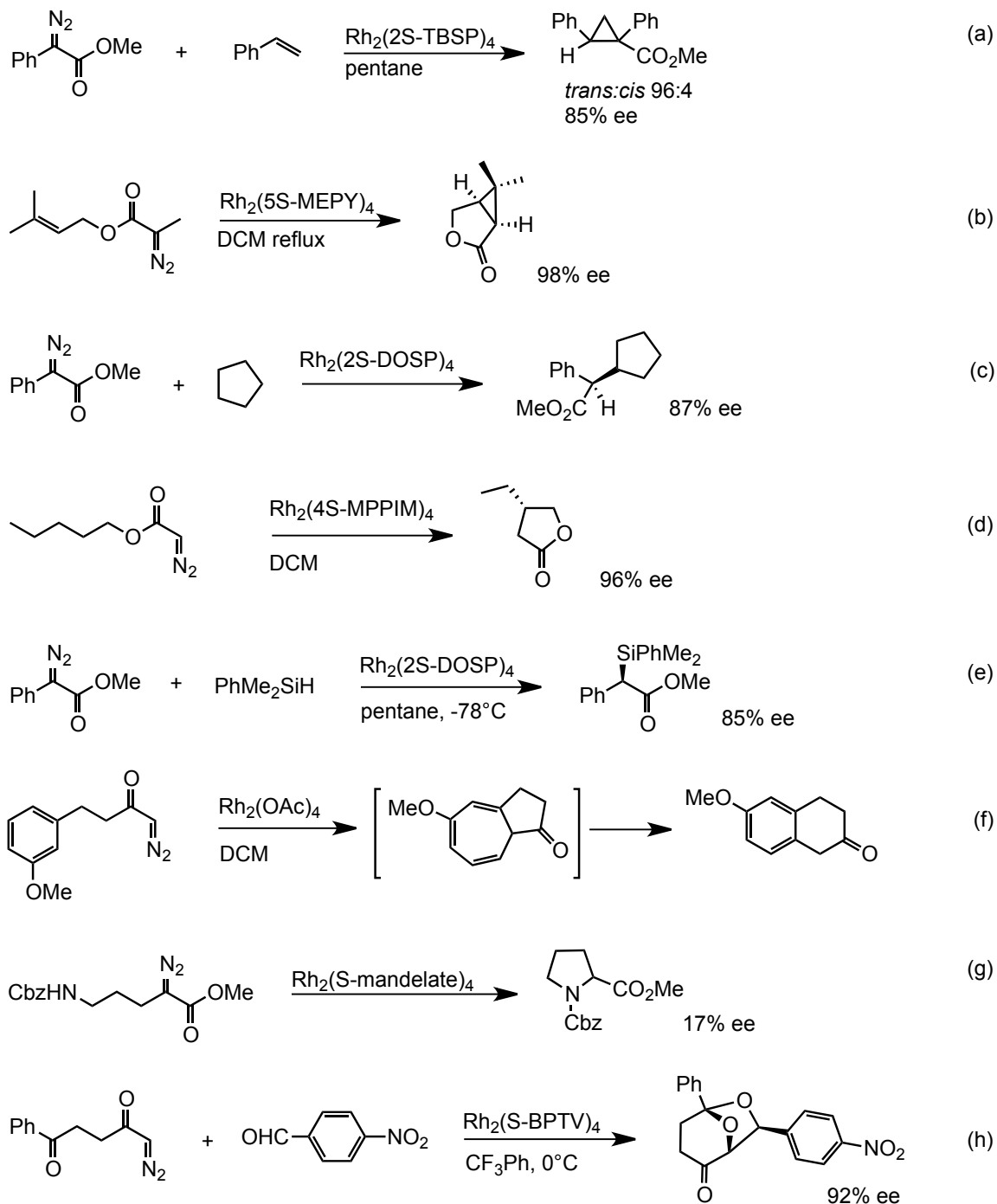


Figure 3-3. Examples of dirhodium catalyzed diazo-reaction: (a) intermolecular cyclopropanation,⁵³ (b) intramolecular cyclopropanation,⁵⁴ (c) intermolecular C-H insertion,⁵⁵ (d) intramolecular C-H insertion,⁵⁶ (e) Si-H insertion,⁵⁷ (f) N-H insertion,⁵⁸ (g) aromatic cycloaddition,⁵⁹ (h) carbonyl ylide formation followed by 1,3-dipolar cycloaddition.⁶⁰ (for ligand structure see **Figure 3-5**)

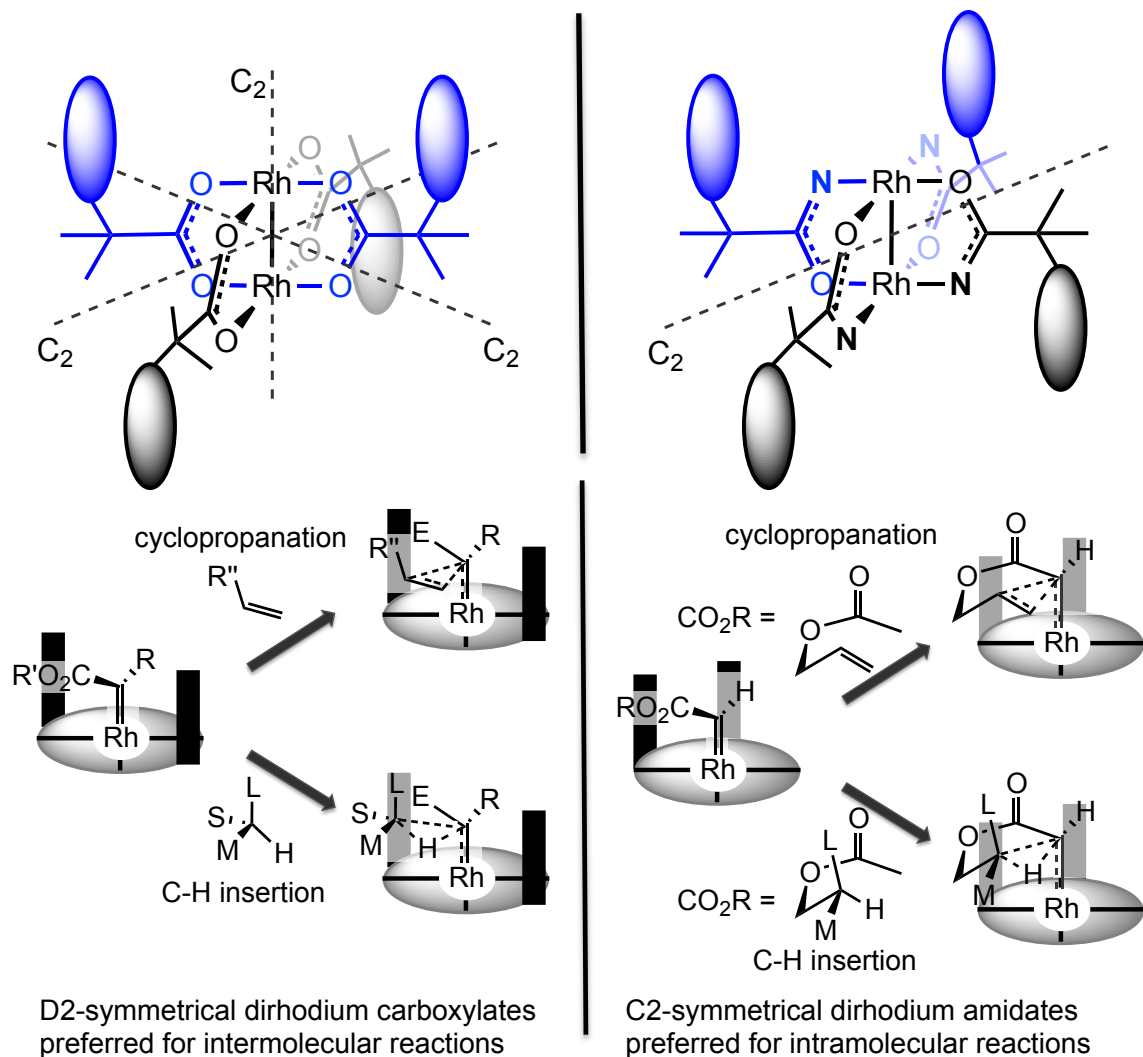


Figure 3-4. Symmetry and transition state of chiral carboxylates and amidate catalysts in cyclopropanation and C-H insertion reactions. Black blocks represent steric hindrance imposed by chiral ligands.^{44,47} (Note: amidate catalyst are typically used in intramolecular reactions and are depicted as such)⁴⁴

the case of amidate complexes that project steric hindrance at the adjacent quadrants (Figure 3-4). Both the orientation of the carbene and the approach of the substrate are controlled by the chiral environment, providing a preference for the formation of one enantiomer.

The most successful chiral carboxylate ligands are derived from amino acids that have chirality at the alpha-carbon (Figure 3-8). Bulky

sulphonyl or phthaloyl groups are attached to the amine and oriented toward the space around the reaction center. Because these structures tend to be rather flexible, the second generation of ligands was designed to allow simultaneous coordination of two equatorial positions in the *cis*-arrangement (Figure 3-8). The series of amidate ligands feature four- and five- member rings with a chiral center in the position α to the amide nitrogen (Figure 3-8). Amidate ligands are subcategorized into pyrrolidines, imidazolidines, oxazolidines and azetidines based on the nature of the amidate ring.

The choice of a catalyst depends on the reactivity of the diazo substrate and the type of reaction.⁴³ Dirhodium carboxylates are more reactive and are preferred catalysts for reactions with acceptor/acceptor and donor/acceptor diazo compounds (Figure 3-6).⁴⁴ The acceptor/acceptor substrates tend to be unreactive and require electron-poor dirhodium complexes for catalysis, making them challenging substrates for enantioselective transformations. The donor/acceptor diazo substrates work the best with most carboxylate complexes, fitting well into their reactivity profile. High reactivity tends to negatively affect selectivity and thus, carboxylate catalysts are often limited to substrates with low reactivity and require reactions to be executed at low temperatures.^{42,44} On the other hand, dirhodium amidates are used with the acceptor substrates and perform best in intramolecular reactions. Due to the limited symmetry of the complexes, they often work poorly in asymmetric intermolecular reactions, where carboxylate complexes are most effective.⁶¹ In addition, the chemoselectivity of these catalysts differs as a function of the electron withdrawing properties

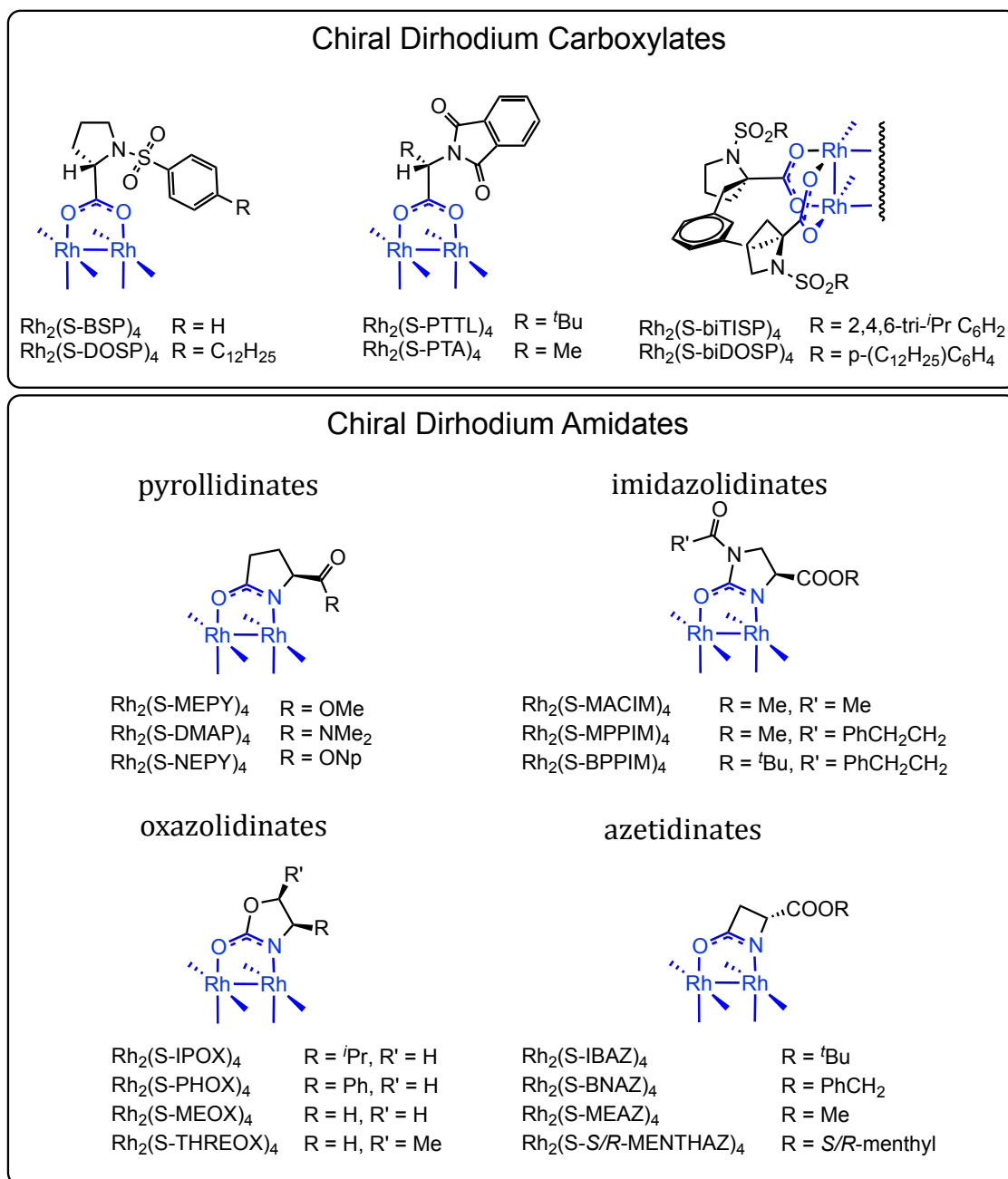


Figure 3-5. Examples of chiral dirhodium carboxylate and amidate catalysts.⁴³

of the equatorial ligands. It was well demonstrated in a competition experiment between intramolecular C-H insertion vs. cyclopropanation reactions. The catalyst with perfluorinated carboxylate ligands are highly selective toward the C-H insertion, the carboxylate complex yields a mixture of both products, and the amidate complex favors a cyclopropanation

pathway.⁶² Thus, multiple factors need to be taken into the consideration when performing dirhodium-catalyzed diazo transformations. Also, the limitations of the catalysts and the diazo substrates leave this area open for further development of chiral complexes with a broader scope of reactivity and selectivity.

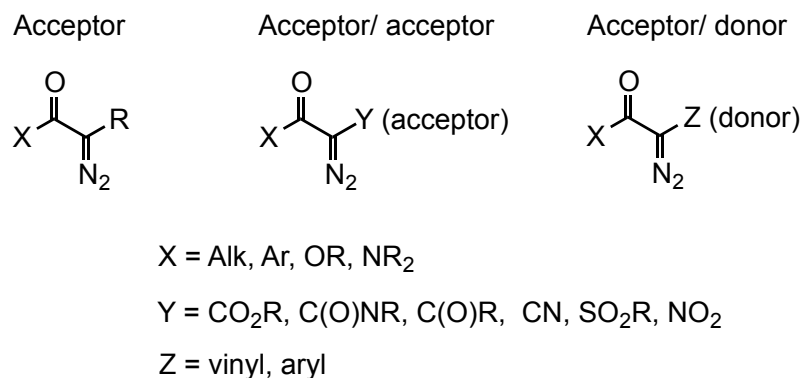


Figure 3-6. Three different classes of diazo substrate depending on the donor/acceptor properties of the adjacent groups.⁴⁴ (Note: α -carbonyl diazo compounds are the most common substrates)

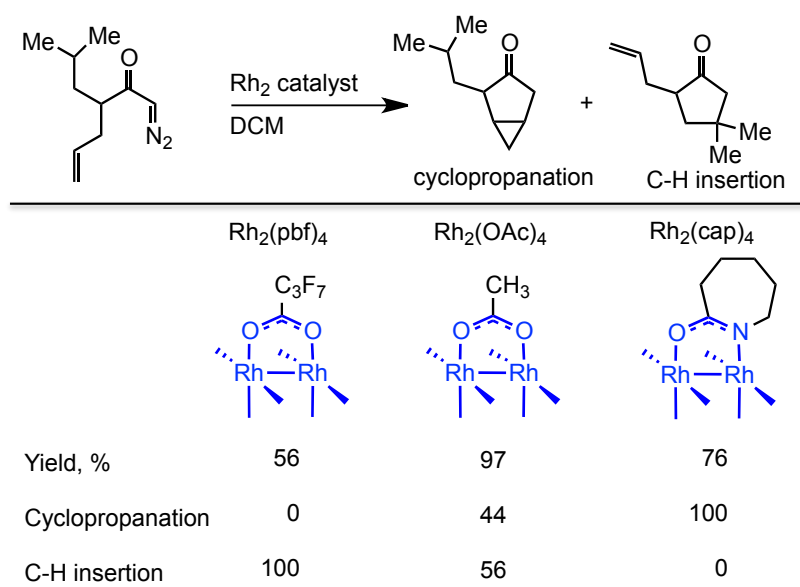


Figure 3-7. Chemoselectivity of dirhodium catalysts.⁶²

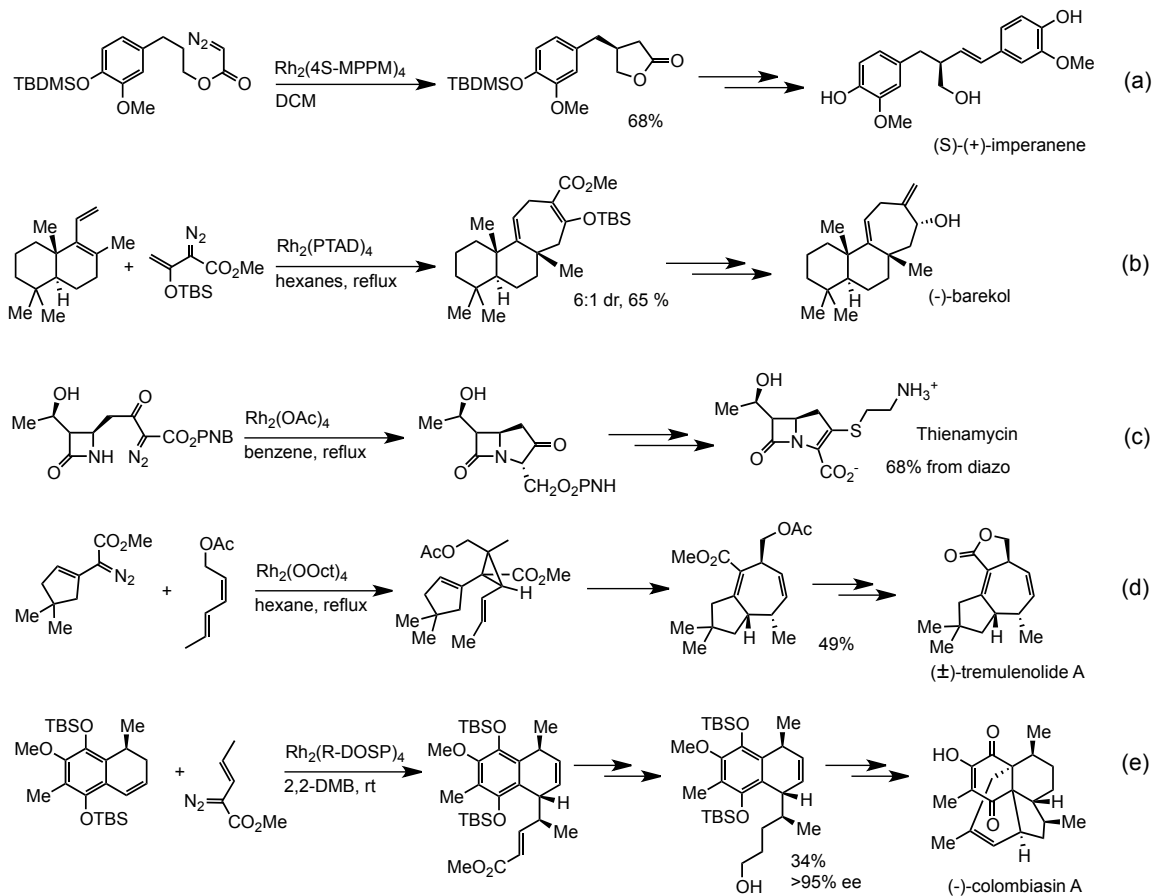


Figure 3-8. Examples of dirhodium catalysis in total synthesis. (a) C-H insertion in the synthesis of (S)-(+)-imperanene⁵⁶ (b) [4+3] dipolar cycloaddition in the synthesis of (-)-barekol⁶³ (c) N-H insertion in the synthesis of thienamycin⁶⁴ (d) cyclopropanation and rearrangement in the synthesis of (±)-tremulenolide A⁶⁵ (e) C-H insertion in the synthesis of (-)-colombiasin A.⁶⁶

Dirhodium catalysis have found utility in the synthesis of natural products and pharmaceuticals with medically valuable properties (Figure 3-8). The asymmetric transformations described above are especially useful, allowing for the installation of stereocenters in a complex molecule with a high degree of control. Achiral dirhodium catalysts were also widely applied, as in the commercialized synthesis of thienamycin antibiotic involving dirhodium-catalyzed N-H insertion step (Figure 3-8, c).

In summary, dirhodium catalysis in the area of diazo chemistry has made great progress in the last few decades and has become an important asset for synthetic organic chemistry. Development of chiral ligands significantly advanced asymmetric cyclopropanation and C–H insertion reactions, while the ability to catalyze oxidation and reduction reactions spurs further interest in utilizing dirhodium complexes toward these transformations. Also, activity toward diazo compounds has recently been recognized as a promising biorthogonal reaction with the capability of covalent modification of peptide and protein substrates (section 3.3).

3.3. Bioorthogonal reactivity

One of the inspirations for my project stems from the work of Antos and Francis, who first evaluated the utility of dirhodium catalysis for site-selective modification of tryptophan residues with diazo reagents.^{67,68} In their search for bioorthogonal methods of protein modification, they explored various transition-metal catalyzed transformations that could selectively modify amino-acid side chains.⁶⁹ The abundance of residues such as cysteine, tyrosine and tryptophan are relatively low in natural proteins, which makes them attractive targets for selective protein labeling. Some methods were available for targeting cysteine or tyrosine residues, yet tryptophan had not been previously investigated.

The tryptophan contains an indole ring that was previously demonstrated to be able undergo dirhodium-mediated insertion reactions with diazo reagents.^{70,71} Because the electron-rich character of indoles makes them reactive substrates for metallocarbenes they could potentially provide the selectivity of modification.⁷² The challenge with carbene chemistry, however, is its intolerance toward water, resulting in the formation of

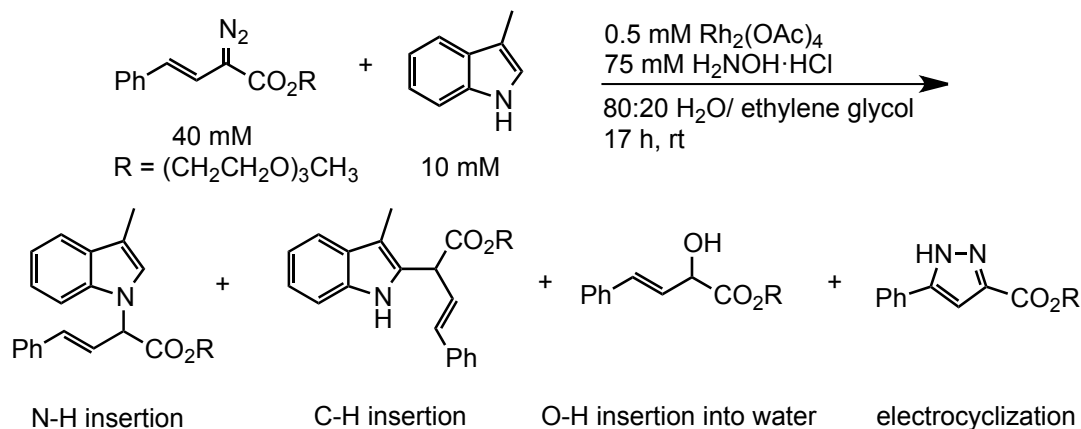


Figure 3-9. Initial reactivity study of dirhodium catalyzed insertion reaction with 3-methyl indole and styryl-diazo reagent in aqueous solution.⁶⁷

an O–H insertion byproduct.⁷³ After screening various diazo compounds, Francis identified styryl-diazoacetate as the best substrate.⁷⁴ The donor/acceptor nature of this reagent provides stabilization of the dirhodium metallocarbene and sets the preference for reaction with the more reactive indole group, rather than water. To improve solubility of the reagent in an aqueous environment, a PEG chain was attached to the ester group. In the initial test of reactivity with 3-methyl indole, two products were observed, corresponding to the C–H and N–H insertions (1.4:1.0 ratio) with an overall 51% yield along with the by-products of O–H insertion and electrocyclization (Figure 3-9).

The optimized reaction conditions were successfully applied to the modification of protein substrates. Based on the MS analysis, the exposed tryptophan residues of myoglobin (Figure 3-10) and subtilisin Carlsberg were labeled in around 50% yield. Selectivity of modification was further confirmed by MS/MS fragmentation, validating the insertion exclusively at the expected residues.⁶⁷ Further studies aimed at improving the methodology by expanding the pH range necessary for efficient modification. A

significant improvement was observed by employing a tert-butyl hydroxylamine buffer (TBHA), allowing the reaction to proceed at a pH up to 9, compared to the prior optimal best results with a hydroxylamine buffer working only at pH < 6.⁶⁸ The melitin peptide could be labeled at 60% conversion in TBHA buffer at pH 6. The protein lysozyme, which does not have any tryptophan residues on the surface, is only labeled under denaturing conditions at the temperatures above 75 °C.⁶⁸

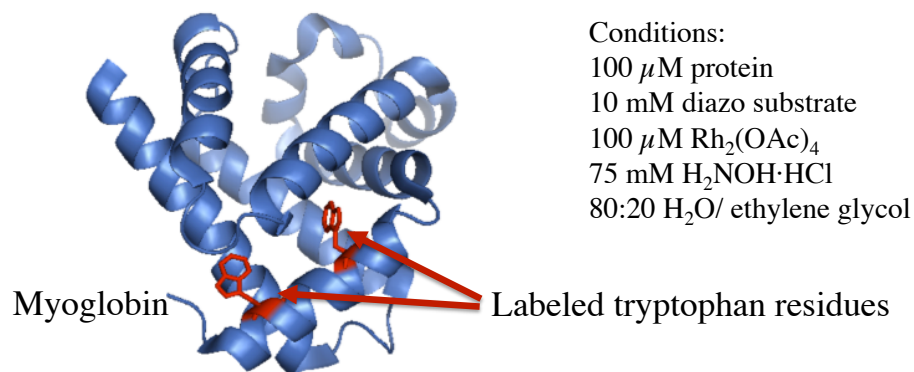


Figure 3-10. Selective labeling of myoglobin at the exposed tryptophan residues with styryl-diazo substrate and dirhodium catalyst.⁶⁷

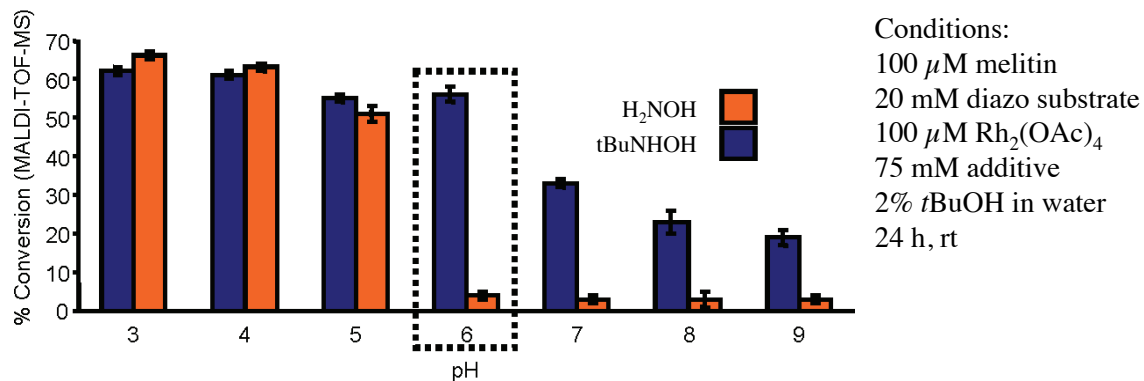


Figure 3-11. pH range improvement of the dirhodium-catalyzed protein labeling by using tert-butyl hydroxylamine buffer (Reprinted with permission from Antos, J. M. et al. *J. Am. Chem. Soc.* **2009**, *131*, 6301. Copyright 2009 American Chemical Society).⁶⁸

This chemistry allows labeling of exposed tryptophan residues under mild aqueous conditions. It displays good chemoselectivity, especially considering the potential reactivity of other electron-rich and often exposed residues, such as histidine and tyrosine. While developing my own project, one goal was to explore the potential of using peptide-dirhodium conjugates to further improve selectivity of this technique. Peptide-protein interactions were envisioned to provide selectivity for the targeting and modification of the protein of interest with the catalytic dirhodium. The foreseen benefits would be an ability to label a specific protein in a mixture, such as a lysate, and an improvement in the efficiency of labeling through an enhanced effective concentration of the substrate, i.e. amino acid side-chain.

3.4. Antitumor properties

Soon after the discovery of dirhodium complexes, they were found to possess anticancer properties.^{75,76} Their activity was suggested to be similar to cisplatin, proceeding via interaction of the metal with nucleotides of DNA. The potency of typical carboxylate complexes, however, was not a match to the cisplatin standard.⁷⁷ Nevertheless, further discoveries demonstrated potential for certain complexes with alternative ligands such as amidates or formamidinates and ligands based on methoxyphenylphosphine.⁷⁸⁻⁸⁰

The Aoki and Dunbar groups made a considerable effort to elucidate the mechanism of the dirhodium anticancer activity and characterize coordination complexes of dirhodium with DNA. It was demonstrated that dirhodium was able to form not only axial-coordination adducts with nucleotides,^{26,81,82} but also bridging equatorial complexes.^{77,83,84} Furthermore, chelate complexes with dinucleotides were prepared and structurally

characterized by NMR and X-Ray.^{77,85,86} The pair of nucleotide bases coordinates in *cis*-geometry to the dirhodium, forming a macrocyclic loop structurally similar to the cisplatin adduct (Figure 3-12). In more recent examples, adducts with oligonucleotides were characterized where dirhodium forms an equatorial type complex with adjacent adenine and cytosine bases.⁸⁷

Heteroleptic (i.e. ligands are not identical) dirhodium complexes with diimine ligands are being investigated by Turro and colleagues as candidates for photochemotherapy. Dirhodium carboxylate complexes can undergo photoexcitation by visible light (300-600 nm) to produce a long-lived excited state.⁸⁸ In the presence of a variety of acceptors, an electron transfer leads to formation of the oxidized Rh^{II}-Rh^{III} species that are capable of DNA cleavage.⁸⁹ Diimine complexes developed by Turro incorporate an acceptor into the dirhodium complex. Bipyridine- and phenanthroline- based ligands

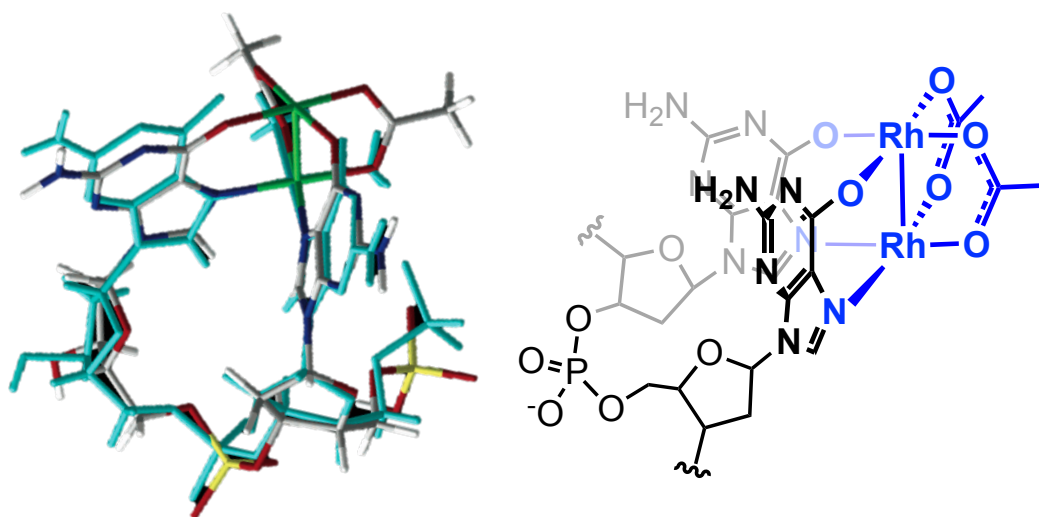


Figure 3-12. (left) Overlay of diguanidine (pGpG) adducts of dirhodium (gray, green and red) and cisplatin (blue).⁸³ (right) Chemdraw structure of the dirhodium adduct. (Reprinted with permission from Chifotides, H. T et al. *J. Am. Chem. Soc.* **2003**, *125*, 10714. Copyright 2003 American Chemical Society).

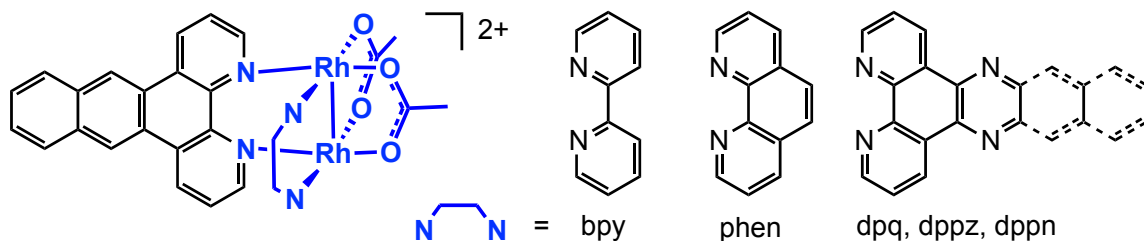


Figure 3-13. Examples of diimine dirhodium complexes developed by Turro for DNA photocleavage and cancer treatment.⁹⁴

(Figure 3-12) serve a dual purpose, providing intercalation into DNA via π -stacking and serving as electron acceptors in the direct DNA photocleavage.⁹⁰⁻⁹³ Significantly, the toxicity of these dirhodium complexes is relatively low in the dark and increases upon illumination.⁹⁴ HeLa and COLO-316 cancer cells were successfully killed with the series of *dppn* complexes with LD₅₀ values in the range 70-200 μ M.⁹⁴ Inducing cell apoptosis with light has the potential to be developed into a technology for cancer treatment.

3.5. References

- (1) I. I. Chernyaev, E. V. S., L. A. Kazarova, and A. S. Antsyshkina In *Abstracts of Papers Presented at 7th International Conference on Coordination Chemistry* Stockholm, 1962.
- (2) Johnson, S. A.; Hunt, H. R.; Neumann, H. M. *Inorg. Chem.* **1963**, 2, 960.
- (3) Porai-Koshits, M. A.; Antsyshkina, A. S. *Dok. Akad. Nauk SSSR* **1962**, 146, 1102.
- (4) Cotton, F. A.; DeBoer, B. G.; LaPrade, M. D.; Pipal, J. R.; Ucko, D. A. *Acta Crystallogr. Sect. B* **1971**, 27, 1664.
- (5) Cotton, F. A.; Murillo, C. A.; Walton, R. A. *Multiple bonds between metal atoms*; Springer Science and Business Media, Inc., 2005.

- (6) Casas, J. M.; Cayton, R. H.; Chisholm, M. H. *Inorg. Chem.* **1991**, *30*, 358.
- (7) Bear, J. L.; Kitchens, J.; Willcott III, M. R. *J. Inorg. Nucl. Chem.* **1971**, *33*, 3479.
- (8) Dunbar, K. R. *J. Am. Chem. Soc.* **1988**, *110*, 8247.
- (9) Maspero, F.; Taube, H. *J. Am. Chem. Soc.* **1968**, *90*, 7361.
- (10) Pruchnik, F. P.; Jutarska, A.; Ciunik, Z.; Pruchnik, M. *Inorg. Chim. Acta* **2003**, *350*, 609.
- (11) Ogoshi, H.; Setsune, J.; Yoshida, Z. *J. Am. Chem. Soc.* **1977**, *99*, 3869.
- (12) Pirrung, M. C.; Liu, H.; Morehead, A. T. *J. Am. Chem. Soc.* **2002**, *124*, 1014.
- (13) Takamizawa, S.; Nakata, E.; Yokoyama, H.; Mochizuki, K.; Mori, W. *Angew. Chem.* **2003**, *115*, 4467.
- (14) Cotton, F. A.; Kim, Y. *J. Am. Chem. Soc.* **1993**, *115*, 8511.
- (15) Legzdins, P.; Mitchell, R. W.; Rempel, G. L.; Ruddick, J. D.; Wilkinson, G. *J. Chem. Soc. A* **1970**, 3322.
- (16) Winkhaus, G.; Ziegler, P. *Z. Anorg. Allg. Chem.* **1967**, *350*, 51.
- (17) Cotton, F.; Han, S.; Wang, W. *Inorg. Chem.* **1984**, *23*, 4762.
- (18) Berry, M.; Garner, C. D.; Hillier, I. H.; Macdowell, A. A.; Clegg, W. *J. Chem. Soc., Chem. Commun.* **1980**, 494.
- (19) Piraino, P.; Bruno, G.; Tresoldi, G.; Lo Schiavo, S.; Zanello, P. *Inorg. Chem.* **1987**, *26*, 91.
- (20) Doyle, M. P.; Winchester, W. R.; Hoorn, J. A. A.; Lynch, V.; Simonsen, S. H.; Ghosh, R. *J. Am. Chem. Soc.* **1993**, *115*, 9968.
- (21) Pimblett, G.; Garner, C. D.; Clegg, W. *J. Chem. Soc., Dalton Trans.* **1986**, 1257.

- (22) Pruchnik, F.; Jezierski, A.; Kalecińska, E. *Polyhedron* **1991**, *10*, 2551.
- (23) Yoshimura, T.; Umakoshi, K.; Sasaki, Y. *Inorg. Chem.* **2003**, *42*, 7106.
- (24) Estevan, F.; Garcia-Bernabe, A.; Garcia-Granda, S.; Lahuerta, P.; Moreno, E.; Perez-Prieto, J.; Sanau, M.; Angeles Ubeda, M. *J. Chem. Soc., Dalton Trans.* **1999**, 3493.
- (25) Cotton, F. A.; Felthouse, T. R. *Inorg. Chem.* **1981**, *20*, 584.
- (26) Aoki, K.; Salam, M. A. *Inorg. Chim. Acta* **2002**, *339*, 427.
- (27) Doyle, M. P.; Terpstra, J. W.; Winter, C. H.; Griffin, J. H. *J. Mol. Catal.* **1984**, *26*, 259.
- (28) Catino, A. J.; Forslund, R. E.; Doyle, M. P. *J. Am. Chem. Soc.* **2004**, *126*, 13622.
- (29) Moody, C. J.; Palmer, F. N. *Tetrahedron Lett.* **2002**, *43*, 139.
- (30) Choi, H.; Doyle, M. P. *Org. Lett.* **2007**, *9*, 5349.
- (31) Doyle, M. P.; Westrum, L. J.; Protopopova, M. N.; Eismont, M. Y.; Jarstfer, M. B. *Mendeleev Commun.* **1993**, *3*, 81.
- (32) Pascoe, W. *Catalysis of organic reactions*; M. Dekker, 1992.
- (33) Doyle, M. P.; Phillips, I. M.; Hu, W. *J. Am. Chem. Soc.* **2001**, *123*, 5366.
- (34) Doyle, M. P.; Shanklin, M. S. *Organometallics* **1994**, *13*, 1081.
- (35) Doyle, M. P.; High, K. G.; Nesloney, C. L.; Clayton, T. W.; Lin, J. *Organometallics* **1991**, *10*, 1225.
- (36) Doyle, M. P.; High, K. G.; Bagheri, V.; Pieters, R. J.; Lewis, P. J.; Pearson, M. M. *J. Org. Chem.* **1990**, *55*, 6082.
- (37) Maxwell, J. L.; Brown, K. C.; Bartley, D. W.; Kodadek, T. *Science* **1992**, *256*, 1544.

- (38) Wong, F. M.; Wang, J.; Hengge, A. C.; Wu, W. *Org. Lett.* **2007**, *9*, 1663.
- (39) Shankar, B. K. R.; Shechter, H. *Tetrahedron Lett.* **1982**, *23*, 2277.
- (40) Doyle, M. P.; McKervey, M. A.; Ye, T. *Modern catalytic methods for organic synthesis with diazo compounds: from cyclopropanes to ylides*; Wiley, 1998.
- (41) Ye, T.; McKervey, M. A. *Chem. Rev.* **1994**, *94*, 1091.
- (42) Doyle, M. P.; Forbes, D. C. *Chem. Rev.* **1998**, *98*, 911.
- (43) Doyle, M. P.; Duffy, R.; Ratnikov, M.; Zhou, L. *Chem. Rev.* **2009**, *110*, 704.
- (44) Davies, H. M. L.; Beckwith, R. E. J. *Chem. Rev.* **2003**, *103*, 2861.
- (45) Jacobsen, E. N.; Pfaltz, A.; Yamamoto, H. *Comprehensive Asymmetric Catalysis*; Springer-Verlag GmbH, 2004.
- (46) Clark, J. S. *Nitrogen, oxygen, and sulfur ylide chemistry: a practical approach in chemistry*; Oxford University Press, 2002.
- (47) Nowlan, D. T.; Gregg, T. M.; Davies, H. M. L.; Singleton, D. A. *J. Am. Chem. Soc.* **2003**, *125*, 15902.
- (48) Hansen, J.; Autschbach, J.; Davies, H. M. L. *J. Org. Chem.* **2009**, *74*, 6555.
- (49) Briones, J. F.; Hansen, J. r.; Hardcastle, K. I.; Autschbach, J.; Davies, H. M. L. *J. Am. Chem. Soc.* **2010**, *132*, 17211.
- (50) Lou, Y.; Remarchuk, T. P.; Corey, E. J. *J. Am. Chem. Soc.* **2005**, *127*, 14223.
- (51) Taber, D. F.; You, K. K.; Rheingold, A. L. *J. Am. Chem. Soc.* **1996**, *118*, 547.
- (52) Nakamura, E.; Yoshikai, N.; Yamanaka, M. *J. Am. Chem. Soc.* **2002**, *124*, 7181.

- (53) Doyle, M. P.; Zhou, Q.-L.; Charnsangavej, C.; Longoria, M. A.; McKervey, M. A.; Garcia, C. F. *Tetrahedron Lett.* **1996**, *37*, 4129.
- (54) Doyle, M. P.; Austin, R. E.; Bailey, A. S.; Dwyer, M. P.; Dyatkin, A. B.; Kalinin, A. V.; Kwan, M. M. Y.; Liras, S.; Oalmann, C. J. *J. Am. Chem. Soc.* **1995**, *117*, 5763.
- (55) Davies, H. M. L.; Hansen, T.; Churchill, M. R. *J. Am. Chem. Soc.* **2000**, *122*, 3063.
- (56) Bode, J. W.; Doyle, M. P.; Protopopova, M. N.; Zhou, Q.-L. *J. Org.Chem.* **1996**, *61*, 9146.
- (57) Davies, H. M. L.; Hansen, T.; Rutberg, J.; Bruzinski, P. R. *Tetrahedron Lett.* **1997**, *38*, 1741.
- (58) Fernandez Garcia, C.; McKervey, M. A.; Ye, T. *ChemInform* **1996**, 27.
- (59) Kennedy, M.; McKervey, M. A.; Maguire, A. R.; Tuladhar, S. M.; Twohig, M. F. *J. Chem. Soc., Perkin Trans. I* **1990**, 1047.
- (60) Tsutsui, H.; Shimada, N.; Abe, T.; Anada, M.; Nakajima, M.; Nakamura, S.; Nambu, H.; Hashimoto, S. *Adv. Synth. Catal.* **2007**, *349*, 521.
- (61) Doyle, M. P. *J. Org.Chem.* **2006**, *71*, 9253.
- (62) Padwa, A.; Austin, D. J.; Price, A. T.; Semones, M. A.; Doyle, M. P.; Protopopova, M. N.; Winchester, W. R.; Tran, A. *J. Am. Chem. Soc.* **1993**, *115*, 8669.
- (63) Lian, Y.; Miller, L. C.; Born, S.; Sarpong, R.; Davies, H. M. L. *J. Am. Chem. Soc.* **2010**, *132*, 12422.
- (64) Melillo, D. G.; Shinkai, I.; Liu, T.; Ryan, K.; Sletzinger, M. *Tetrahedron Lett.* **1980**, *21*, 2783.
- (65) Davies, H. M. L.; Doan, B. D. *J. Org.Chem.* **1998**, *63*, 657.

- (66) Davies, H. M. L.; Dai, X.; Long, M. S. *J. Am. Chem. Soc.* **2006**, *128*, 2485.
- (67) Antos, J. M.; Francis, M. B. *J. Am. Chem. Soc.* **2004**, *126*, 10256.
- (68) Antos, J. M.; McFarland, J. M.; Iavarone, A. T.; Francis, M. B. *J. Am. Chem. Soc.* **2009**, *131*, 6301.
- (69) Antos, J. M.; Francis, M. B. *Curr. Opin. Chem. Biol.* **2006**, *10*, 253.
- (70) Gibe, R.; Kerr, M. A. *J. Org. Chem.* **2002**, *67*, 6247.
- (71) Salim, M.; Capretta, A. *Tetrahedron* **2000**, *56*, 8063.
- (72) Davies, H. M. L. *ChemInform* **1995**, *26*, no.
- (73) Miller, D. J.; Moody, C. J. *Tetrahedron* **1995**, *51*, 10811.
- (74) Antos, J. Ph.D., University of California, Berkeley, 2006.
- (75) Erck, A.; Rainen, L.; Whileyman, J.; Chang, I. M.; Kimball, A. P.; Bear, J. L. *Experimental Biology and Medicine* **1974**, *145*, 1278.
- (76) Bear, J. L.; Gray, H. B. J.; Rainen, L.; Chang, I. M.; Howard, R.; Serio, G.; Kimball, A. P. *Cancer Chemother Rep.* **1975**, *59*, 611.
- (77) Chifotides, H. T.; Dunbar, K. R. *Acc. Chem. Res.* **2005**, *38*, 146.
- (78) Espósito, B. P.; Zyngier, S. B.; de Souza, A. R.; Najjar, R. *Met-Based. Drugs* **1997**, *4*, 333.
- (79) Pruchnik, F. P.; Starosta, R.; Ciunik, Z.; Opolski, A.; Wietrzyk, J.; Wojdat, E.; Dus, D. *Can. J. Chem.*, *79*, 868.
- (80) Pruchnik, F.; Duś, D. *J. Inorg. Biochem.* **1996**, *61*, 55.
- (81) Aoki, K.; Hoshino, M.; Okada, T.; Yamazaki, H.; Sekizawa, H. *J. Chem. Soc., Chem. Commun.* **1986**, 314.
- (82) Aoki, K.; Salam, M. A. *Inorg. Chim. Acta* **2001**, *316*, 50.
- (83) Chifotides, H. T.; Koshlap, K. M.; Perez, L. M.; Dunbar, K. R. *J. Am. Chem. Soc.* **2003**, *125*, 10714.

- (84) Chifotides, H. T.; Koshlap, K. M.; Perez, L. M.; Dunbar, K. R. *J. Am. Chem. Soc.* **2003**, *125*, 10703.
- (85) Chifotides, H. T.; Dunbar, K. R. *J. Am. Chem. Soc.* **2007**, *129*, 12480.
- (86) Chifotides, H. T.; Dunbar, K. R. *Chem. Eur. J.* **2008**, *14*, 9902.
- (87) Kang, M.; Chifotides, H. T.; Dunbar, K. R. *Biochemistry* **2008**, *47*, 2265.
- (88) Fu, P. K. L.; Bradley, P. M.; Turro, C. *Inorg. Chem.* **2001**, *40*, 2476.
- (89) Dunham, S. U.; Chifotides, H. T.; Mikulski, S.; Burr, A. E.; Dunbar, K. R. *Biochemistry* **2004**, *44*, 996.
- (90) Bradley, P. M.; Angeles-Boza, A. M.; Dunbar, K. R.; Turro, C. *Inorg. Chem.* **2004**, *43*, 2450.
- (91) Angeles-Boza, A. M.; Bradley, P. M.; Fu, P. K. L.; Wicke, S. E.; Bacsa, J.; Dunbar, K. R.; Turro, C. *Inorg. Chem.* **2004**, *43*, 8510.
- (92) Aguirre, J. D.; Angeles-Boza, A. M.; Chouai, A.; Turro, C.; Pellois, J.-P.; Dunbar, K. R. *Dalton Trans.* **2009**, 10806.
- (93) Aguirre, J. D.; Angeles-Boza, A. M.; Chouai, A.; Pellois, J.-P.; Turro, C.; Dunbar, K. R. *J. Am. Chem. Soc.* **2009**, *131*, 11353.
- (94) Joyce, L. E.; Aguirre, J. D.; Angeles-Boza, A. M.; Chouai, A.; Fu, P. K. L.; Dunbar, K. R.; Turro, C. *Inorg. Chem.* **2010**, *49*, 5371.

Chapter 4

Synthesis of dirhodium metallopeptides

4.1. Introduction

The development of the procedures for the synthesis of dirhodium metallopeptides was one of the initial challenges faced in the beginning stages of this project. The difficulties arise from the harsh conditions that are used in typical methods of dirhodium complex synthesis as described in detail in Chapter 3. Specifically, procedures requiring high temperatures and organic solvents are not well-suited for peptide chemistry. Although high stability and exchange-inertness of tetracarboxylate complexes were the reasons that drew our interest, the same attributes had complicated the synthesis of metallopeptides with dirhodium center. In search of a new approach, a few other precursors were found in the literature, aside from the common dirhodium tetraacetate. The benefits of alternative precursors arise either from the point of aqueous synthesis as with dirhodium tetracarbonate or lower temperatures as with dirhodium complexes bearing nitrile or trifluoroacetate equatorial ligands.

Dirhodium carbonate is prepared as a sodium salt and is completely soluble in water.¹⁻³ Carbonate ligands undergo exchange with carboxylates in aqueous solution at reflux (100 °C). The exchange is irreversible due to formation of carbon dioxide and does not require excess of the carboxylate ligands. The method is attractive because the reaction proceeds in aqueous

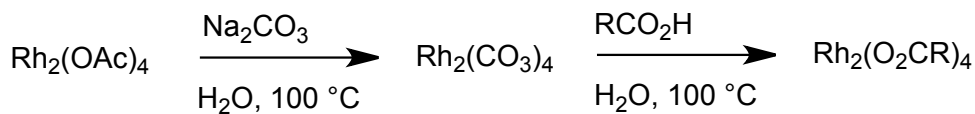


Figure 4-1. Synthesis of dirhodium complexes with dirhodium tetracarboxylate precursor.^{1,2}

solution and ligand substitution can potentially be optimized to proceed at lower temperatures (Figure 4-1).

Cotton et al. employed cationic dirhodium complexes with four acetonitrile ligands to synthesize organometallic macrocycles where three dirhodium centers are bridged via dicarboxylate ligands.^{4,5} This precursor undergoes fast ligand exchange at rt in acetonitrile as the solvent (Figure 4-2). High reactivity of the complex could provide a necessary improvement for development of milder conditions of metalloprotein synthesis.

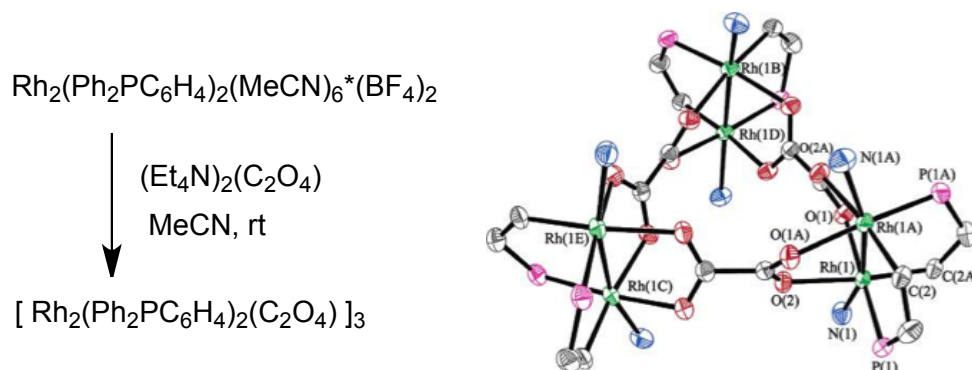


Figure 4-2. Synthesis of dirhodium complexes from dirhodium precursor with acetonitrile ligands and crystal structure of organometallic macrocyclic product.⁴

In the most recent example, dirhodium complexes with trifluoroacetate ligands were used to produce mixed-ligand complexes containing amidate and carboxylate ligands.⁶ As in the previous case, the advantage of this method comes from the mild exchange conditions (Figure 4-3). However, the use of organic solvents like acetonitrile or THF remains an obstacle for application of these methods to peptide substrates.

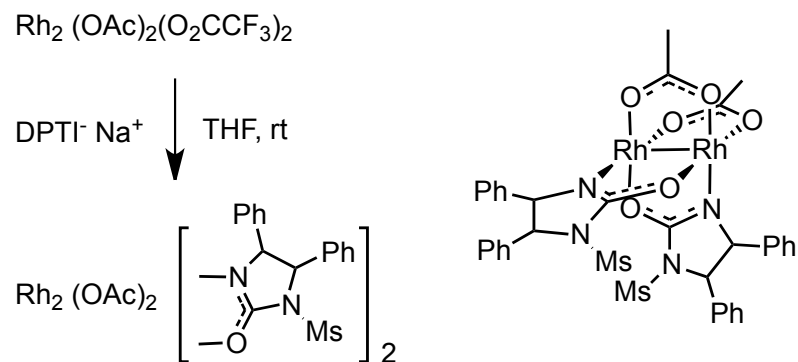


Figure 4-3. Synthesis of dirhodium complexes from dirhodium precursor with trifluoroacetate ligands (DPTI is the amidate with its structure displayed in the product).⁶

In the development of a protocol of dirhodium metallopeptide synthesis, I have tested dirhodium tetraacetate as well as the new precursors similar to the ones described above. Small-molecule carboxylate ligands, a short dipeptide and longer chain peptides were tried as substrates for carboxylate exchange. As a result of these studies, I was able to achieve an efficient method that allows synthesis of dirhodium metallopeptides under mild aqueous conditions.

4.2. Development of metalation conditions

The four dirhodium complexes shown in Figure 4-4 were examined as precursors for the synthesis of dirhodium metallopeptides. An initial screening of the reaction conditions for carboxylate exchange was primarily performed with the small dipeptide aspartame that is used as a sweetener.

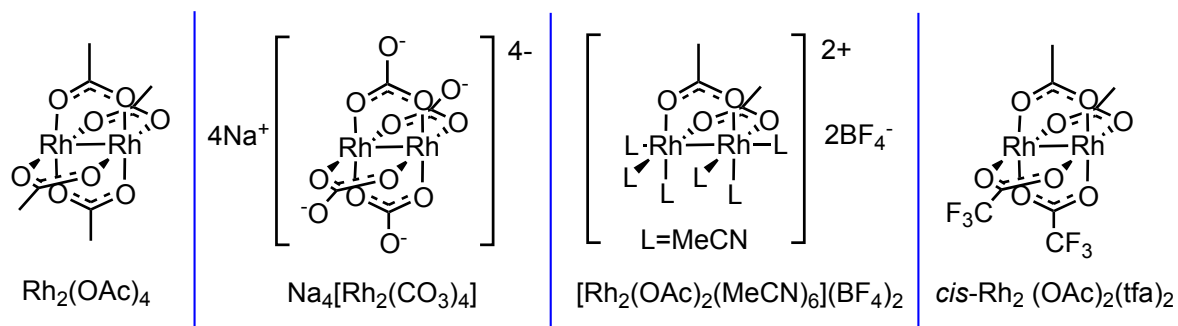


Figure 4-4. Dirhodium precursors used in developing peptide metalation conditions.

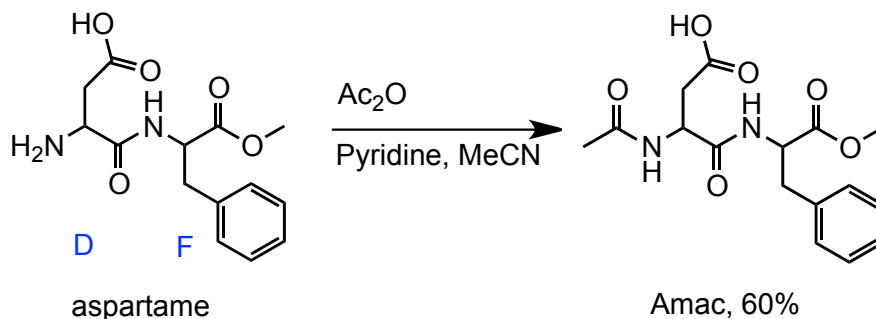


Figure 4-5. Synthesis of acetylated aspartame (Amac).

The structure of aspartame is surprisingly convenient for these studies. It features aspartate as the carboxylate source and phenylalanine as the handle for UV detection. The methylated C-terminus eliminates the problem of multiple carboxylates that can complicate results via formation of oligomeric structures. The only modification that was performed to aspartame was acetylation of N-terminal amine (“Amac” substrate, Figure 4-5) to increase solubility and exclude a potentially reactive group.

In spite of the complications with dirhodium tetraacetate precursor $\text{Rh}_2(\text{OAc})_4$ described above, this precursor was also evaluated. Heating a mixture of this precursor and Amac in a sealed vial at $100\text{ }^\circ\text{C}$ overnight gave a range of products as a result of mono-, di-, tri- and tetra- substitution (Figure 4-6). The reaction can be shifted towards mostly the tetra-substituted product by using an excess of the dipeptide or/and using a Soxhlet extractor (Figure 4-7). Attempts to use the described conditions for oligopeptide metalation have failed.

Simultaneously I pursued ligand exchange with the other precursor—dirhodium acetonitrile complex $[\text{Rh}_2(\text{OAc})_2(\text{MeCN})_6](\text{BF}_4)_2$. All attempts to achieve ligand exchange with Amac were unsuccessful. Though some results were obtained with phenylacetic acid and its sodium salt as substrates, a mixture of products was typically observed resulting from the

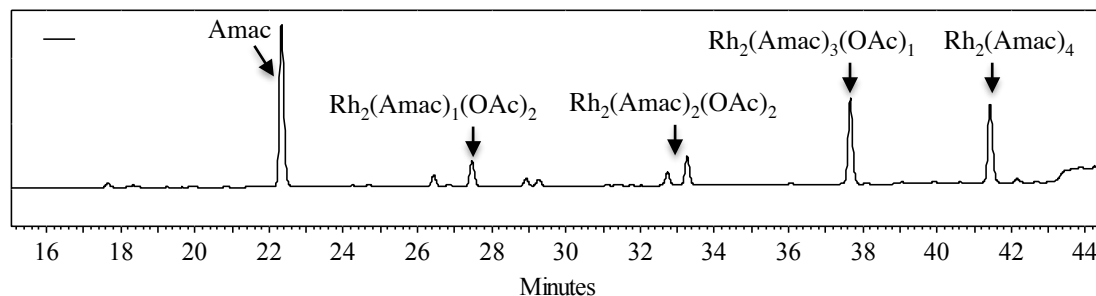


Figure 4-6. HPLC of crude ligand exchange reaction between Amac and $\text{Rh}_2(\text{OAc})_4$ via the sealed vial procedure.

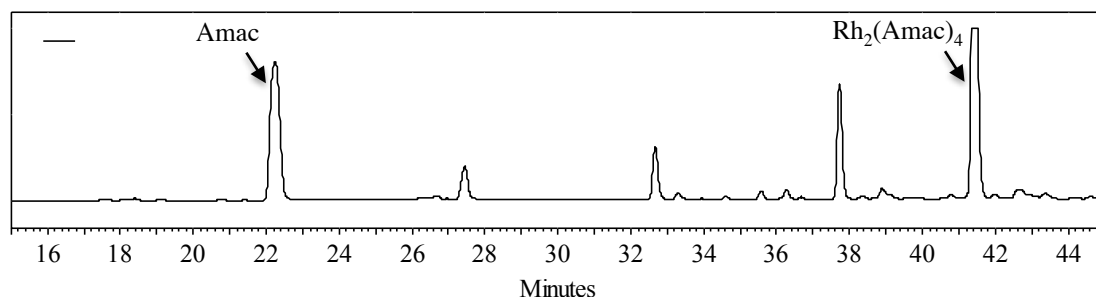


Figure 4-7. HPLC of crude ligand exchange reaction between Amac and $\text{Rh}_2(\text{OAc})_4$ via Soxhlet extraction procedure.

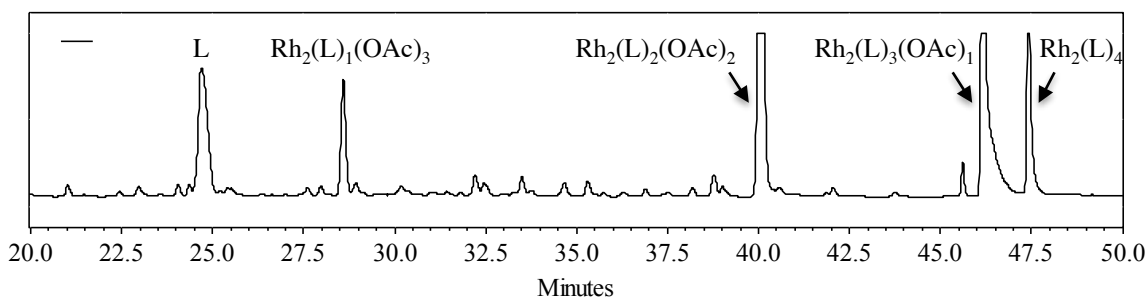


Figure 4-8. HPLC of crude ligand exchange reaction between phenylacetic acid (L) and $[\text{Rh}_2(\text{OAc})_2(\text{MeCN})_6](\text{BF}_4)_2$ precursor.

replacement of conditions worked for Amac or aspartame systems and resulted in either no reaction or an unidentified mixture of products.

After positive results were attained with the dirhodium-trifluoroacetate complexes, studies with the other precursors were discontinued. Screening was mostly focused on the *cis*- $\text{Rh}_2(\text{OAc})_2(\text{tfa})_2$ complex which is similar to the acetonitrile complex in that the labile

ligands are in a *cis* conformation. Such arrangement of the ligands was viewed to be important for potentially bridging two carboxylates chains on the same secondary structure elements like a β -hairpin or an α -helix. Clean exchange was observed with Amac substrate in various aprotic organic solvents in the presence of DIEA as base (Figure 4-9). More importantly, the ligand exchange can proceed in aqueous solution buffered with MES (Figure 4-10). The success of this reaction was found to be strongly dependent on pH. Displacement of trifluoroacetates was observed even in unbuffered conditions as long as the pH remains in the range of 4.5-6. Lower pH causes carboxylates on the side chains of aspartate to be protonated and higher pH affects efficiency of the exchange. The effect of free amine was tested via addition of butyl amine to mimic side chain of lysine residues.

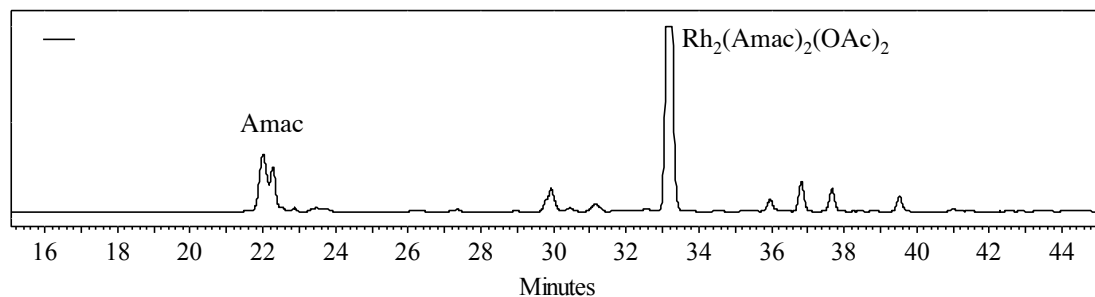


Figure 4-9. HPLC of crude ligand exchange reaction between Amac and *cis*- $\text{Rh}_2(\text{tfa})_2(\text{OAc})_2$ in THF.

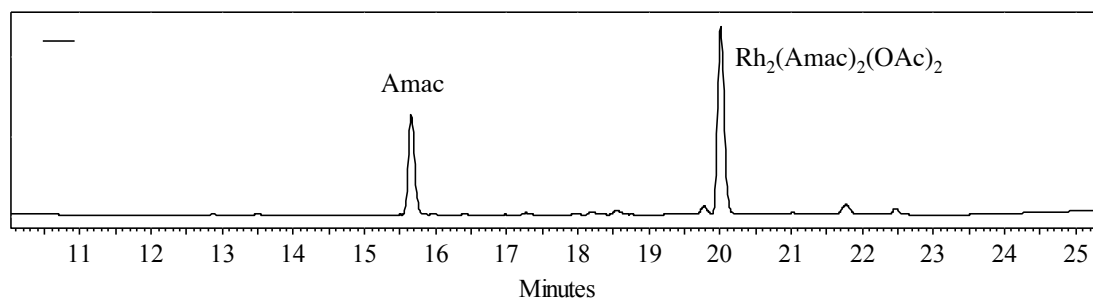


Figure 4-10. HPLC trace of metalation reaction between acetylated aspartame (Amac, 3 equiv) and $\text{Rh}_2(\text{OAc})_2(\text{tfa})_2$ (1 equiv) in MES buffer (pH 5.1), 50 °C, 3h.

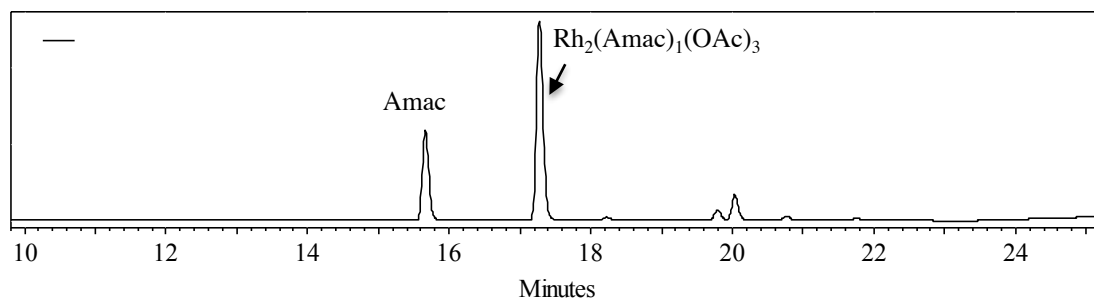


Figure 4-11. HPLC trace of metalation reaction between acetylated aspartame (Amac, 3 equiv) and $\text{Rh}_2(\text{OAc})_3(\text{tfa})_1$ (1 equiv) in MES buffer (pH 5.1), 50 °C, 3h.

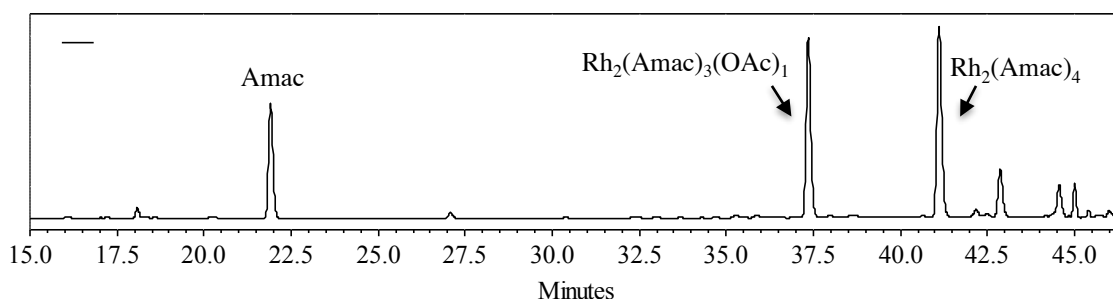


Figure 4-12. HPLC of crude ligand exchange reaction between Amac and 1:1 mixture of $\text{Rh}_2(\text{tfa})_3(\text{OAc})_1$ and $\text{Rh}_2(\text{tfa})_4$ under aqueous reaction conditions.

No negative effect was observed if the pH was adjusted to the proper value. Other precursors with trifluoroacetate ligands $\text{Rh}_2(\text{OAc})_n(\text{tfa})_{4-n}$ also react successfully under the described conditions (Figure 4-11 and Figure 4-12).

4.3. Synthesis of the “zinc finger” (ZF) dirhodium metallopeptide

The oligopeptide employed for initial studies was derived from *bis*-cysteine hairpin domain from a typical zinc finger protein, ZIF268.⁷ I chose to examine the generality of the zinc-binding domain to determine if it could serve as the basis for new dirhodium-binding domains through amino-acid substitutions to position two Asp residues in place of the zinc-binding Cys. The peptide sequence **ZF**, derived from the ZIF268 fragment P62–A73, contains a number of functional groups. Although I considered selective

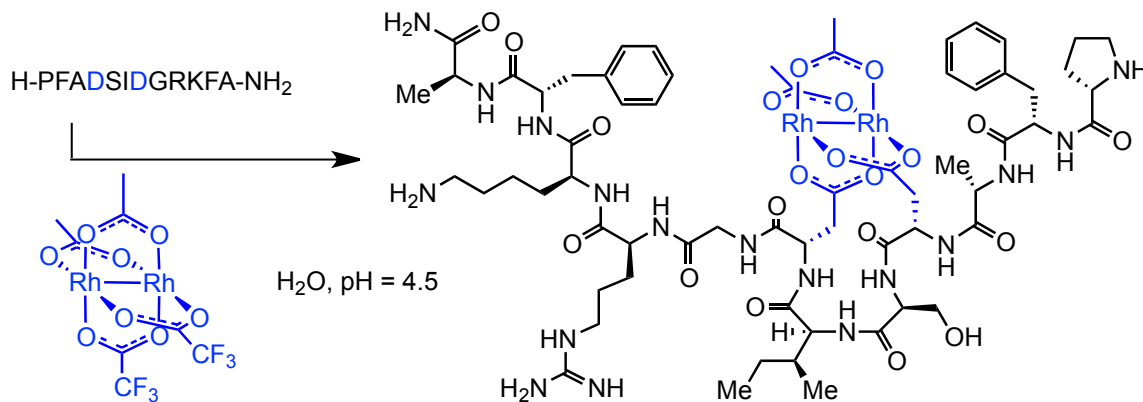


Figure 4-13. Synthesis of a dirhodium metallopeptide **ZF-Rh₂(OAc)₂**.

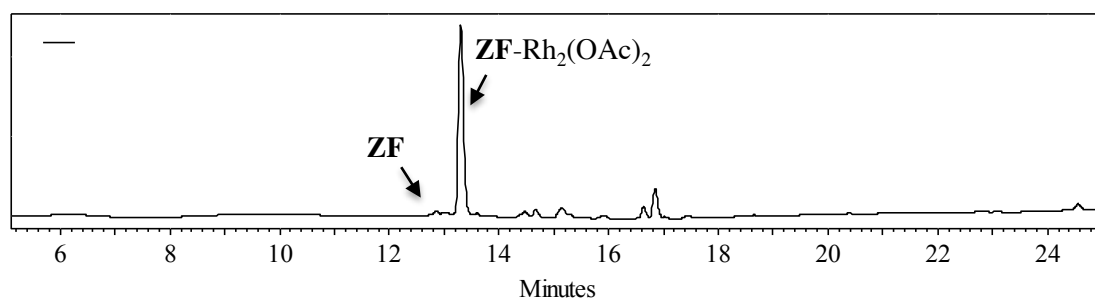


Figure 4-14. HPLC of crude metalation reaction demonstrating complete conversion of peptide **ZF** into metallopeptide **ZF-Rh₂(OAc)₂** (starting from a 1:1 ratio of peptide and precursor).

protection strategies to mask potentially reactive groups, I have discovered that developed method provides selective reactivity toward carboxylate side chains and enables access to a single dirhodium metallopeptide complex **ZF-Rh₂(OAc)₂** (Figure 4-13).

HPLC analysis indicates an efficient transformation with complete conversion of the peptide (Figure 4-14). The metallopeptide can be purified to homogeneity by RP-HPLC and isolated in 70% yield. Trifluoroacetic acid used in the HPLC purification does not affect the structure or function of the adduct. The method affords a remarkably efficient synthesis in the presence of numerous functional groups, including free amines and potential bridging ligands for dirhodium such as terminal carboxamide and guanidine groups.

Although at that point I had not yet attempted the metalation of peptides containing every natural amino acid side chain, I had tested the inclusion of models for His- and Met-containing peptides, two amino acids that show a high affinity for other transition metals. The metalation succeeds in the presence of 2 equiv of Ac-His-NHMe, allowing isolation of the same metallopeptide **ZF**-Rh₂(OAc)₂ in >50% yield. The desired metalation is observed in the presence of 2 equiv of Ac-Met-OMe as well, but in lower yield (ca. 40%), together with unidentified adducts.

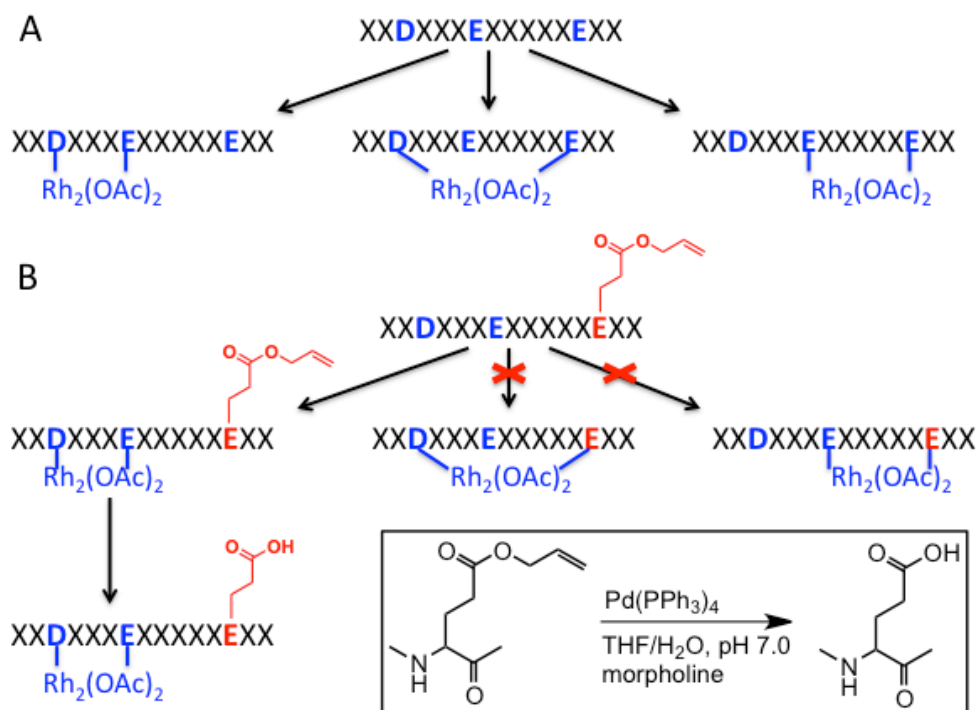
Noteworthy is the ease of macrocyclic ring formation. Bridging the dirhodium tetracarboxylate core with traditional ligands has proven challenging. Preparative yields of bridged structures have been largely limited to *m*-phenylene structures,^{3,8-11} and it has been reported that aliphatic α,ω -diacids give product mixtures and low yields of chelate products.¹² Here I demonstrate a dirhodium-bridged, 17-membered ring product that can be formed in very high yields.

4.4. Synthesis of metallopeptides with free carboxylates

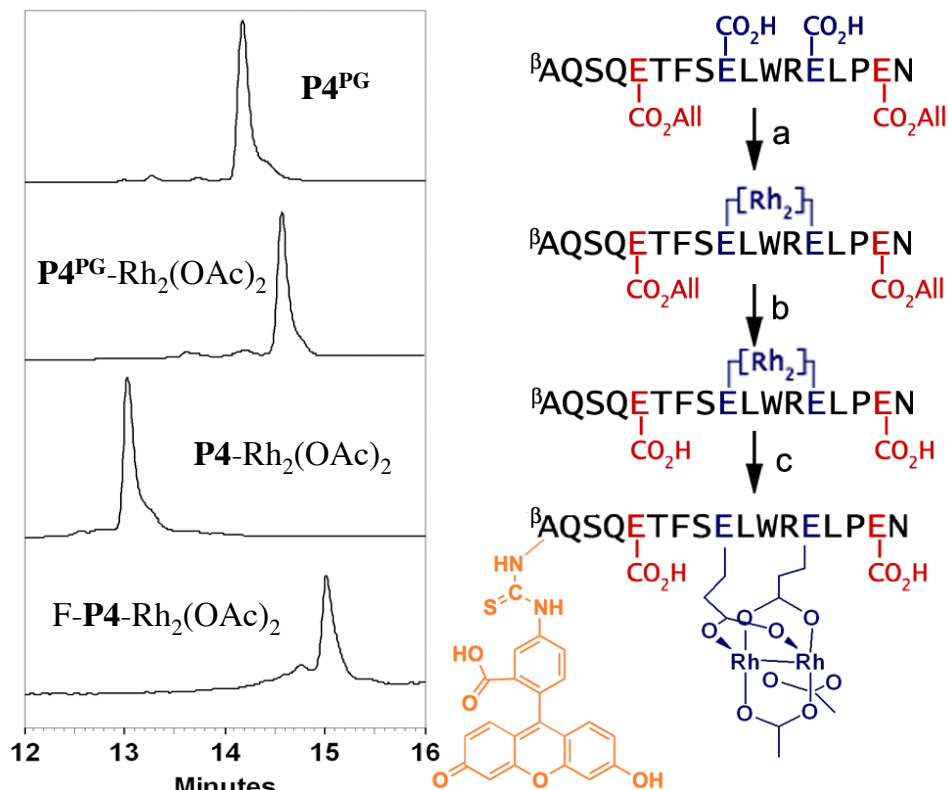
Dirhodium metalation at carboxylate side chains is a kinetic, irreversible, and largely non-selective process; multicarboxylate peptides yield isomeric mixtures of metalated products. As in a generalized example shown in Scheme 4-1, metalation with *bis*-trifluoroacetate precursor of a peptide containing three carboxylate side chains would yield a mixture of three major products. In some cases it is more expedient to separate the statistical mixture of metalated peptides. For example, treatment of the peptide Ac-VQDTRL-OH with 1 equiv Rh₂(OAc)₃(tfa) under developed metalation conditions (aq. buffer, pH 4.5, 50 °C) afforded a mixture of 49% side-chain metalation, 30% C-terminal metalation, and 21% bis-metalation.

These species could be separated by preparative HPLC, but more complex peptides with three or more carboxylates make the statistical approach unproductive, so a more general synthetic approach was needed.

The capability to preserve free carboxylates became important in designing dirhodium metalloptides as ligands for proteins. Carboxylate residues are often found to be highly conserved and crucial for binding in protein–protein interactions, as for example in the interaction between proteins with BH3 domain and Bcl-2 protein.¹³ The overall charge of the peptide also has an impact on its solubility, cellular uptake, and electrostatic interactions at the protein interface.^{14,15} I wanted to assess the importance of carboxylate-containing residues in the peptide derived from the helical domain of the p53 protein (Chapter 7).



Scheme 4-1. (A) Dirhodium metalation is non-selective process that results in formation of multiple products in case of polycarboxylate peptide (B) Orthogonal protection scheme via allyl ester and palladium-catalyzed deprotection.



Scheme 4-2. (right) Synthesis of fluorescein-labeled metallopeptide **F-P4-Rh₂(OAc)₂** and (left) HPLC traces of reaction products. Conditions: (a) *cis*-Rh₂(tfa)₂(OAc)₂, MES buffer (pH 4.5), 50 °C, 70% isolated yield. (b) 0.5 equiv Pd(PPh₃)₄, morpholine, THF/water, 53% isolated yield for in-situ deprotection (i.e. over two steps). (c) 1.5 equiv FITC, DIEA, DMSO. FITC = fluorescein isothiocyanate (yields not determined).

To accomplish that I turned to orthogonal carboxylate protection as an allyl ester.¹⁶ This approach provides a rare example of a transition-metal-catalyzed transformation on a transition-metal complex as substrate and avoids potential complications from dirhodium carboxylate instability under acidic, basic, or redox conditions. As shown in Scheme 4-2, metalation of peptide **P4^{PG}** was followed by palladium-catalyzed deprotection of the allyl esters. No interference from dirhodium and complete de-allylation were observed. In the last step, a fluorescein dye was attached to the N-terminal β-alanine to afford the final product **F-P4-Rh₂(OAc)₂**. Because fluorescein

contains a carboxylate group, it was necessary to delay fluorescent labeling to the end of the synthesis. This example also demonstrates ability of dirhodium metallopeptide to undergo multiple transformations without deterioration of metal complex.

4.5. Solution structure and stability of zinc-finger metallopeptide

To understand the effects of a bridging **ZF**-Rh₂(OAc)₂ center on peptide structure, the solution structure of the metallopeptide in water was examined, first by circular dichroism (Figure 4-15). The CD spectrum for peptide **ZF** displays a strong negative peak, diagnostic of a random coil conformation, at 200 nm. Upon binding to dirhodium, this feature disappears and a new negative feature was observed at 235 nm. These changes are consistent with the appearance of a turn element; similar spectra have been reported for short turn structures enforced with disulfide bond formation at similar (*i, i+3*) spacing.^{17,18}

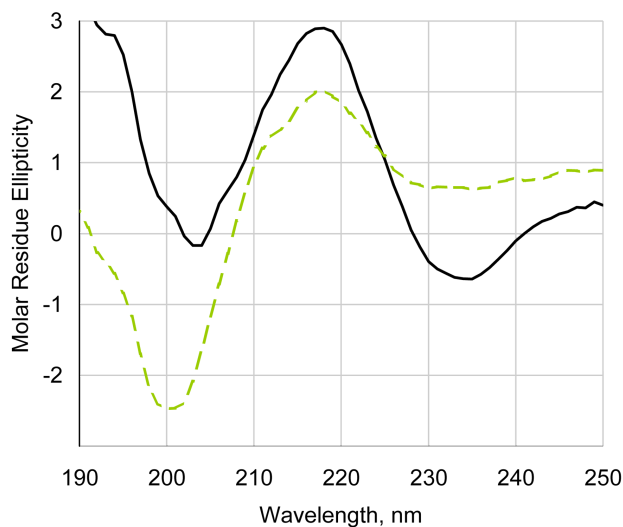


Figure 4-15. CD spectra (residual molar ellipticity in $\text{deg cm}^2 \text{dmol-res}^{-1} \times 10^3$) of the free peptide **ZF** (broken line) and metallopeptide **ZF**-Rh₂(OAc)₂ (solid line) at pH = 7 in water.

The structure in aqueous solution was further probed by NMR, employing COSY, NOESY, ROESY, HSQC-13C and HSQC-15N experiments. Distance, dihedral, and coupling restraints from 2D NMR experiments were used in simulated-annealing molecular dynamics calculations with CNS software (Figure 4-16).¹⁹ An overlay of 16 representative structures (Figure 4-16) indicates that the Phe2 to Gly8 region of **ZF**-Rh₂(OAc)₂ is well ordered in solution, while the C-terminal domain is best described as a random coil.²⁰ Comparison of the structure of **ZF**-Rh₂(OAc)₂ with that of the parent zinc-finger protein indicates that the turn domain, D4–D7, exhibits a similar backbone structure. However, the ligating Asp residues project into the opposite face of the turn structure compared to the zinc-finger structure, a change that alters the direction of both chains and greatly alters their orientation.

Table 4-1. Statistics for 16 representative solution structures of the **ZF**-Rh₂(OAc)₂ from molecular dynamics simulations.

restraining constraints		constraint violations	
total:	103	distance violations, >0.5 Å	0
distance, i=j	51	rms deviations	0.03
distance, i - j = 1	32	dihedral violations, >5°	1
distance, i - j > 1	10	rms deviations	3.35
dihedral	3	J coupling violations, >1 Hz	3.13
J coupling	7	rms deviations	0.98
constraints/ residue	9.4		
		rmsd for selection (Ala ³ -Gly ⁸ and dirhodium center):	
		backbone and rhodium atoms	0.27
		all heavy atoms	0.40

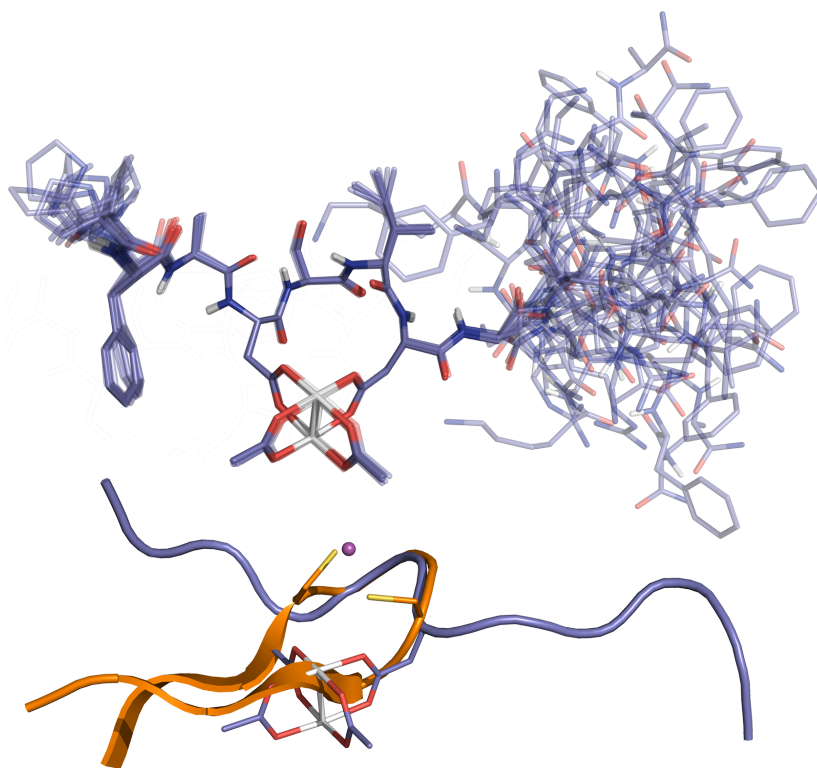


Figure 4-16. (top) Overlay of 16 representative conformations of **ZF**-Rh₂(OAc)₂ metallopeptide from simulated annealing molecular dynamics calculations based on NMR structural constraints and (bottom) overlay of one calculated conformation (blue) with that of the analogous zinc-finger sequence (orange).

The dirhodium metallopeptide was found to be stable to a variety of buffers and pH. Nevertheless I have observed slow decomposition of **ZF**-Rh₂(OAc)₂ in acetate buffer (pH 7) with clean formation of free peptide **ZF**. Further exploration has revealed that the dirhodium center can be cleaved from the peptide under relatively mild conditions (Figure 4-17): treatment of a solution of **ZF**-Rh₂(OAc)₂ with acetate buffer (0.1 M) at pH = 6 results in ligand substitution that produces the original peptide **ZF** and dirhodium tetraacetate complex Rh₂(OAc)₄. The release of dirhodium from the peptide is slow at room temperature, requiring days to reach completion. Mild heating (50 °C) allows this process to be complete within a few hours, and increased potassium acetate concentrations also accelerate the reaction. The

mild metalation and cleavage conditions allow cycling between bound and unbound states in a single pot. Thus, treatment of the peptide **ZF** with developed metalation conditions affords quantitative conversion of the peptide to the bridging dirhodium structure **ZF-Rh₂(OAc)₂**. Direct treatment of the reaction mixture with an acetate solution reverses this transformation, reforming the free peptide without significant by-products being observed.

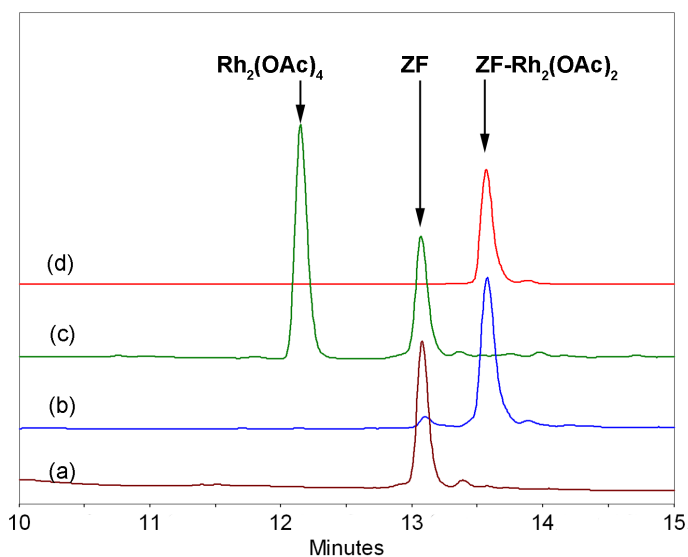


Figure 4-17. HPLC analysis of reversible dirhodium metalation of peptide **ZF**. (a) Peptide **ZF**. (b) Crude reaction of the complex $\text{Rh}_2(\text{tfa})_2(\text{OAc})_2$ with peptide **ZF** to form **ZF-Rh₂(OAc)₂**. (c) Direct treatment of the crude metalation reaction with KOAc, demonstrating reversibility of the complexation process through release of $\text{Rh}_2(\text{OAc})_4$ in a single reaction pot. (d) Metallopeptide **ZF-Rh₂(OAc)₂** after purification by RP-HPLC.

4.6. Conclusion

I present an efficient and reversible method of bridging distal carboxylate side chains with a dirhodium metal center. The method is compatible with aqueous, non-denaturing conditions and features chemistry that is orthogonal to other peptide cross-linking strategies. I demonstrate that dirhodium binding can be used to control the conformation of the bound peptide via formation of a macrocycle. Further investigations that utilize this

concept are described in the other chapters of this thesis and demonstrate control of peptide secondary structure and coiled coil heterodimerization. Peptide-dirhodium conjugates offer unique and modular control over the ligand environment around a dirhodium center. Thus dirhodium reactivity and selectivity might be controlled by appropriate polypeptide ligands. This essential development of dirhodium metallopeptide synthesis and initial tests of their catalytic activity have further led to application of peptides as ligands in dirhodium catalysis.

4.7. Experimental section

4.7.1. General information

Peptide synthesis. All peptides were synthesized with an Advanced ChemTech APEX 396 Automated Multipetide Synthesizer using standard solid-phase Fmoc protocols. The purification was accomplished by reverse-phase HPLC with gradients of water-acetonitrile containing 0.1% trifluoroacetic acid, and peptides were isolated by lyophilization. Analysis and purity assessment was attained by mass spectrometry and analytical HPLC. Peptides were prepared using Rink amide MBHA resin (AAPTEC) to afford the C-terminal amide and were acetylated at the N-terminus prior to cleavage from the resin.

Circular Dichroism Spectroscopy. CD spectra were obtained on Jasco-J810 spectropolarimeter using a 0.01 cm cell. The spectra were acquired with a 1 nm interval in the range of 180–250 nm. The temperature was maintained at 20 °C by Jacso PTC423S water bath. Peptide concentrations were 0.5 mM in buffer (50 mM PO₄, 100 mM KCl). The results were converted to mean residual ellipticity by the equation below:

$$[\theta] = \theta_{\text{obs}} / (10 \times l \times C \times N)$$

where θ_{obs} is the ellipticity in millidegrees of rotation, l is the optical path length of the cell in cm, C is the concentration of the peptide in mol/L, and N is the number of residues in the peptide.

HPLC analysis and purification. HPLC was performed on a Shimadzu CBM-20A instrument with Phenomenex Jupiter 4 μ Proteo 90A (250 \times 15 mm preparative) and Phenomenex Jupiter 4 μ Proteo 90A (250 \times 4.6 mm analytical) columns. Flow rates of 8 mL/min and 1 mL/min were used for preparative and analytical columns, respectively. Analytical and preparative HPLC were performed with gradient of acetonitrile in water. Both solvents contained 0.1% trifluoroacetic acid (TFA) unless otherwise noted. Two wavelengths — 220 nm and 300 nm — were used to allow for independent analysis of peptides and dirhodium complexes.

Mass Spectrometry. MALDI-MS and MS/MS analyses were performed on a Bruker Daltonics Autoflex MALDI- TOF/TOF mass spectrometer with CHCA matrix (10 mg/mL, Thermo Scientific Pierce). ESI-MS was performed on Bruker Daltonics micrOTOF instrument.

NMR Spectroscopy. 1D Spectra were measured with Bruker 500 UltraShield™ (500 MHz) spectrometer or Oxford (400 MHz) spectrometer. ^1H NMR are reported in units of part per million (ppm). Standard abbreviations are used to indicate signal multiplicity: s, singlet; d, doublet; t, triplet; q, quartet; m, multiplet. Coupling constants are reported as J value in Hertz (Hz). nH describes the number of protons (n) from integration. All 2D NMR spectra were acquired on 500 MHz Varian Inova NMR Spectrometer at 25°C. Samples were prepared in 90:10 H₂O/D₂O at 6 mM concentration and were buffered to pH 5.5 with sodium acetate-d₃. Mixing time used for NOESY was 400 ms and for ROESY, 200 ms. Acquisition times of 500 ms (ROESY) and 1000 ms (NOESY) were used in the direct dimension and 100

ms in the indirect dimension. 2D NMR data were processed with NMRPipe¹⁹ and analyzed using the Sparky program⁽²¹⁾ (Table 4-2).

4.7.2. Synthetic procedures

Synthesis of known compounds. The dirhodium complexes *cis*-Rh₂(tfa)₂(OAc)₂, Rh₂(OAc)₂(MeCN)₆•(BF₄)₂ and Rh₂(CO₃)₄ were prepared according the published procedures.^{2,5,6} Rh₂(tfa)₁(OAc)₃, Rh₂(tfa)₃(OAc)₁ and Rh₂(tfa)₄ was isolated as the byproducts of *cis*-Rh₂(tfa)₂(OAc)₂ synthesis.

Synthesis of N-acetyl-L-aspartyl-L-phenylalanine methyl ester (Amac). Aspartame (100 mg, 0.34 mmol, 1 equiv) was suspended in acetonitrile (1.15 mL) and pyridine (275 μ L, 3.4 mmol, 10 equiv) was added. Acetic anhydride (64 μ L, 0.68 mmol, 2 equiv) in acetonitrile (0.85 mL) was then added to a stirring mixture. After 5 minutes the solvent was removed by nitrogen stream and solid was dissolved in 5 mL of 0.5 M KHSO₄. The solution was extracted with 3 portions of EtOAc. The organic phase was dried with anhydrous Na₂SO₄ and solvent removed in vacuo. No purification was needed and product was isolated as white solid (87.8 mg, 77%). ¹H NMR (MeOD, 400MHz): 1.93 (s, 3H, CH₃-C(O)), 2.59 (dd, 1H, J=7.6 Hz, J=16.8 Hz, CH(H)-COOH), 2.77 (dd, 1H, J=6 Hz, J=16.8 Hz, CH(H)-COOH), 3.03 (dd, 1H, J=3.6 Hz, J=14 Hz, CH(H)-Ph), 3.13 (dd, 1H, J=5.6 Hz, J=14 Hz, CH(H)-Ph), 3.69 (s, 3H, COOCH₃), 4.65 (dd, 1H, J=3.6 Hz, J=5.6 Hz, CH(Phe)), 4.72 (dd, 1H, J=7.6 Hz, J=6 Hz, CH(Asp)), 7.17-7.29 (m, 5H, PhH).

Procedure for ligand exchange on Rh₂(OAc)₄ precursor in sealed vial. The dipeptide Amac (2.3 mg, 6 equiv) and Rh₂(OAc)₄ (0.5 mg, 1 equiv) were placed in a 4mL vial. The vial was tightly closed with a screw cap with PTFI/SIL septum. Atmosphere inside the vial was replaced with nitrogen

and a solvent (0.5 ml per 1 mg of rhodium acetate) was added. The cap wrapped by Teflon tape and reaction was heated at 100 °C for overnight. After mixture was cooled to rt, 1 mL of 50:50 water/MeCN solvent was added and filtered through 13 mm/ 0.2 µm syringe filter. Analysis and separation were done by HPLC (Figure 4-6) and products were analyzed by MALDI-MS.

Procedure for ligand exchange on $\text{Rh}_2(\text{OAc})_4$ precursor with Soxhlet extraction. The dipeptide Amac (40 mg, 12 eq), $\text{Rh}_2(\text{OAc})_4$ (5 mg, 1 equiv) and a stir bar were placed in two-necked round bottom flask. The Soxhlet extractor was filled with potassium carbonate-sand mixture and installed on the top of the flask. The second neck was tightly closed with a screw cap with PTFI/SIL septum. A condenser was mounted on the top of the extractor and all joint were tightly secured. Atmosphere inside the system was replaced with nitrogen and 5 mL of solvent (THF, dioxane or PhCl) was added. The assembly was connected to nitrogen line through the top of the condenser and was heated at 120-180 °C for 12-72 hours. Mixture was cooled to rt; the solvent was removed by a nitrogen jet; 1 mL of 50:50 water/MeCN solvent was added and solution was filtered through 13 mm/ 0.2 µm syringe filter. Analysis and separation were done by HPLC (Figure 4-7) and products were analyzed by MALDI-MS. Tetra-substituted product $\text{Rh}_2(\text{Amac})_4$ was isolated by lyophilization (12.2 mg, 70 %).

Procedure for ligand exchange reaction between phenylacetic acid and $\text{Rh}_2(\text{OAc})_2(\text{MeCN})_6 \cdot (\text{BF}_4)_2$ precursor. Sodium salt of phenylacetic acid (6.2 mg, 5 equiv), $\text{Rh}_2(\text{OAc})_2(\text{MeCN})_6 \cdot (\text{BF}_4)_2$ precursor (5.77 mg, 1 equiv) and a stir bar were placed in a 4 mL vial. Vial is sealed with a screw cap with PTFI/SIL septum and atmosphere inside the system was replaced with nitrogen. Methanol (0.5 mL) was added via syringe and reaction is

heated at 50 °C overnight. Analysis and separation were done by HPLC (Figure 4-8).

General procedure for ligand exchange with *cis*-Rh₂(tfa)₂(OAc)₂ precursor in organic solvents. Aspartame or Amac (3 equiv), *cis*-Rh₂(tfa)₂(OAc)₂ (1 equiv) and a stir bar were placed in the 4 mL vial. A solvent (1 mL per 3 mg of the precursor) was added. DIEA (10 equiv) was added and reaction stirred at rt overnight. Analysis and separation were done by HPLC and products were analyzed by MALDI-MS. Using this procedure Rh precursor (3 mg) was converted into Rh₂(Amac)₂(OAc)₂ product (4.1 mg, 75% yield) in THF as the solvent (Figure 4-9).

Procedure for ligand exchange with *cis*-Rh₂(tfa)₂(OAc)₂ precursor in aqueous solution. Amac (1.8 mg, 3 equiv), *cis*-Rh₂(tfa)₂(OAc)₂ (1 mg, 1 equiv) and a stir bar were placed in a 4 mL vial. The mixture was dissolved in water (0.33 mL) and pH adjusted to 5.1 with 0.1 M NaOH. The reaction was heated at 50 °C for 3 h and monitored by HPLC (Figure 4-10). (Note: initial screening conditions; for optimized conditions, refer to general procedure for synthesis of metallopeptides)

Procedure for ligand exchange with Rh₂(tfa)₁(OAc)₃ precursor in aqueous solution. Amac (2.0 mg, 3 equiv), Rh₂(tfa)₁(OAc)₃ (1 mg, 1 equiv) and a stir bar were placed in a 4 mL vial. MES buffer (0.33 mL) was added and pH adjusted to 4.4 with 0.1 M NaOH. The reaction was heated at 50 °C overnight and analyzed by HPLC (Figure 4-11).

Procedure for ligand exchange with a 1:1 mixture of Rh₂(tfa)₃(OAc)₁ and Rh₂(tfa)₄ precursors in aqueous solution. Amac (2.27 mg, ~5 equiv), precursors mixture (1 mg) and a stir bar were placed in a 4 mL vial. MES buffer (0.4 mL) was added and pH adjusted to 4.5 with

0.1 M NaOH. The reaction was heated at 50 °C overnight and analyzed by HPLC (Figure 4-12).

Synthesis of dirhodium-peptide complex ZF-Rh₂(OAc)₂. Peptide **ZF** (18.6 mg, 0.014 mmol, 1 eq), *cis*-Rh₂(tfa)₂(OAc)₂ (7.7 mg, 0.014 mmol, 1 eq), MES (108 mg, 0.56 mmol, 40 eq) and a stir bar were placed in a 4 mL vial. Water (2.6 mL) was added and pH adjusted to 4.5 with 0.1 M NaOH. The reaction was heated to 50 °C for 3 h and monitored by HPLC (Figure 4-19). The complex was purified by HPLC and was isolated in pure form upon lyophilization. Isolated product is a green solid (16.1 mg, 70 %).

In situ formation and cleavage of the dirhodium-peptide complex ZF-Rh₂(OAc)₂ (Figure 4-17). Peptide **ZF** (1.0 mg, 0.76 μmol), *cis*-Rh₂(tfa)₂(OAc)₂ (7.7 mg, 0.76 μmol), MES (5.9 mg, 0.15 mmol) and a stir bar were placed in a 4-mL vial. Water (0.3 mL) was added and the pH adjusted to 4.1 with NaOH (0.1M aq. solution). The reaction was heated to 50 °C for 2.5 h and monitored by HPLC. After complex formation was complete KOAc (59.0 mg, 0.60 mmol) was added as a solid. The reaction proceeded at 50 °C and was monitored by HPLC.

Synthesis of dirhodium metallopeptide P4^{PG}-Rh₂(OAc)₂. Peptide **P4^{PG}** (18.6 mg, 0.014 mmol, 1 eq), *cis*-Rh₂(tfa)₂(OAc)₂ (7.7 mg, 0.014 mmol, 1 eq), and a stir bar were placed in a 4 mL vial. MES buffer (0.1 M, pH 4.9) was added and the reaction was heated to 50 °C for 3 h. The complex was purified by HPLC and was isolated in pure form upon lyophilization. Isolated product is a green solid (16.1 mg, 70 %) (Figure 4-23).

General procedure for palladium deprotection. Allyl deprotection was performed directly on the crude metalation reaction (1 mM in MES buffer, pH 4.5). A solution of Pd(PPh₃)₄ (0.5 equiv) and morpholine (10

equiv) in THF (volume is equivalent to the volume of buffer solution in the preceding reaction, i.e. 50:50 THF/water final solution) were added to the crude metalation reaction and the pH was adjusted to 7.0 with KOH (0.1 M aq solution).²² The reaction was monitored by HPLC, reaching completion after 0.5–1.5 h. Metallopeptides were purified by RP-HPLC, isolated by lyophilization, and characterized by ESI-MS. Using this general procedure P4 peptide (1.80 mg) was converted to the unlabeled **P4**-Rh₂(OAc)₂ metallopeptide (1.06 mg, 53%) (Figure 4-21). (Note: deprotection can be performed on isolated metallopeptide as well)

4.7.3. NMR study and structure calculation.

Structure calculations were performed with the software program CNS using three-stage simulated annealing in cartesian molecular dynamics.¹⁹ We used 103 distance restraints, 3 dihedral restraints and 7 coupling restraints for the 12 residue peptide, for an average of 9.4 restraints per residue (Figure 4-16). Topology and parameter files for the dirhodium core were created based on the Cambridge Structural Database entry KABWOZ (dirhodium tetraacetate). To ensure that the topological constraints of ligation to the dirhodium core did not bias the computational sampling of structures consistent with our experimental NMR data, we treated the dirhodium diacetate, ligand and the peptide as initially distinct molecules, with a starting structure for our conformational search consisting of the fully extended peptide chain and the newly described DRA (dirhodium acetate) residue. The metal core was represented as dirhodium tetraacetate but with non-bonded interactions eliminated for the atoms of two cis acetates, and distance restraints were used to superimpose the CG, OD1, and OD2 atoms of Asp4 and Asp7 on the carboxylate carbons and

oxygens of the replaced acetate ligands. Simulated annealing was used to search for conformations that simultaneously satisfy the experimental NOE and dihedral restraints as well as the distance restraints that position the Asp carboxylates so that they ligate the dirhodium. The results of these searches did not change significantly when the force constants for distance restraints connecting the Asp side chains to the dirhodium core were varied. From 30 simulated annealing structures, 16 structures were accepted that had low overall energy, good bonded geometry, and no NOE violations larger than 0.5 Å. Atoms for the replaced acetates were deleted from the PDB files but can be regenerated by superimposing the coordinates of KABWOZ on the rhodium and acetate atoms.

4.7.4. Experimental data

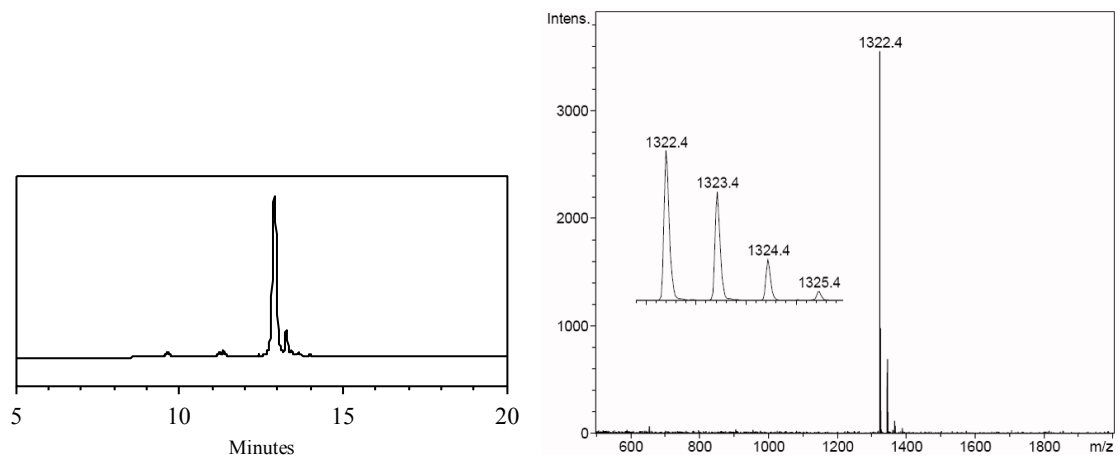


Figure 4-18. HPLC and MALDI-TOF MS of the peptide **ZF**. Calculated mass $[M+H]^+$: 1322.7; found: 1322.4.

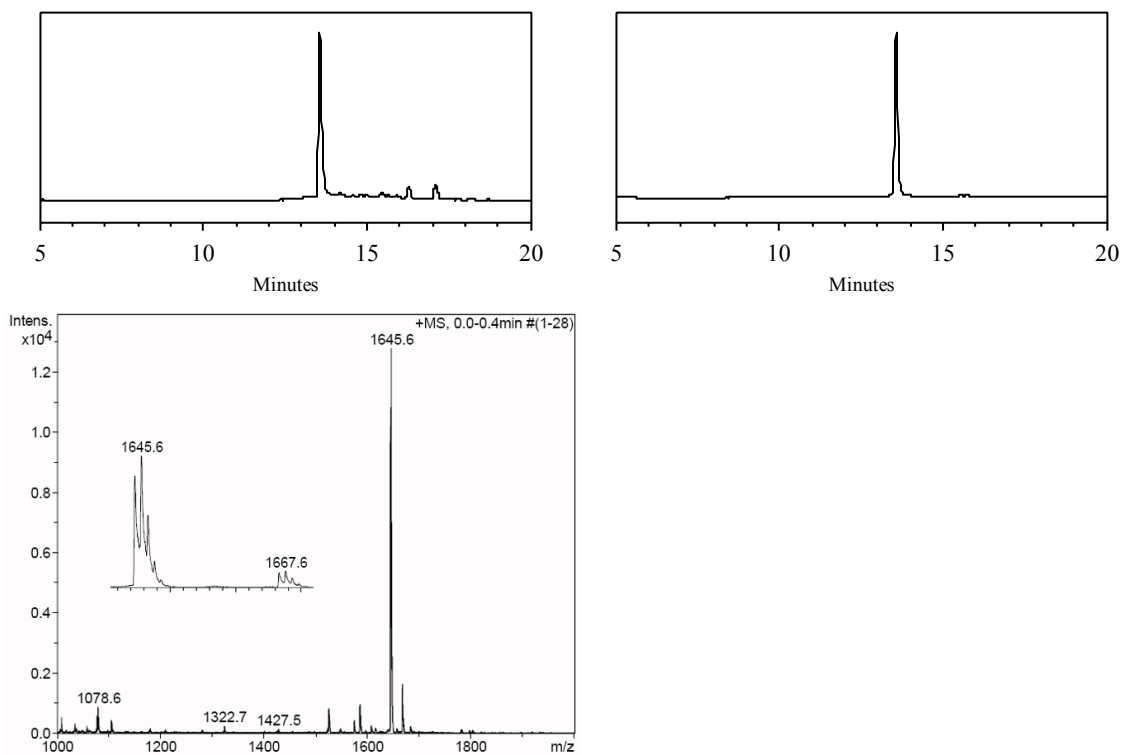


Figure 4-19. HPLC of the crude coupling reaction (left) and of the isolated complex **ZF-Rh₂(OAc)₂** (right) and ESI-MS of the isolated complex **ZF-Rh₂(OAc)₂**. Calculated mass $[M+H]^+$: 1644.6; found: 1644.6.

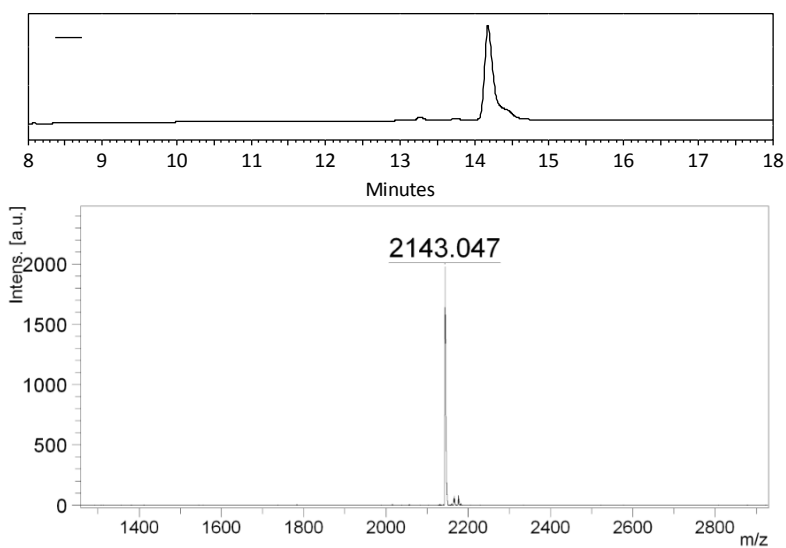


Figure 4-20. HPLC trace and MS data for isolated **P4^{PG}** peptide. Calculated mass $[M+H]^+$: 2143.0; found: 2143.0.

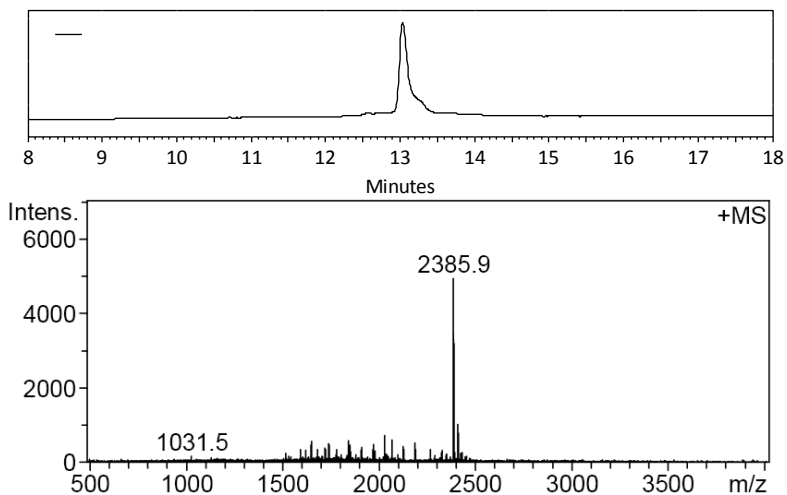


Figure 4-21. HPLC trace and MS data of purified metalloprotein **P4-Rh₂(OAc)₂**. Calculated mass [M+H]⁺: 2384.8; found: 2385.9.

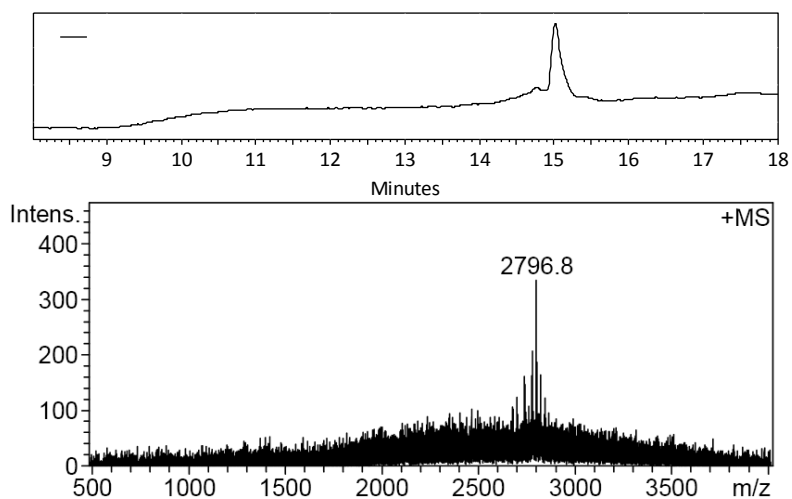
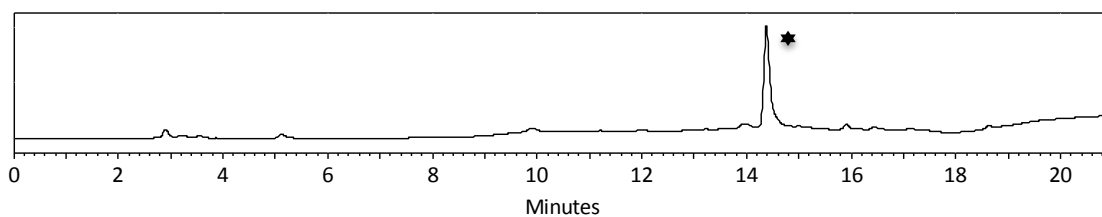


Figure 4-22. HPLC trace and MS data of purified fluorescein-labeled metalloprotein **F-P4-Rh₂(OAc)₂**. Calculated mass [M+Na]⁺: 2796.2; found: 2796.8.



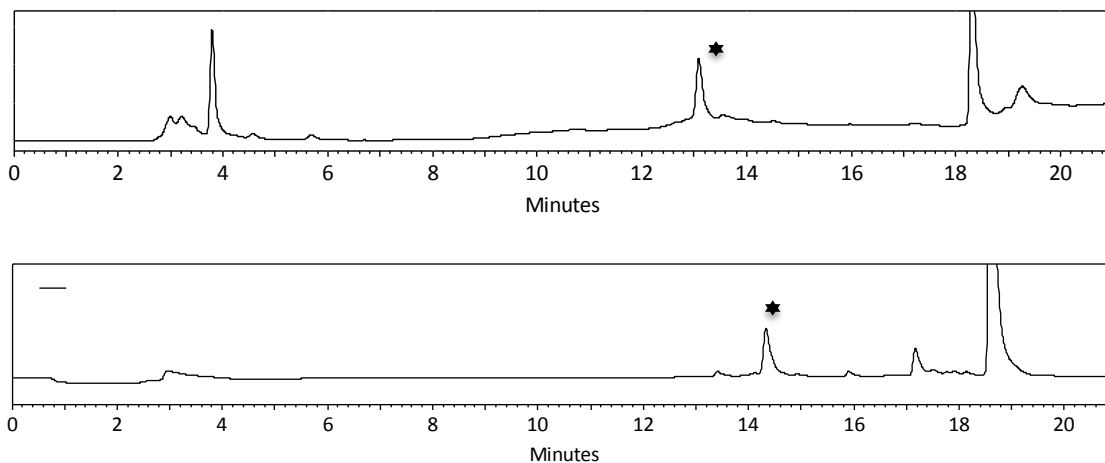


Figure 4-23. HPLC trace of crudes of metalation reaction (top), in-situ palladium deprotection (center) and fluorescein labeling with FITC (bottom) for **P4** metallopeptide synthesis.

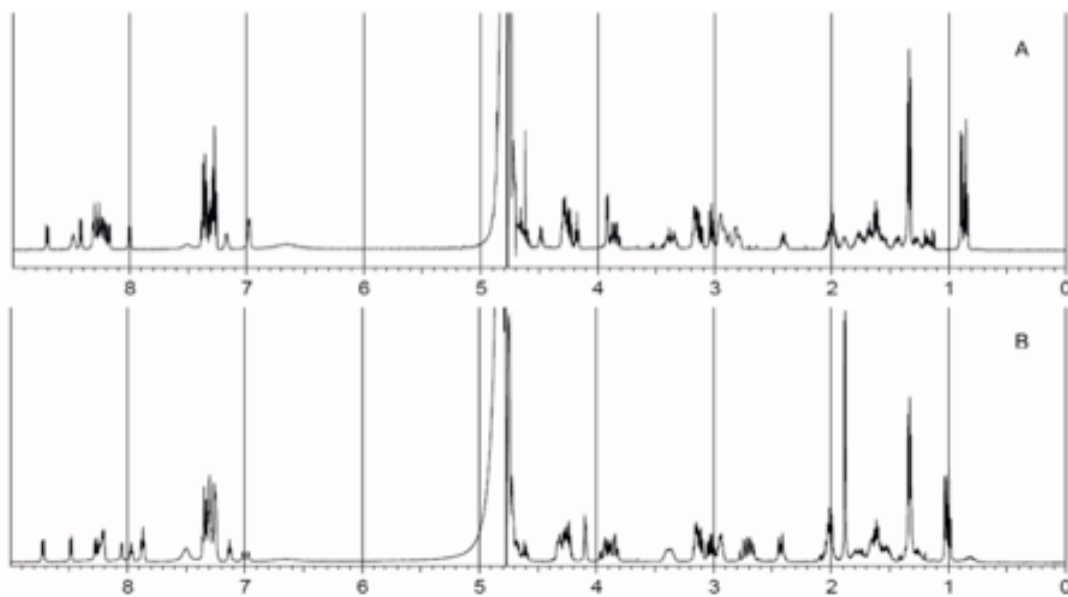


Figure 4-24. $^1\text{H-NMR}$ in 90:10 $\text{H}_2\text{O}/\text{D}_2\text{O}$ of peptides and their dirhodium complexes (A) peptide **ZF**, and (B) metallopeptide **ZF-Rh₂(OAc)₂**.

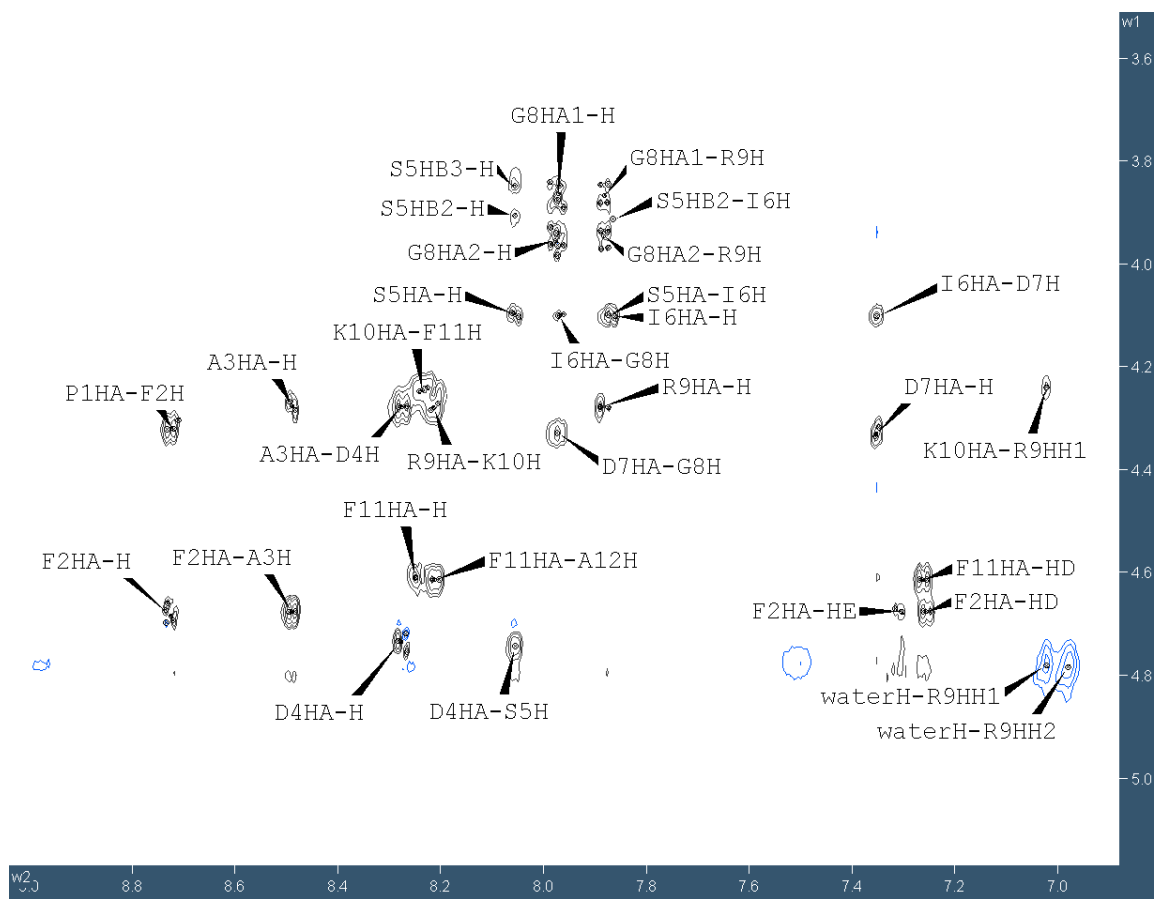


Figure 4-25. Representative region of the ROESY spectrum for **ZF-Rh₂(OAc)₂** metallopeptide.

Table 4-2. Chemical shifts of **ZF-Rh₂(OAc)₂** metallopeptide.

Residue	Atom name	Atom type	Shift (ppm)	Residue	Atom name	Atom type	Shift (ppm)
Pro1	HA	H	4.31	Ser5	HN	H	8.05
	HB2	H	2.42		HA	H	4.1
	HB3	H	2		HB2	H	3.91
	HG	H	2.01		HB3	H	3.84
	HD	H	3.37	CA	C	62.15	
	CA	C	62.42	CB	C	63.03	
	CB	C	32.57	Ile6	HN	H	7.87
	CE	C	49.48		HA	H	4.1
	CG	C	26.54		HB	H	2.03
Phe2	HN	H	8.73		HG1	H	1.03
	HA	H	4.67		HG21	H	1.34
	HB2 or HB3	H	3.04		HG22	H	1.52
	HB2 or HB3	H	3.12		HD	H	1
	HD	H	7.26		CA	C	60.58
	HE	H	7.31	CB	C	38.15	
	HH	H	7.3	CD	C	13.93	
	HZ	H	7.3	CG1	C	18.12	
	CA	C	62.42	CG2	C	28.09	
Ala3	CB	C	32.57	Asp7	HN	H	7.35
	HN	H	8.49		HA	H	4.32
	HA	H	4.27		HB2 or HB3	H	2.73
	HB	H	1.33		HB2 or HB3	H	2.69
	CA	C	52.73	CA	C	54.57	
Asp4	CB	C	18.91	CB	C	39.48	
	HN	H	8.27	Gly8	HN	H	7.97
HA	H	4.74	HA1		H	3.86	
Asp4	HB2	H	2.43		HA2	H	3.95
	HB3	H	2.69	CA	C	45.55	
	CB		40.02				

Continued on the next page

Continued

Residue	Atom name	Atom type	Shift (ppm)	Residue	Atom name	Atom type	Shift (ppm)	
Arg9	HN	H	7.88	Phe11	HN	H	8.24	
	HA	H	4.28		HA	H	4.61	
	HB2 or HB3	H	1.75		HB2 or HB3	H	3.02	
	HB2 or HB3	H	1.79		HB2 or HB3	H	3.15	
	HG	H	1.57		HD	H	7.26	
	HD	H	3.16		HE	H	7.31	
	HE	H	7.13		HH	H	7.3	
	HH1	H	7.02		HZ	H	7.3	
	HH2	H	6.98		CA	C	57.65	
	CA	C	56.26		CB	C	43.51	
	CB	C	30.8		Ala12	HN	H	8.21
	CG	C	27.05			HA	H	4.24
	Lys10	HN	H			8.21	HB	H
HA		H	4.24	CA	C	52.34		
HB		H	1.66	CB	C	19.57		
HG1		H	1.26	OAc1	H	H	1.88	
HG2		H	1.32		C	C	25.57	
HD		H	1.61	OAc2	H	H	1.89	
HE		H	2.94		C	C	25.57	
HZ		H	7.5					
CA		C	56.46					
CB		C	33.1					
CD		C	29.09					
CE		C	42.22					
CG		C	24.72					

4.8. References

- (1) Roos, G. H. P.; McKervey, M. A. *ChemInform* **1992**, *23*, 1751.
- (2) Wilson, C. R.; Taube, H. *Inorg. Chem.* **1975**, *14*, 405.
- (3) Gallagher, J. F.; Ferguson, G.; McAlees, A. J. *Acta Crystallogr. Sect. C* **1997**, *53*, 576.
- (4) Cotton, F. A.; Murillo, C. A.; Wang, X.; Yu, R. *Inorg. Chem.* **2004**, *43*, 8394.
- (5) Pimblett, G.; Garner, C. D.; Clegg, W. *J. Chem. Soc., Dalton Trans.* **1986**, 1257.
- (6) Lou, Y.; Remarchuk, T. P.; Corey, E. J. *J. Am. Chem. Soc.* **2005**, *127*, 14223.
- (7) Pavletich, N. P.; Pabo, C. O. *Science* **1991**, *252*, 809.
- (8) Taber, D. F.; Meagley, R. P.; Louey, J. P.; Rheingold, A. L. *Inorg. Chim. Acta* **1995**, *239*, 25.
- (9) Espino, C. G.; Fiori, K. W.; Kim, M.; Du Bois, J. *J. Am. Chem. Soc.* **2004**, *126*, 15378.
- (10) Davies, H. M. L.; Panaro, S. A. *Tetrahedron Lett.* **1999**, *40*, 5287.
- (11) Seitz, J.; Maas, G. *Chem. Comm.* **2002**, 338.
- (12) Bickley, J.; Bonar-Law, R.; McGrath, T.; Singh, N.; Steiner, A. *New J. Chem.* **2004**, *28*, 425.
- (13) Lessene, G.; Czabotar, P. E.; Colman, P. M. *Nat. Rev. Drug Discovery* **2008**, *7*, 989.
- (14) Wagstaff, K. M.; Jans, D. A. *Curr. Med. Chem.*, *13*, 1371.
- (15) Cserhati, T.; Szogyi, M. *Peptides* **1995**, *16*, 165.
- (16) Trzeciak, A.; Bannwarth, W. *Tetrahedron Lett.* **1992**, *33*, 4557.

- (17) Nguyen, M. T.; Beck, J.; Lue, H.; Fünfzig, H.; Kleemann, R.; Koolwijk, P.; Kapurniotu, A.; Bernhagen, J. *J. Biol. Chem.* **2003**, *278*, 33654.
- (18) Brahms, S.; Brahms, J. *J. Mol. Biol.* **1980**, *138*, 149.
- (19) Brunger, A. T.; Adams, P. D.; Clore, G. M.; DeLano, W. L.; Gros, P.; Grosse-Kunstleve, R. W.; Jiang, J.-S.; Kuszewski, J.; Nilges, M.; Pannu, N. S.; Read, R. J.; Rice, L. M.; Simonson, T.; Warren, G. L. *Acta Crystallogr. Sect. D* **1998**, *54*, 905.
- (20) (BMRB entry 20084)
- (21) Goddard, T. D. and D. G. Kneller SPARKY 3, University of California, San Francisco.
- (22) Ohmori, K.; Ogawa, Y.; Obitsu, T.; Ishikawa, Y.; Nishiyama, S.; Yamamura, S. *Angew. Chem. Int. Ed.* **2000**, *39*, 2290.

Chapter 5

Dirhodium based control of peptide folding and assembly

5.1. Introduction

Peptide secondary structure drives molecular functions such as binding to target proteins and aggregation into defined supramolecular materials. As such, there is a long-standing interest in chemistries that control secondary structure in a well-defined manner. One powerful way to affect polypeptide structure is through methods that link, or bridge, two amino-acid side chains to form a cyclic product. Metal ions serve structural roles in metalloproteins, where side chains act as ligands, which are bridged by a metal ion. Taking a cue from these biological examples, the effects of metal binding on peptide structures is an active area of study.¹⁻⁹ Peptide-metal interactions have been used to understand metalloprotein folding and energetics and to shed light on potential toxicity pathways.^{10,11} Many transition metals can bind to peptides in aqueous solution, most commonly through cysteine or histidine residues.¹²⁻¹⁸

In this chapter, I describe the utility of dirhodium to control peptide structure by bridging two carboxylate residues. In the first part, reversible dirhodium metalation is evaluated as an approach to control assembly of a coiled-coil structure and in the second part, bridging metalation is utilized as a technique to stabilize or induce peptide helical conformation.

I sought to establish if reversible dirhodium binding could be used to control the supramolecular association and ordering of multiple peptides. Coiled coils are peptide assemblies that play key roles in biological processes, such as signal transduction. Altering these interactions allows elucidation of important pathways and also forms the basis for new therapeutic strategies. These studies were focused on the model E3/K3 heterodimeric coiled-coil system (Figure 5-1), initially reported by Hodges¹⁹ and widely utilized by others.²⁰⁻²³ Based on naturally occurring coiled-coil protein domains, coiled-coil systems feature a heptad repeat (denoted *abcdefg*) in which hydrophobic residues at positions *a* and *d* are situated along one side of an α -helix structure, providing a driving force for peptide dimerization through the hydrophobic effect.²⁴ A heterodimeric coiled coil can be achieved through additional interactions.²⁵ In the E3/K3 system, charged residues flanking the hydrophobic interface (positions *g* and *e*) create salt bridges stabilizing the heterodimer assembly. Thus, the

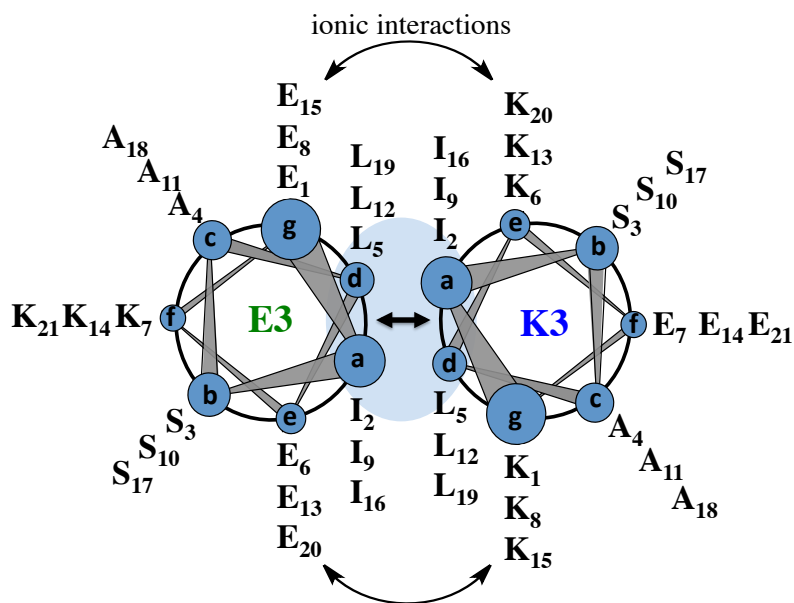


Figure 5-1. E3/K3 heterodimeric coiled coil (ISAL series) developed by Hodges.¹⁹

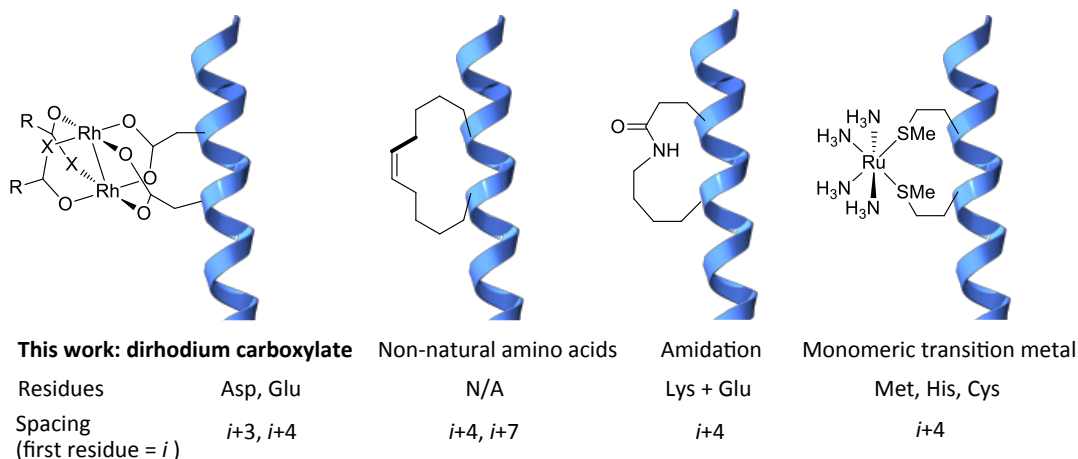
polycationic K3 dimerizes in the presence of the polyanionic E3, while charge-charge repulsion prevents homodimerization. Finally, the peptides E3 and K3 adopt α -helical conformations only when present as dimeric coiled-coils. Otherwise, they exist as random coils.

At the same time, I became interested in using dirhodium centers as ligands for carboxylate side chains to stabilize helical structure. Helix stabilization is an established method to improve or re-establish the binding affinity of peptides and hence, to improve the biological function.²⁶ To achieve structure stabilization, a variety of methods have been explored by others.²⁷⁻³⁰ Non-natural amino acids have been employed in covalently-bridging distal amino acids to favor helix formation.³¹ Covalent modifications by ring-closing metathesis³²⁻³⁴ and 1,3-dipolar cycloaddition³⁵ have enabled the creation of helical structures in short peptide sequences. Wholly non-natural peptide mimics, such as β peptides and aryl-based oligomers, have also been shown to achieve improved helicity.³⁶⁻⁴⁴ Although progress has been made in this area, the requirement for non-natural amino acids represents a considerable drawback. Control of peptide secondary structure with organic reagents through selective bioconjugation methodologies also remains limited.⁴⁵⁻⁵⁵ Alternatively, metal-polypeptide interactions are a long-standing area of study that enables the control of structure and function in metallopeptide complexes.^{2-6,9,56-60}

A new strategy employing a dirhodium linker could address a number of limitations of current methods.^{61,62} First, carboxylate side chains are largely unexplored as sites for selective reactivity or metal binding.⁶²⁻⁶⁷ Well-defined metal binding to natural polypeptides in water typically has been confined to histidine, cysteine, and methionine residues that contain “soft” ligands for monomeric metal centers (see Scheme 5-1).^{56,57,68-74}

Whereas selective binding of carboxylate residues in a fully deprotected peptide remains a challenge, dirhodium is well suited for carboxylate metalation, in part because carboxylates coordinate through a κ^2 orientation that bridges the Rh–Rh bond and engenders increased stability against ligand substitution.

Second, previous studies of metal-mediated helix induction typically examine peptides under controlled conditions. Metallopeptides with non-biological metal centers ligated by natural amino acid side chains that are stable in the presence of diverse biomolecules are rare,^{75,76} and the toxicity of metallopeptides is largely unexplored. Third, the extent of helical stabilization in metallopeptides is limited or difficult to predict, and the structural requirements for efficient helix induction are not fully understood. For example, simple hydrocarbon tethers have been successfully used to induce helicity,³⁴ but tethered peptides do not necessarily show significant increases in helicity—the impact of tether length, tether structure, and peptide sequence on the extent of increased helicity is not clear. Computational progress toward a predictive model for helical induction for hydrocarbon tethers has recently been reported.⁷⁷



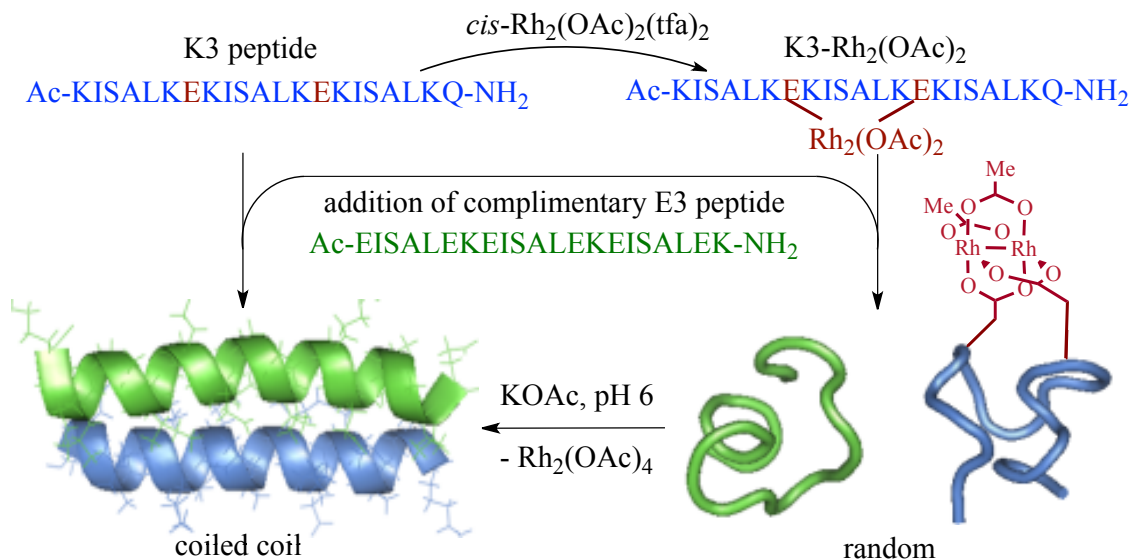
Scheme 5-1. Strategies to stabilize or induce α -helical secondary structure in peptides.

5.2. Control of coiled coil heterodimerization

Based on the previous reports, I synthesized **E3** and **K3** peptides identical to those of Hodges except for an isostructural C-terminal modification of **K3** (E21Q) to remove the third glutamate residue to simplify product analysis. According to the theory of coiled-coil peptides, this modification should not affect interstrand interactions. Metalation of **K3** peptide affords **K3-Rh₂(OAc)₂**, which can be analyzed by mass spectrometry and purified to homogeneity by HPLC. The dirhodium efficiently bridges carboxylates to afford a cyclic product with 30 atoms in the ring.

As anticipated, **E3**, **K3**, and **K3-Rh₂(OAc)₂** all exist as random coils when examined separately in aqueous solution, as evidenced by their CD spectra (Figure 5-2). Consistent with previous work, a 1:1 mixture of the peptides **E3** and **K3** dimerize to give a coiled-coil structure (Scheme 5-2 and Figure 5-3).¹⁹ The **K3** peptide has two Glu residues with *i, i+7* spacing. In an α -helix, Glu side chains are not long enough to span the *i, i+7* spacing (Scheme 5-2), so that dirhodium adduct **K3-Rh₂(OAc)₂** should not be capable of achieving an α -helical structure. In line with my hypothesis, mixtures of **E3** and **K3-Rh₂(OAc)₂** display no evidence of coiled-coil structure (Figure 5-2), remaining as random coils even in the presence of the complementary peptide. Thus, dirhodium bridging allows us to prevent the folding and binding of the complementary peptide **E3** as well. Dirhodium binding is readily reversible in this case as well; treatment of the mixture of **E3** and **K3-Rh₂(OAc)₂** with potassium acetate at pH 6 allows facile removal of the dirhodium center. CD analysis indicates that the coiled-coil secondary structure is reestablished upon dirhodium cleavage (Figure 5-3). The full magnitude of the ellipticity at 222 nm for the coiled-coil structure is restored

upon dirhodium cleavage, indicating the high yield and lack of side reactions in the cleavage step.



Scheme 5-2. Reversible control of coiled-coil heterodimerization.

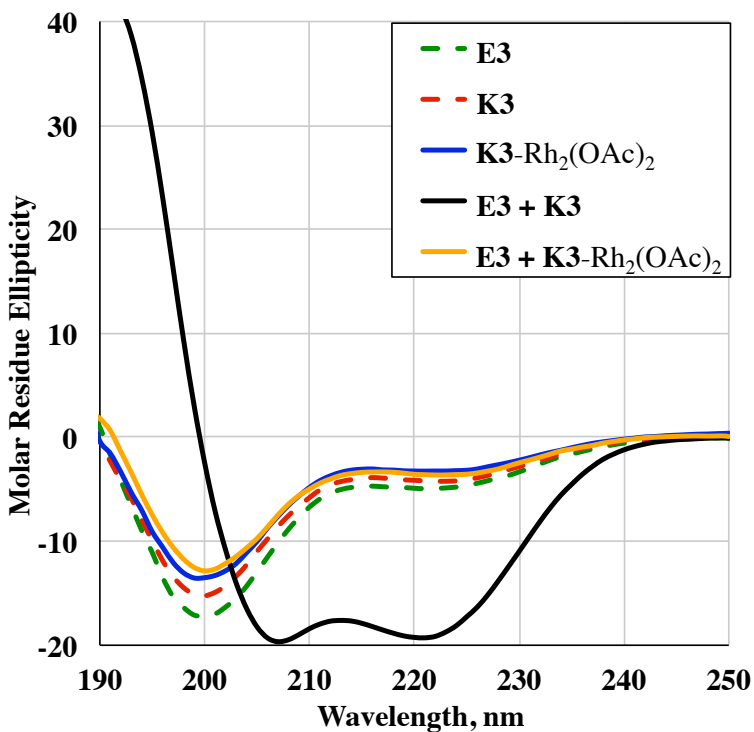


Figure 5-2. CD spectra of peptide coiled coil systems. Residual molar ellipticity in deg cm² dmol-res⁻¹ × 10³. All spectra taken in water at 20 °C and pH 6.

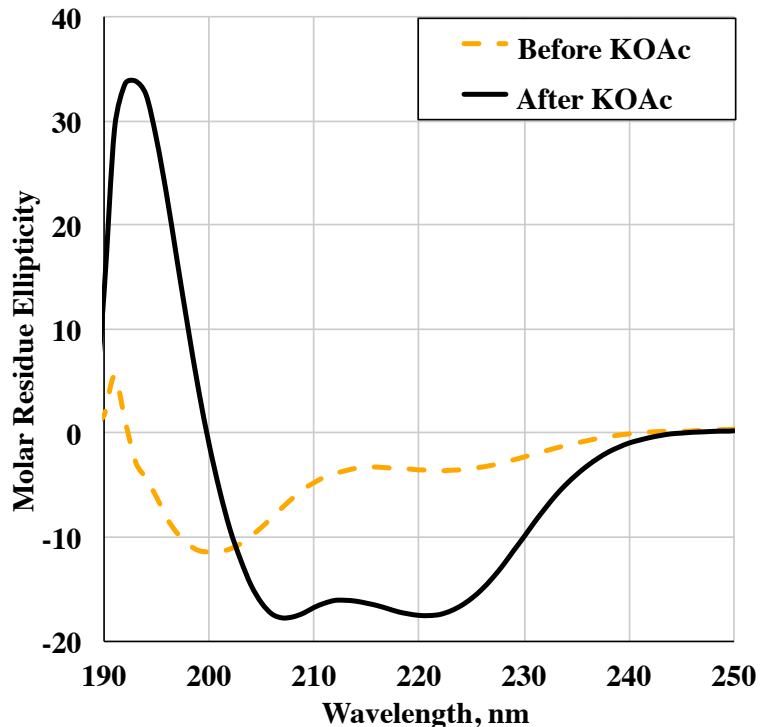


Figure 5-3. Cleavage of the dirhodium-peptide adduct re-establishes coiled-coil structure. Spectra given for a mixture of E3 and K3-Rh₂(OAc)₂ at pH 6 before and after treatment with 0.2 M KOAc for 90 h at 40 °C. (Residual molar ellipticity in deg cm² dmol-res⁻¹ × 10³. All spectra taken in water at 20 °C and pH 6.)

5.3. Stabilization of helical conformation with dirhodium linker

To probe ability of dirhodium to form metallopeptides that retain helical conformation, a series of peptides were designed. They are 18 amino acids in length and have helical propensity due to an alanine-rich sequence (Table 5-1).⁷⁸ A complete turn of an α helix requires between three and four amino acids, so carboxylate side chains (Asp, Glu) were placed in i , $i+3$ or i , $i+4$ relationships. Bridging amino acids in an i , $i+4$ arrangement has been studied extensively for helix stabilization as well as a some examples of helix stabilization by means of an i , $i+3$ arrangement.⁷⁹ As expected, all free peptides exhibit some degree of helicity in water (Figure 5-4). Owing to the helix-disrupting properties of Asp residues, peptides containing this amino

acid exhibit substantially less helicity than comparable Glu-containing sequences (see, Figure 5-4, A).⁸⁰

The peptides react with *cis*-Rh₂(OAc)₂(tfa)₂ to produce adducts with bridging dirhodium centers for both *i, i+3* and *i, i+4* carboxylate spacing (Scheme 5-3). Circular dichroism (CD) spectroscopy was employed to assess the effect of dirhodium binding on helicity. In the *i, i+4* series, both Asp (**DD4**) and Glu (**EE4**) peptides exhibit increased helicity on dirhodium binding (Figure 5-4 (A) and Figure 5-5). The effect of binding is most pronounced in the Asp case; the helix-destabilizing influence of hydrogen bonding from the carboxylate side chain to the amide backbone is removed upon binding dirhodium.⁸⁰ Next, I considered peptides with *i, i+3* carboxylate spacing. The free peptide **EE3** is helical in solution, and binding to a dirhodium center results in increased helical content, in line with *i, i+4* examples discussed above (Figure 5-4, D). However, the structural requirements for helix stabilization in *i, i+3* peptides are clearly stricter than those for the *i, i+4* case: all sequences with at least one Asp residue binding to dirhodium (peptides **DD3**, **ED3**, and **DE3**) display complete disruption of helicity upon binding to dirhodium (Figure 5-4, B). The data suggest that the extra methylene unit in the Glu side chain is necessary to allow proper positioning at a dirhodium center. Although residues at *i, i+3* spacing are proximal in space in a helical structure, the side chains project in different directions and there is no previous examples of helix induction or stabilization through metal binding in an *i, i+3* fashion.

Table 5-1. Helicity of free peptides and dirhodium metallopeptide complexes.

<i>Peptides</i>	<i>Sequence</i>	$[\Theta]_{220}^a$	f_H^b	$f_{H(TFE)}^c$	<i>Rel. Hel^d, %</i>	<i>Yield, %</i>
EE3	Ac-YGKAAAAEAAEKAAAAK-NH ₂	-11.49	39	44	70	
EE3-Rh₂(OAc)₂		-13.8	45	51	82	70
EE3-Rh₂(pyrr)₂-A		-12.55	42	47	76	50
EE3-Rh₂(pyrr)₂-B		-10.42	36	40	65	29
(EE3)₂Rh₂-A		-7.71	26	31	51	25
(EE3)₂Rh₂-B		-7.55	25	31	50	25
DD3	Ac-YGKAAAADAADAKAAAAK-NH ₂	-5.3	21	24	39	
DD3-Rh₂(OAc)₂		-1.47	10	12	19	80
DE3	Ac-YGKAAAADAEEKAAAAK-NH ₂	-7.97	29	32	52	
DE3-Rh₂(OAc)₂		-0.89	11	10	16	67
ED3	Ac-YGKAAAAEAADAKAAAAK-NH ₂	-11.4	38	43	70	
ED3-Rh₂(OAc)₂		-1.69	11	12	20	59
EE3G	Ac-YGKAAAAEAGEAKAAAAK-NH ₂	-2.46	13	15	24	
EE3G-Rh₂(OAc)₂		-9.62	33	38	61	80
EE4	Ac-YGKAAAAEAAEKAAAAK-NH ₂	-12.34	41	46	75	
EE4-Rh₂(OAc)₂		-17.26	55	62	100	65
<i>trans-EE4-</i>		0.3	5	6	10	19
(EE4)₂Rh₂-A		-9.81	31	38	62	30
(EE4)₂Rh₂-B		-10.97	34	42	68	24
sEE4	Ac-KAEAAAEAK-NH ₂	-0.38	9	8	13	
sEE4-Rh₂(OAc)₂		-11.64	48	44	71	58
DD4	Ac-YGKAAAADAAADKAAAAK-NH ₂	-5.72	22	25	41	
DD4-Rh₂(OAc)₂		-16.01	51	58	94	73
EE4G	Ac-YGKAAAAEAGAEEKAAAAK-NH ₂	-1.88	12	13	21	
EE4G-Rh₂(OAc)₂		-8.34	30	34	54	73
<i>trans-EE4G-</i>		0.47	5	6	9	65
ED4G	Ac-YGKAAAAEAGADKAAAAK-NH ₂	-1.08	9	10	17	
ED4G-Rh₂(OAc)₂		-12.14	40	46	74	57
DD4G	Ac-YGKAAAADAGADKAAAAK-NH ₂	-1.12	9	11	17	
DD4G-Rh₂(OAc)₂		-10.8	37	41	67	70

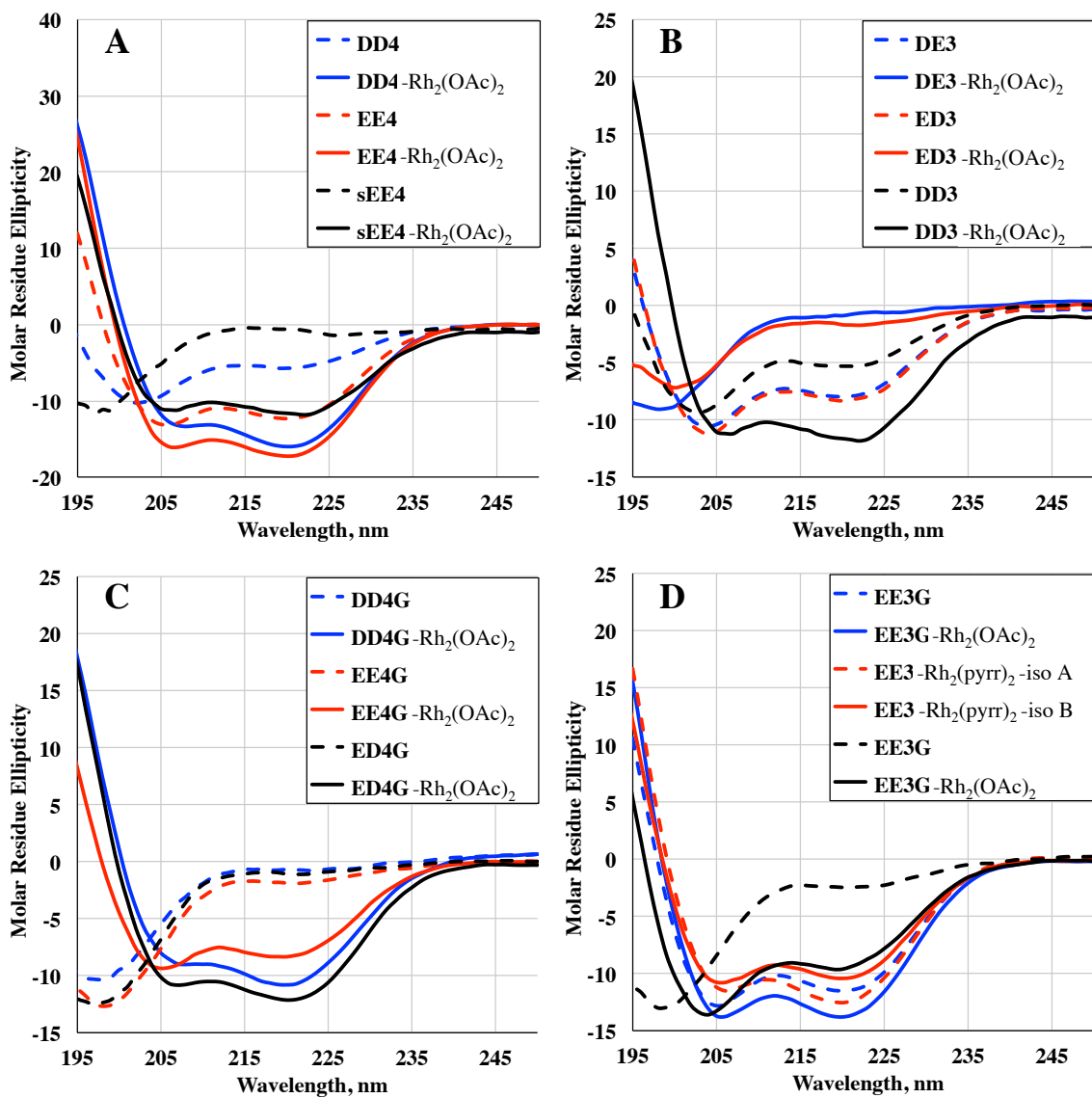


Figure 5-4. Circular dichroism spectra demonstrating the effect of dirhodium binding on the secondary structure of *bis*-carboxylate peptides. For sequences, see Table 5-1.

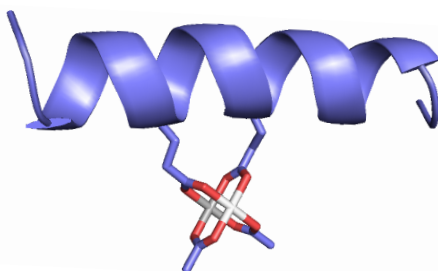
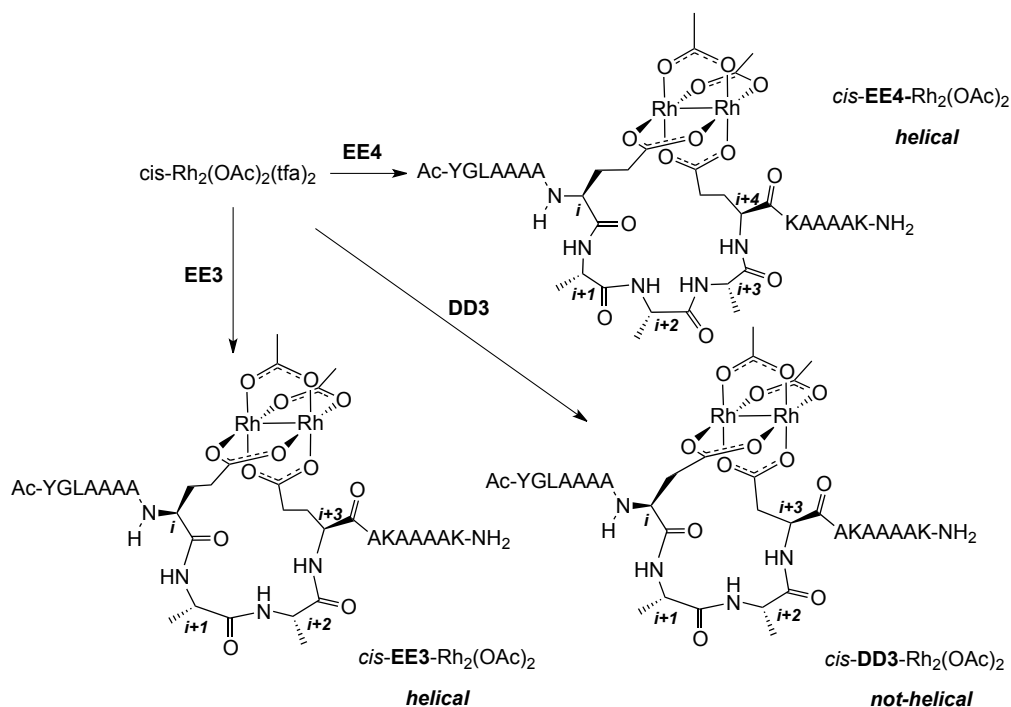


Figure 5-5. A model structure of the **EE4**-Rh₂(OAc)₂ metallopeptide (structure is generated in PyMOL).



Scheme 5-3. Dirhodium metallopeptides with i , $i+4$ (**EE4**) and i , $i+3$ (**EE3** and **DD3**) residue spacing.

5.4. Induction of helical conformation with dirhodium linker

Producing secondary structure upon metal binding in otherwise unstructured peptides potentially allows metal-based switching of molecular function. The polyalanine sequences discussed above contain at least some helical bias in the unbound state, and upon dirhodium binding appear more strongly helical. Inducing helicity in unstructured peptides is a more stringent test, and to probe helix induction in otherwise random-coil peptides, I introduced glycine—a powerful helix disrupting residue—into my peptide sequences at the $i+2$ position.⁸¹ All of the glycine-containing peptides exhibit a random-coil structure in aqueous solution. CD analysis of the metallopeptide adducts, however, indicates a helical structure (Figure 5-4, C). For peptides with i , $i+4$ spacing, as before, good helix induction was observed regardless of whether the binding residues are Asp or Glu. A

glycine-containing peptide with $i, i+3$ carboxylate spacing (**EE3G**) was also prepared. The peptide **EE3G** is a random coil in the unbound state but becomes helical following metalation by dirhodium, as evidenced by the appearance of a negative feature at $\lambda = 220$ nm (Figure 5-4, D). This result extends the possibilities for metal-induced helicity beyond the $i, i+4$ systems reported with other metals to Glu-Xaa-Xaa-Glu sequences. The assignment of helical structure to the adduct **EE3G**-Rh₂(OAc)₂ is further supported by NMR spectroscopy experiments. Due to the repetitive nature of these sequences, unambiguous assignment of peaks was not possible at the periphery of the **EE3G** sequence (Y1–A5 and K13–K18). Nonetheless, peaks in the key dirhodium-binding region were readily identified through COSY experiments. Within the dirhodium-binding region (A6–A12), the ³J_{HN}–Ha coupling constants are all less than 6 Hz, consistent with a helical structure. In addition, unambiguous long-range α N $i, i+3$ NOEs were observed, together with short-range $i, i+1$ interactions (α N and NN) to residues in proximity to dirhodium-bound glutamates (Figure 5-6).⁸²

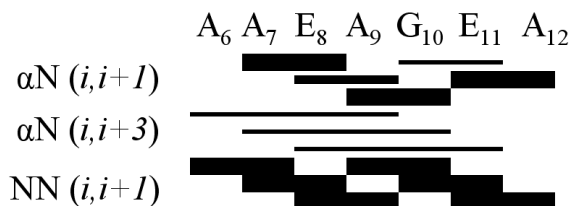
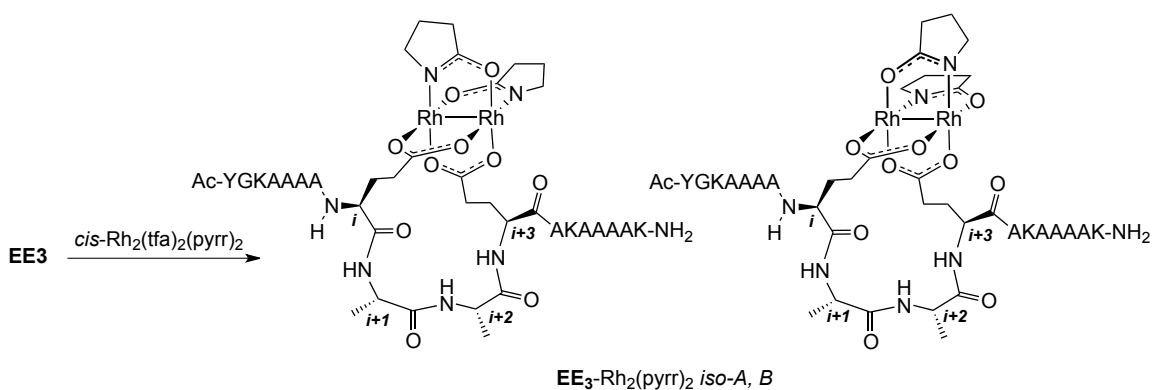


Figure 5-6. ³J_{HN-HA} coupling constants and NOE connectivity for the metal-binding region of the **EE3G**-Rh₂(OAc)₂ complex. The NOE intensity is represented by the thickness of the bars.

The ability of dirhodium complexes to induce peptide helicity has proven to be quite general. For example, a significantly shorter peptide, KAEAAEAK (**sEE4**), which is too short to exist with defined secondary structure in the free state, adopts a helical structure upon dirhodium binding

(see Table 5-1, entry 21 and 22 and Figure 5-4). In addition, variation of the dirhodium-reagent structure is tolerated both in the synthesis and in the secondary structure of metallopeptides. For example, the *bis*-amidate complex $\text{cis-Rh}_2(\text{tfa})_2(\text{pyrr})_2$ (pyrr = pyrrolidonate) reacts cleanly with the peptide **EE3** to afford the *bis*-carboxylate, *bis*-amidate product as two stereoisomers, which are separable by preparative HPLC (Scheme 5-4). Both isomers display helicity similar to the corresponding *bis*-acetate complex (Figure 5-4, D).



Scheme 5-4. Synthesis of a peptide–dirhodium complex with amidate ligands. The identity of the product stereoisomers has not been assigned.

5.5. *Bis*-peptide and *trans*-complexes with dirhodium

In addition to 1:1 dirhodium:helix adducts, I was able to produce adducts with 1:2 dirhodium:peptide stoichiometry with the reagent $\text{Rh}_2(\text{tfa})_4$ ⁸³. Treatment of peptide **EE4** with $\text{Rh}_2(\text{tfa})_4$ results in the formation of a $\text{Rh}_2(\text{EE4})_2$ adduct. The CD spectrum indicates helical structure for the dipeptide adduct as well, which identifies the adduct stereochemistry as that in which each peptide chelates to the dirhodium center in a *cis* geometry (Figure 5-7). The observation of *cis* binding is opposite that which might be predicted on the basis of the *trans* ligand effect: dirhodium complexes of the type $\text{Rh}_2(\text{RCO}_2)(\text{tfa})_3$ are known to react in ligand exchange processes to

give the *trans bis-tfa* product.⁸⁴ Labilization of the *trans*-trifluoroacetate ligand should form the *trans* product, rather than the observed *cis*. Potential explanations for this observation include fast intermolecular ligations relative to intramolecular *trans* chelate formation, *cis-trans* isomerization of an intermediate *trans*-complex, associative displacement of a *cis*-trifluoroacetate ligand by the second chelating-carboxylate ligand, and trifluoroacetate displacement due to a competing *cis*-ligand effect via a dissociative interchange (I_d) mechanism.⁸⁵ Further mechanistic investigations will be necessary to identify the origin of this result.

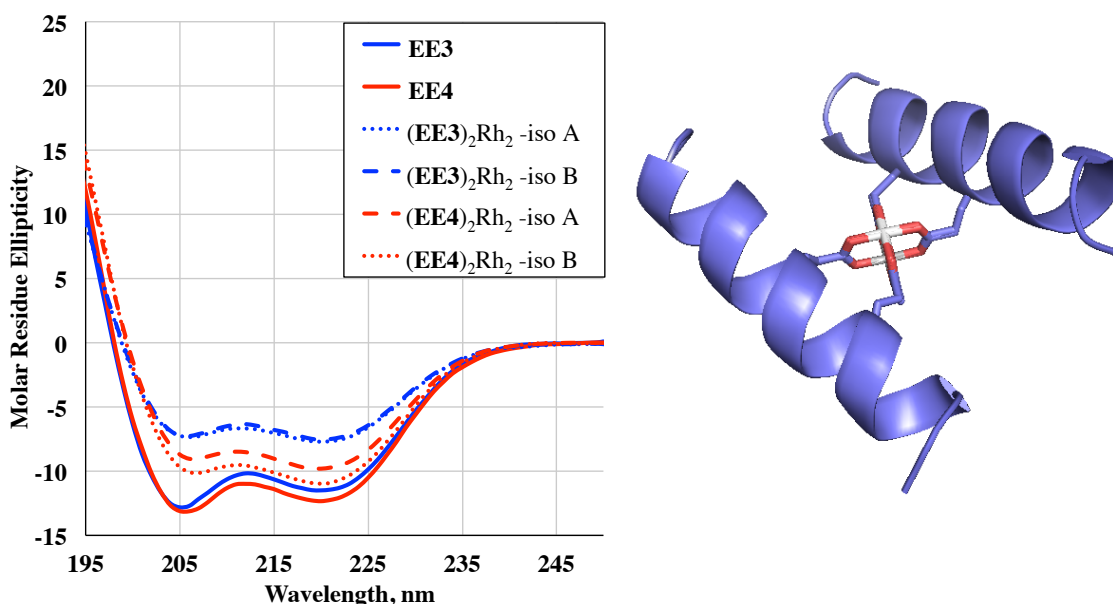


Figure 5-7. Circular dichroism spectra of *bis*-peptide–dirhodium complexes and a model structure of the antiparallel $(EE4)_2Rh_2$ metallopeptide (structure was generated in PyMOL). Isomers A and B correspond to parallel or antiparallel orientation of the two peptide chains, but exact correlation was not identified.

Because dirhodium *bis*-acetate complexes described here can exist in *cis* or *trans* isomeric forms, I was interested in examining the effects of coordination stereochemistry on helix induction. Modeling indicates that only *cis* coordination should be compatible with a helical structure, and this

is born out by experiment. Treatment of peptide **EE4** with the isomeric *trans*-Rh₂(OAc)₂(tfa)₂ complex⁸⁴ results in the formation of the bridged dirhodium complex, *trans*-**EE4**-Rh₂(OAc)₂ (Scheme 5-5). The structure of this complex can be inferred from mass spectrometry and the fact that *trans*-**EE4**-Rh₂(OAc)₂ exhibits different HPLC run times and markedly a different CD spectrum from that of the *cis* isomer. Consistent with expectations from modeling, the CD spectrum of *trans*-**EE4**-Rh₂(OAc)₂ exhibits none of the features above 200 nm that would imply helical structure (Figure 5-8). The *trans*-dirhodium linkage appears to destroy any helical propensity, despite the significant helical bias of the free peptide.

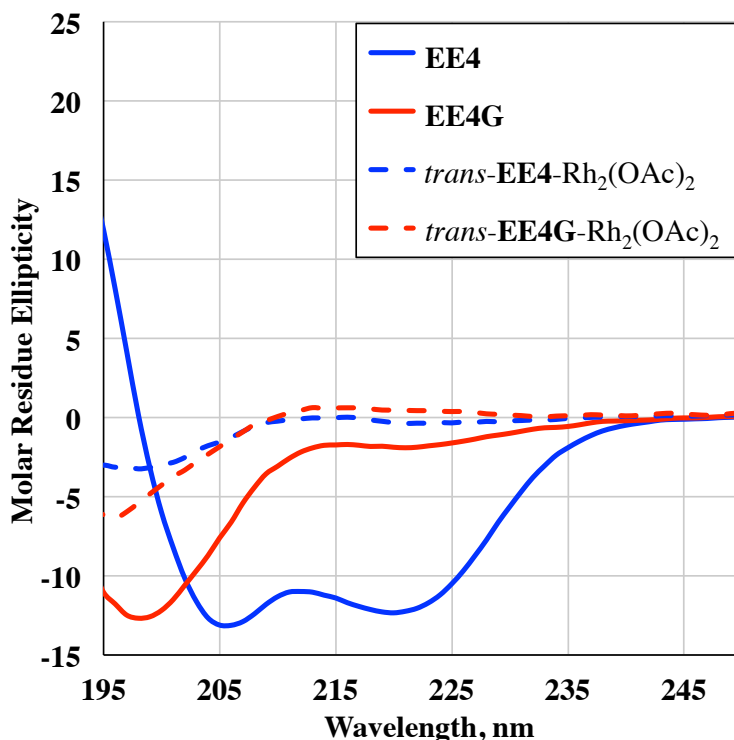
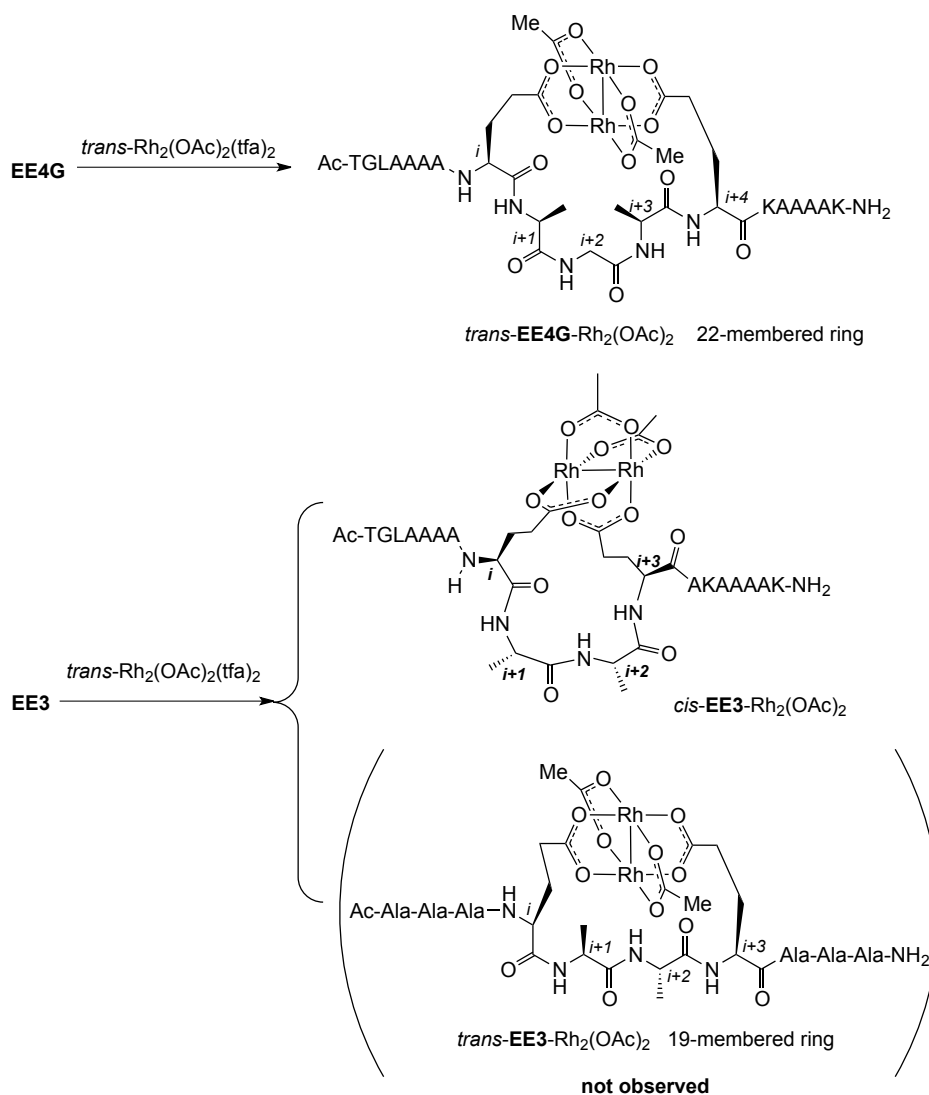


Figure 5-8. Circular dichroism spectra of *trans*-dirhodium-peptide complexes.



Scheme 5-5. Synthesis of metallopeptides from dirhodium precursors that have trans geometry.

5.6. Conclusions

Efficient and reversible means of bridging distal carboxylate side chains with a dirhodium metal center are presented. The method is compatible with aqueous, non-denaturing conditions and features chemistry that is orthogonal to other peptide cross-linking strategies. I demonstrate that dirhodium binding can be used to control the conformation of the bound peptide as well as the structure and aggregation state of complementary

peptides. These properties make dirhodium ligation an attractive platform for examining the alteration of peptide function through control of secondary structure.

Coiled coil E3/K3 heterodimer provides a simplistic model of protein-protein interaction. Various cellular pathways are mediated via network of interacting proteins and peptide mimics of their binding domains are becoming promising candidates for therapeutic applications. Reversible dirhodium metalation provides a unique release mechanism that is based on the regulation of the peptide folding state. Aside from controllable release of an active peptide; dirhodium metalloptides might be used to control the growth of supramolecular materials.

Dirhodium-carboxylate ligation was demonstrated to have powerful helix-inducing properties. Helix induction upon dirhodium binding is extremely general for *bis*-carboxylates with *i, i+4* spacing, and this work also expands the scope of known metal-binding topologies to include helix induction in peptides with *i, i+3* spacing. The tolerance of this method for other metal-binding side chains is particularly significant as it may make it possible to switch the structure of a peptide among multiple states through the use of complementary metal-ligation strategies.

Finally, peptide-dirhodium conjugates offer unique and modular control over the ligand environment around a dirhodium center. Well-folded helical peptide ligands can be used to introduce chirality at the catalytic center and the unique architecture of *bis*-peptide complexes provides the symmetry of the two dirhodium sites. On the other hand, the catalytic activity of dirhodium can be modulated with hybrid amidate/peptide complexes. Dirhodium metalloptide catalysis with diazo compounds in the

contexts of small molecule enantioselective synthesis and peptide/protein modification became the consequence of studies.⁸⁶⁻⁹⁰

5.7. Experimental section

5.7.1. General information

Peptide synthesis. All peptides were synthesized with an Advanced ChemTech APEX 396 Automated Multipetide Synthesizer using standard solid-phase Fmoc protocols. The purification was accomplished by reverse-phase HPLC with gradients of water-acetonitrile containing 0.1% trifluoroacetic acid, and peptides were isolated by lyophilization. Analysis and purity assessment was attained by mass spectrometry and analytical HPLC. Peptides were prepared using Rink amide MBHA resin (AAPTEC) to afford the C-terminal amide and were acetylated at the N-terminus prior to cleavage from the resin.

Circular Dichroism Spectroscopy. CD spectra were obtained on Jasco-J810 spectropolarimeter using a 0.01 cm cell. The spectra were acquired with a 1 nm interval in the range of 180–250 nm. Millidegrees of rotation were converted to mean residual ellipticity.

HPLC analysis and purification. HPLC was performed on a Shimadzu CBM-20A instrument with Phenomenex Jupiter 4 μ Proteo 90A (250 \times 15 mm preparative) and Phenomenex Jupiter 4 μ Proteo 90A (250 \times 4.6 mm analytical) columns. Flow rates of 8 mL/min and 1 mL/min were used for preparative and analytical columns, respectively. Analytical and preparative HPLC were performed with gradient of acetonitrile in water. Both solvents contained 0.1% trifluoroacetic acid (TFA) unless otherwise noted. Two wavelengths — 220 nm and 300 nm — were used to allow for independent analysis of peptides and dirhodium complexes.

Mass Spectrometry. MALDI-MS and MS/MS analyses were performed on a Bruker Daltonics Autoflex MALDI- TOF/TOF mass spectrometer with CHCA matrix (10 mg/mL, Thermo Scientific Pierce). ESI-MS was performed on Bruker Daltonics micrOTOF instrument.

NMR Spectroscopy. 1D Spectra were measured with Bruker 500 UltraShield™ (500 MHz) spectrometer or Oxford (400 MHz) spectrometer. ¹H NMR are reported in units of part per million (ppm). Standard abbreviations are used to indicate signal multiplicity: s, singlet; d, doublet; t, triplet; q, quartet; m, multiplet. Coupling constant are reported as *J* value in Hertz (Hz). nH describes the number of protons (n) from integration. All 2D NMR spectra were acquired on 500 MHz Varian Inova NMR Spectrometer at 25°C. Samples were prepared in 90:10 H₂O/D₂O at 6 mM concentration and were buffered to pH 5.5 with sodium acetate-d₃. Mixing time used for NOESY was 400 ms and for ROESY, 200 ms. Acquisition times of 500 ms (ROESY) and 1000 ms (NOESY) were used in the direct dimension and 100 ms in the indirect dimension. 2D NMR data were processed with NMRPipe⁹¹ and analyzed using the Sparky program.⁹²

5.7.2. Synthetic procedures

Synthesis of known compounds. The dirhodium precursors *cis*-Rh₂(tfa)₂(OAc)₂ and *trans*-Rh₂(tfa)₂(OAc)₂ were prepared according to the published procedures.⁹³

General procedure for the synthesis of dirhodium metallopeptides from *cis*-Rh₂(tfa)₂(OAc)₂. Peptide (1 equiv), *cis*-Rh₂(tfa)₂(OAc)₂ (1 equiv), MES (40 equiv), and a stir bar were placed in the 4 mL vial. Water (calculated for 2.5 mM peptide concentration) was added and the pH was adjusted to 4.5 with NaOH (0.1 M). The reaction was heated to 50 °C for 2-4

h and monitored by HPLC. Purification of the metallopeptides was performed by direct injection of the reaction mixture on a preparative RP-HPLC column. All complexes were isolated as a green solid upon lyophilization (Table 5-2).

Synthesis of K3-Rh₂(OAc)₂ metallopeptide. Peptide **K3** (5.93 mg, 2.5 μmol), *cis*-Rh₂(TFA)₂(OAc)₂ (1.38 mg, 2.5 μmol), MES (19.5 mg, 0.1 mmol) and a stir bar were placed in the 4-mL vial. Water (1 mL) was added and the pH adjusted to 4.5 with NaOH (0.1 M aq soln). The reaction was heated to 50 °C for 3 h and monitored by HPLC (Figure 5-13). Two wavelengths were used (220 nm and 300 nm) to allow for independent analysis of peptides and dirhodium complexes. Purification of the metallopeptides was performed by direct injection of the reaction mixture on a preparative RP-HPLC column. The product was isolated as a green solid (4.11 mg, 61 %) upon lyophilization.

Cleavage of the metallopeptide K3-Rh₂(OAc)₂ in presence of the peptide E3. KOAc (4.91 mg) was added to the mixture of the complex **K3**-Rh₂(OAc)₂ and peptide **E3** in the buffered solution (0.5 mL, 50 mM phosphate, 0.1 M KCl) to achieve a 0.1 M KOAc soln (pH 6.8). The cleavage of the complex **K3**-Rh₂(OAc)₂ (at rt and 50 °C) was monitored by HPLC and CD (Figure 5-10).

Synthesis of dirhodium-peptide complex *trans*-EE4-Rh₂(OAc)₂. Peptide **EE4** (4.51 mg, 2.64 μmol), *trans*-Rh₂(tfa)₂(OAc)₂ (1.45 mg, 2.64 μmol), MES (20.7 mg, 0.11 mmol) and a stir bar were placed in the 4-mL vial. Water (1.06 mL) was added and the pH adjusted to 4.5 with NaOH (0.1M). The reaction was heated to 50 °C for 24 h and monitored by HPLC. Purification of the metallopeptides was performed by direct injection of the

reaction mixture on a preparative RP-HPLC column and lyophilization affords the product as a green solid (1.0 mg, 19%).

Synthesis of dirhodium-peptide complex *trans*-EE4G-Rh₂(OAc)₂. Peptide **EE4G** (0.92 mg, 0.54 μmol), *trans*-Rh₂(tfa)₂(OAc)₂ (0.27 mg, 0.49 μmol), MES (3.8 mg, 0.02 mmol) and a stir bar were placed in the 4-mL vial. Water (0.19 mL) was added and the pH adjusted to 4.5 with NaOH (0.1M). The reaction was heated to 50 °C for 8 h and monitored by HPLC. Purification of the metallopeptides was performed by direct injection of the reaction mixture on a preparative RP-HPLC column and lyophilization affords the product as a green solid (0.64 mg, 65%).

Synthesis of the *cis*-Rh₂(pyrr)₂(tfa)₂ precursor. Rh₂(OAc)₄ (30 mg, 68 mmol) and 2-pyrrolidinone (2.7g, 32 mmol) were heated at 125 °C for 20 h under nitrogen atmosphere. The excess of 2-pyrrolidinone was removed by Kugelrohr distillation at 125 °C and 0.4 torr. The solid was dissolved in trifluoroacetic acid (2mL) and stirred for 3 h at rt. The product was isolated by HPLC as a violet solid (10.1mg, 21%). ¹H NMR (CD₃CN, 500 MHz): 1.82-1.95 (m, 4H), 2.20-2.35 (m, 4H), 3.38-3.50 (m, 4H). ¹³C NMR (CD₃CN, 500 MHz): 21.32, 33.00, 54.86, 118.41, 191.02.

Synthesis of dirhodium-peptide complex EE3-Rh₂(pyrr)₂*iso*-A and EE3-Rh₂(pyrr)₂ *iso*-B. Peptide **EE3** (3.60 mg, 2.11 μmol), *cis*-Rh₂(pyrr)₂(tfa)₂ (1.44 mg, 2.11 μmol), MES (16.5 mg, 0.084 mmol) and a stir bar were placed in the 4-mL vial. Water (0.84 mL) was added and the pH adjusted to 4.5 with NaOH (0.1M). The reaction was heated to 50 °C for 2 h and monitored by HPLC. Purification of the metallopeptides was performed by direct injection of the reaction mixture on a preparative RP-HPLC column. The products were isolated as a violet solid upon

lyophilization. **EE3**-Rh(pyrr)₂ *iso-A*: 2.27 mg, 50%. **EE3**-Rh(pyrr)₂ *iso-B*: 1.30 mg, 29%.

Synthesis of dirhodium-peptide complex (EE3)₂Rh₂ iso-A and (EE3)₂Rh₂ iso-B. Peptide **EE3** (4.70 mg, 2.76 μmol), Rh₂(tfa)₄ (0.89 mg, 1.57 μmol), MES (21.6 mg, 0.11 mmol) and a stir bar were placed in the 4-mL vial. Water (1.1 mL) was added and the pH adjusted to 4.5 with NaOH (0.1M). The reaction was heated to 50 °C for 22 h and monitored by HPLC. Purification of the metallopeptides was performed by direct injection of the reaction mixture on a preparative RP-HPLC column. The products were isolated as a violet solid upon lyophilization. **(EE3)₂Rh₂ iso-A**: 1.41 mg, 25%. **(EE3)₂Rh₂ iso-B**: 1.43 mg, 25%.

Synthesis of dirhodium-peptide complex (EE4)₂Rh₂ iso-A and (EE4)₂Rh₂ iso-B. Peptide **EE4** (12.0 mg, 7.05 μmol), Rh₂(tfa)₄ (2.0 mg, 3.52 μmol), MES (27 mg, 0.14 mmol) and a stir bar were placed in the 4-mL vial. Water (2.8 mL) was added and the pH adjusted to 4.5 with NaOH (0.1M). The reaction was heated to 50 °C for 3 h and monitored by HPLC. Purification of the metallopeptides was performed by direct injection of the reaction mixture on a preparative RP-HPLC column. The products were isolated as violet solids upon lyophilization. **(EE4)₂Rh₂ iso-A**: 3.78 mg, 30%. **(EE4)₂Rh₂ iso-B**: 3.00 mg, 24%.

Table 5-2. Yields of the metallopeptides obtained from *cis*-Rh₂(tfa)₂(OAc)₂ precursor using general procedure for synthesis of dirhodium metallopeptides described above.

Metallopeptide	Isolated mass, mg	Yield
EE3 -Rh ₂ (OAc) ₂	2.58	70%
DD3 -Rh ₂ (OAc) ₂	1.68	80%
DE3 -Rh ₂ (OAc) ₂	1.60	67%
ED3 -Rh ₂ (OAc) ₂	1.40	59%
EE4 -Rh ₂ (OAc) ₂	2.41	65%
DD4 -Rh ₂ (OAc) ₂	1.76	73%
DD4G -Rh ₂ (OAc) ₂	2.51	70%
EE4G -Rh ₂ (OAc) ₂	1.44	73%
ED4G -Rh ₂ (OAc) ₂	1.96	57%
sEE4 -Rh ₂ (OAc) ₂	1.31	58%
EE3G -Rh ₂ (OAc) ₂	2.93	80%

5.7.3. Analytical data

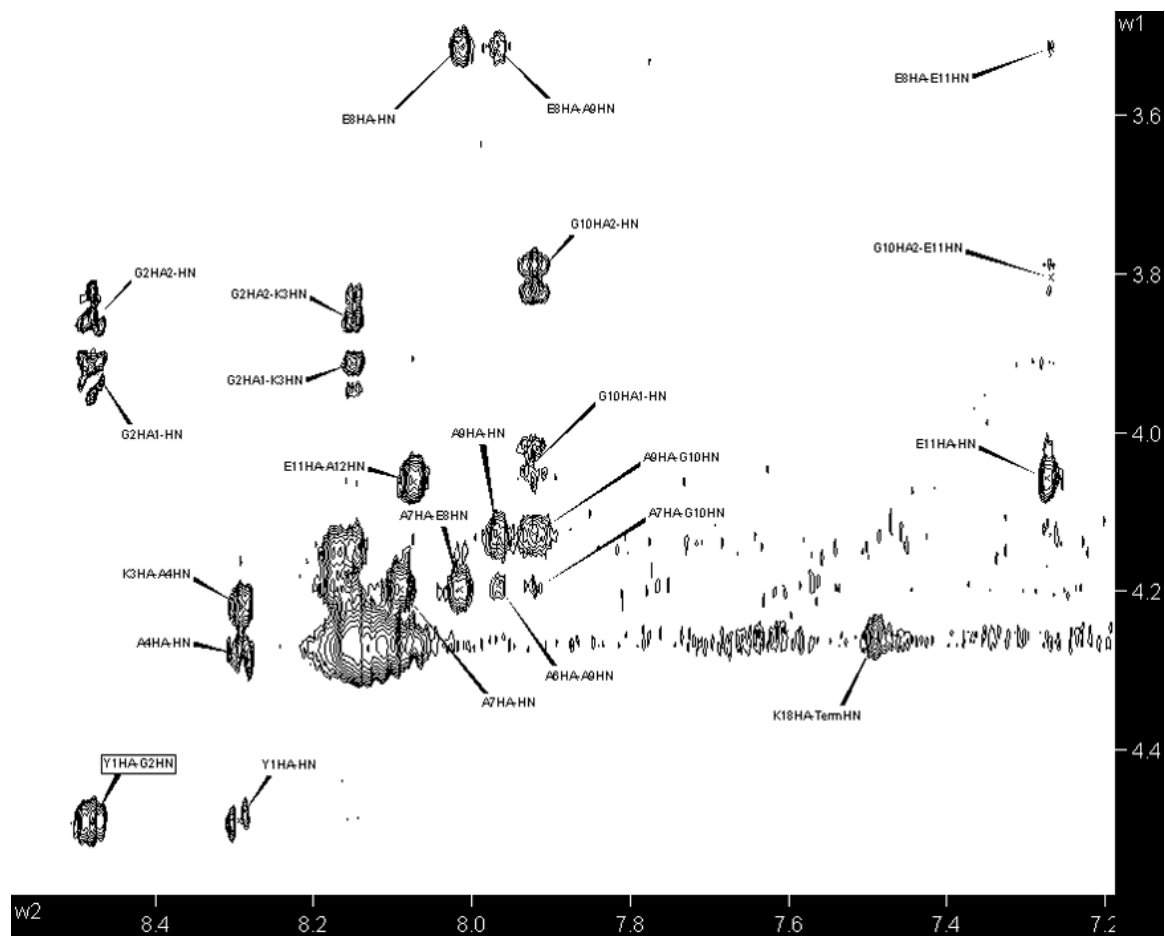


Figure 5-9. NH-H α region of the ROESY spectrum of the **EE4G**-Rh₂(OAc)₂ complex.

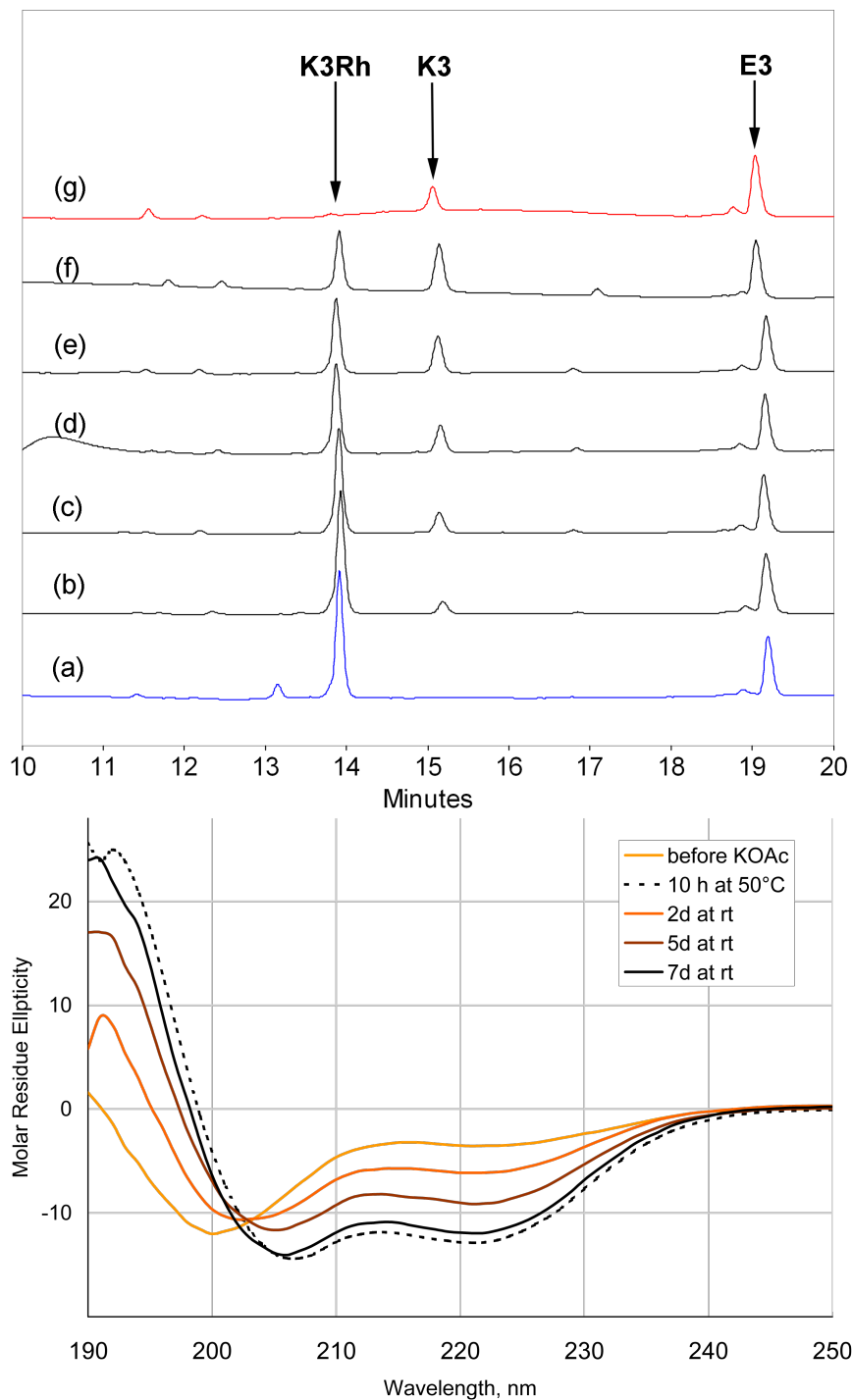


Figure 5-10. HPLC (left) and CD spectroscopy (right) of a mixture of **E3** and **K3-Rh₂(OAc)₂** demonstrating the time course of dirhodium cleavage in KOAc solution (0.1 M). For HPLC: (a) time = 0 (b) 22 h at rt (c) 2 d at rt (d) 3 d at rt (e) 5 d at rt (f) 7 d at rt (g) 10 h at 50 °C.

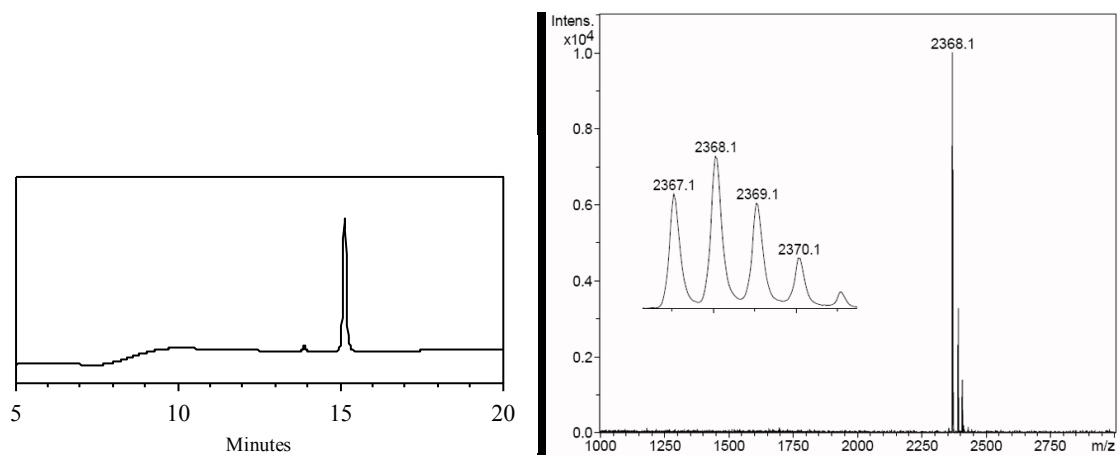


Figure 5-11. HPLC and MALDI-TOF MS of the peptide **K3**. Calculated mass $[M+H]^+$: 2367.5; found: 2367.1

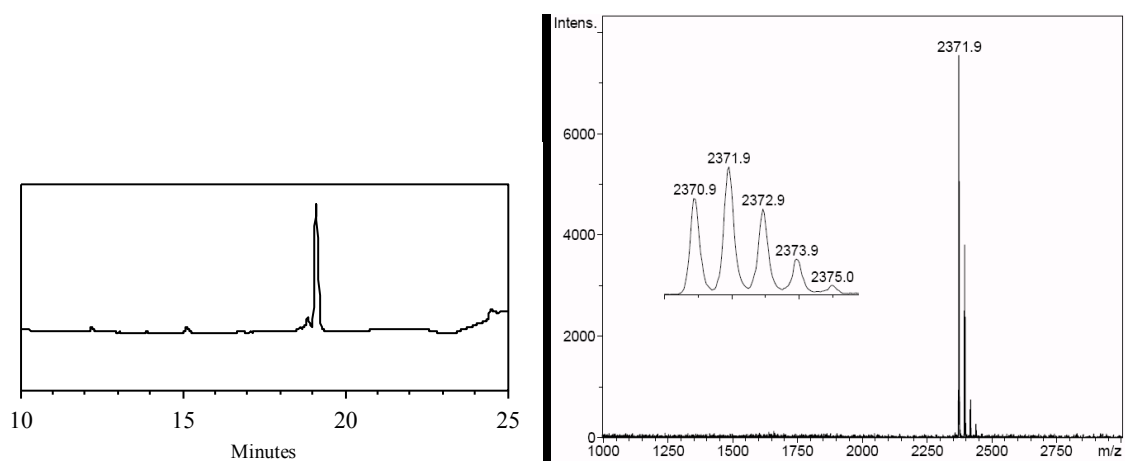


Figure 5-12. HPLC and MALDI-TOF MS of the peptide **E3**. Calculated mass $[M+H]^+$: 2371.3; found: 2370.9.

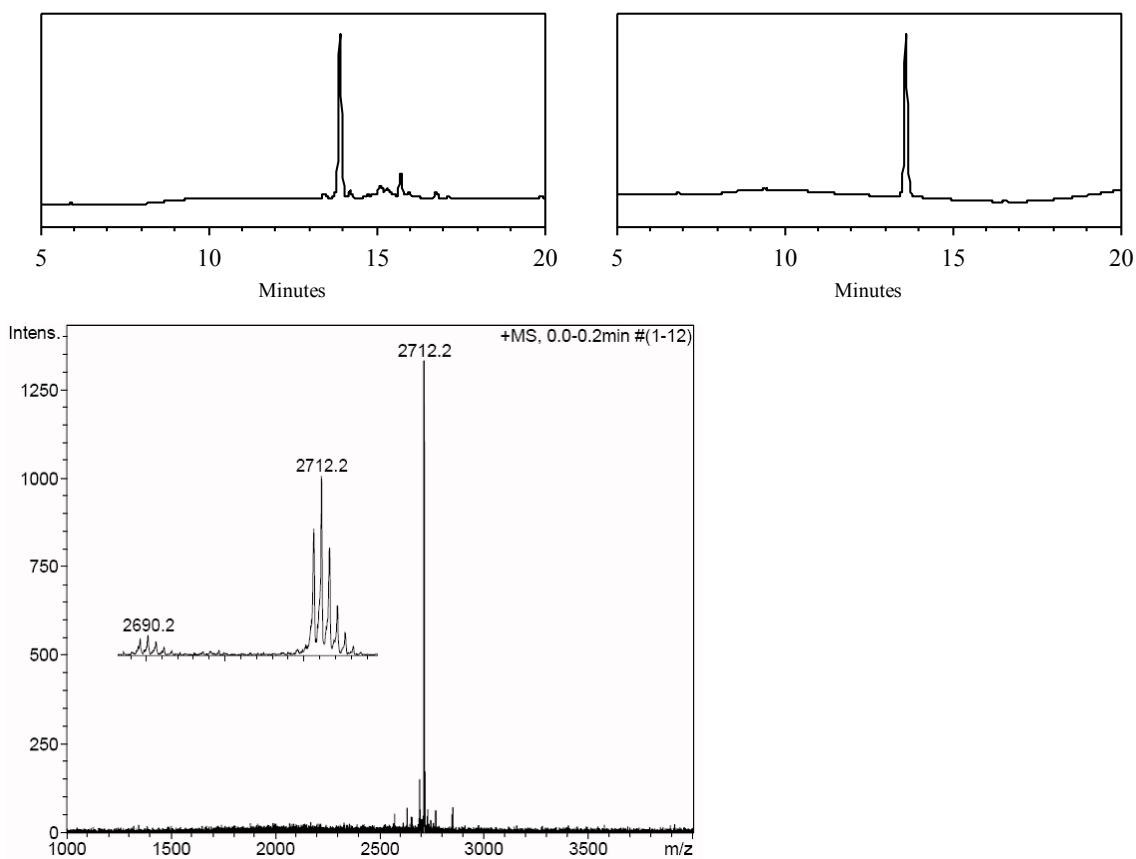


Figure 5-13. HPLC of the crude coupling reaction (left) and of the isolated complex **K3-Rh₂(OAc)₂** (right), and ESI-MS of the isolated complex **K3-Rh₂(OAc)₂** (bottom). Calculated mass $[M+H]^+$: 2689.4; found: 2689.2.

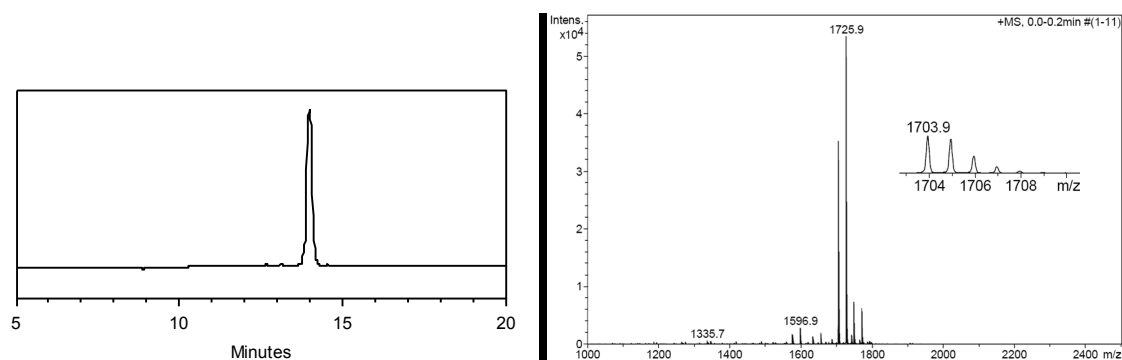


Figure 5-14. HPLC and MALDI-TOF MS of the peptide **EE3**. Calculated mass $[M+H]^+$: 1703.9; found: 1703.9.

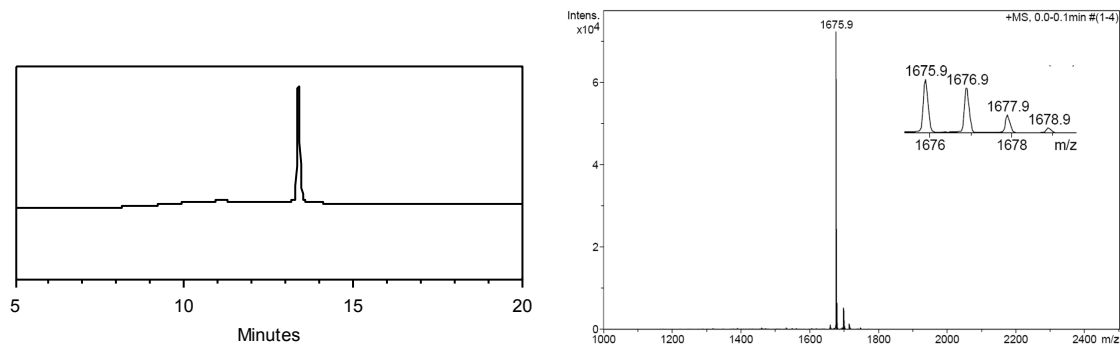


Figure 5-15. HPLC and MALDI-TOF MS of the peptide **DD3**. Calculated mass $[M+H]^+$: 1675.9; found: 1675.9.

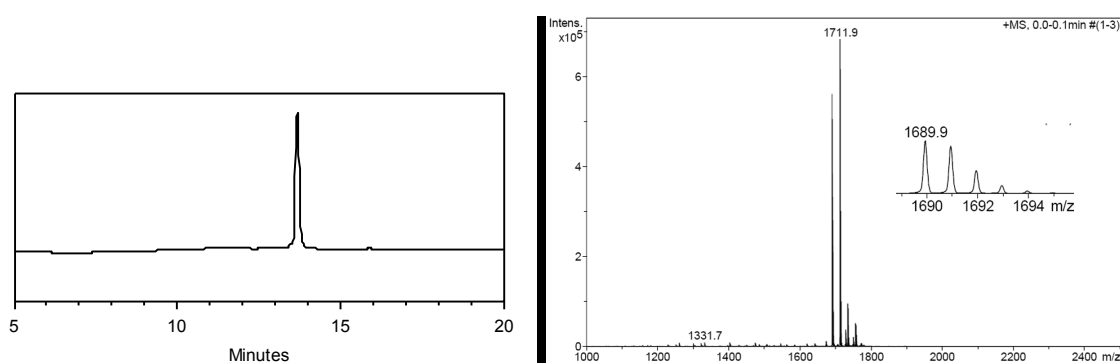


Figure 5-16. HPLC and MALDI-TOF MS of the peptide **DE3**. Calculated mass $[M+H]^+$: 1689.9; found: 1689.9.

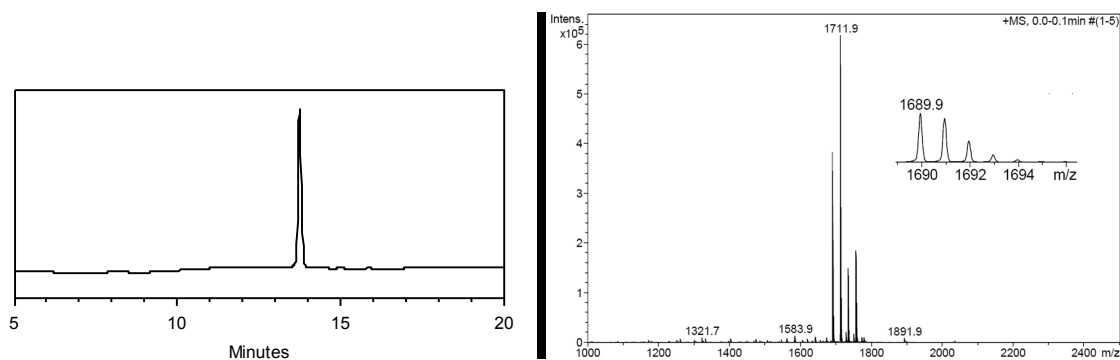


Figure 5-17. HPLC and MALDI-TOF MS of the peptide **ED3**. Calculated mass $[M+H]^+$: 1689.9; found: 1689.9.

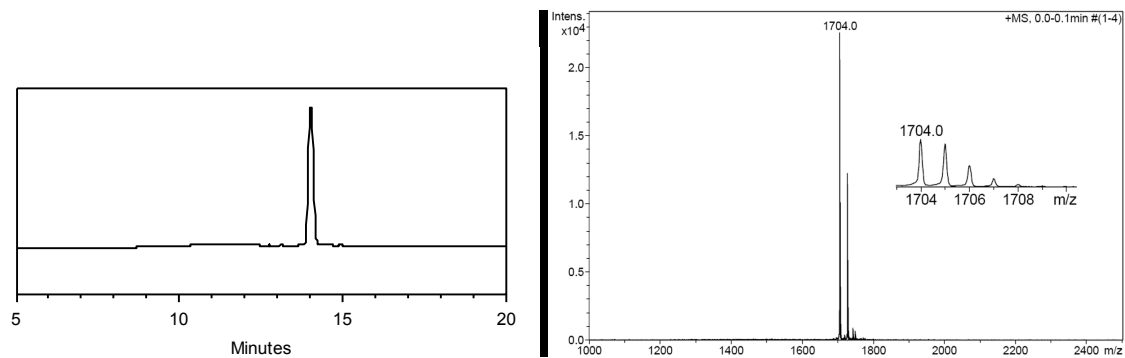


Figure 5-18. HPLC and MALDI-TOF MS of the peptide **EE4**. Calculated mass $[M+H]^+$: 1703.9; found: 1322.4.

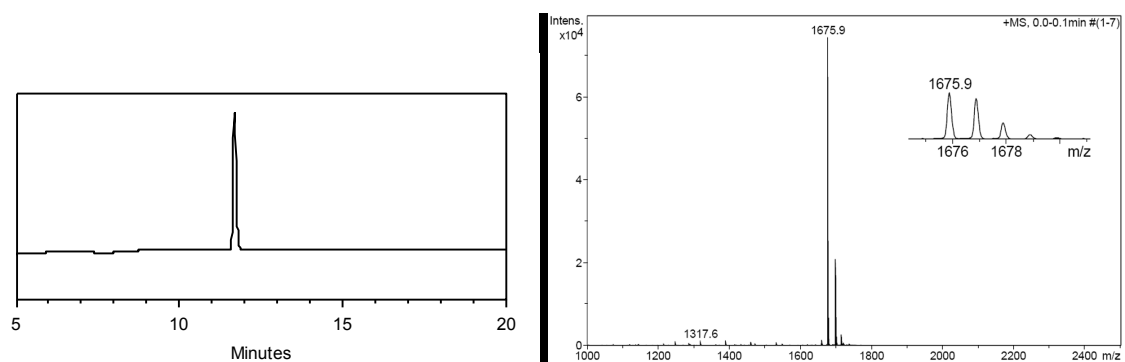


Figure 5-19. HPLC and MALDI-TOF MS of the peptide **DD4**. Calculated mass $[M+H]^+$: 1675.9; found: 1675.9.

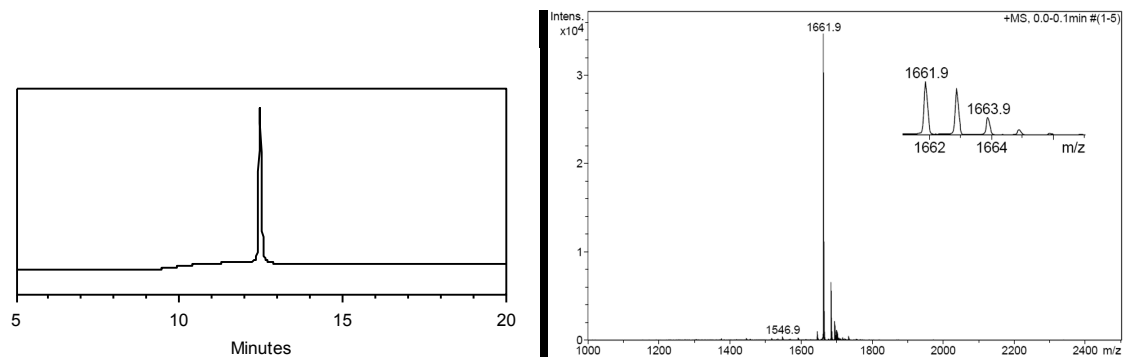


Figure 5-20. HPLC and MALDI-TOF MS of the peptide **DD4G**. Calculated mass $[M+H]^+$: 1661.9; found: 1661.9.

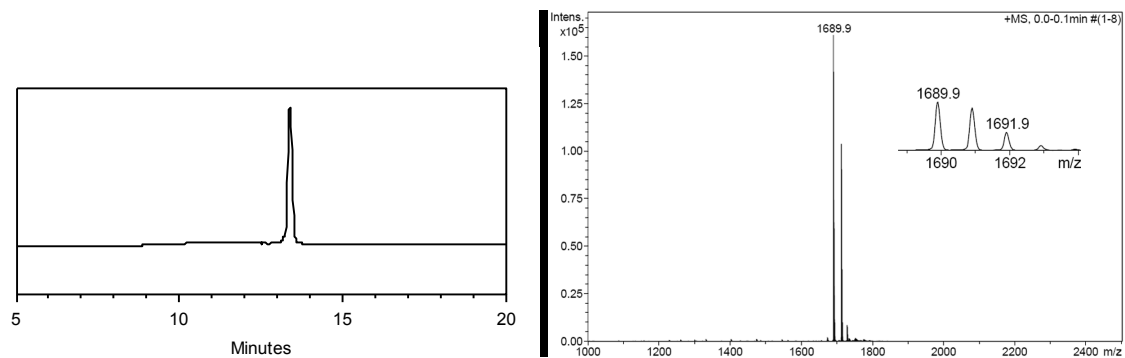


Figure 5-21. HPLC and MALDI-TOF MS of the peptide **EE4G**. Calculated mass $[M+H]^+$: 1689.9; found: 1689.9.

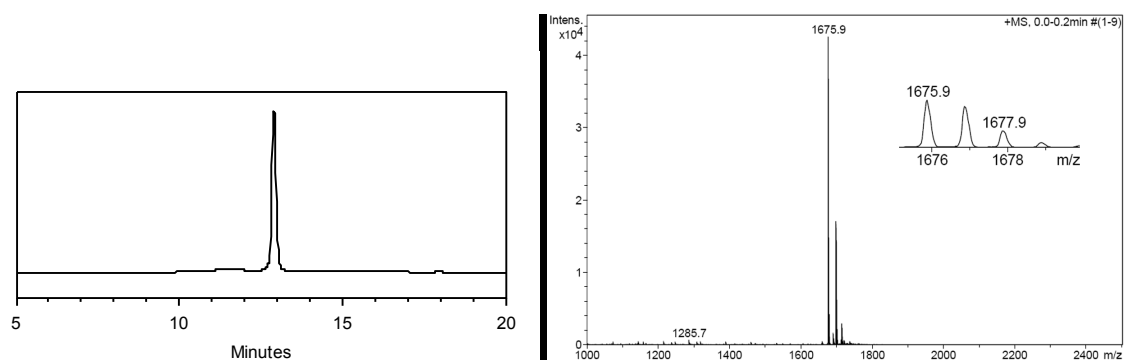


Figure 5-22. HPLC and MALDI-TOF MS of the peptide **ED4G**. Calculated mass $[M+H]^+$: 1675.9; found: 1675.9.

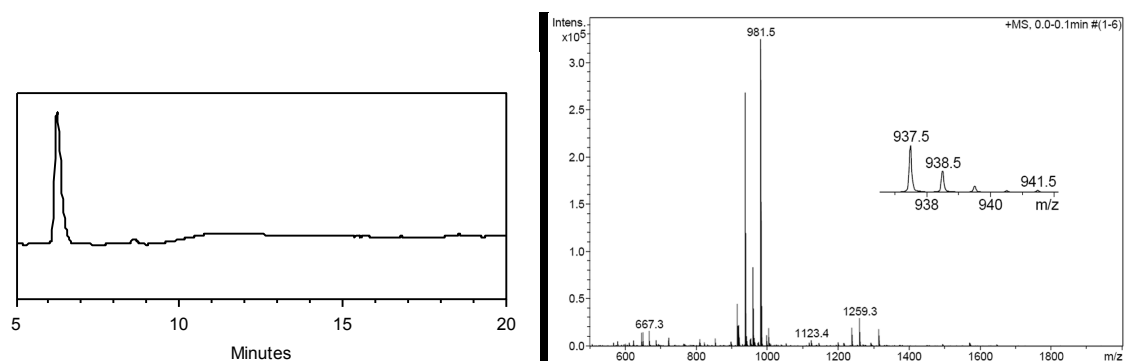


Figure 5-23. HPLC and MALDI-TOF MS of the peptide **sED4**. Calculated mass $[M+Na]^+$: 937.5; found: 937.5.

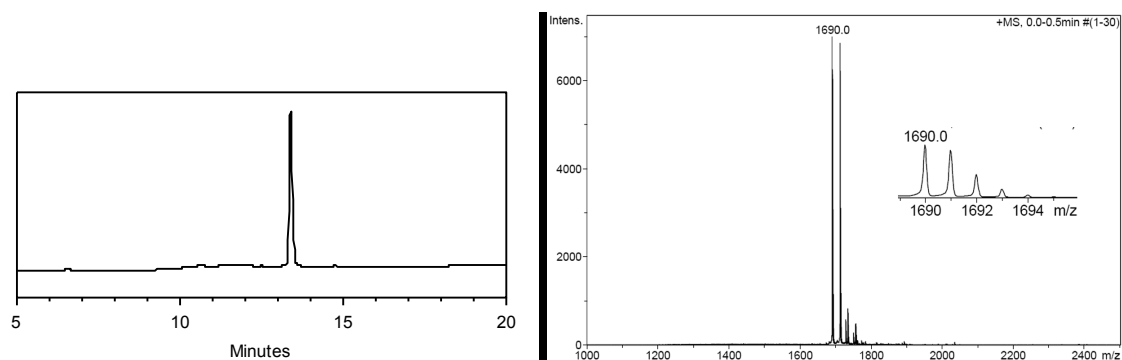


Figure 5-24. HPLC and MALDI-TOF MS of the peptide **EE3G**. Calculated mass $[M+H]^+$: 1689.9; found: 1690.0.

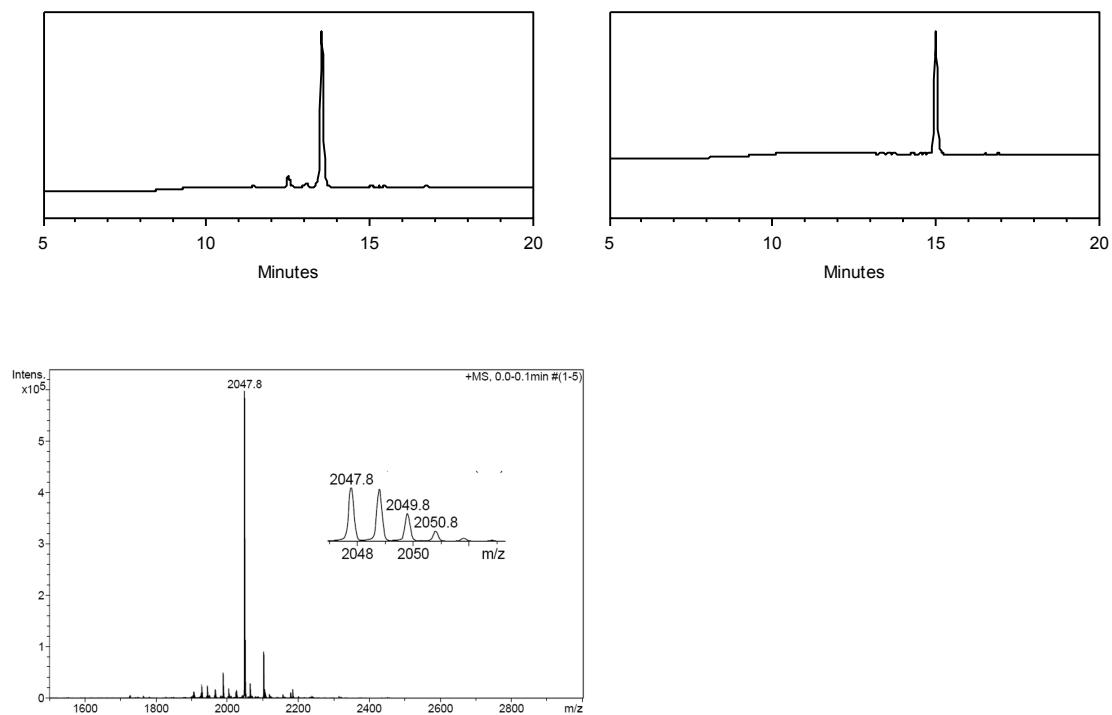


Figure 5-25. HPLC of the crude coupling reaction (left) and of the isolated complex **EE3-Rh₂(OAc)₂** (right) and ESI-MS of the isolated complex **EE3-Rh₂(OAc)₂**. Calculated mass $[M+Na]^+$: 2047.8; found: 2047.8.

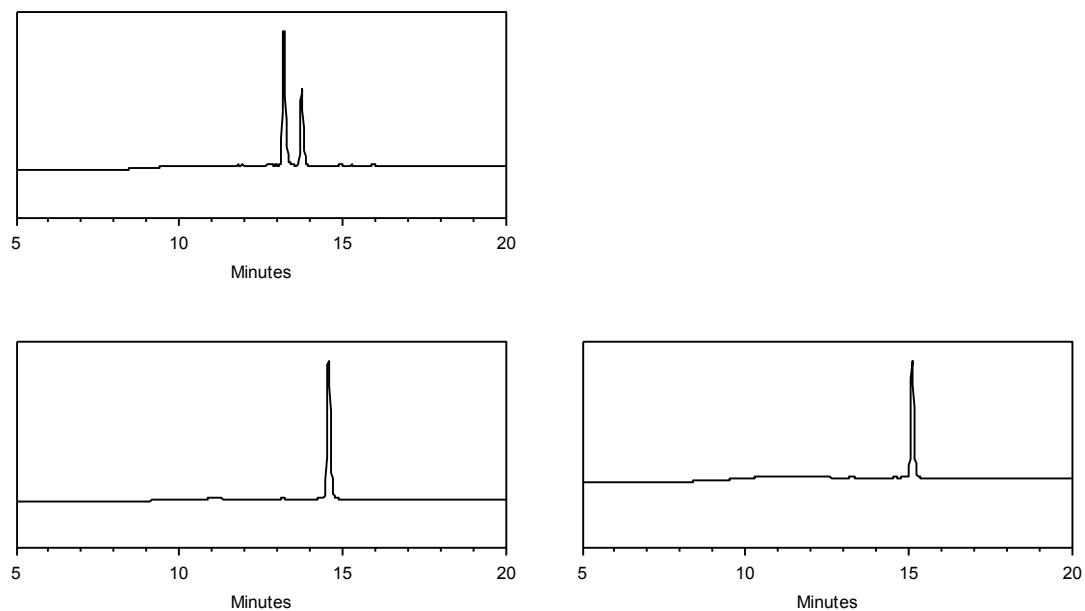


Figure 5-26. HPLC of the crude coupling reaction (top) and of the isolated complex **EE3-Rh₂(pyrr)₂ iso-A** (bottom left), **EE3-Rh₂(pyrr)₂ iso-B** (bottom right).

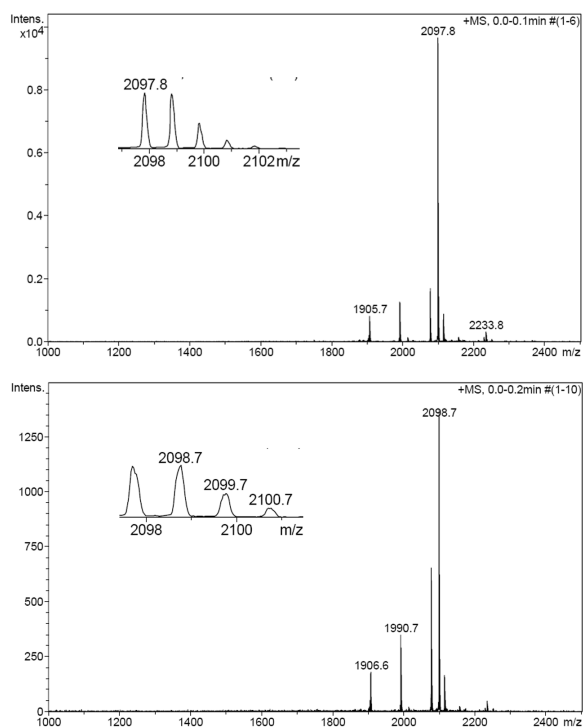


Figure 5-27. ESI-MS of the isolated complex **EE3-Rh₂(pyrr)₂ iso-A** (top), **EE3-Rh₂(pyrr)₂ iso-B** (bottom). Calculated mass for **EE3-Rh₂(pyrr)₂ iso-A** [M+Na]⁺: 2097.9; found: 2097.8. Calculated mass for **EE3-Rh₂(pyrr)₂ iso-B** [M+Na]⁺: 2097.9; found: 2097.7.

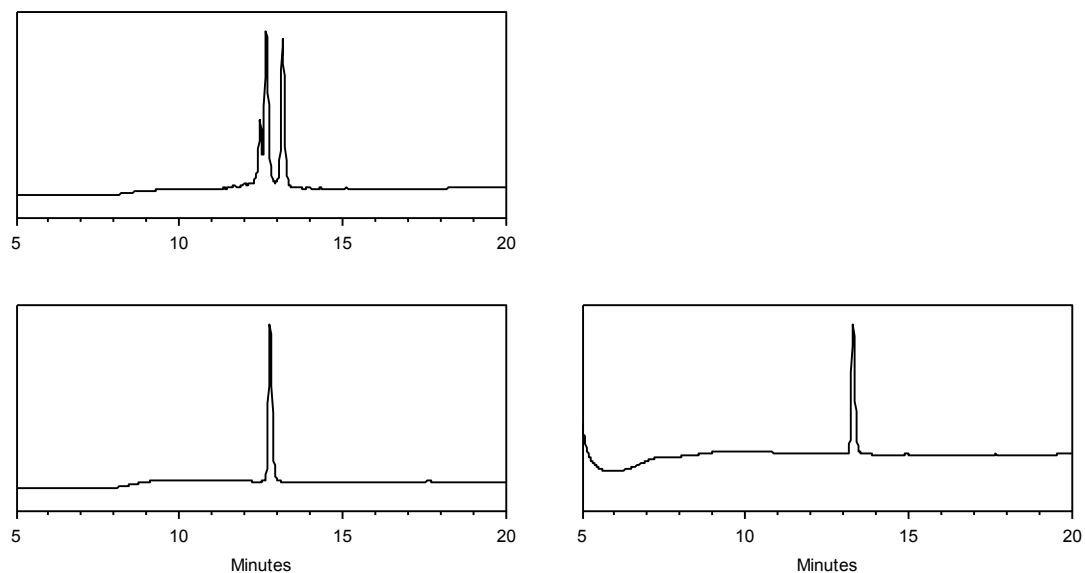


Figure 5-28. HPLC of the crude coupling reaction (top) and of the isolated complex $(\text{EE3})_2\text{Rh}_2$ *iso-A* (bottom left), $(\text{EE3})_2\text{Rh}_2$ *iso-B* (bottom right).

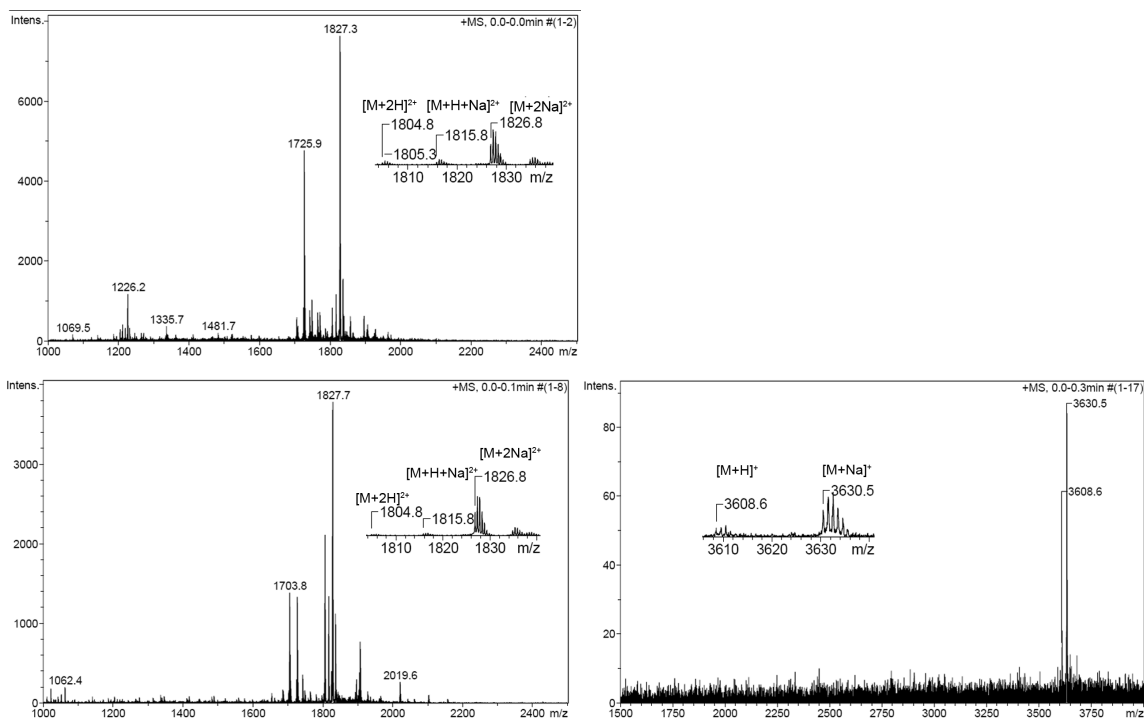


Figure 5-29. ESI-MS of the isolated complex $(\text{EE3})_2\text{Rh}_2$ *iso-A* (top), $(\text{EE3})_2\text{Rh}_2$ *iso-B* (bottom). Calculated mass for $(\text{EE3})_2\text{Rh}_2$ *iso-A*: $[\text{M}+2\text{H}]^{2+}$ 1804.8, $[\text{M}+\text{H}+\text{Na}]^{2+}$ 1815.8, $[\text{M}+2\text{Na}]^{2+}$ 1826.8; found: 1804.8, 1815.8, 1826.8. Calculated mass for $(\text{EE3})_2\text{Rh}_2$ *iso-B*: $[\text{M}+\text{H}]^+$ 3608.6, $[\text{M}+2\text{H}]^{2+}$ 1804.8, $[\text{M}+\text{H}+\text{Na}]^{2+}$ 1815.8, $[\text{M}+2\text{Na}]^{2+}$ 1826.8; found: 3608.6, 1804.8, 1815.8, 1826.8.

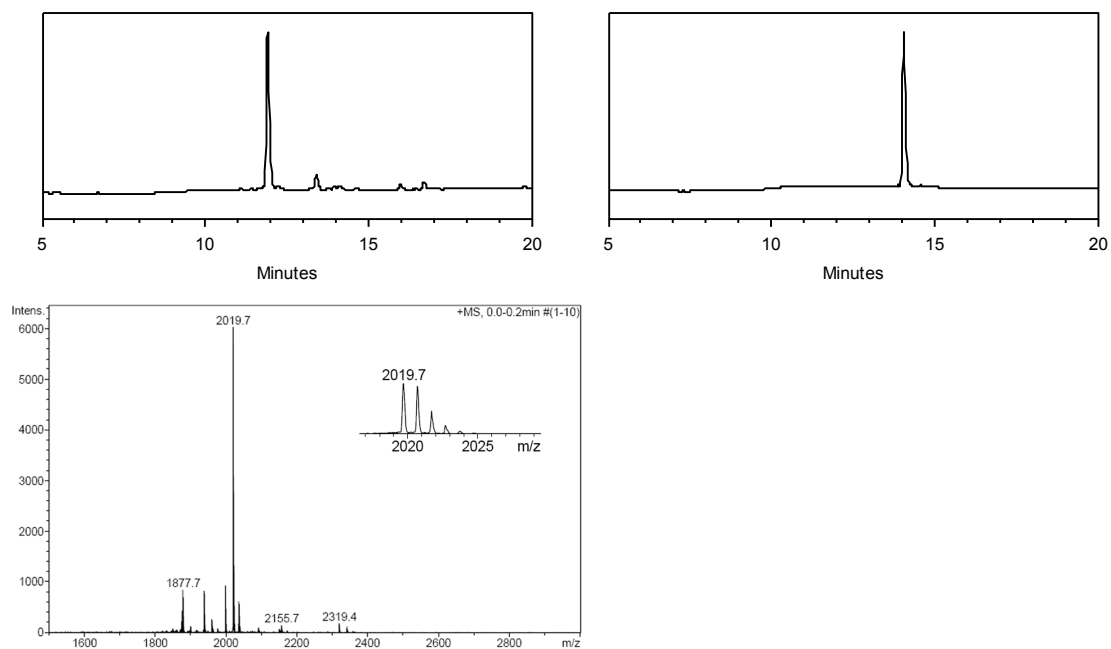


Figure 5-30. HPLC of the crude coupling reaction (left) and of the isolated complex **DD3-Rh₂(OAc)₂** (right) and ESI-MS of the isolated complex **DD3-Rh₂(OAc)₂**. Calculated mass $[M+Na]^+$: 2019.8; found: 2019.7.

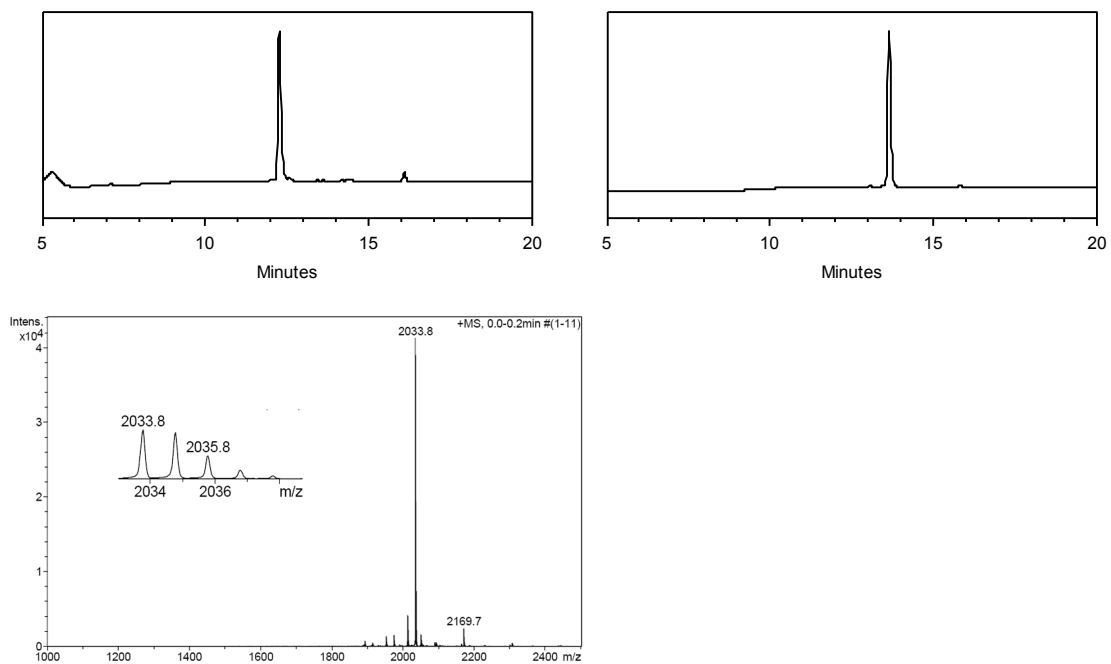


Figure 5-31. HPLC of the crude coupling reaction (left) and of the isolated complex **DE3-Rh₂(OAc)₂** (right) and ESI-MS of the isolated complex **DE3-Rh₂(OAc)₂**. Calculated mass $[M+Na]^+$: 2033.8; found: 2033.8.

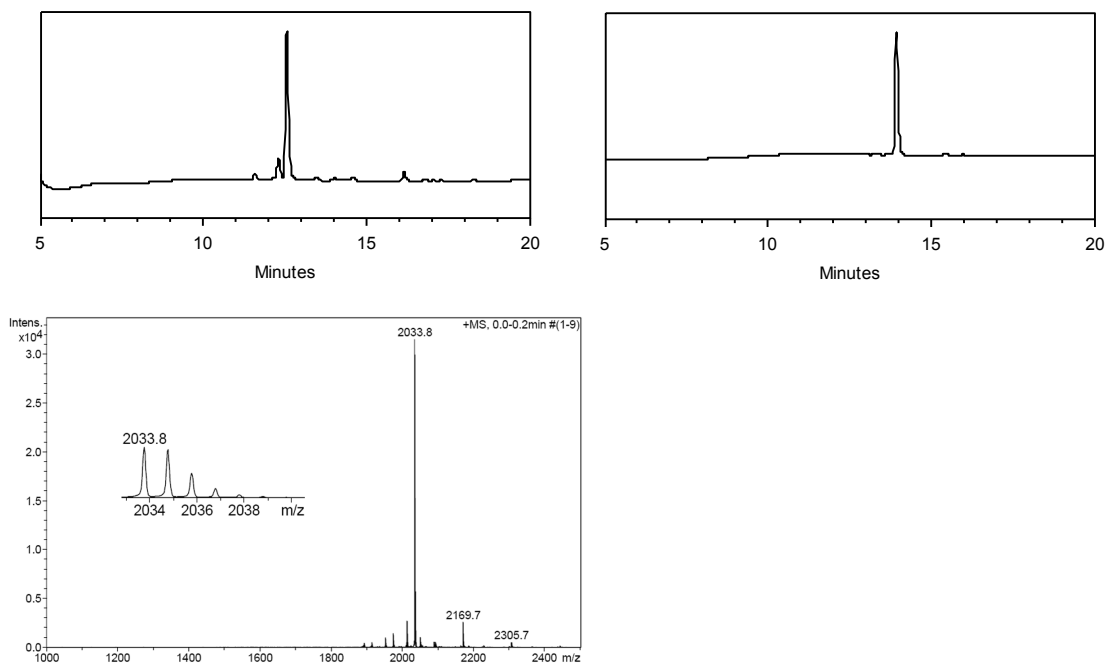


Figure 5-32. HPLC of the crude coupling reaction (left) and of the isolated complex **ED3-Rh₂(OAc)₂** (right) and ESI-MS of the isolated complex **ED3-Rh₂(OAc)₂**. Calculated mass $[M+Na]^+$: 2033.8; found: 2033.8.

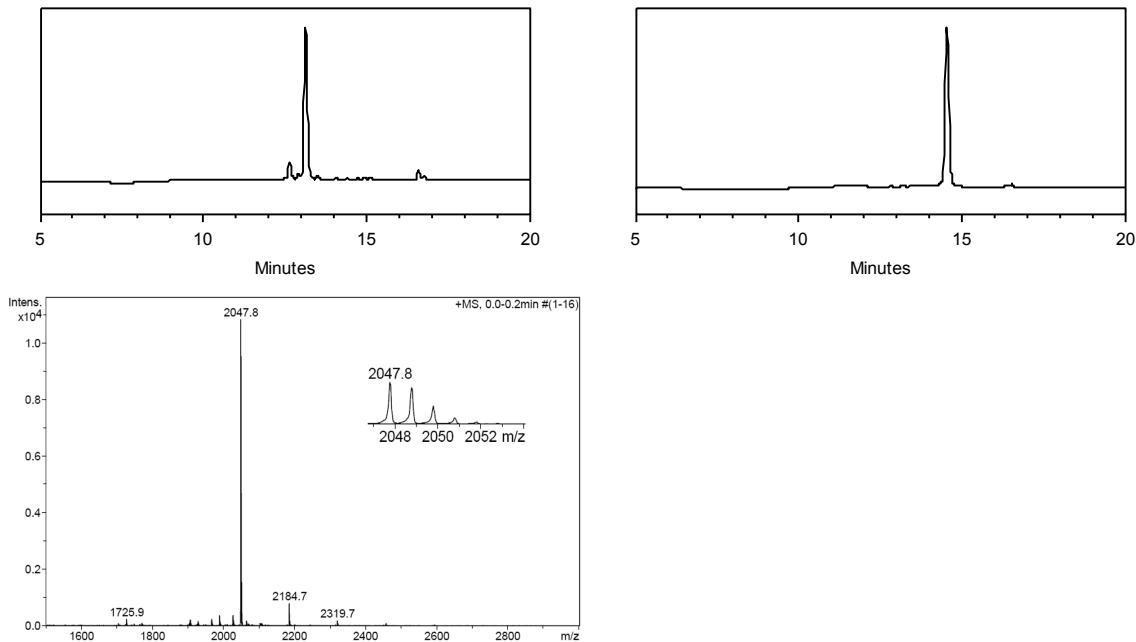


Figure 5-33. HPLC of the crude coupling reaction (left) and of the isolated complex **EE4-Rh₂(OAc)₂** (right) and ESI-MS of the isolated complex **EE4-Rh₂(OAc)₂**. Calculated mass $[M+Na]^+$: 2047.8; found: 2047.8.

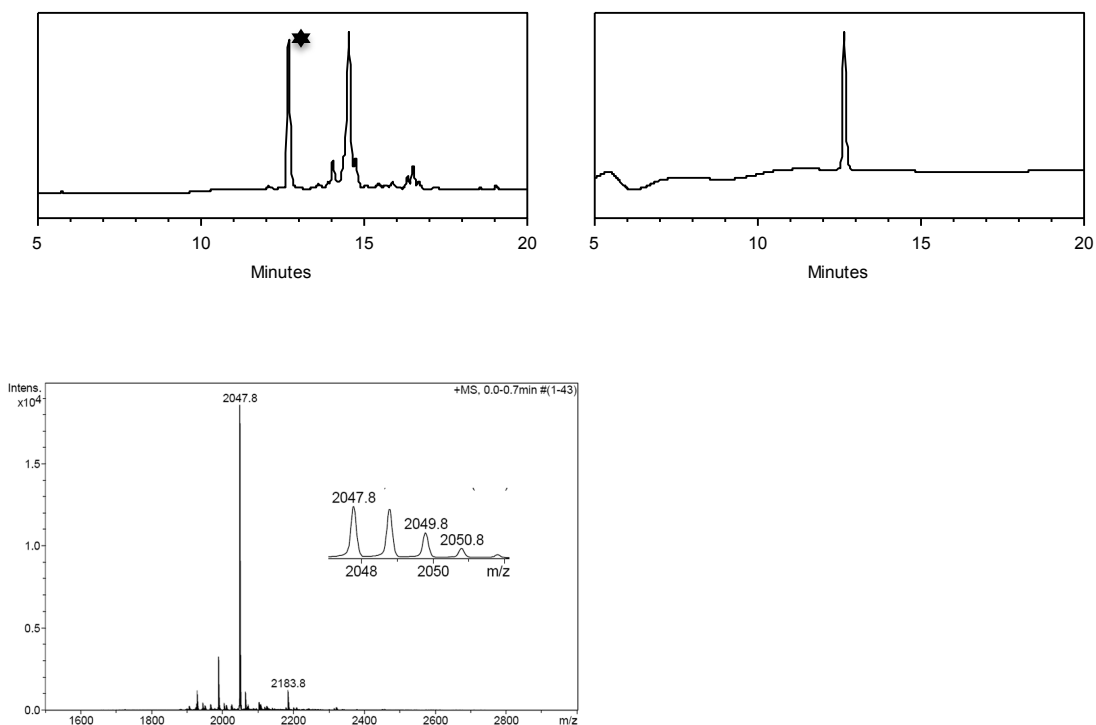


Figure 5-34. HPLC of the crude coupling reaction (left) and of the isolated complex *trans*-EE4-Rh₂(OAc)₂ (right) and ESI-MS of the isolated complex *trans*-EE4-Rh₂(OAc)₂. Calculated mass [M+Na]⁺: 2047.8; found: 2047.8.

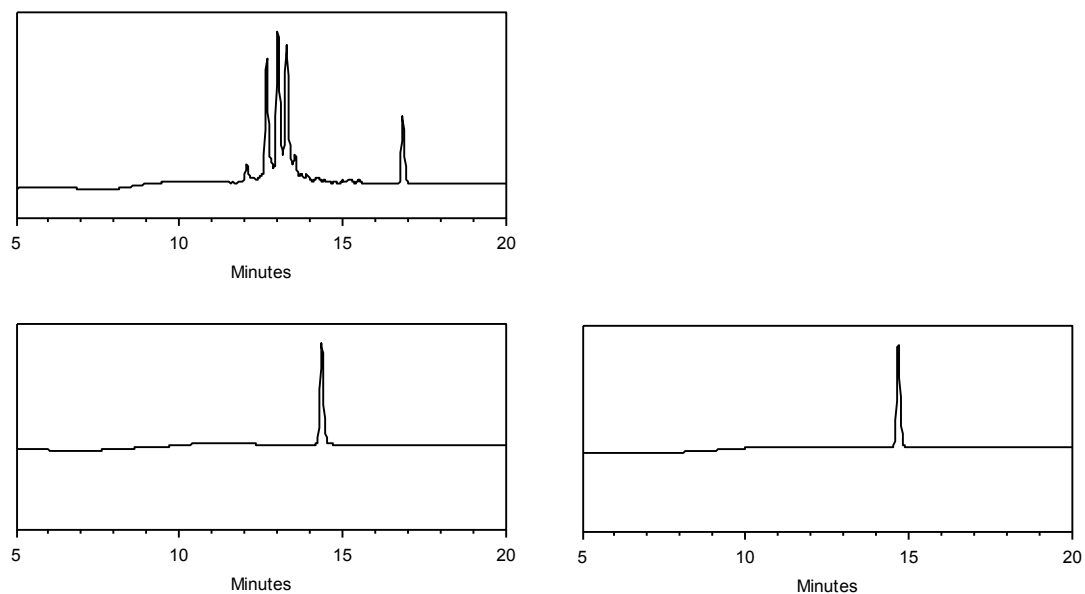


Figure 5-35. HPLC of the crude coupling reaction (top) and of the isolated complex (EE4)₂Rh₂ iso-A (bottom left), (EE4)₂Rh₂ iso-B (bottom right).

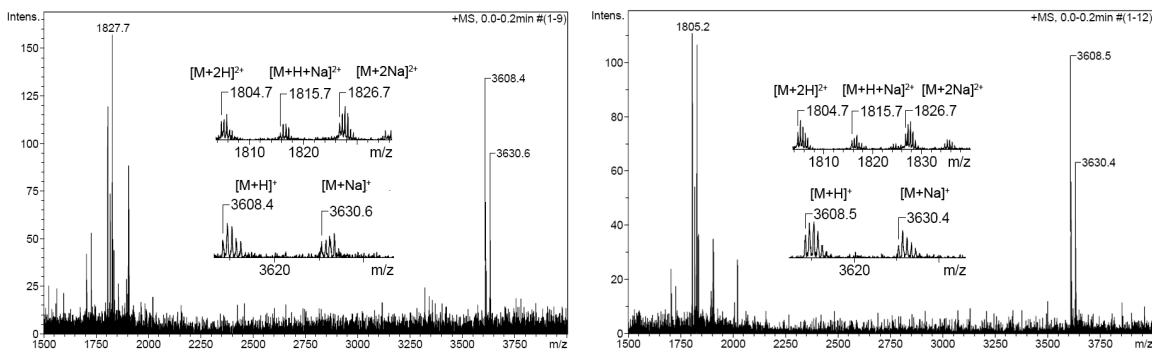


Figure 5-36. ESI-MS of the isolated complex complex $(\mathbf{EE4})_2\text{Rh}_2$ *iso-A* (top), $(\mathbf{EE4})_2\text{Rh}_2$ *iso-B* (bottom). Calculated mass for $(\mathbf{EE4})_2\text{Rh}_2$ - Rh_2 *iso-A*: $[\text{M}+\text{H}]^+$ 3608.6, $[\text{M}+2\text{H}]^{2+}$ 1804.8, $[\text{M}+\text{H}+\text{Na}]^{2+}$ 1815.8, $[\text{M}+2\text{Na}]^{2+}$ 1826.8; found: 3608.4, 1804.7, 1815.7, 1826.7. Calculated mass for $(\mathbf{EE4})_2\text{Rh}_2$ *iso-B*: $[\text{M}+\text{H}]^+$ 3608.6, $[\text{M}+2\text{H}]^{2+}$ 1804.8, $[\text{M}+\text{H}+\text{Na}]^{2+}$ 1815.8, $[\text{M}+2\text{Na}]^{2+}$ 1826.8; found: 3608.5, 1804.7, 1815.7, 1826.7

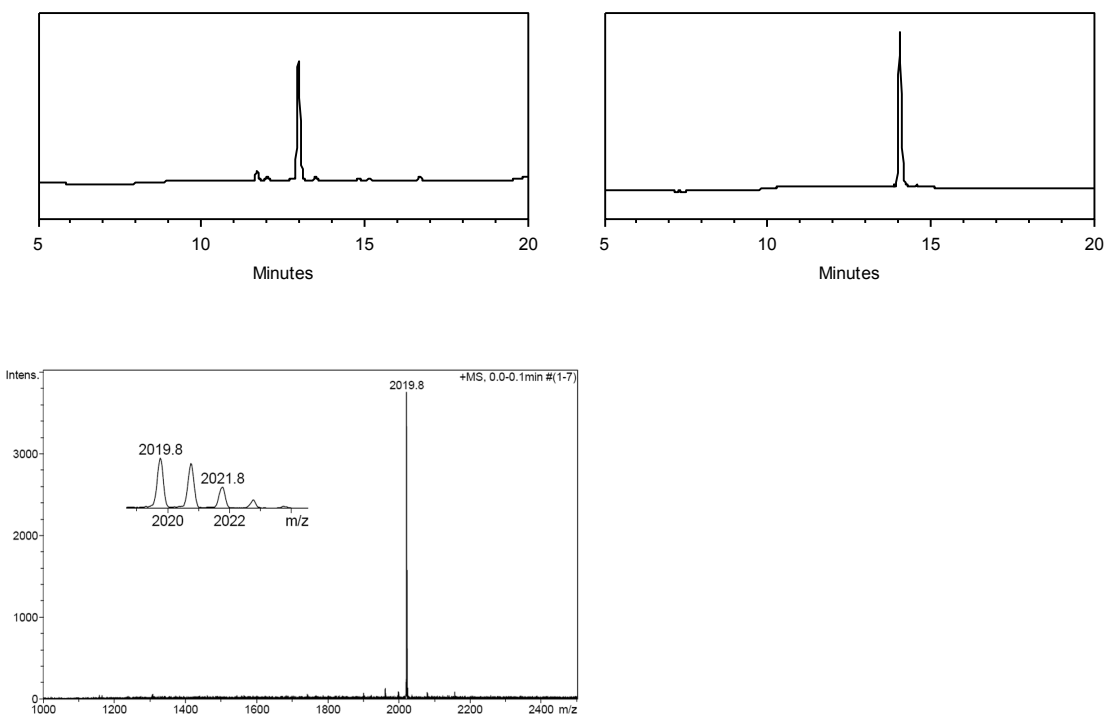


Figure 5-37. HPLC of the crude coupling reaction (left) and of the isolated complex $\mathbf{DD4-Rh}_2(\text{OAc})_2$ (right) and ESI-MS of the isolated complex $\mathbf{DD4-Rh}_2(\text{OAc})_2$. Calculated mass $[\text{M}+\text{H}]^+$: 1921.8; found: 1921.8.

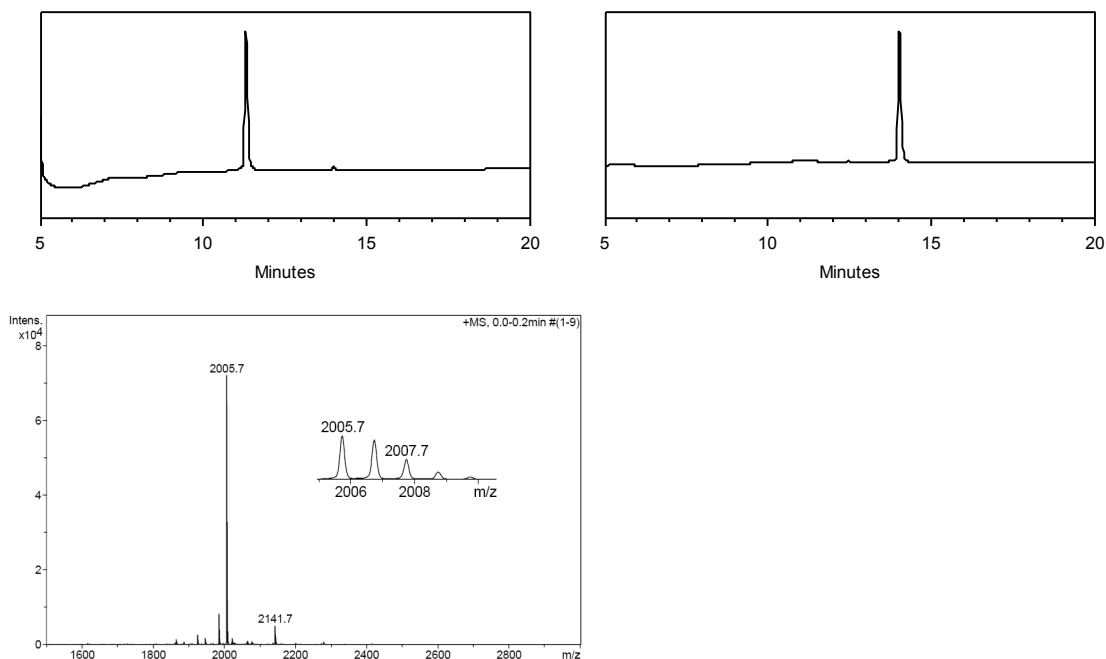


Figure 5-38. HPLC of the crude coupling reaction (left) and of the isolated complex **DD4G-Rh₂(OAc)₂** (right) and ESI-MS of the isolated complex **DD4G-Rh₂(OAc)₂**. Calculated mass $[M+Na]^+$: 1983.8; found: 1644.6.

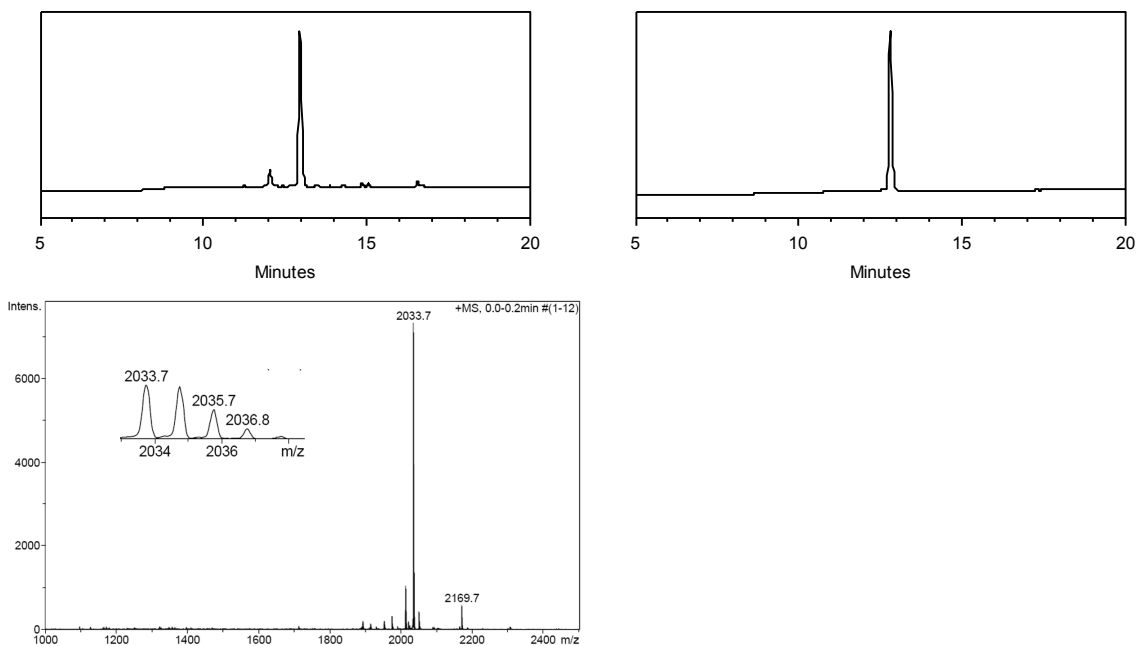


Figure 5-39. HPLC of the crude coupling reaction (left) and of the isolated complex **EE4G-Rh₂(OAc)₂** (right) and ESI-MS of the isolated complex **EE4G-Rh₂(OAc)₂**. Calculated mass $[M+Na]^+$: 2033.8; found: 2033.7.

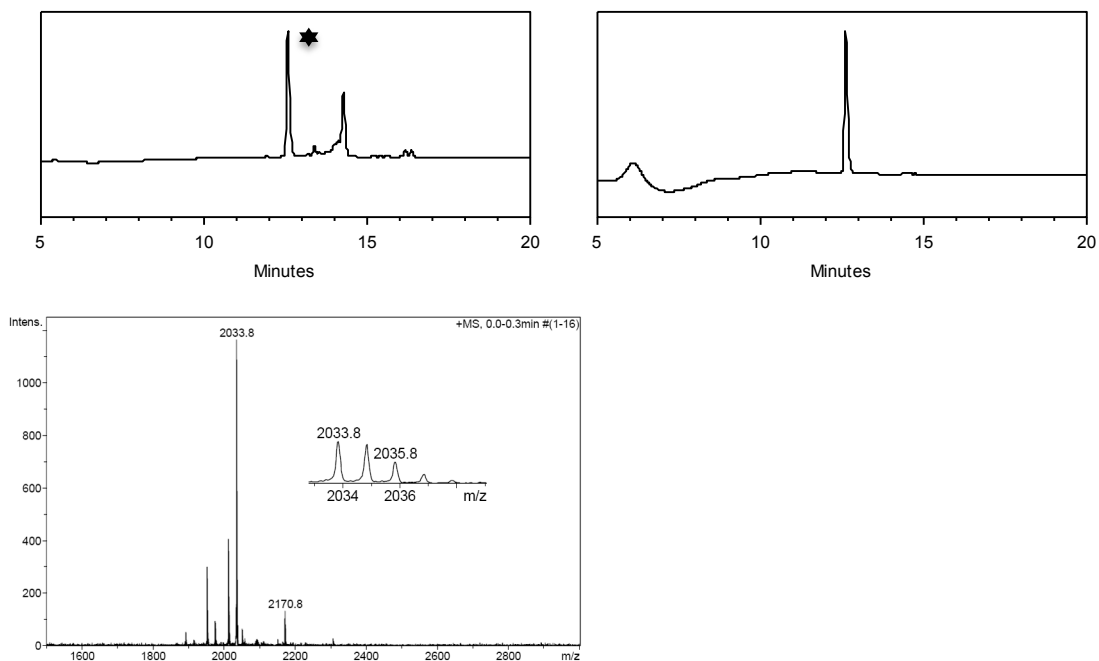


Figure 5-40. HPLC of the crude coupling reaction (left) and of the isolated complex *trans-EE4G-Rh₂(OAc)₂* (right) and ESI-MS of the isolated complex *trans-EE4G-Rh₂(OAc)₂*. Calculated mass $[M+H]^+$: 2011.8; found: 1644.6.

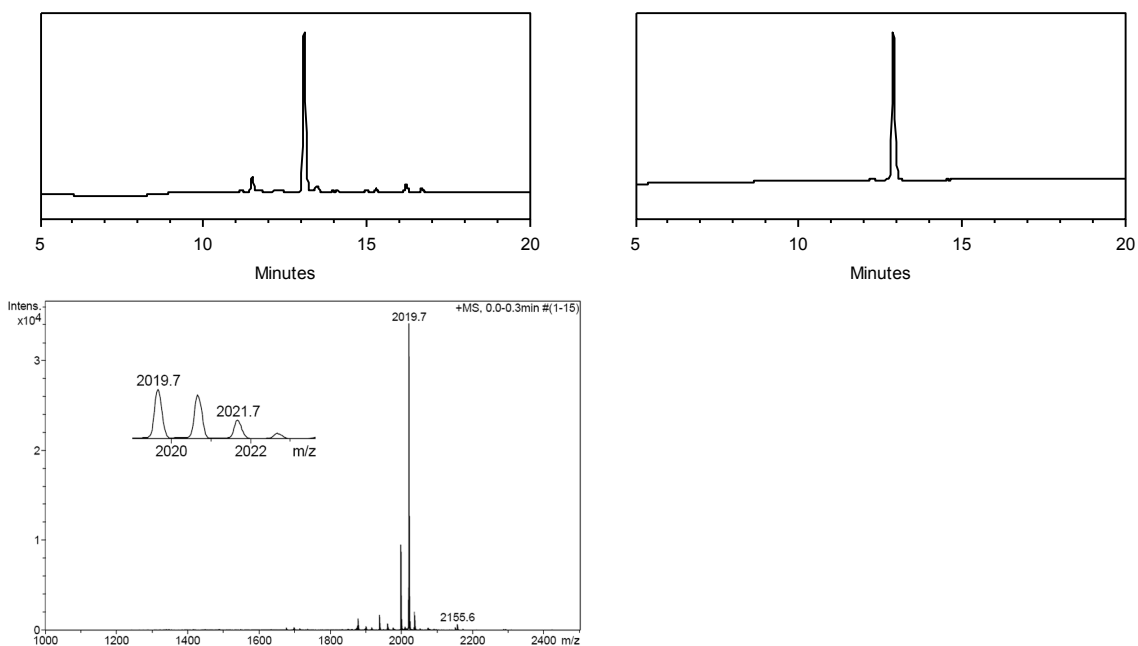


Figure 5-41. HPLC of the crude coupling reaction (left) and of the isolated complex **ED4G-Rh₂(OAc)₂** (right) and ESI-MS of the isolated complex **ED4G-Rh₂(OAc)₂**. Calculated mass $[M+Na]^+$: 2019.8; found: 2019.7.

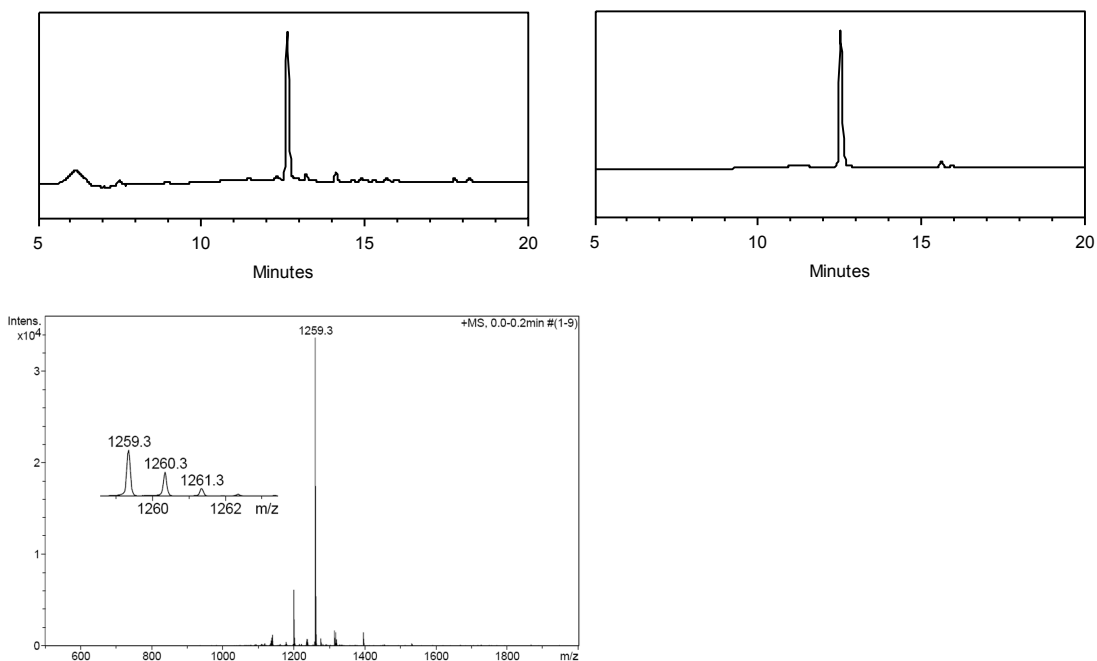


Figure 5-42. HPLC of the crude coupling reaction (left) and of the isolated complex **sED4-Rh₂(OAc)₂** (right) and ESI-MS of the isolated complex **sED4-Rh₂(OAc)₂**. Calculated mass $[M+Na]^+$: 1259.4; found: 1259.3.

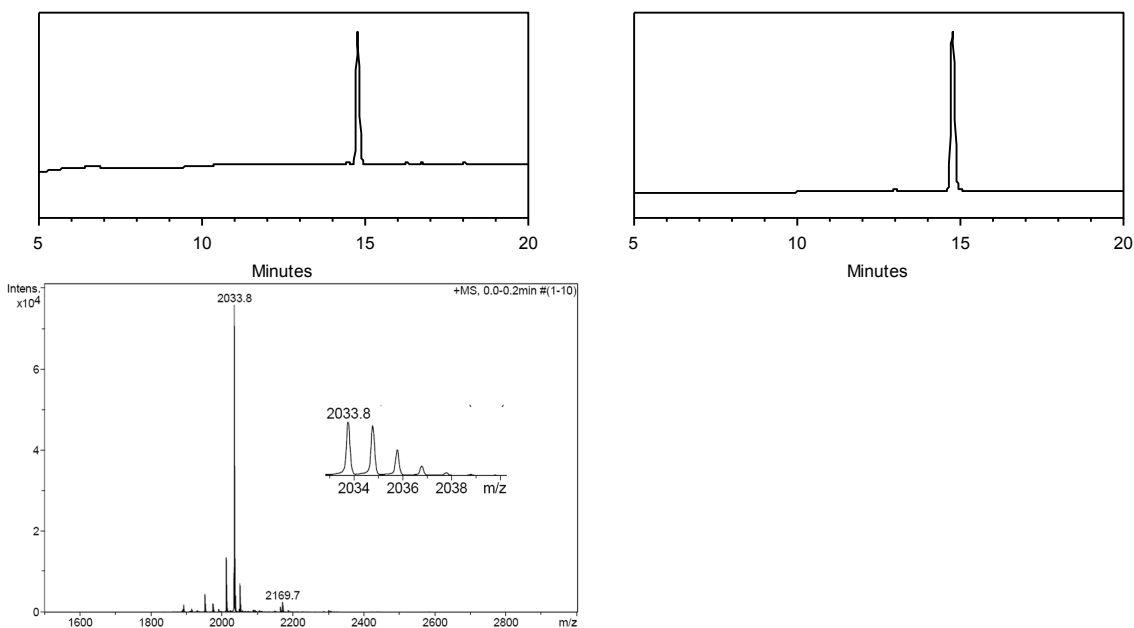


Figure 5-43. HPLC of the crude coupling reaction (left) and of the isolated complex **EE3G-Rh₂(OAc)₂** (right) and ESI-MS of the isolated complex **EE3G-Rh₂(OAc)₂**. Calculated mass $[M+Na]^+$: 2033.8; found: 2033.8.

5.8. References

- (1) Koder, R. L.; Valentine, K. G.; Smith, K. M.; Wand, A. J.; Dutton, P. L. *Biophys. J.* **2004**, *86*, 627A.
- (2) Shifman, J. M.; Moser, C. C.; Kalsbeck, W. A.; Bocian, D. F.; Dutton, P. L. *Biochemistry* **1998**, *37*, 16815.
- (3) Gibney, B. Ä.; Mulholland, S. Ä.; Rabanal, F.; Dutton, P. Ä. *Proc. Natl. Acad. Sci. USA* **1996**, *93*, 15041.
- (4) Laplaza, C. E.; Holm, R. H. *J. Am. Chem. Soc.* **2001**, *123*, 10255.
- (5) Nomura, A.; Sugiura, Y. *Inorg. Chem.* **2002**, *41*, 3693.
- (6) Long, E. C. *Acc. Chem. Res.* **1999**, *32*, 827.
- (7) DeGrado, W. F.; Summa, C. M.; Pavone, V.; Nistri, F.; Lombardi, A. *Annu. Rev. Biochem.* **1999**, *68*, 779.
- (8) Lombardi, A.; Summa, C. M.; Geremia, S.; Randaccio, L.; Pavone, V.; DeGrado, W. F. *Proc. Natl. Acad. Sci. U. S. A.* **2000**, *97*, 6298.
- (9) Bender, G. M.; Lehmann, A.; Zou, H.; Cheng, H.; Fry, H. C.; Engel, D.; Therien, M. J.; Blasie, J. K.; Roder, H.; Saven, J. G.; DeGrado, W. F. *J. Am. Chem. Soc.* **2007**, *129*, 10732.
- (10) Ramadan, D.; Cline, D. J.; Bai, S.; Thorpe, C.; Schneider, J. P. *J. Am. Chem. Soc.* **2007**, *129*, 2981.
- (11) Touw, D. S.; Nordman, C. E.; Stuckey, J. A.; Pecoraro, V. L. *Proc. Natl. Acad. Sci. U. S. A.* **2007**, *104*, 11969.
- (12) Geremia, S.; Di Costanzo, L.; Randaccio, L.; Engel, D. E.; Lombardi, A.; Nistri, F.; DeGrado, W. F. *J. Am. Chem. Soc.* **2005**, *127*, 17266.
- (13) Maglio, O.; Nistri, F.; Calhoun, J. R.; Lahr, S.; Wade, H.; Pavone, V.; DeGrado, W. F.; Lombardi, A. *J. Biol. Inorg. Chem.* **2005**, *10*, 539.

- (14) Negi, S.; Imanishi, M.; Matsumoto, M.; Sugiura, Y. *Chem. Eur. J.* **2008**, *14*, 3236.
- (15) Singh, U. P.; Singh, R. K.; Isogai, Y.; Shiro, Y. *Int. J. Pept. Res. Ther.* **2006**, *12*, 379.
- (16) Long, E. C. *Acc. Chem. Res.* **1999**, *32*, 827.
- (17) Gibney, B. R.; Mulholland, S. E.; Rabanal, F.; Dutton, P. L. *Proc. Nat. Acad. Sci. U.S.A.* **1996**, *93*, 15041.
- (18) Gibney, B. R.; Dutton, P. L. *Prot. Sci.* **1999**, *8*, 1888.
- (19) Litowski, J. R.; Hodges, R. S. *J. Biol. Chem.* **2002**, *277*, 37272.
- (20) Apostolovic, B.; Klok, H.-A. *Biomacromolecules* **2008**, *9*, 3173.
- (21) Marsden, H. R.; Korobko, A. V.; van Leeuwen, E. N. M.; Pouget, E. M.; Veen, S. J.; Sommerdijk, N. A. J. M.; Kros, A. *J. Am. Chem. Soc.* **2008**, *130*, 9386.
- (22) Yano, Y.; Yano, A.; Oishi, S.; Sugimoto, Y.; Tsujimoto, G.; Fujii, N.; Matsuzaki, K. *ACS Chem. Biol.* **2008**, *3*, 341.
- (23) Kwok, S. C.; Hodges, R. S. *J. Pept. Sci.* **2004**, *76*, 378.
- (24) Parry, D. A. D.; Fraser, R. D. B.; Squire, J. M. *J. Struct. Biol.* **2008**, *163*, 258.
- (25) Dong, H.; Hartgerink, J. D. *Biomacromolecules* **2006**, *7*, 691.
- (26) Alonso De Diego, S. A.; Gutiérrez-Rodríguez, M.; Pérez de Vega, M. J.; Gonzalez-Muniz, R.; Herranz, R.; Martin-Martinez, M.; Cenarruzabeitia, E.; Frechilla, D.; Rio, J. D.; Jimeno, M. L.; Garcia-Lopez, M. T. *Bioorg. Med. Chem. Lett.* **2006**, *16*, 3396.
- (27) Henchey, L. K.; Jochim, A. L.; Arora, P. S. *Curr. Opin. Chem. Biol.* **2008**, *12*, 692.
- (28) Garner, J.; Harding, M. M. *Org. Biomol. Chem.* **2007**, *5*, 3577.

- (29) Venkatraman, J.; Shankaramma, S. C.; Balaram, P. *Chem. Rev.* **2001**, *101*, 3131.
- (30) Schneider, J. P.; Kelly, J. W. *Chem. Rev.* **1995**, *95*, 2169.
- (31) Jackson, D. Y.; King, D. S.; Chmielewski, J.; Singh, S.; Schultz, P. G. *J. Am. Chem. Soc.* **1991**, *113*, 9391.
- (32) Blackwell, H. E.; Grubbs, R. H. *Angew. Chem.* **1998**, *110*, 3469.
- (33) Schafmeister, C. E.; Po, J.; Verdine, G. L. *J. Am. Chem. Soc.* **2000**, *122*, 5891.
- (34) Kim, Y.-W.; Verdine, G. L. *Bioorg. Med. Chem. Lett.* **2009**, *19*, 2533.
- (35) Cantel, S.; Le Chevalier Isaad, A.; Scrima, M.; Levy, J. J.; DiMarchi, R. D.; Rovero, P.; Halperin, J. A.; D'Ursi, A. M.; Papini, A. M.; Chorev, M. *J. Org. Chem.* **2008**, *73*, 5663.
- (36) Goodman, C. M.; Choi, S.; Shandler, S.; DeGrado, W. F. *Nat. Chem. Biol.* **2007**, *3*, 252.
- (37) Andrews, M. J. I.; Tabor, A. B. *Tetrahedron* **1999**, *55*, 11711.
- (38) Appella, D. H.; Christianson, L. A.; Klein, D. A.; Powell, D. R.; Huang, X.; Barchi, J. J.; Gellman, S. H. *Nature* **1997**, *387*, 381.
- (39) Cheng, R. P.; Gellman, S. H.; DeGrado, W. F. *Chem. Rev.* **2001**, *101*, 3219.
- (40) Horne, W. S.; Gellman, S. H. *Acc. Chem. Res.* **2008**, *41*, 1399.
- (41) Seebach, D.; Gardiner, J. *Acc. Chem. Res.* **2008**, *41*, 1366.
- (42) Cabezas, E.; Satterthwait, A. C. *J. Am. Chem. Soc.* **1999**, *121*, 3862.
- (43) Patgiri, A.; Jochim, A. L.; Arora, P. S. *Acc. Chem. Res.* **2008**, *41*, 1289.
- (44) Saraogi, I.; Hamilton, A. D. *Chem. Soc. Rev.* **2009**, *38*, 1726.
- (45) Ravi, A.; Prasad, B. V. V.; Balaram, P. *J. Am. Chem. Soc.* **1983**, *105*, 105.

- (46) Osapay, G.; Taylor, J. W. *J. Am. Chem. Soc.* **1990**, *112*, 6046.
- (47) Osapay, G.; Taylor, J. W. *J. Am. Chem. Soc.* **1992**, *114*, 6966.
- (48) Bracken, C.; Gulyas, J.; Taylor, J. W.; Baum, J. *J. Am. Chem. Soc.* **1994**, *116*, 6431.
- (49) Albert, J. S.; Hamilton, A. D. *Biochemistry* **1995**, *34*, 984.
- (50) Houston, M. E.; Campbell, A. P.; Lix, B.; Kay, C. M.; Sykes, B. D.; Hodges, R. S. *Biochemistry* **1996**, *35*, 10041.
- (51) Phelan, J. C.; Skelton, N. J.; Braisted, A. C.; McDowell, R. S. *J. Am. Chem. Soc.* **1997**, *119*, 455.
- (52) Schievano, E.; Bisello, A.; Chorev, M.; Bisol, A.; Mammi, S.; Peggion, E. *J. Am. Chem. Soc.* **2001**, *123*, 2743.
- (53) Fujimoto, K.; Oimoto, N.; Katsuno, K.; Inouye, M. *Chem. Comm.* **2004**, 1280.
- (54) Fujimoto, K.; Kajino, M.; Inouye, M. *Chem. Eur. J.* **2008**, *14*, 857.
- (55) Ousaka, N.; Sato, T.; Kuroda, R. *J. Am. Chem. Soc.* **2007**, *130*, 463.
- (56) Ghadiri, M. R.; Fernholz, A. K. *J. Am. Chem. Soc.* **1990**, *112*, 9633.
- (57) Lieberman, M.; Sasaki, T. *J. Am. Chem. Soc.* **1991**, *113*, 1470.
- (58) Anzellotti, A. I.; Farrell, N. P. *Chem. Soc. Rev.* **2008**, *37*, 1629.
- (59) Krizek, B. A.; Amann, B. T.; Kilfoil, V. J.; Merkle, D. L.; Berg, J. M. *J. Am. Chem. Soc.* **1991**, *113*, 4518.
- (60) Merkle, D. L.; Schmidt, M. H.; Berg, J. M. *J. Am. Chem. Soc.* **1991**, *113*, 5450.
- (61) Chen, J.; Kostic, N. M. *Inorg. Chem.* **1988**, *27*, 2682.
- (62) Dennis, A. M.; Howard, R. A.; Bear, J. L. *Inorg. Chim. Acta* **1982**, *66*, L31.
- (63) Imperiali, B. *Biochemistry* **2003**, *42*, 8604.

- (64) Kohn, W. D.; Kay, C. M.; Sykes, B. D.; Hodges, R. S. *J. Am. Chem. Soc.* **1998**, *120*, 1124.
- (65) Nitz, M.; Sherawat, M.; Franz, K. J.; Peisach, E.; Allen, K. N.; Imperiali, B. *Angew. Chem.* **2004**, *116*, 3768.
- (66) Martin, L. J.; Hähnke, M. J.; Nitz, M.; Wöhnert, J.; Silvaggi, N. R.; Allen, K. N.; Schwalbe, H.; Imperiali, B. *J. Am. Chem. Soc.* **2007**, *129*, 7106.
- (67) Su, X.-C.; McAndrew, K.; Huber, T.; Otting, G. *J. Am. Chem. Soc.* **2008**, *130*, 1681.
- (68) Ma, M. T.; Hoang, H. N.; Scully, C. C. G.; Appleton, T. G.; Fairlie, D. P. *J. Am. Chem. Soc.* **2009**, *131*, 4505.
- (69) Hoang, H. N.; Bryant, G. K.; Kelso, M. J.; Beyer, R. L.; Appleton, T. G.; Fairlie, D. P. *Inorg. Chem.* **2008**, *47*, 9439.
- (70) Kelso, M. J.; Beyer, R. L.; Hoang, H. N.; Lakdawala, A. S.; Snyder, J. P.; Oliver, W. V.; Robertson, T. A.; Appleton, T. G.; Fairlie, D. P. *J. Am. Chem. Soc.* **2004**, *126*, 4828.
- (71) Beyer, R. e. L.; Hoang, H. N.; Appleton, T. G.; Fairlie, D. P. *J. Am. Chem. Soc.* **2004**, *126*, 15096.
- (72) Kelso, M. J.; Hoang, H. N.; Oliver, W.; Sokolenko, N.; March, D. R.; Appleton, T. G.; Fairlie, D. P. *Angew. Chem.* **2003**, *115*, 437.
- (73) Hoang, H. N.; Bryant, G. K.; Kelso, M. J.; Beyer, R. L.; Appleton, T. G.; Fairlie, D. P. *J. Inorg. Biochem.* **2003**, *96*, 146.
- (74) Kelso, M. J.; Hoang, H. N.; Appleton, T. G.; Fairlie, D. P. *J. Am. Chem. Soc.* **2000**, *122*, 10488.
- (75) Sculimbrene, B. R.; Imperiali, B. *J. Am. Chem. Soc.* **2006**, *128*, 7346.
- (76) Reynolds, A. M.; Sculimbrene, B. R.; Imperiali, B. *Bioconjugate Chem.* **2008**, *19*, 588.

- (77) Kutchukian, P. S.; Yang, J. S.; Verdine, G. L.; Shakhnovich, E. I. *J. Am. Chem. Soc.* **2009**, *131*, 4622.
- (78) Marqusee, S.; Robbins, V. H.; Baldwin, R. L. *Proc. Natl. Acad. Sci. USA* **1989**, *86*, 5286.
- (79) Huyghues-Despointes, B. M. P.; Martin Scholtz, J.; Baldwin, R. L. *Prot. Sci.* **1993**, *2*, 80.
- (80) Huyghues-Despointes, B. M. P.; Scholtz, J. M.; Baldwin, R. L. *Prot. Sci.* **1993**, *2*, 1604.
- (81) O'Neil, K. T.; DeGrado, W. F. *Science* **1990**, *250*, 646.
- (82) Q. Teng, *Structural Biology: Practical NMR Applications*, Springer, New York, 2005
- (83) Hansen, J.; Davies, H. M. L. *Coord. Chem. Rev.* **2008**, *252*, 545.
- (84) Lou, Y.; Remarchuk, T. P.; Corey, E. J. *Journal of the American Chemical Society* **2005**, *127*, 14223.
- (85) Jordan, R. B. *Reaction Mechanisms of Inorganic and Organometallic Systems*,; 2nd ed. ed.; Oxford University Press: New York, 1998.
- (86) Chen, Z.; Popp, B. V.; Bovet, C. L.; Ball, Z. T. *ACS Chem. Biol.* **2011**, *6*, 920.
- (87) Zaykov, A. N.; Ball, Z. T. *Tetrahedron* **2011**, *67*, 4397.
- (88) Popp, B. V.; Ball, Z. T. *Chem. Sci.* **2011**, *2*, 690.
- (89) Sambasivan, R.; Ball, Z. T. *J. Am. Chem. Soc.* **2010**, *132*, 9289.
- (90) Popp, B. V.; Ball, Z. T. *J. Am. Chem. Soc.* **2010**, *132*, 6660.
- (91) Brunger, A. T.; Adams, P. D.; Clore, G. M.; DeLano, W. L.; Gros, P.; Grosse-Kunstleve, R. W.; Jiang, J. S.; Kuszewski, J.; Nilges, M.; Pannu, N. S.; Read, R. J.; Rice, L. M.; Simonson, T.; Warren, G. L. *Acta Crystallogr., Sect D: Biol. Crystallogr.* **1998**, *54*, 905.

- (92) Goddard, T. D.; Kneller, D. G.; University of California, San Francisco.
- (93) Lou, Y.; Remarchuk, T. P.; Corey, E. J. *J. Am. Chem. Soc.* **2005**, *127*, 14223.

Chapter 6

Kinetic and stereoselectivity effects of phosphite ligands in dirhodium catalysis

6.1. Introduction

Dirhodium complexes are one of the most synthetically useful examples of homogenous catalysts containing multiple metal atoms.¹⁻³ A large number of enantioselective reactions have been developed through the design of chiral carboxylate and carboxamidate ligands for the bridging equatorial sites of the dirhodium core, and these reactions play important roles in the synthesis of diverse classes of chiral targets. The development of selective dirhodium catalysts for diazo decomposition has typically treated a dirhodium complex as though it were a mono-metallic site. Reaction with diazo compounds is assumed to result in the formation of a metallocarbene intermediate with loss of dinitrogen. The reactive metallocarbene intermediate then undergoes reaction with substrate through X–H insertion, cyclopropanation, ylide formation, or other processes.^{3,4} Because the two labile, axial coordination sites point in opposite directions, they are typically assumed to catalyze reactions independently. Homoleptic (i.e. all ligands are identical) tetracarboxylate and tetraamidate complexes have an axis of symmetry perpendicular to the metal-metal bond, and so the two metal sites are chemically equivalent as well. However, polymetallic complexes offer attractive targets for the development of selective catalysts precisely because

metals can interact in diverse ways, allowing dual binding of substrate(s) or influencing the catalytic cycle through steric or electronic effects.

In the context of examining peptide ligands for enantioselective catalysis, I decided to examine the potential for improving the enantioselectivity through the addition of labile axial ligands. In pursuing this line of inquiry, I was aware that added ligands almost certainly inhibit diazo decomposition (Figure 6-1). Indeed, a previous kinetic study with other ligand classes concluded that ligated dirhodium complexes are not competent catalysts for diazo decomposition, even if one of the two rhodium atoms remains free of ligand.^{5,6} Despite efforts to understand the mechanism of dirhodium-catalyzed diazo reactions,⁵⁻¹² mechanistic understanding of product-determining steps, which occur after the turnover-limiting diazo-decomposition step, is limited. The effects of the coordination environment of the distal rhodium atom on catalytic reactivity may be an important variable in determining catalytic selectivity and efficiency, yet is little studied. Sporadic evidence indicates that catalysis can be altered with solution additives,¹³⁻¹⁵ including an observation that phosphate and phosphine-oxide additives can rescue enantioselectivity from the detrimental effects of trace water in asymmetric cyclopropanation reactions.¹⁴ Recently the catalytic activity of dirhodium complexes with exchange-inert NHC ligands bound to an axial site has been described.¹⁶⁻¹⁹ In this chapter, I present the discovery that phosphite complexes improve the enantioselectivity observed in silane insertion reactions²⁰⁻²⁷ catalyzed by peptide-dirhodium complexes.^{28,29} Presented is a kinetic analysis of the process that sheds light on the equilibrium and kinetic parameters involved in reaction with phosphite ligands.

Dirhodium metallopeptides are kinetically inert coordination complexes that are readily synthesized by direct metalation of a fully deprotected peptide ligand²⁸ and adopt discrete secondary structures that are stabilized by chelate binding to the dirhodium center.²⁹ While in a typical catalyst four molecules of chiral ligand around the dirhodium center are required for asymmetric catalysis, I have been interested in asymmetric catalysis with a single chelating *bis*-carboxylate peptide ligand at a rhodium center that also contains two (achiral) acetate ligands. In general, these mono-peptide catalysts provide modest stereoselectivity in silane insertion reactions (Table 6-1).

Selectivity is improved in *bis*-peptide catalysts,²⁷ but the development of selective mono-peptide catalysts is desirable for many purposes, including screening peptide ligands directly on solid support.

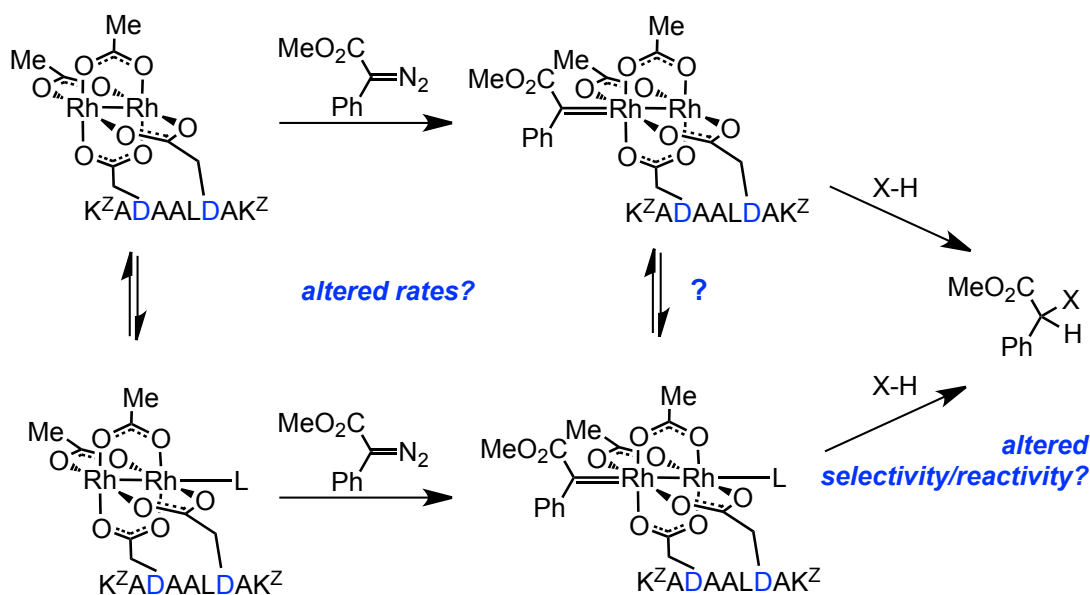
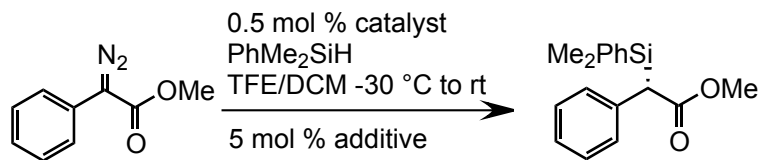
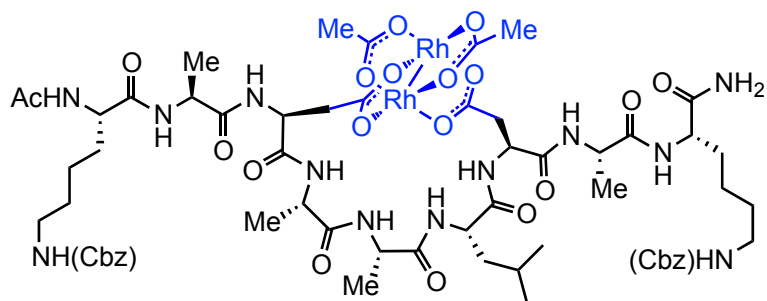


Figure 6-1. Distal ligation and X-H insertion of dirhodium metalcarbene intermediates.

Table 6-1. Screen of additives for increased enantioselectivity.



catalyst = Rh₂(OAc)₂(K^ZADAALDAK^Z)



additive	% ee
none	50
Tris(2,4-di-tert-butylphenyl) phosphite	52
(PhO)₃P	66
(EtO) ₃ P	50
(MeO) ₃ P	53
DMSO	51
Et ₂ NOH	51
Pyridine	48
(<i>i</i> -Pr) ₂ EtN	52
9-Cyanoanthracene	42
PhCN	48
(biphenyl)(tBu) ₂ P	54
Ad ₂ PhP	53
(Ph) ₃ P	46

6.2. Phosphite additives and enantioselectivity

Upon initial screening, the complex $\text{Rh}_2(\mathbf{L1})(\text{OAc})_2$, containing one chelating peptide ligand and two achiral acetate groups, catalyzes the silane insertion reaction of dimethylphenylsilane and ethyl phenyldiazoacetate with 50% ee (Table 6-1). I examined additives that might bind to the dirhodium core and affect enantioselectivity. Although most additives had a negligible or negative effect on enantioselectivity, the addition of triphenylphosphite improved the product ee to 66%.

The beneficial effect on product ee was general across a variety of peptide ligands; the addition of 10 equiv, relative to dirhodium, produced modest increases (5–18%) in ee across catalysts with a variety of peptide sequences (Table 6-2). The best results were observed with catalyst $\text{Rh}_2(\mathbf{L2})(\text{OAc})_2$, which afforded the product in 88% ee, and the best enhancement in ee was observed with the $\text{Rh}_2(\mathbf{L1})(\text{OAc})_2$ catalyst.

6.3. Kinetics

To shed light on the effect of phosphite on enantioselective dirhodium catalysis, a kinetic analysis of the process was performed. The loss of dinitrogen to form a metallocarbene is irreversible and turnover limiting, so that the kinetics of the reaction can be expressed as a function of two ligand association constants (K_{i1} and K_{i2}), a rate constant for reaction in the absence of phosphite (k_1), and a constant (γ) that describes the catalytic power of the phosphite complex relative to the free catalyst, as shown in Figure 6-4. The association constants were determined by fitting UV-vis absorption spectra as a function of phosphite concentration (Figure 6-2 and Figure 6-3).³⁰⁻³³ For $\text{Rh}_2(\mathbf{L1})(\text{OAc})_2$, $\log K_{i1}$ and $\log K_{i2}$ are 5.38 and 3.31, respectively (Table 6-

2). These values are consistent with negative cooperativity binding typical of dirhodium complexes.³⁰⁻³³

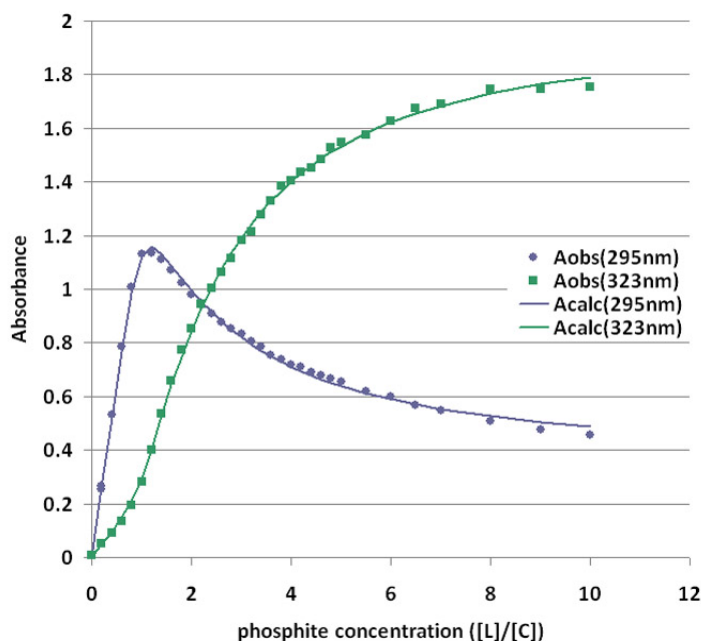


Figure 6-2. Fitting of UV-vis data for $(L1)Rh_2(OAc)_2$. Absorbance at 323 nm and 295 nm correspond to the complexes with a one and two axial ligands respectively.

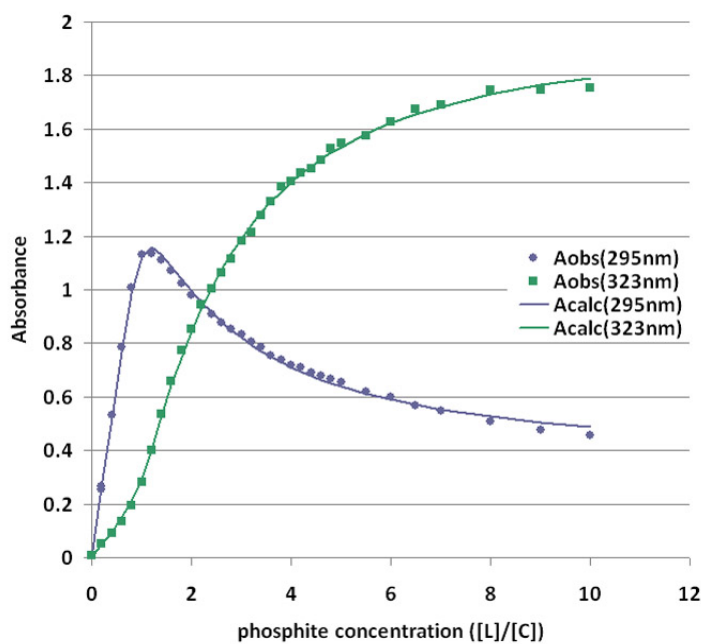


Figure 6-3. Fitting of UV-vis data for $Rh_2(OAc)_4$. Absorbance at 323 nm and 295 nm correspond to the complexes with a one and two axial ligands respectively.

Table 6-2. Triphenylphosphite as an additive for enantioselective dirhodium reactions at 0 °C. ^a Scaled up reaction afforded 84% yield.

ligand	sequence	ee, %	
		no additive	P(OPh) ₃
L1	K ^Z ADAALDAK ^Z	40	58
L2	K ^Z TDAAIDAK ^Z	77	88 ^a
L3	K ^Z TDGATDAK ^Z	61	76
L4	K ^Z NDAAIDAK ^Z	82	87

The values for Rh₂(**L1**)(OAc)₂ are somewhat lower than those for the parent compound, Rh₂(OAc)₄ (6.09 and 3.96), indicating that the bulky peptide ligand disfavors axial ligation. The rate constant k_c can be measured for reactions without phosphite or fit numerically. The relationship between phosphine concentration and reaction rate provides a plot of concentration vs. 1/rate that allows determination of the reactivity ratio, γ . Disappearance of the diazo substrate was monitored by HPLC and/or UV absorption at varying concentrations of phosphite. Individual reactions displayed linear plots of $-\log([\text{diazo}]/[\text{diazo}]_0)$ vs. time, indicative of clean kinetics that are first-order in substrate (Figure 6-14). The constant γ was obtained by fitting the rate constants to the kinetic data using a least-squares fitting method (Figure 6-5).³⁴ A value of 0.013 was obtained for γ (Table 6-3).

Table 6-3. Experimentally determined kinetic and thermodynamic parameters.

$\log K_{il}$ (M ⁻¹)	5.38
$\log K_{il}$ (M ⁻¹)	3.31
k_c (M ⁻¹ s ⁻¹)	5.46
γ	0.013

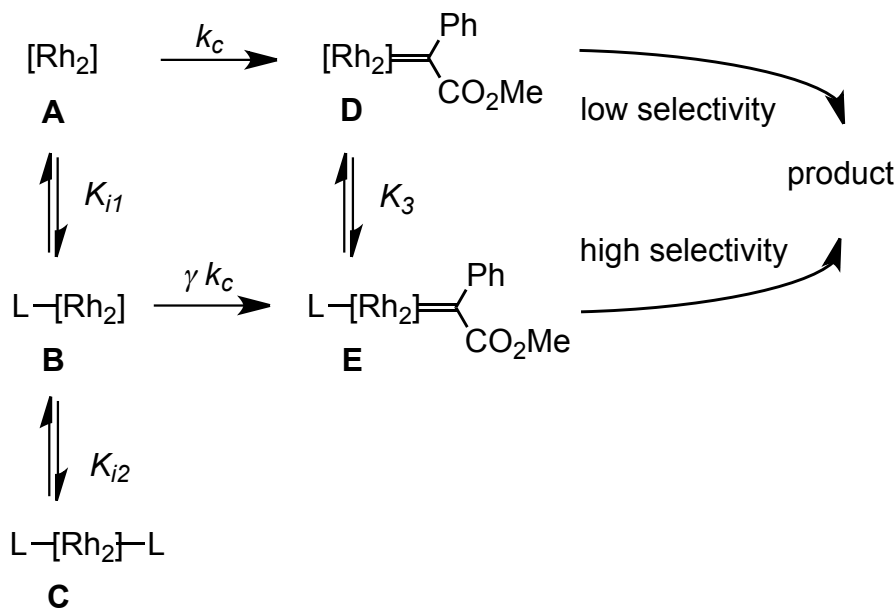


Figure 6-4. Mechanism of dual-path enantioselective catalysis.

6.4. Discussion

It is not apparent that ligand additives should be a successful strategy for altering selectivity in dirhodium catalysis. Each metal center contains a single open coordination site, so that ligand-bound rhodium atoms are necessarily catalytically inactive. In addition, the two axial sites of the dirhodium core point in opposite directions, projecting into very different regions of space. Finally, a previous kinetic study of dirhodium catalysis in nonpolar solvent in the presence of weak ligands (such as THF) concluded that ligand-bound catalysts (Figure 6-4 **B**) are unreactive.^{5,6} Nonetheless, it is clear that triphenylphosphite provides an enhancement in enantioselectivity with the dirhodium metallopeptide catalysts described here. The basis for this additive effect is difficult to establish. In the presence of a single peptide ligand, there is no symmetry in the complex and the two dirhodium sites are chemically nonequivalent. Part of the initial rationale for the use of added ligand was the belief that axial ligands might bind and change the site of

catalysis. However, the difference between two association constants K_{i1} and K_{i2} are comparable to the observed with dirhodium tetraacetate, implying that the two non-equivalent rhodium atoms bind phosphite with similar affinity. Alternatively, electronic or steric effects of distal ligand binding may alter selectivity.

The acquired kinetic data is inconsistent with $\gamma=0$, as would be the case if ligand-bound catalysts (Figure 6-4, **B**) are not kinetically competent in diazo decomposition reactions. Least-squares fitting of the kinetic data provides a measured γ of 1.3% (Figure 6-5). Fitting the data in Figure 6-5 under the alternative assumption that $\gamma=0$ provides a model that is inconsistent with the obtained data (Figure 6-5, dashed curve). Indeed, the apparent linear relationship in Figure 6-5 requires either that $\gamma=0$ and $K_{i2}=0$ reducing the system to simple, single-site inhibition, or else that both γ and K_{i2} are non-zero. This differs from a previous report, which determined that $\gamma=0$ for a series of weak oxygen donor ligands.^{5,6} Despite the fact that ligand-bound

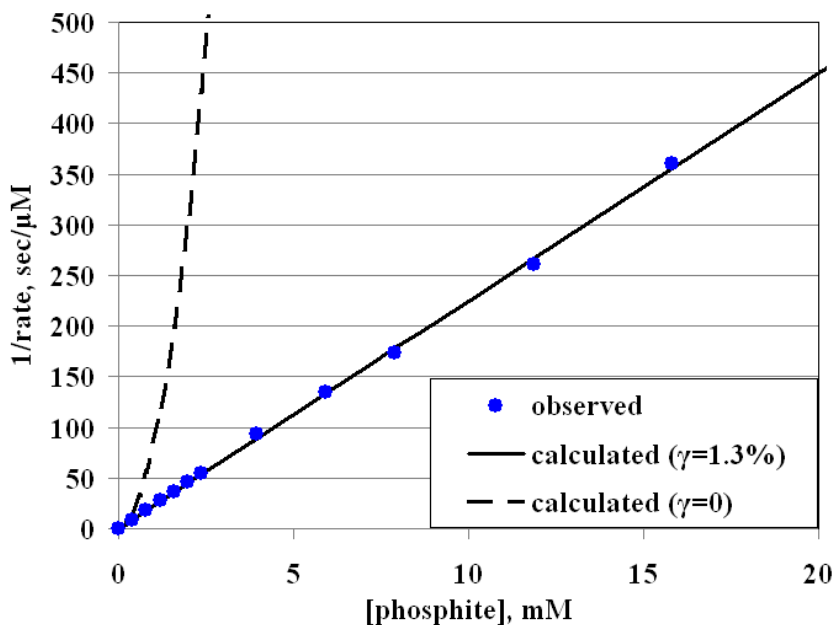


Figure 6-5. Plot of kinetic data and fit for the reactivity ratio, γ .

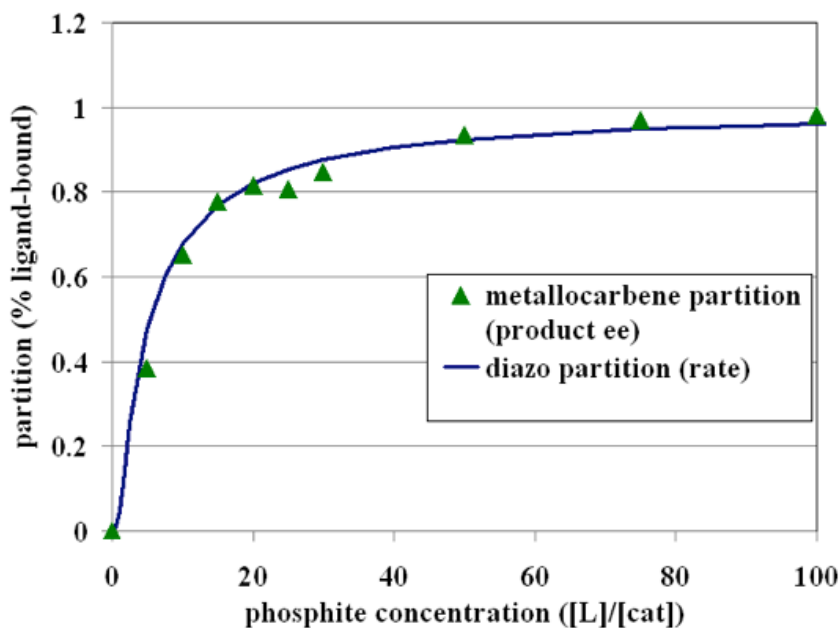


Figure 6-6. Experimental measurement of partitioning between phosphite-bound and unligated catalyst for the two steps of the reaction, diazo decomposition and silane insertion. Diazo partition determined from kinetic data; metallocarbene partition determined from product ee.

catalysts are less reactive ($\gamma < 1$), ligand-bound intermediates (**B,E**) can still be the predominant pathway in catalytic reactions. For example, in the reaction described in the Table 6-1, ligand-bound intermediates (**B,E**) are on the predominant catalytic pathway (i.e., partition > 0.5 , see Figure 6-6) for phosphite concentrations ≥ 6 mol %.

Changes in product enantioselectivity as a function of phosphite concentration require that triphenylphosphite is involved in the enantio-determining step. Because the turnover-limiting step in dirhodium-catalyzed diazo reactions is irreversible diazo decomposition to afford the metallocarbene, it is difficult to use kinetic methods to probe the subsequent steps that determine product selectivity. Gleaning information about steps

after the formation of the metallocarbene requires creative substrate design to derive kinetic and mechanistic information from product ratios.^{11,12}

Assuming two reactive metallocarbenes are involved in catalysis—a (less selective) free metallocarbene and a (more selective) phosphite-bound metallocarbene—it is possible to define a metallocarbene partition, the percentage of silane insertion that occurs through the ligand-bound metallocarbene (Figure 6-4, **E**). Examining the product *ee* as a function of ligand concentration provides a measure of this metallocarbene partition (Figure 6-6). The measurement of reaction kinetics was used to define a diazo partition—a function of catalyst and ligand concentration—that defines the percentage of diazo decomposition through the ligand-bound catalyst (Figure 6-4, **B**). In a general sense, these two partitions will be rigorously identical only if silane insertion is faster than ligand exchange of the metallocarbene intermediate. However, coincidental overlapping partition curves is possible for individual reactions, even if insertion is not faster than ligand exchange, based on the rates of metallocarbene interconversion and product formation. As shown in the Figure 6-6, the diazo partition, derived from kinetics experiments, is identical to the metallocarbene partition. In other words, the fraction of substrate following the bottom path (Figure 6-4) during diazo decomposition is the same as that during product formation. This observation implies that metallocarbene intermediates do not interconvert through ligand exchange, subject to the caveat of possible coincidental overlap described above. Future work with other substrates may enable to address this possibility. The presented analysis carries with it a number of assumptions that could affect the results. The mono-ligated species (Figure 6-4, **B**), as well as both metallocarbene

intermediates, represent a mixture of ligand isomers. Because kinetic analysis is based on the steady-state approximation, the ratio of these species must remain constant during a reaction and thus the existence of these isomers does not affect the kinetic results described here. This analysis also ignores ligation to the axial sites by solvent molecules. Although trifluoroethanol certainly does bind to the axial sites, this binding is weak and transient and is accounted for under steady-state assumptions. Finally, a previous study modeled the diazo decomposition process as a combination of substrate binding and dinitrogen expulsion steps. This approach is compatible with the analysis presented here, and the reactivity ratio γ is equivalent to the ratio of two constants, β/α , used in that approach.^{5,6}

6.5. Conclusion

This work demonstrates the potential of axial ligands as a control element in dirhodium-catalysis. In the present context, a phosphite additive enables synthetically useful enantioselectivity in a dirhodium mono-peptide complex. In the absence of phosphite additives, achieving synthetically useful levels of enantioselectivity required the use of *bis*-peptide complexes, which require chromatographic separation of the two isomers that differ in the orientation of the ligated peptides (parallel and antiparallel in the respect to the N and C termini).^{27,29} Because axial ligands inherently inhibit catalysis through both competitive and non-competitive mechanisms, it may be possible to build carboxylate ligands with a single pendant axial ligand to achieve improved selectivity with minimal sacrifice of reactivity.

Axial-bound dirhodium centers have been proposed in a few circumstances, beyond enantioselectivity questions, to play a role in chemoselectivity and reaction efficiency. However, it has been difficult to

establish the role of added ligand and its presence on the catalytic pathway. In providing the first nonzero measurement of the reactivity ratio, γ , this paper provides a framework for investigating other instances of ligand effects and provides a foundation for the use of ligands to alter other selectivity types in dirhodium catalysis.

6.6. Experimental Section

6.6.1. General information

Peptide synthesis. All peptides were synthesized with an Advanced ChemTech APEX 396 Automated Multipetide Synthesizer using standard solid-phase Fmoc protocols. The peptides are acetylated at N-termini and amides at the C-termini. All lysine side chains are capped with carboxybenzyl protecting group (Z) and remain unprotected. The purification was accomplished by reverse-phase HPLC with gradients of water-acetonitrile containing 0.1% trifluoroacetic acid, and peptides were isolated by lyophilization. Analysis and purity assessment was attained by mass spectrometry and analytical HPLC.

HPLC analysis and purification. HPLC was performed on a Shimadzu CBM-20A instrument with Phenomenex Jupiter 4 μ Proteo 90A (250 \times 15 mm preparative) and Phenomenex Jupiter 4 μ Proteo 90A (250 \times 4.6 mm analytical) columns. Flow rates of 8 mL/min and 1 mL/min were used for preparative and analytical columns, respectively. Analytical and preparative HPLC were performed with gradient of acetonitrile in water. Both solvents contained 0.1% trifluoroacetic acid (TFA) unless otherwise noted. Two wavelengths — 220 nm and 300 nm — were used to allow for independent analysis of peptides and dirhodium complexes.

Mass Spectrometry. MALDI-MS and MS/MS analyses were performed on a Bruker Daltonics Autoflex MALDI- TOF/TOF mass spectrometer with CHCA matrix (10 mg/mL, Thermo Scientific Pierce). ESI-MS was performed on Bruker Daltonics micrOTOF instrument.

NMR Spectroscopy. 1D Spectra were measured with Bruker 500 UltraShield™ (500 MHz) spectrometer or Oxford (400 MHz) spectrometer. ¹H NMR are reported in units of part per million (ppm). Standard abbreviations are used to indicate signal multiplicity: s, singlet; d, doublet; t, triplet; q, quartet; m, multiplet. Coupling constant are reported as *J* value in Hertz (Hz). nH describes the number of protons (n) from integration.

6.6.2. Synthetic procedures

Phenyl diazo acetate was prepared according to the published procedure.³⁵

General procedure for the synthesis of dirhodium metallopeptides from *cis*-Rh₂(tfa)₂(OAc)₂. Peptide (1 equiv) and *cis*-Rh₂(tfa)₂(OAc)₂ (1 equiv) were dissolved in TFE (calculated for 1.0 mM peptide concentration). The reaction was heated to 50 °C for 3 h and monitored by HPLC. Purification of the metallopeptides was performed by direct injection of the reaction mixture on a preparative RP-HPLC column. All complexes were isolated as a green solid upon lyophilization: (**L1**)Rh₂(OAc)₂ (2.3 mg, 60% yield), (**L2**)Rh₂(OAc)₂ (1.7 mg, 67% yield), (**L3**)Rh₂(OAc)₂ (1.4 mg, 50% yield), (**L4**)Rh₂(OAc)₂ (2.2 mg, 70% yield).

6.6.3. Analytical data

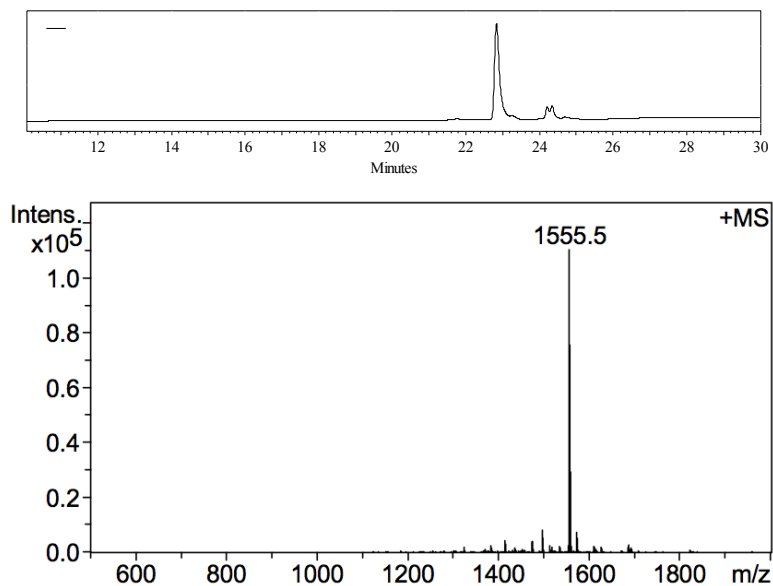


Figure 6-7. HPLC trace and ESI-MS of the (L1)Rh₂(OAc)₂ metallopeptide. Calculated mass [M+Na]⁺: 1555.5; found: 1555.5.

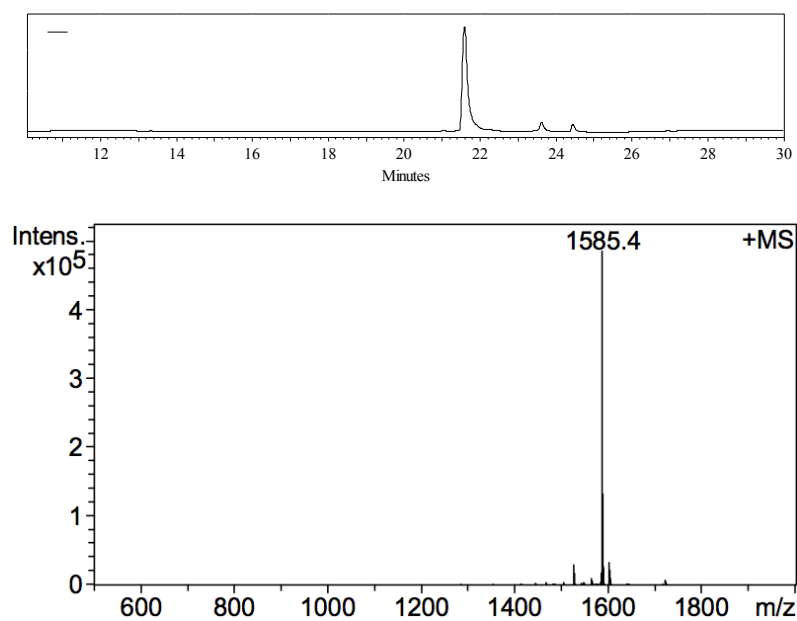


Figure 6-8. HPLC trace and ESI-MS of the (L2)Rh₂(OAc)₂ metallopeptide. Calculated mass [M+Na]⁺: 1585.5; found: 1585.4.

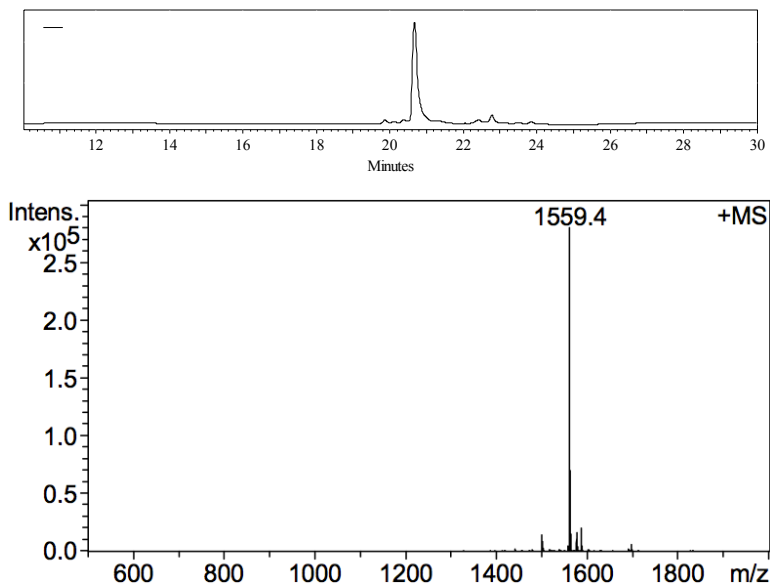


Figure 6-9. HPLC trace and ESI-MS of the (L3)Rh₂(OAc)₂ metallopeptide. Calculated mass [M+Na]⁺: 1559.4; found: 1559.4.

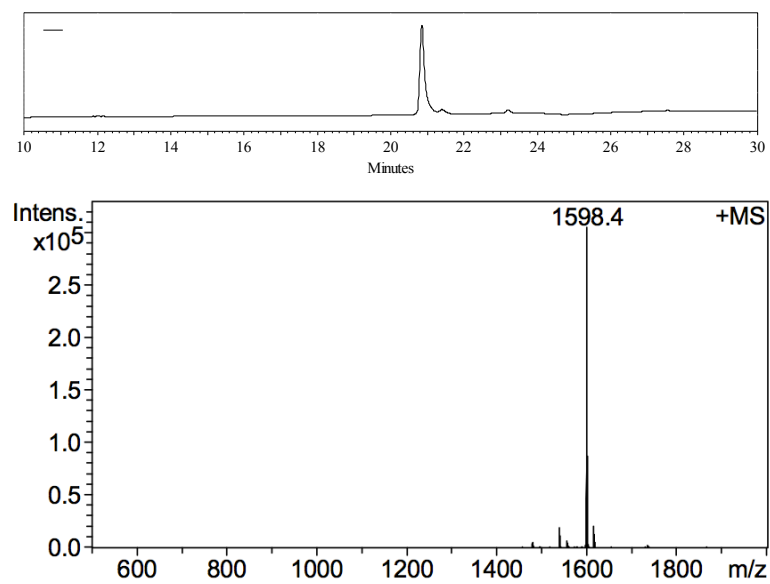


Figure 6-10. HPLC trace and ESI-MS of the (L4)Rh₂(OAc)₂ metallopeptide. Calculated mass [M+Na]⁺: 1598.5; found: 1598.4.

6.6.4. Ligand screening

General procedure for enantioselective silane insertion with phosphite additives. Methyl phenyldiazoacetate (1 equiv, 7.8 μmol) was mixed with silane (2 equiv, 15.6 μmol) in trifluoroethanol (200 μL) and equilibrated to $-30\text{ }^{\circ}\text{C}$ in Neslab CB-80 cold bath; peptide catalyst (0.5 %, 39 nmol) is dissolved and trifluoroethanol (100 μL) and ligand (5 %, 390 nmol) was added in DCM solution (200 μL). After equilibration of the catalyst solution to $-30\text{ }^{\circ}\text{C}$, the mixture of starting materials was added and reaction proceeded overnight. The reactions were moved to ice ($0\text{ }^{\circ}\text{C}$) and allowed to warm up to rt. The crude mixtures were dried under nitrogen jet and the product was isolated by silica-gel column, eluting with ether/hexanes (1:99). Enantioselectivity was determined by chiral HPLC (Phenomenex Lux 5 μ , eluent: isopropanol-hexanes (10:90). Analytical data for the product (S)-Methyl 2-dimethylphenylsilyl-2-phenylacetate can be found in the previous work.²⁷

6.6.5. Equilibrium constants.

The equilibrium constants, K_{i1} and K_{i2} , were determined from UV-vis titration experiments according to the method of Bear.⁸ Measurements were taken on Jasco spectropolarimeter at $0\text{ }^{\circ}\text{C}$. The sample of dirhodium complex in 3:2 mixture of trifluoroethanol/DCM (78 μM , 4 mL) and solution of triphenyl phosphite in DCM (6.24 mM) were equilibrated at $0\text{ }^{\circ}\text{C}$. The dirhodium solution was titrated with phosphite and UV-vis spectra were acquired at each increment. The absorption data at 295 nm and 323 nm (Equation 6-1) were fitted using least-square procedure to three-state equilibrium model (Figure 6-2 and Figure 6-3) using method implemented in

Equation 6-1. Absorption values at each wavelength are compound of contribution from CL and CL2 species.

$$A_{calc(295)} = \varepsilon_{295}^{CL} \times [CL] + \varepsilon_{295}^{CL2} \times [CL2]$$

$$A_{calc(323)} = \varepsilon_{323}^{CL} \times [CL] + \varepsilon_{323}^{CL2} \times [CL2]$$

Excel.¹¹. The fitting parameters are equilibrium constants K_{i1} and K_{i2} , extinction coefficients of CL and CL2 complexes at both 295 nm and 323 nm.

Determining the concentration of free phosphite, [L], requires solving the third-degree polynomial obtained upon solving the equilibrium expressions in Equation 6-2:

Equation 6-2. Third-degree polynomial describing the equilibrium in **Figure 6-4**.

$$K_{i1}K_{i2}[L]^3 + (2[C]_0K_{i1}K_{i2} - [L]_0K_{i1}K_{i2} + K_{i1})[L]^2 + ([C]_0K_{i1} - [L]_0K_{i1} + 1)[L] - [L]_0 = 0$$

for $[C]_0$ = total metalloprotein concentration and $[L]_0$ = total phosphite concentration. Solving this equation was accomplished with an add-in for Excel.³⁶

Concentrations of free metalloprotein, [C]; the monophosphite complex, [CL]; and the *bis*-phosphite complex, [CL₂], were determined from the Equation 6-3 (Figure 6-13).

Equation 6-3. Equilibrium concentrations of the dirhodium species.

$$[C] = \frac{[C]_0}{(1 + K_{i1}[L] + K_{i1}K_{i2}[L]^2)}$$

$$[CL] = \frac{K_{i1}[L][C]_0}{1 + K_{i1}[L] + K_{i1}K_{i2}[L]^2}$$

$$[CL_2] = \frac{K_{i1}K_{i2}[L]^2[C]_0}{(1 + K_{i1}[L] + K_{i1}K_{i2}[L]^2)}$$

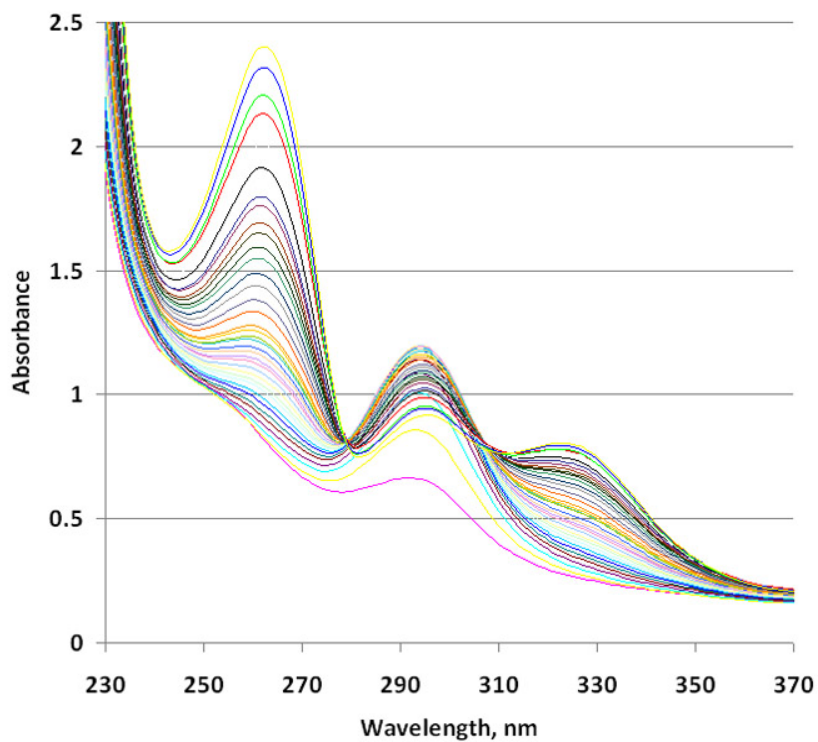


Figure 6-11. Raw UV-vis data for $(L1)Rh_2(OAc)_2$.

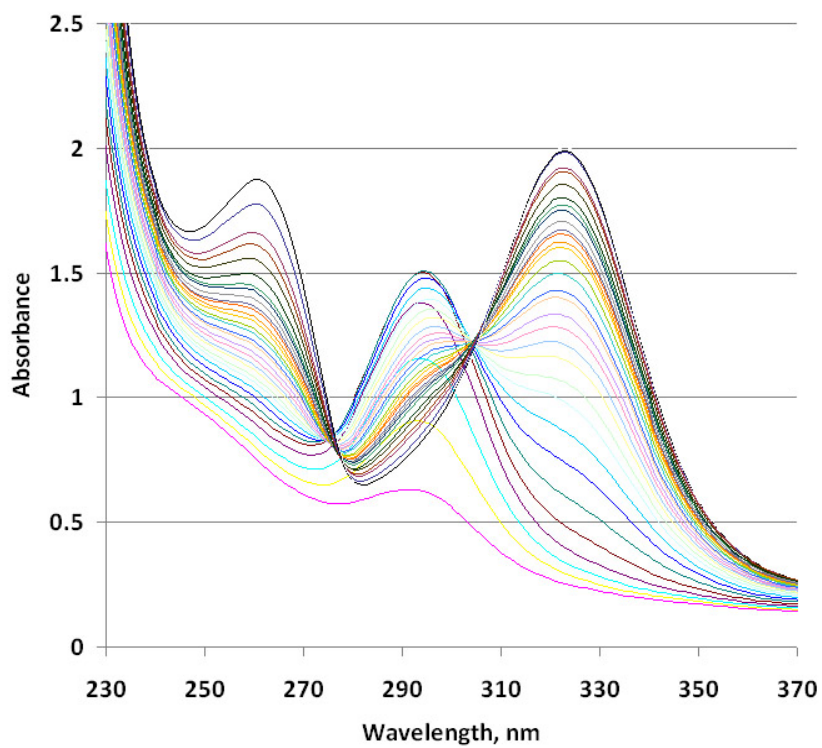


Figure 6-12. Raw UV-vis data for $Rh_2(OAc)_4$.

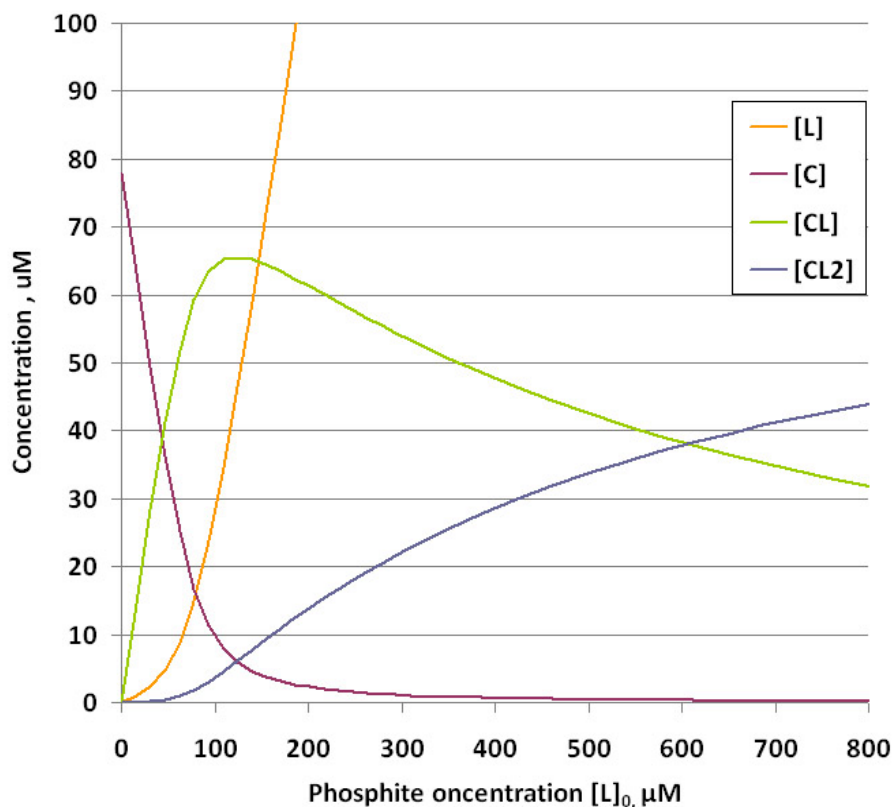


Figure 6-13. Concentrations of the dirhodium species and the ligand.

6.6.6. Rate measurements.

Methyl phenyldiazoacetate (1 equiv, 6.2 μmol) was mixed with silane (2 equiv, 12.4 μmol) in trifluoroethanol (160 μL) and cooled to 0 °C. In a separate vial, solid Rh₂(**L1**)(OAc)₂ (0.5 %, 31 nmol) was dissolved in trifluoroethanol (80 μL) and ligand (variable amounts) was added in CH₂Cl₂ (160 μL). After cooling to 0 °C, the solution of starting materials was added. Aliquots (10 μL) were taken from the reaction mixture at various times and quenched with acetonitrile (90 μL). The conversion of the reaction was determined by analytical HPLC (Phenomenex Kinetex 2.6μ, water-acetonitrile gradient). Graphs of $-\log([\text{diazo}]/[\text{diazo}]_0)$ vs. time were linear, indicating clean first-order kinetics (Figure 6-14).

The reactivity ratio, γ , was fit using the least-squares method referenced above, according to the rate law,

Equation 6-4. Overall rate of the reaction.

$$rate = k_c[C] + \gamma k_c[CL]$$

where k_c = rate constant measured in the absence of phosphite and $[C]$ and $[CL]$ were determined from the equilibrium constants measured above.

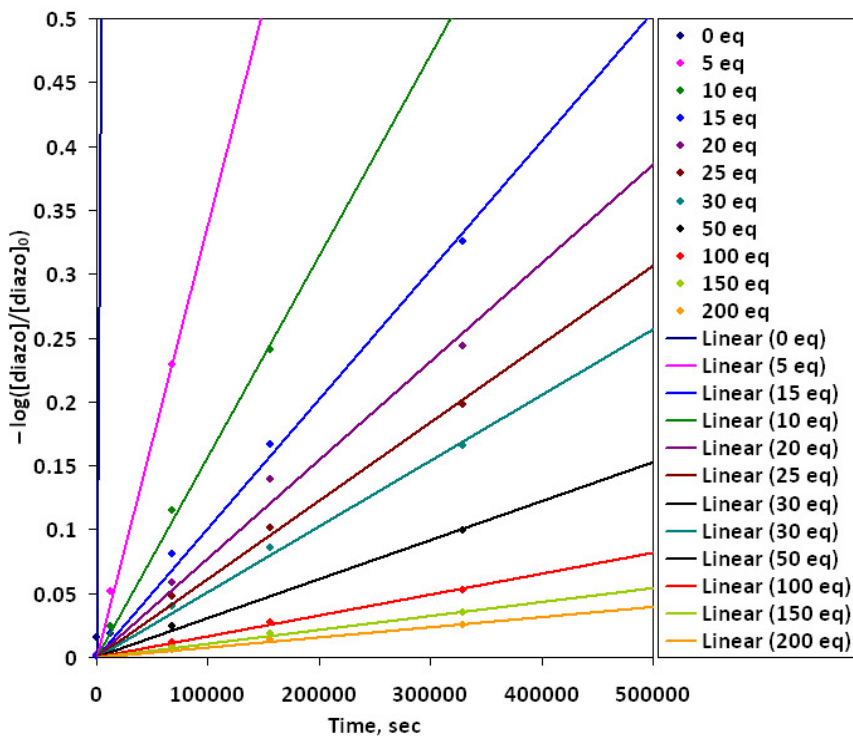


Figure 6-14. Linear relationship between $-\log([diazol]/[diazol]_0)$ and time at various concentrations of triphenyl phosphite.

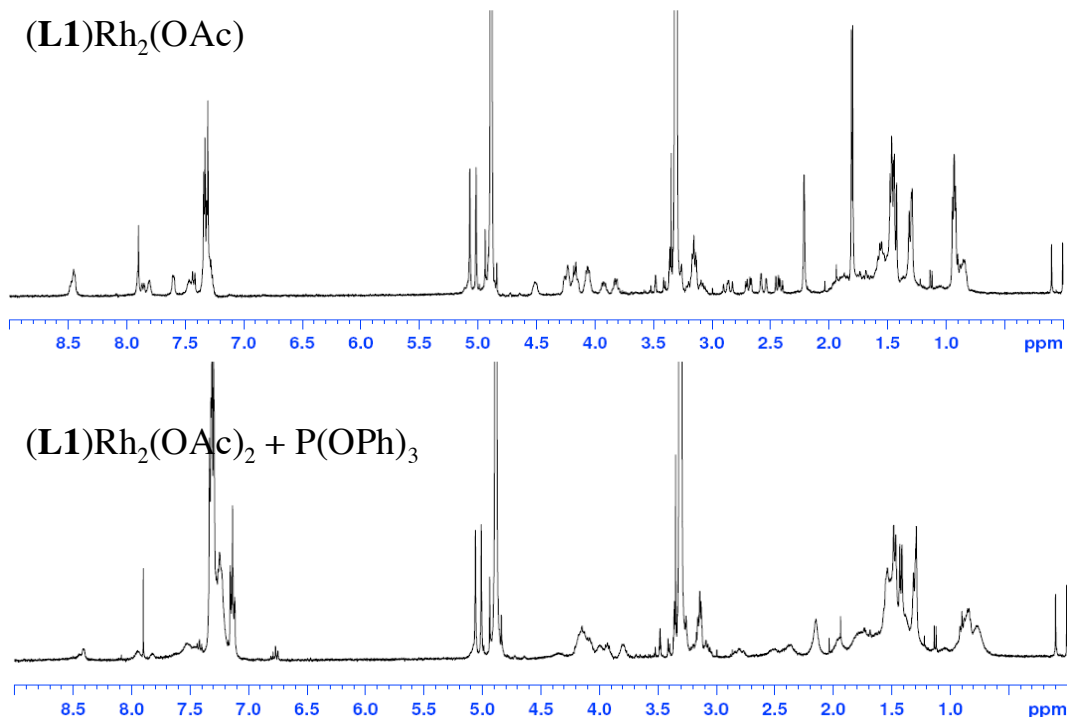


Figure 6-15. ¹H NMR of (L1)Rh₂(OAc)₂ (top) compared with ¹H NMR of (L1)Rh₂(OAc)₂ with 1 equiv of triphenylphosphite (bottom). Spectra were taken in MeOD at 2.6 mM concentration of metalloprotein.

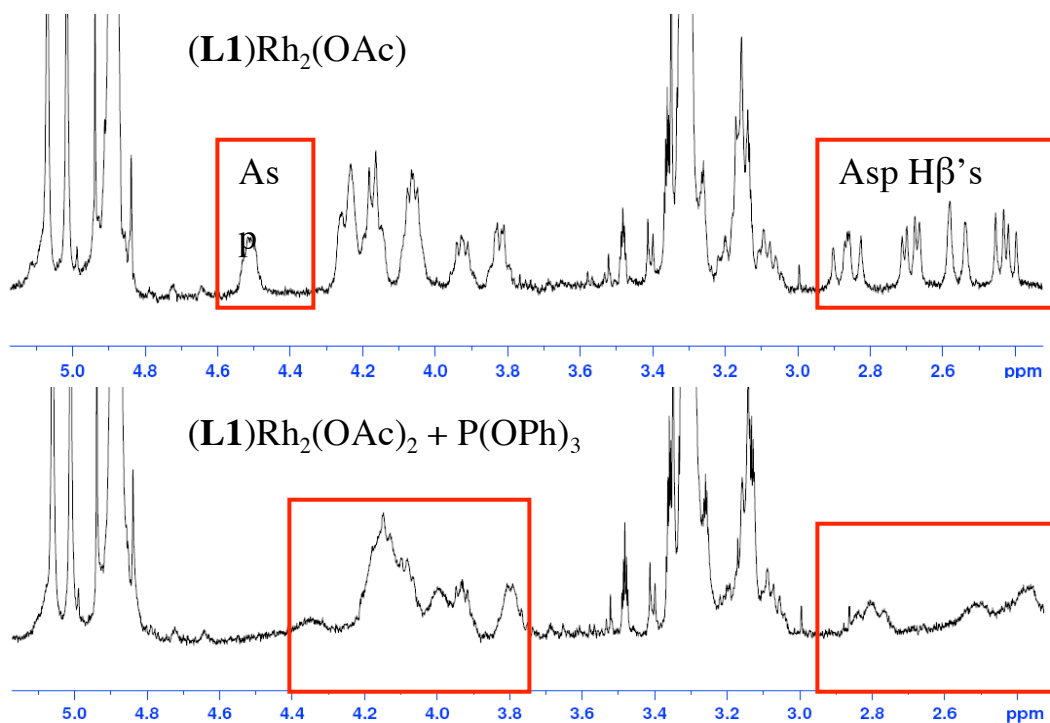


Figure 6-16. ¹H NMR in the region 2.3-5.2 ppm.

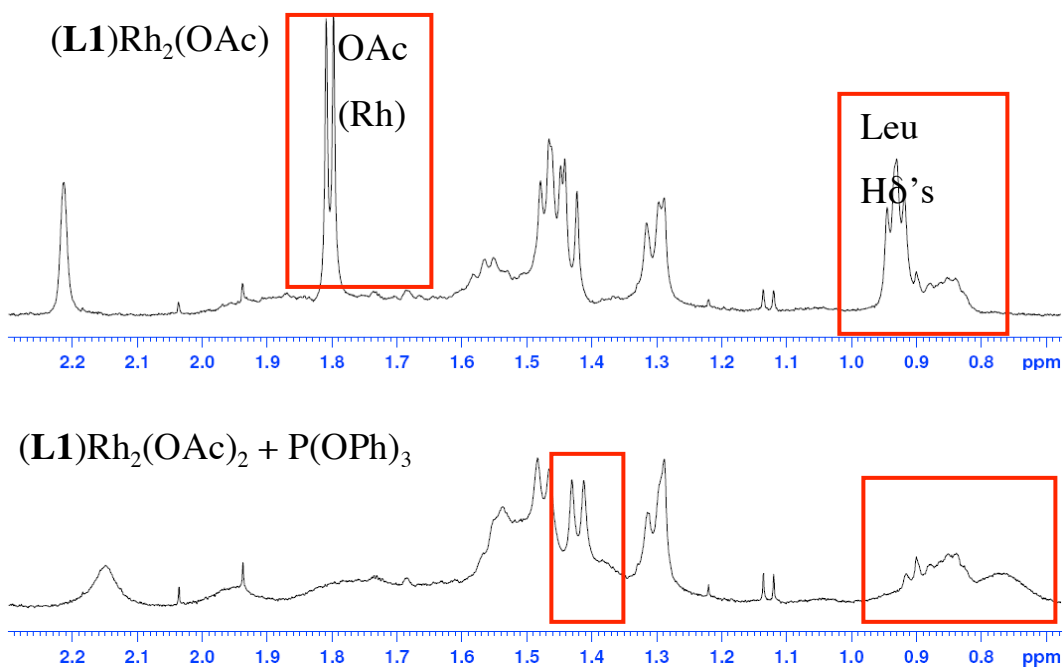


Figure 6-17. ¹H NMR in the region 0.7-2.3 ppm.

6.7. References

- (1) Messerle, L. *Chem. Rev.* **1988**, 88, 1229.
- (2) Cotton, F. A. W., R. A. *Multiple Bonds between Metal Atoms*; Wiley: New York, NY, 1982.
- (3) Cotton, F. A. *Acc. Chem. Res.* **1978**, 11, 225.
- (4) Doyle, M. P.; Forbes, D. C. *Chem. Rev.* **1998**, 98, 911.
- (5) Pirrung, M. C.; Liu, H.; Morehead, A. T. *J. Am. Chem. Soc.* **2002**, 124, 1014.
- (6) Pirrung, M. C.; Morehead, A. T. *J. Am. Chem. Soc.* **1994**, 116, 8991.
- (7) Wong, F. M.; Wang, J.; Hengge, A. C.; Wu, W. *Org. Lett.* **2007**, 9, 1663.
- (8) Nakamura, E.; Yoshikai, N.; Yamanaka, M. *J. Am. Chem. Soc.* **2002**, 124, 7181.

- (9) Davies, H. M. L.; Jin, Q.; Ren, P.; Kovalevsky, A. Y. *J. Org.Chem.* **2002**, *67*, 4165.
- (10) Qu, Z.; Shi, W.; Wang, J. *J. Org.Chem.* **2001**, *66*, 8139.
- (11) Wang, P.; Adams, J. *J. Am. Chem. Soc.* **1994**, *116*, 3296.
- (12) Stokes, B. J.; Richert, K. J.; Driver, T. G. *J. Org.Chem.* **2009**, *74*, 6442.
- (13) Nelson, T. D.; Song, Z. J.; Thompson, A. S.; Zhao, M.; DeMarco, A.; Reamer, R. A.; Huntington, M. F.; Grabowski, E. J. J.; Reider, P. J. *Tetrahedron Lett.* **2000**, *41*, 1877.
- (14) Wynne, D. C.; Olmstead, M. M.; Jessop, P. G. *J. Am. Chem. Soc.* **2000**, *122*, 7638.
- (15) Davies, H. M. L.; Venkataramani, C.; Hansen, T.; Hopper, D. W. *J. Am. Chem. Soc.* **2003**, *125*, 6462.
- (16) Gomes, L. F. R.; Trindade, A. F.; Candeias, N. R.; Gois, P. M. P.; Afonso, C. A. M. *Tetrahedron Lett.* **2008**, *49*, 7372.
- (17) Trindade, A. F.; Gois, P. M. P.; Veiros, L. F.; AndreÅ, V.; Duarte, M. T.; Afonso, C. A. M.; Caddick, S.; Cloke, F. G. N. *J. Org.Chem.* **2008**, *73*, 4076.
- (18) Trindade, A. F.; Andre, V.; Duarte, M. T.; Veiros, L. F.; Gois, P. M. P.; Afonso, C. A. M. *ChemInform* **2011**, *42*, no.
- (19) Trindade, A. F.; André, V.; Duarte, M. T.; Veiros, L. F.; Gois, P. M. P.; Afonso, C. A. M. *Tetrahedron* **2010**, *66*, 8494.
- (20) Zhang, Y.-Z.; Zhu, S.-F.; Wang, L.-X.; Zhou, Q.-L. *Angew. Chem.* **2008**, *120*, 8624.
- (21) Buck, R. T.; Coe, D. M.; Drysdale, M. J.; Moody, C. J.; Pearson, N. D. *Tetrahedron Lett.* **1998**, *39*, 7181.

- (22) Buck, R. T.; Coe, D. M.; Drysdale, M. J.; Ferris, L.; Haigh, D.; Moody, C. J.; Pearson, N. D.; Sanghera, J. B. *Tetrahedron Asymm.* **2003**, *14*, 791.
- (23) Davies, H. M. L.; Hansen, T.; Rutberg, J.; Bruzinski, P. R. *Tetrahedron Lett.* **1997**, *38*, 1741.
- (24) Kitagaki, S.; Kinoshita, M.; Takeba, M.; Anada, M.; Hashimoto, S. *Tetrahedron Asymm.* **2000**, *11*, 3855.
- (25) Landais, Y.; Planchenault, D.; Weber, V. r. *Tetrahedron Lett.* **1995**, *36*, 2987.
- (26) Landais, Y.; Planchenault, D.; Weber, V. r. *Tetrahedron Lett.* **1994**, *35*, 9549.
- (27) Sambasivan, R.; Ball, Z. T. *J. Am. Chem. Soc.* **2010**, *132*, 9289.
- (28) Zaykov, A. N.; MacKenzie, K. R.; Ball, Z. T. *Chem. Eur. J.* **2009**, *15*, 8961.
- (29) Zaykov, A. N.; Popp, B. V.; Ball, Z. T. *Chem. Eur. J.* **2010**, *16*, 6651.
- (30) L. Bear, J.; Howard, R. A.; E. Korn, J. *Inorg. Chim. Acta* **1979**, *32*, 123.
- (31) Rainen, L.; Howard, R. A.; Kimball, A. P.; Bear, J. L. *Inorg. Chem.* **1975**, *14*, 2752.
- (32) Drago, R. S.; Long, J. R.; Cosmano, R. *Inorg. Chem.* **1981**, *20*, 2920.
- (33) Aquino, M. A. S.; Macartney, D. H. *Inorg. Chem.* **1987**, *26*, 2696.
- (34) Kemmer, G.; Keller, S. *Nat. Protocols* **2010**, *5*, 267.
- (35) Davies, H. M. L.; Hansen, T.; Churchill, M. R. *J. Am. Chem. Soc.* **2000**, *122*, 3063.
- (36) <http://www.tushar-mehta.com/excel/software/polynomials/index.html>.

Chapter 7

Dirhodium metallopeptide as MDM2 ligands

7.1. Introduction

Multi-functional therapeutic and probe agents are increasingly important for the future of chemical biology and drug design. Different regions of a biologically active molecule may serve complementary roles, as in fragment-based drug design,¹ or probes may include differing functions, incorporating binding and chemical function in a single unit.² Metallopeptides are attractive targets to be developed as biological probes. As hybrid structures of a metal complex and a polypeptide, they conveniently combine biochemical properties of peptides as protein ligands and various functions of metal that now can be directed to the protein interface. A transition-metal center may serve diverse roles, including stabilizing ligand secondary structure,³⁻⁵ increasing potency through secondary binding interactions,⁶ serving as spectroscopic handles,⁷ or facilitating electron transfer⁸⁻¹⁰ or catalytic activity.¹¹⁻¹³

As described in Chapter 4 and in the examples reported by others, metalation of a peptide can be used as a means of enforcing peptide helical conformation.³⁻⁵ Stabilization of the peptide secondary structure has the potential for improving activity of the peptide-based therapeutic agents. A large number of proteins utilize helical domains in protein-protein interactions that are often transient in nature and involved in signal transduction pathways.¹⁴⁻¹⁶ Targeting protein-protein interactions is an

important goal of today's medicinal chemistry.¹⁷ Inhibition of these proteins with small-molecule drugs however is quite challenging due to a shallow binding interface, a fact that led to their label as "undruggable."¹⁸ As a result, there is a growing interest in peptide- and protein- based therapeutics because of the benefits such as larger interaction surface and higher specificity. A success with peptide "stapling" methodology, where helical peptide structure is stabilized by a hydrocarbon tether, encourages development of other techniques that influence peptide conformation.¹⁹⁻²²

Interaction of metal chaperon proteins is mediated by metal binding to both of the interaction partners.⁶ The fact that metal ligation can provide a thermodynamic force for interaction in these systems suggests that a similar concept could be utilized in metallopeptide-protein interactions. Again, the idea would be highly beneficial for targeting proteins with weak affinities. Cooperative binding of the peptide ligand and the attached metal will provide both selectivity and an enhanced affinity that could lead to a more potent therapeutic (Figure 7-1, A). Protein domains are categorized into the families based on their structure and interacting partners. High similarity of the binding domains between many proteins creates a selectivity issue when only an individual protein needs to be targeted. These domains however may vary in position and distribution of the residues that are preferential for metal ligation, such as Lewis-basic residues histidine, cysteine and methionine. Thus improved selectivity can be attained with metallopeptide that spatially positions metal in the proximity to the ligating residue and ensures their interaction.

Dirhodium has several advantages over other metal centers. Unlike many metal-ion-peptide interactions,^{23,24} dirhodium metalation of

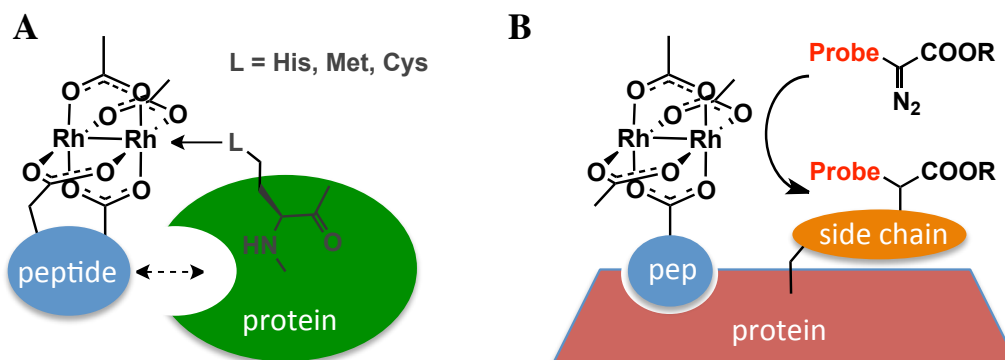


Figure 7-1. Conceptual scheme depicting (A) cooperative interaction of a peptide and a dirhodium center with a protein's binding pocket and (B) site-specific labeling of a protein catalyzed by the proximal dirhodium.

side chains yields kinetically inert coordination complexes, enabling purification and isolation.³ The covalent-like character of a dirhodium bond to the equatorial carboxylates ensures irreversible attachment of metal center to the peptide. The unique structure of the dirhodium core separates the equatorial sites that provide a robust connection to the peptide from the Lewis-acidic axial sites that are capable of reversible binding to electron-donor ligands. Though complete studies of dirhodium metallopeptide biocompatibility, stability in biological environment, and cell permeability are yet to come, initial results demonstrate reasonable stability in cellular media and low toxicity.³

In addition, dirhodium has useful catalytic, redox,^{25,26} and medicinal properties.^{27,28} Exciting results demonstrating utility of dirhodium metallopeptides for site-specific labeling of interacting partners has recently been presented from our lab.²⁹⁻³¹ Coiled-coil assembly that serves as a model of protein-protein interaction was used to bring a dirhodium center on one peptide into the proximity to the amino-acid side chains on the complimentary peptide. Treatment of the assembly with a diazo reagent

leads to the catalytic decomposition of the reagent at the dirhodium to form a reactive metallocarbene intermediate. This intermediate undergoes an insertion reaction with the local amino acid on the complimentary peptide resulting in the covalent modification of the peptide substrate.^{30,31} The diazo reagent was further designed to carry a biotin affinity probe or a fluorophore. This technology can be potentially extended to enable protein functionalization by localizing a dirhodium core at the binding interface of the protein of interest (Figure 7-1, B). Targeting specific proteins with a dirhodium metallopeptide can be used to exploit and improve dirhodium's ability for small-molecule sensing³² and DNA binding³³ in the biological context.

7.2. MDM2 protein

The protein MDM2 is well studied, owing to its role in oncogenesis.³⁴ MDM2 regulates the p53 protein, which controls cell cycle and cellular responses to various stress factors (Figure 7-2). It is estimated that MDM2 is overexpressed in 50 % of cancers , resulting in suppression of p53 activity and survival of the tumor cells.³⁵ Inhibition of the MDM2-p53 interaction is a validated approach to restore p53 function and activate natural cancer-defense mechanisms.³⁶ Significant efforts were made to invent potent inhibitors of MDM2, including small molecule, peptide and peptidomimetic structures (Figure 7-3).^{37,38} The binding domain of the p53 protein adopts an α -helical conformation and binds into the exposed hydrophobic pocket of MDM2 (Figure 7-4, A).³⁹ A peptide fragment derived from the p53 domain displays reasonable affinity for MDM2 that was significantly improved by sequence optimization and utilization of unnatural amino acids.⁴⁰⁻⁴³ Stabilization of the helical conformation by bridging peptide side chains is

another approach to improve ligand potency, as in the example of “stapled” peptides, and the metalloptides presented here were designed according to this concept.^{22,44}

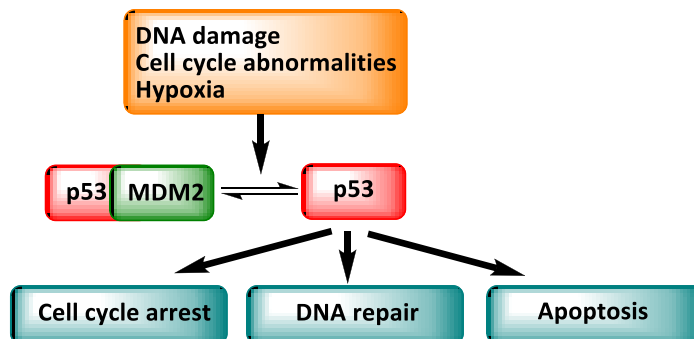


Figure 7-2. Defense function of the p53 protein and its regulation by the MDM2. Overexpression of MDM2 in cancers results in suppression of p53 activity.

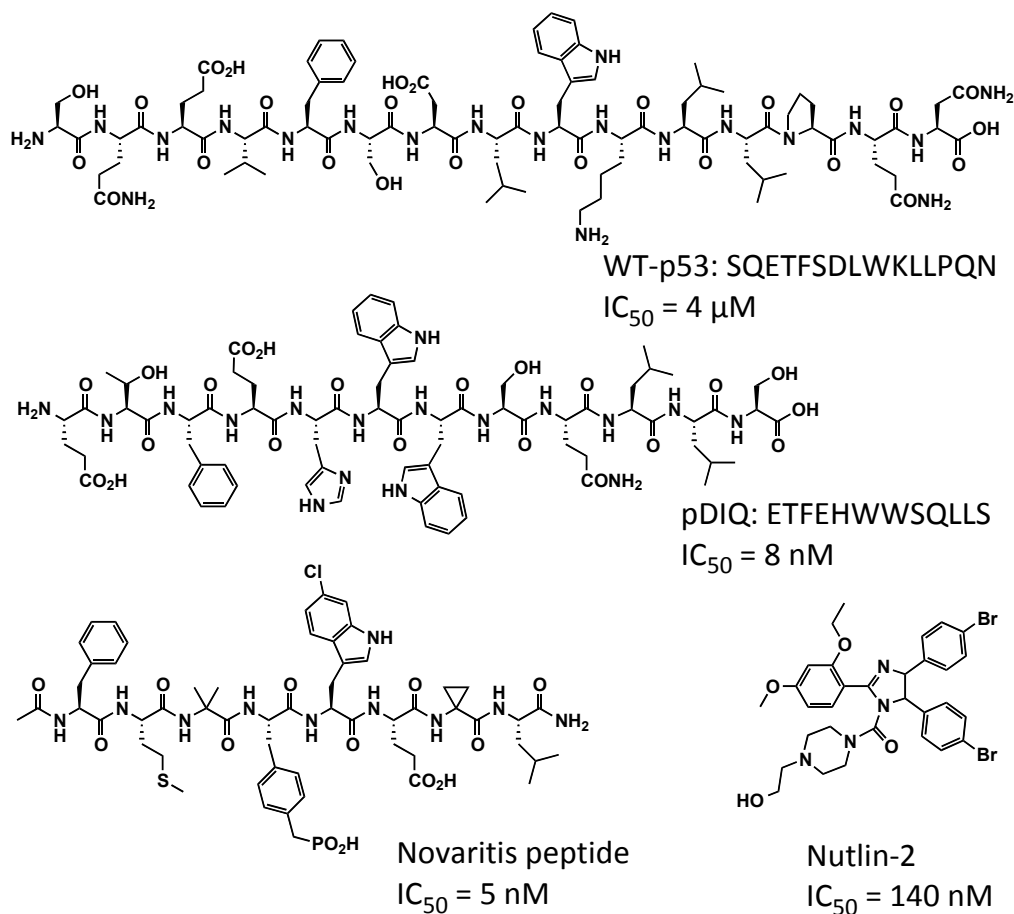


Figure 7-3. Peptide based on the wild type p53 sequence (top) and a few examples peptide and small molecule inhibitors of the MDM2.

7.3. Dirhodium metallopeptide design

Four metallopeptides were designed that are based on the wild-type sequence of the MDM2 binding domain. The natural sequence contains three carboxylate residues that can contribute to protein-protein interaction. Aspartate and glutamate residues often play crucial role for binding, such as in the example of highly conserved aspartate of BH3-Bcl2 interactions.⁴⁵ To evaluate importance of the acidic residues in this case, two peptides (P2-Rh₂(OAc)₂ and P4-Rh₂(OAc)₂) were made using an orthogonal protection scheme described in Chapter 4, preserving one or both of the native glutamate residues (Table 7-1). In addition, two other metallopeptides (P6-Rh₂(OAc)₂ and P7-Rh₂(OAc)₂) were synthesized with the sequence derived from an alternative peptide (P5) with improved affinity (Table 7-1).⁴⁶ Two glutamate residues were positioned in the *i, i+4* arrangement to provide ligand sites for metalation with bidentate *cis*-Rh₂(tfa)₂(OAc)₂ precursor. Two

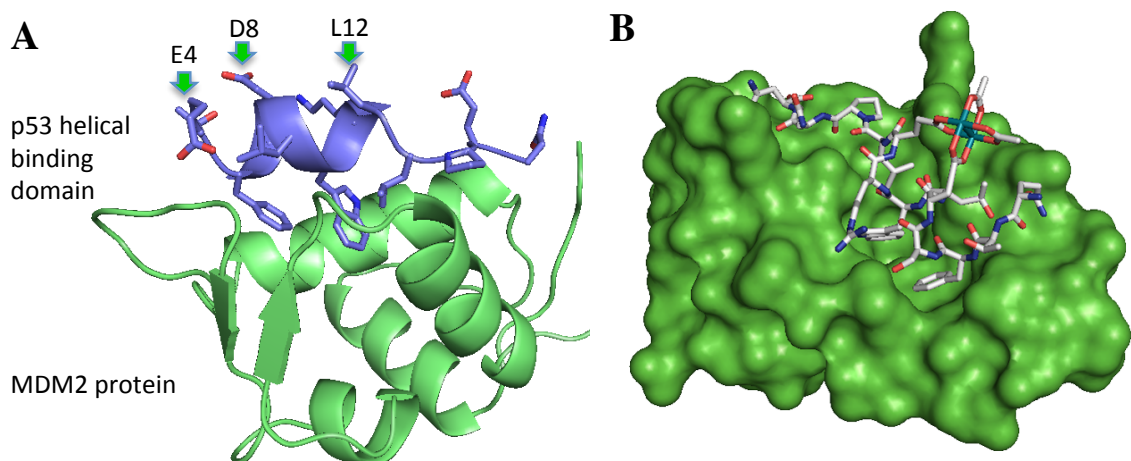


Figure 7-4. (A) MDM2 protein with bound p53 helical peptide. Annotated residues (based on the sequence in the Table 7-1 are positioned on the exposed side of the helix and were chosen as the dirhodium metalation sites. (B) Model of the metallopeptide **P7**-Rh₂(OAc)₂ bound to the MDM2. The model is created using Spartan, starting from a reported MDM2-peptide structure (PDB ID: 1YCR).

Table 7-1. Peptide sequences and MDM2 affinity (K_d) obtained by a fluorescence polarization assay. [Rh₂] stands for bridging Rh₂(OAc)₂ metallocenter and * indicates that metalloptides are functionalized with fluorescein bound through β -alanine linker.

entry	name	sequence	$K_d(\mu\text{M})$
1	WT	*LSQ ET FS D LWKLL PEN	1.9±0.3
2	P1-Rh₂(OAc)₂	*QSQ ET FS EL WRLL PQN [Rh ₂]	3.0±0.5
3	P2-Rh₂(OAc)₂	*QSQ ET FS EL WRLL PEN [Rh ₂]	2.0±0.7
4	P3-Rh₂(OAc)₂	*QS Q TFS EL WR EL PQN [Rh ₂]	7.0±1.0
5	P4-Rh₂(OAc)₂	*QSQ ET FS EL WR EL PEN [Rh ₂]	9.0±1.2
6	P5	*LTFSDYWAQLTS [Rh ₂]	0.066±0.013
7	P6-Rh₂(OAc)₂	* ET FS E YWAQLTS [Rh ₂]	0.77±0.020
8	P7-Rh₂(OAc)₂	*LTFSEYWA EL TS [Rh ₂]	0.131±0.030

registers of metalation were tested, with the dirhodium bridging residues in positions 4 and 8 or 8 and 12 (Figure 7-4, A). The positions of glutamate residues were chosen based on the previous structural data to ensure the metal core is directed away from the binding interface, thus avoiding steric clashes with the protein surface (Figure 7-4, B).³⁹ Peptides were synthesized with N-terminal β -alanine amino acid as a linker to a fluorescein moiety that is necessary for the fluorescence polarization studies.

7.4. Fluorescence polarization affinity measurements

Affinities for MDM2 were assessed by fluorescence polarization anisotropy (Figure 7-5).⁴⁷ The p53-binding region of MDM2, residues 5–109, was prepared using a published method for high-yielding protein expression.⁴⁸ In our hands, MDM2 [5–109] binds the wild-type sequence

(WT) with $K_d = 1.9 \mu\text{M}$, consistent with a previous report for the MDM2 peptide-binding domain without N-terminal truncation.^{47,49} For metallopeptide variants based on p53-WT, the register of metalation has an impact on binding affinity, despite the fact that both registers should position the dirhodium core away from the binding interface (Figure 7-4, A). Dirhodium chelation at residues 4 and 8 (**P1**-Rh₂(OAc)₂ and **P2**-Rh₂(OAc)₂) provides affinity comparable to the wild-type sequence, while chelation at residues 8 and 12 (**P3**-Rh₂(OAc)₂ and **P4**-Rh₂(OAc)₂) provides considerably

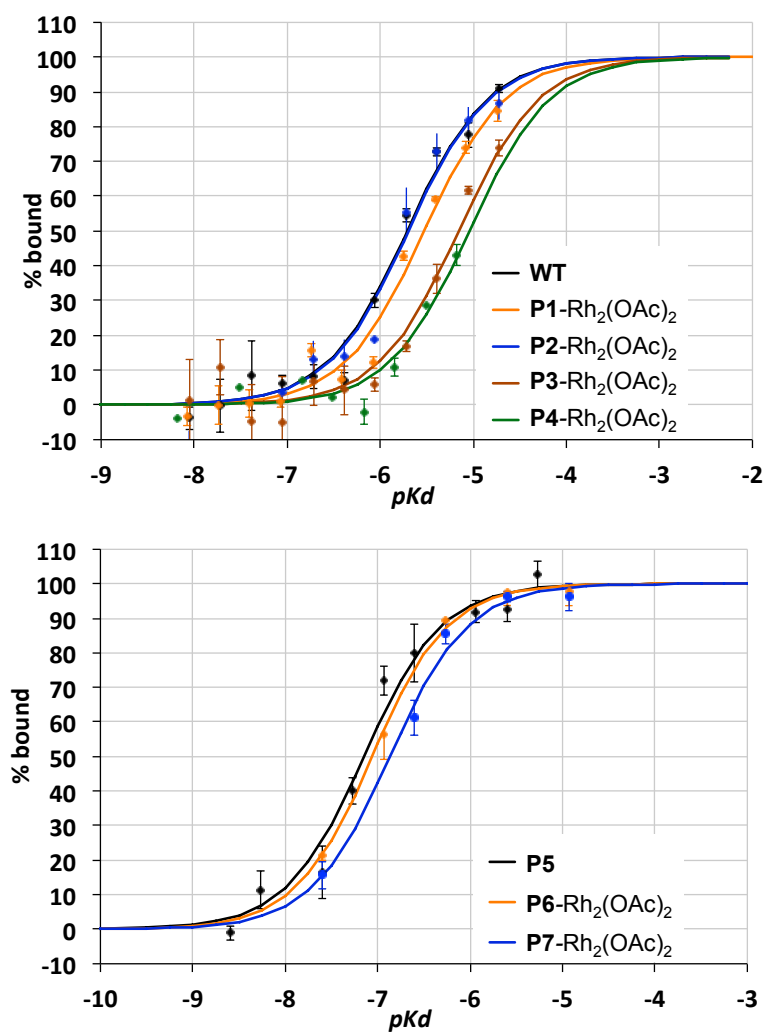


Figure 7-5. Fluorescence polarization assays with FITC-dirhodium peptides and MDM2 [5-109] protein.

weaker affinity. This trend between metal-binding registers is mirrored in two other metallopeptides (**P6**-Rh₂(OAc)₂ and **P7**-Rh₂(OAc)₂) based on a previously reported sequence (**P5**) with improved affinity.⁵⁰ The peptide **P5** bound MDM2 with $K_d = 66$ nM. The corresponding metallopeptide with the N-terminal binding register (**P6**-Rh₂(OAc)₂) demonstrated comparable affinity (77 nM), while that with the C-terminal binding register (**P7**-Rh₂(OAc)₂) exhibited decreased affinity. Although register does impact affinity significantly, peptide charge and the free carboxylate side chains have a surprisingly minimal effect, especially given the close proximity of E4 and E15 to the binding interface.

7.5. Conclusions

This chapter describes multifunctional MDM2 ligands that incorporate a peptide binding sequence, an organic dye molecule, and a catalytically active transition-metal center. The designed metallopeptides were demonstrated to retain high affinity to the MDM2 protein with bridging metalation not interfering with binding. The chelated metallopeptides employed here were in part designed to stabilize helical secondary structure.^{3,22,51} However the examined metallopeptides do not exhibit increased affinity compared to corresponding free peptides. Evidence indicates that the benefits of helix stabilization go beyond simple affinity concerns. In Verdine's work stapling non-natural alkenyl side chains in the MDM2-p53 system, a modest increase in K_d (from 100 to 55 nM over an unstapled control) led to a large improvement in apoptosis reactivation, suggesting that stapling offers other benefits such as cell permeability, degradative stability, and/or target specificity.

The ability to produce a complex dirhodium metallopeptide that bind to natural protein targets provides a foundation for various applications, such as development of stable hybrid inorganic-organic structures as therapeutic agents and dirhodium-catalyzed site-specific functionalization with diazo reagents.³¹ It also offers tools to localize dirhodium centers for applications as diverse as electron-transfer, small molecule sensing,³² and UV-vis spectroscopy.

7.6. Experimental section

7.6.1. General considerations

Peptide synthesis. All peptides were synthesized with an Advanced ChemTech APEX 396 Automated Multipetide Synthesizer using standard solid-phase Fmoc protocols. The purification was accomplished by reverse-phase HPLC with gradients of water-acetonitrile containing 0.1% trifluoroacetic acid, and peptides were isolated by lyophilization. Analysis and purity assessment was attained by mass spectrometry and analytical HPLC. Peptides were prepared using Rink amide MBHA resin (AAPPTeC) to afford the C-terminal amide.

HPLC. HPLC was performed on a Shimadzu CBM-20A instrument with Phenomenex Jupiter 4 μ Proteo 90A (250 \times 15 mm preparative) and Phenomenex Jupiter 4 μ Proteo 90A (250 \times 4.6 mm analytical) columns. Flow rates of 8 mL/min and 1 mL/min were used for preparative and analytical columns, respectively. Analytical and preparative HPLC were performed with gradient of acetonitrile in water. Both solvents contained 0.1% trifluoroacetic acid (TFA) unless otherwise noted. Spectra were obtained using UV-vis detection at 220 nm and 300 nm.

Mass Spectrometry. MALDI-MS and MS/MS were performed on a Bruker Daltonics Autoflex MALDI- TOF/TOF mass spectrometer with CHCA matrix (10 mg/mL, Thermo Scientific Pierce) for peptide analyses and DHAP matrix (10 mg/mL) for protein analyses. ESI-MS was performed on Bruker Daltonics micrOTOF instrument.

7.6.2. Experimental Procedures

General procedure for metallopeptide synthesis. Peptide (1 equiv) and *cis*-Rh₂(tfa)₂(OAc)₂ precursor (1 equiv) were dissolved in MES buffer (0.1 M, volume calculated for 1 mM concentration of peptide) and pH adjusted to 4.5 with NaOH (0.1 M) if necessary. The reaction was heated to 50 °C for 3 h and monitored by HPLC. Purification of the metallopeptides was performed by direct injection of the reaction mixture on a preparative RP-HPLC column. All complexes were isolated as a green solid upon lyophilization.

General procedure for palladium deprotection. Allyl deprotection was performed directly on the crude metalation reaction (1 mM in MES buffer, pH 4.5). A solution of Pd(PPh₃)₄ (0.5 equiv) and morpholine (10 equiv) in tetrahydrofuran (volume is equivalent to the volume of buffer solution in the preceding reaction, i.e. 50/50 THF:water final solution) were added to the crude metalation reaction and the pH was adjusted to 7.0 with KOH (0.1 M aq solution).⁵² The reaction was monitored by HPLC, reaching completion after 0.5–1.5 h. Metallopeptides were purified by RP-HPLC, isolated by lyophilization, and characterized by ESI-MS. Using this general procedure **P4** peptide (1.80 mg) was converted to the unlabeled **P4**-Rh₂(OAc)₂ metallopeptide (1.06 mg, 53%). (note: deprotection can be performed on isolated metallopeptide as well)

General procedure for labeling with fluorescein. Solution of fluorescein isothiocyanate (FITC) (1.5 equiv) in DMSO (volume is calculated for a final 0.1 mM concentration of metallopeptide) was added to a lyophilized metallopeptide (typically 0.1-0.2 mg), followed by addition of diisopropylethylamine (5 equiv). The reaction mixture was quenched with methanol (5x rxn volume), diluted with water (5x rxn volume), purified by RP-HPLC (without TFA in the eluent) and characterized by ESI-MS. Lyophilized labeled metallopeptides were dissolved in DMSO (50 μ L) and concentrations of these solutions were determined by absorbance at 492 nm ($\epsilon = 83000 \text{ M}^{-1}\text{cm}^{-1}$) after dilution in Tris buffer (20 mM Tris pH 8, 200 mM NaCl) to achieve 0.2-1.0 absorbance values.⁵⁰ Using this general procedure **P3-Rh₂(OAc)₂** unlabeled metallopeptide (0.64 mg) was converted to the fluorescein-**P3-Rh₂(OAc)₂** metallopeptide (0.49 mg, 68%).

Protein expression. The protein MDM2 [5-109] was expressed in BL21 *E. coli* (Rosetta) cells as a fusion with its interaction partner, the p53 transactivation peptide, which has been shown to afford dramatically higher yields.⁴⁸ The MDM2 plasmid was purchased from Genscript in pET15b vector. After expression, cells were lysed by freezing at $-80 \text{ }^{\circ}\text{C}$. Due to instability of the protein, subsequent steps should be performed in minimal time. The lysate was purified on Ni-NTA affinity column with stepwise increase in concentration of imidazole in the eluent buffer 50 mM/ 100 mM/ 300 mM (Figure 7-26). After analysis by SDS-PAGE gel, most concentrated and clean fractions were combined and dialyzed. His-tag and the fusion peptide were cleaved with 100 U/mg TEV protease at rt overnight or $4 \text{ }^{\circ}\text{C}$ for 48 h (Figure 7-27). MDM2 protein was purified by a second Ni-column and used immediately in binding measurements. Concentration of the protein was determined by absorbance at 280 nm ($\epsilon = 8960 \text{ M}^{-1}\text{cm}^{-1}$)

Fluorescence polarization. Fluorescence polarization data were acquired on Nanolog (Horiba Jobin Yvon) Spectrometer with 16.5F-Q-10 quartz cells (1 cm path length). 200-nM stock solutions of the labeled metallopeptides in DMSO were prepared. Samples were made by adding 4 μ L of metallopeptide solution (10 nM final concentration) to 76 μ L of MDM2 solution of various concentrations in Tris buffer (20 mM Tris pH 8.0, 200 mM NaCl, 2 μ M mercaptoethanol) and incubation for 30 min at rt. Measurements were obtained by excitation at 485 nm with 6 nm slit width and emission detection at 512 nm with 6 nm slit width. 10 data points each integrated over 3 seconds were collected. Binding curves and K_d values were generated in Excel using a non-linear least-squares fit to the equation⁵³:

$$FP = FP_{\min} \times PL \times \frac{(FP_{\max} - FP_{\min})}{FP_{\max}}$$

$$PL = L_0 + P_0 + K_d - \frac{\sqrt{(L_0 + K_d + P_0)^2 - 4 \times L_0 \times P_0}}{2}$$

where L_0 is the concentration of the peptide, P_0 is the concentration of the protein, K_d is the dissociation constant, FP_{\min} is the low limit of the curve and FP_{\max} is the high limit of the curve.²² K_d , FP_{\min} and FP_{\max} were all floating parameters during the non-linear least-squares fitting.

MDM2 model (Figure 7-4). Model structure was prepared based on PDB coordinates 1YCR of p53-wild type peptide and N-terminal binding domain MDM2 [17-125]. The coordinates for p53 peptide were manually extracted into a separate file (pdb) and the structure was altered in Spartan to represent **P1**-Rh₂(OAc)₂. The complete assembly was “frozen” and only the side chains of glutamates that are bound to the dirhodium core were released for molecular mechanic (MMFF) optimization. The optimized **P1**-

$\text{Rh}_2(\text{OAc})_2$ structure was exported in PDB format and overlaid with MDM2 in PyMOL.

7.6.3. Analytical data

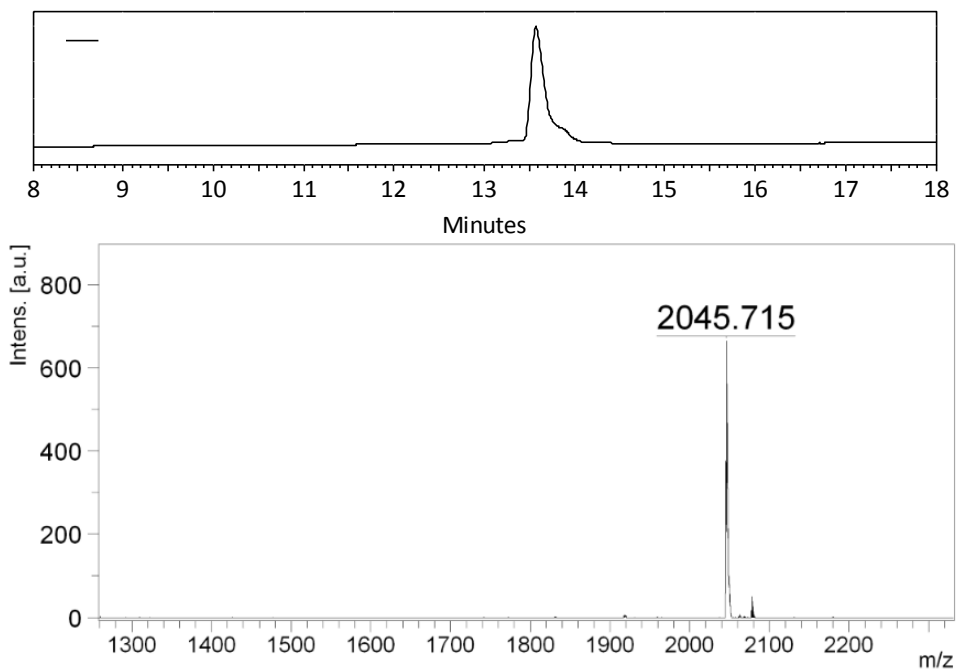


Figure 7-6. HPLC trace and MS data for isolated **P1** peptide.

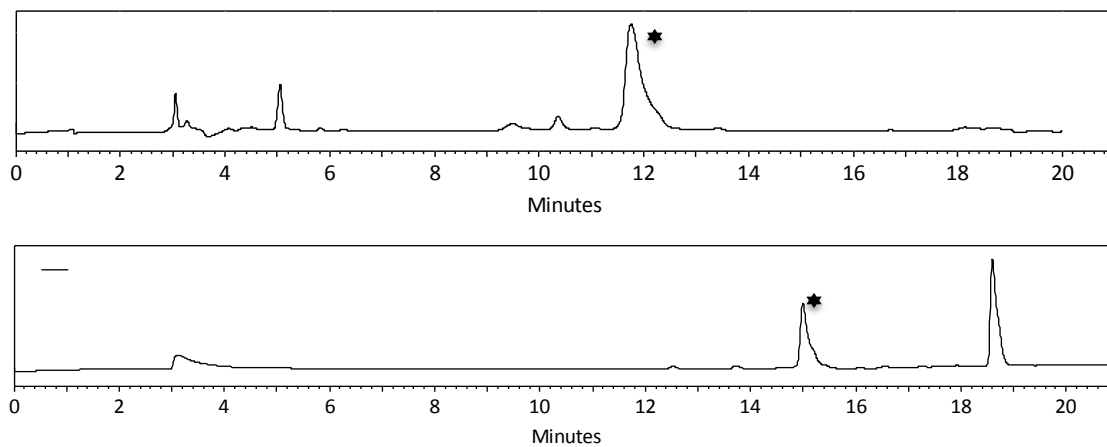


Figure 7-7. HPLC trace of crudes of metalation reaction (top) and fluorescein labeling with FITC (bottom) for **P1**- $\text{Rh}_2(\text{OAc})_2$ metalloprotein synthesis.

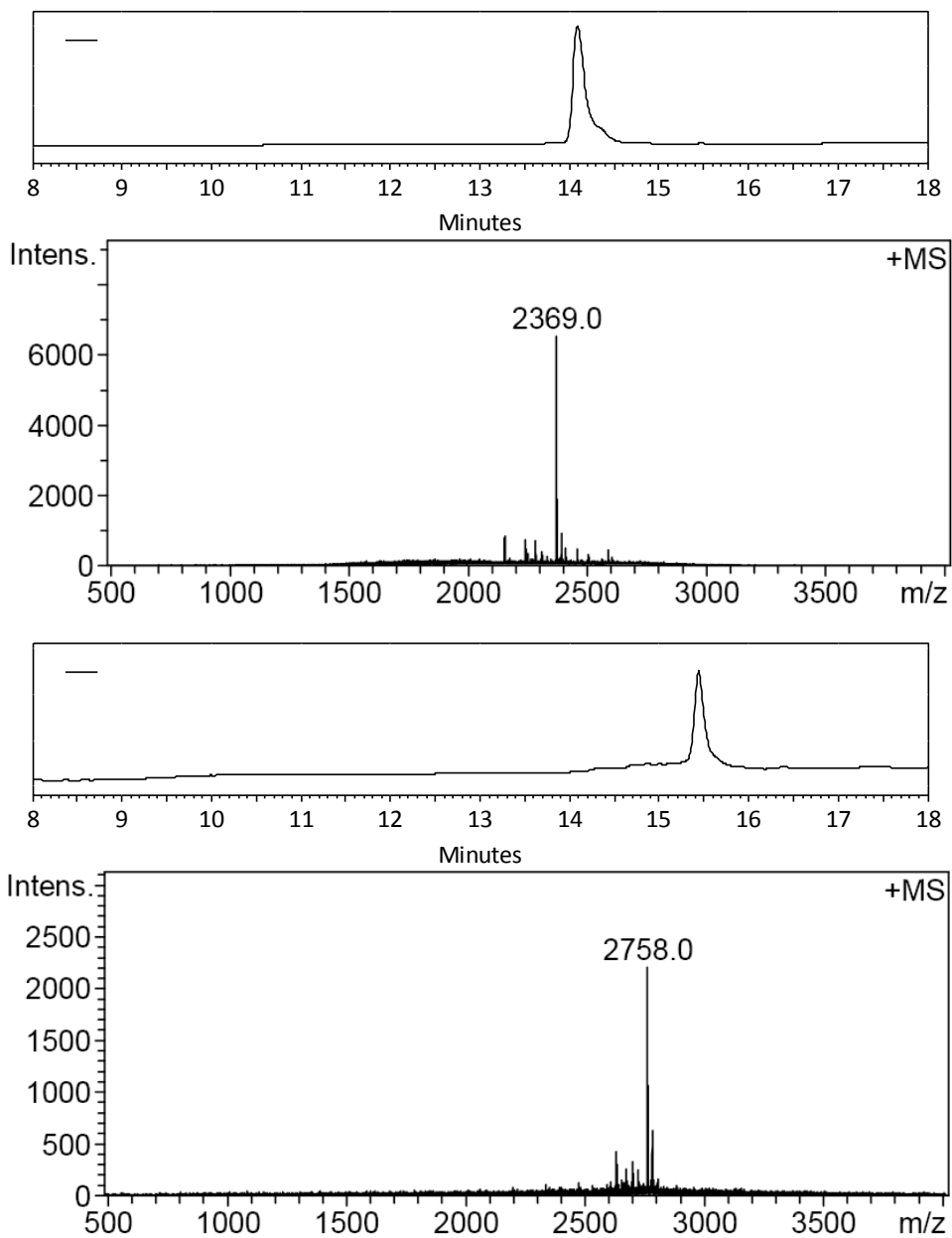


Figure 7-8. HPLC trace and MS data of purified product for **P1-Rh₂(OAc)₂** metalloprotein synthesis before (top) and after (bottom) fluorescein labeling with FITC.

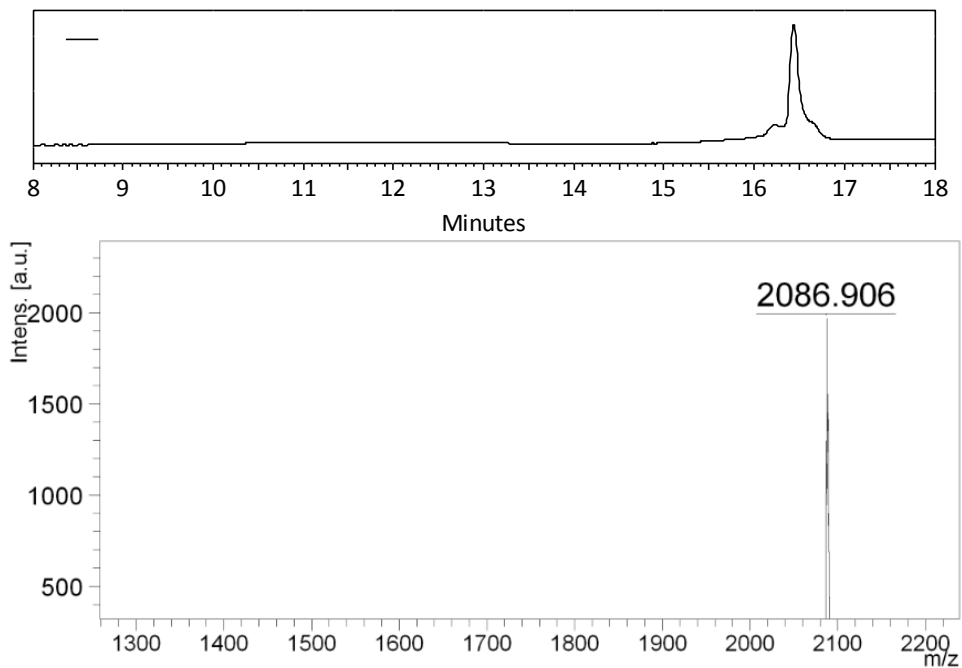


Figure 7-9. HPLC trace and MS data for isolated **P2** peptide.

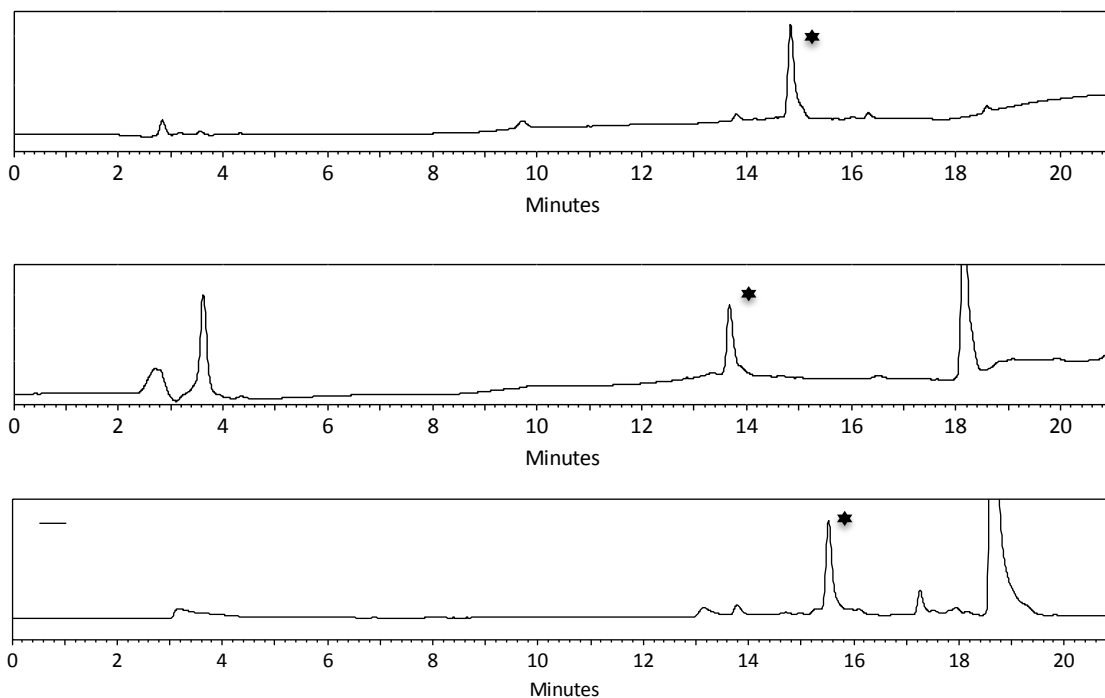


Figure 7-10. HPLC trace of crudes of metalation reaction (top), in-situ palladium deprotection (center) and fluorescein labeling with FITC (bottom) for **P2-Rh₂(OAc)₂** metallopeptide synthesis.

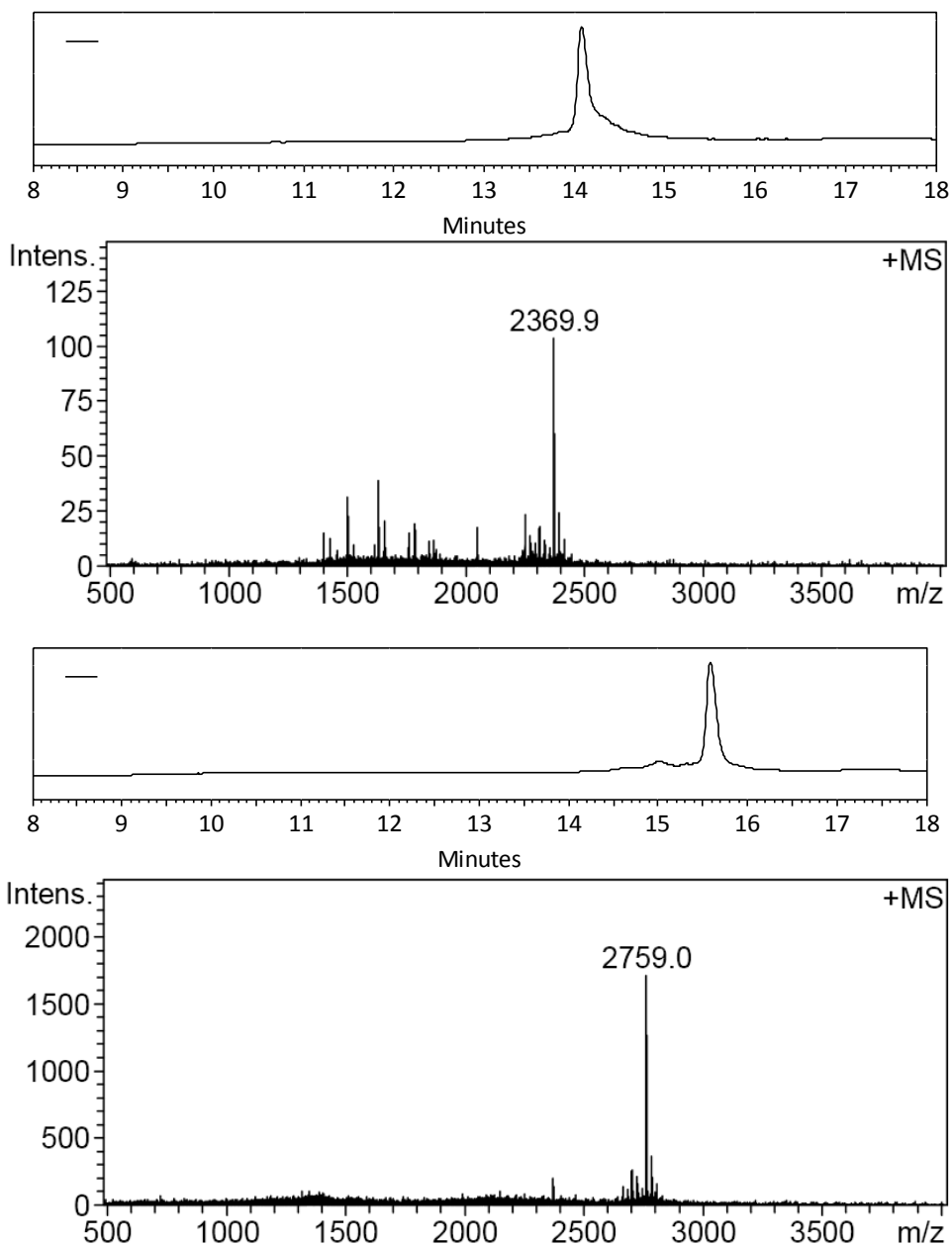


Figure 7-11. HPLC trace and MS data of purified product for **P2-Rh₂(OAc)₂** metallopeptide synthesis before (top) and after (bottom) fluorescein labeling with FITC.

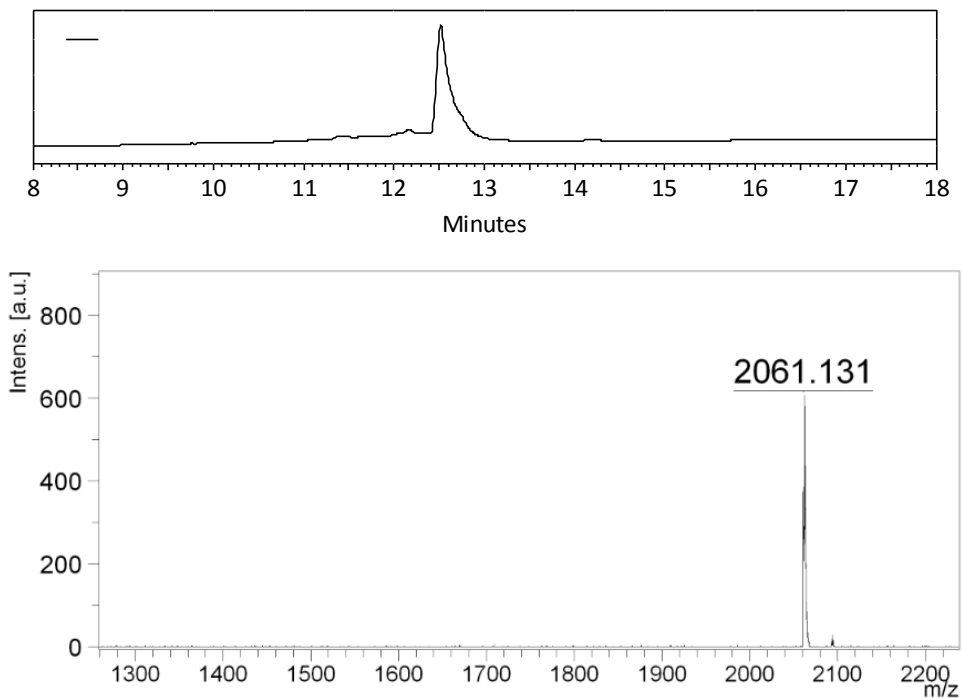


Figure 7-12. HPLC trace and MS data for isolated **P3** peptide.

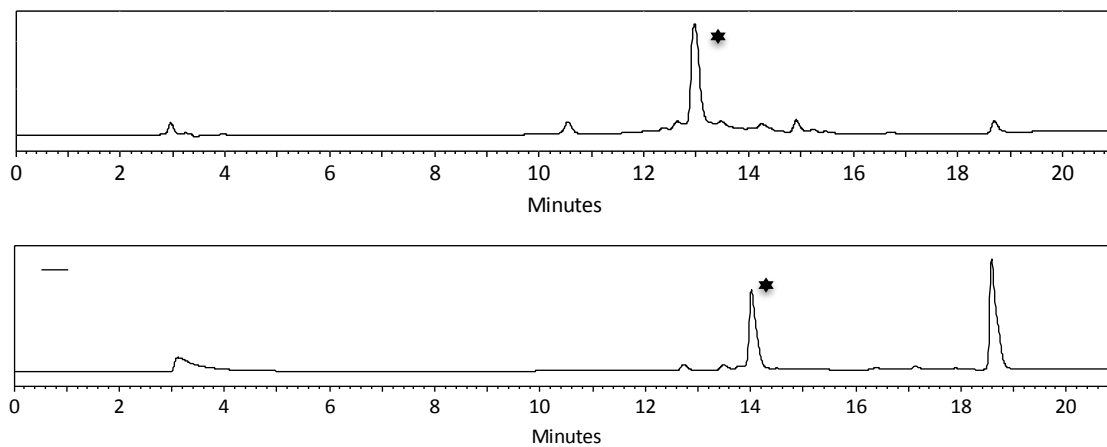


Figure 7-13. HPLC trace of crudes of metalation reaction (top) and fluorescein labeling with FITC (bottom) for **P3**-Rh₂(OAc)₂ metalloprotein synthesis.

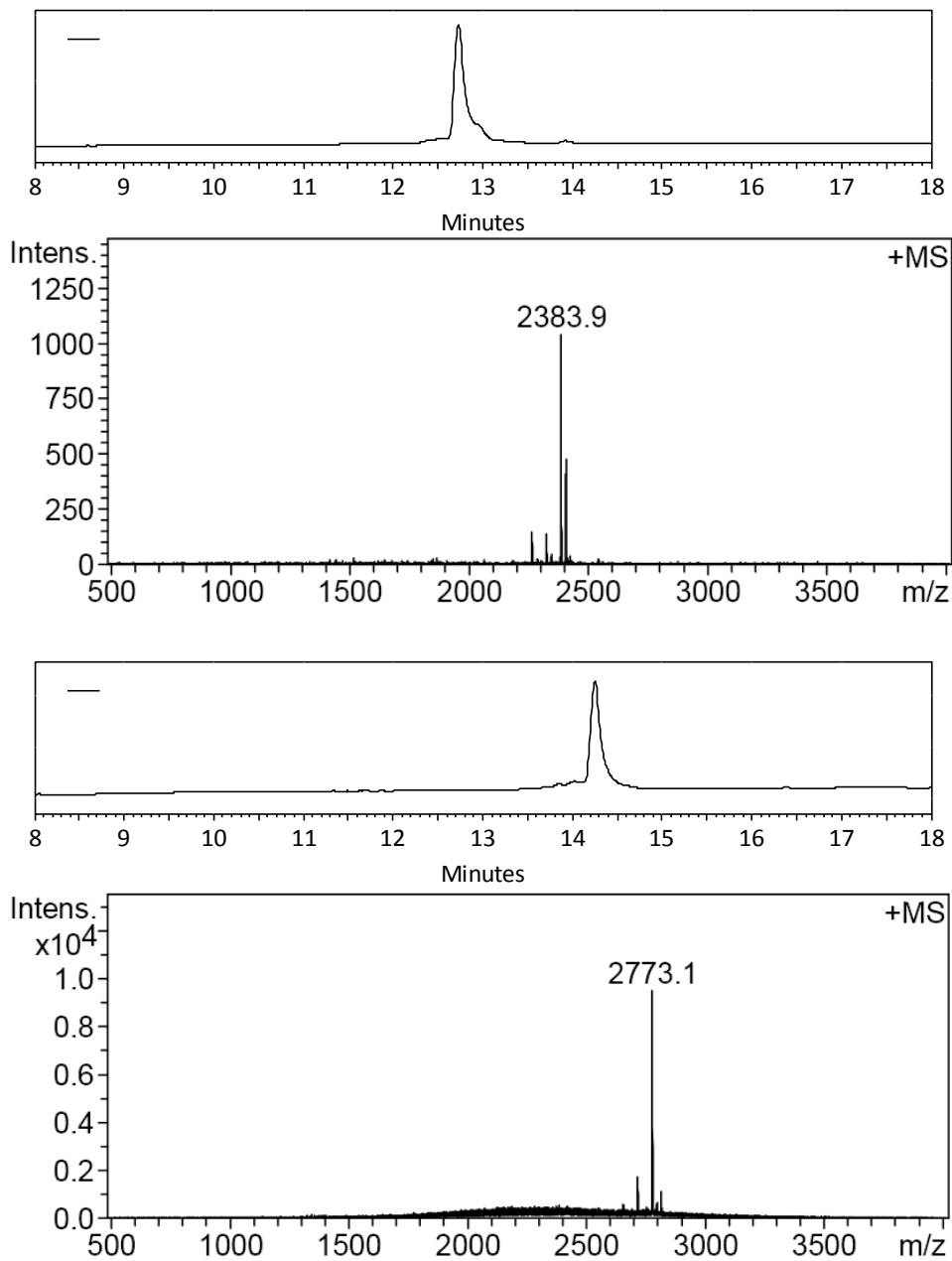


Figure 7-14. HPLC trace and MS data of purified product for **P3-Rh₂(OAc)₂** metallopeptide synthesis before (top) and after (bottom) fluorescein labeling with FITC.

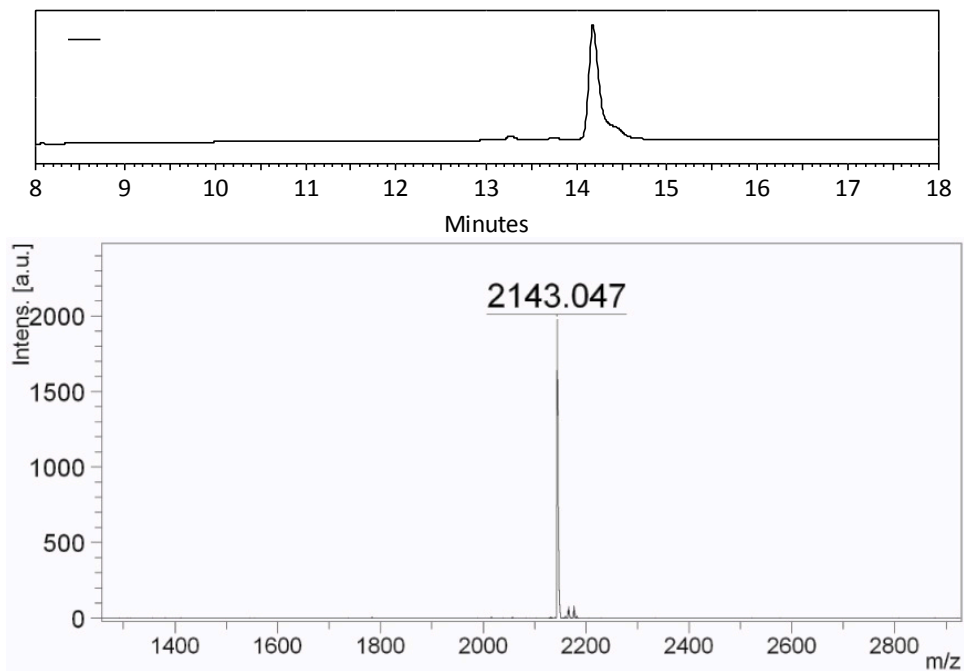


Figure 7-15. HPLC trace and MS data for isolated **P4** peptide.

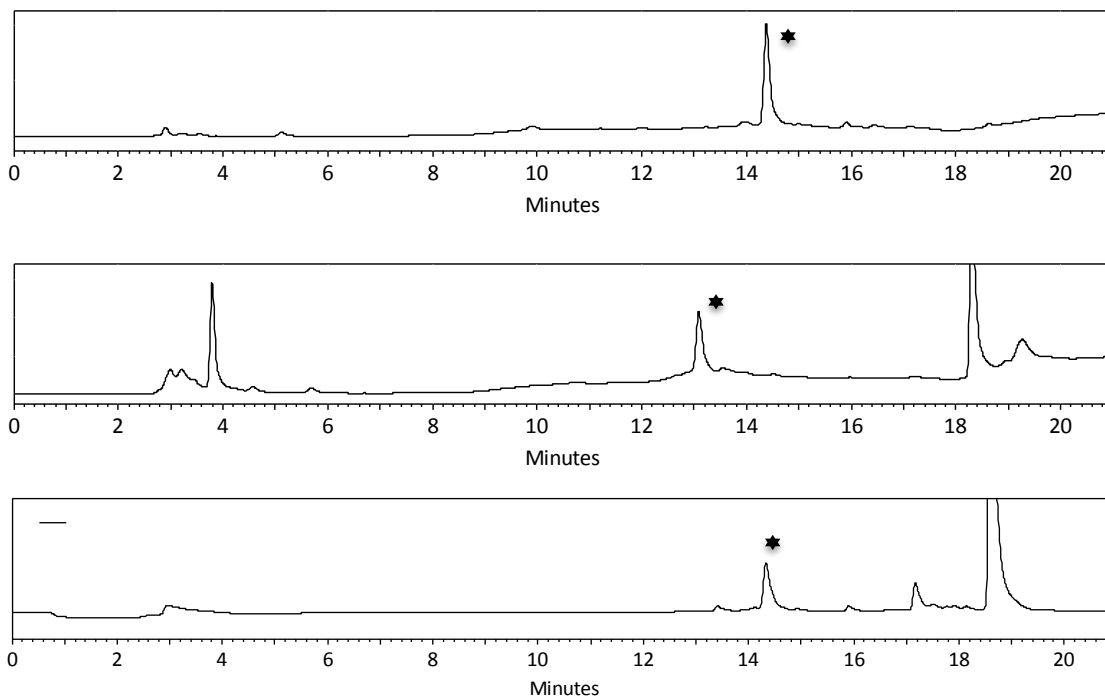


Figure 7-16. HPLC trace of crudes of metalation reaction (top), in-situ palladium deprotection (center) and fluorescein labeling with FITC (bottom) for **P4-Rh₂(OAc)₂** metallopeptide synthesis.

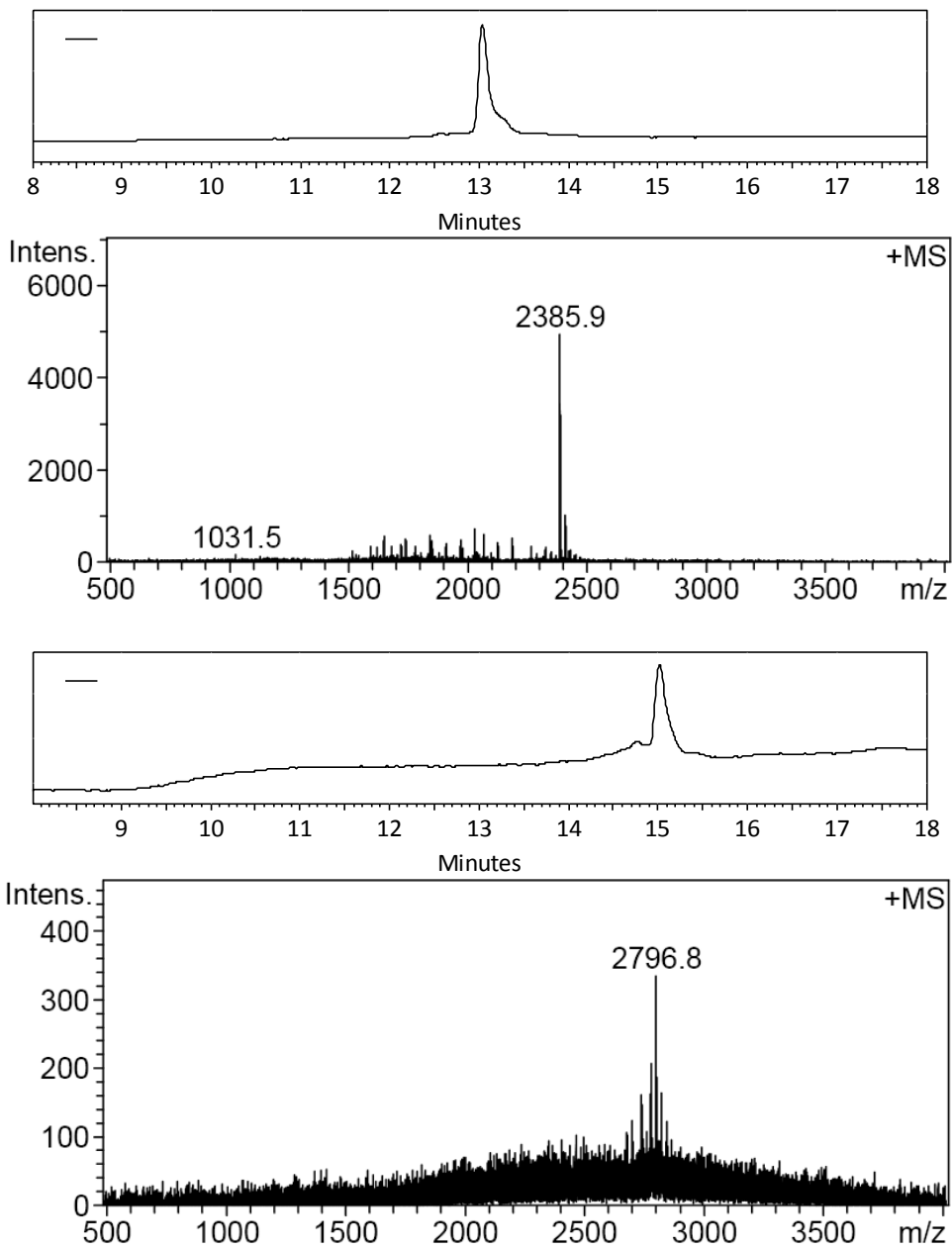


Figure 7-17. HPLC trace and MS data of purified product for **P4-Rh₂(OAc)₂** metallopeptide synthesis before (top) and after (bottom) fluorescein labeling with FITC.

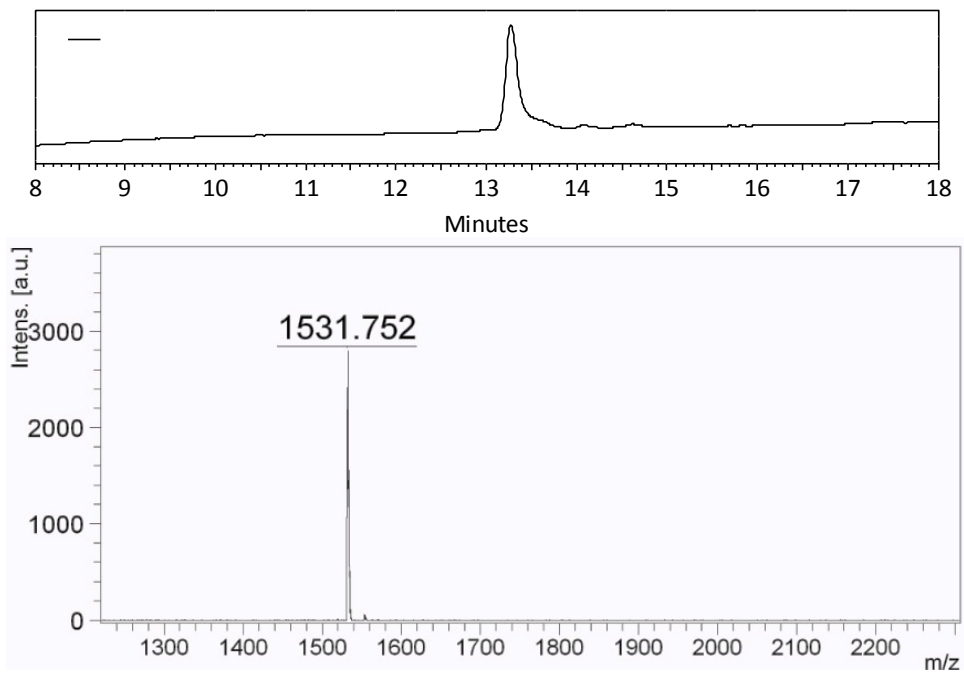


Figure 7-18. HPLC trace and MS data for isolated **P6** peptide.

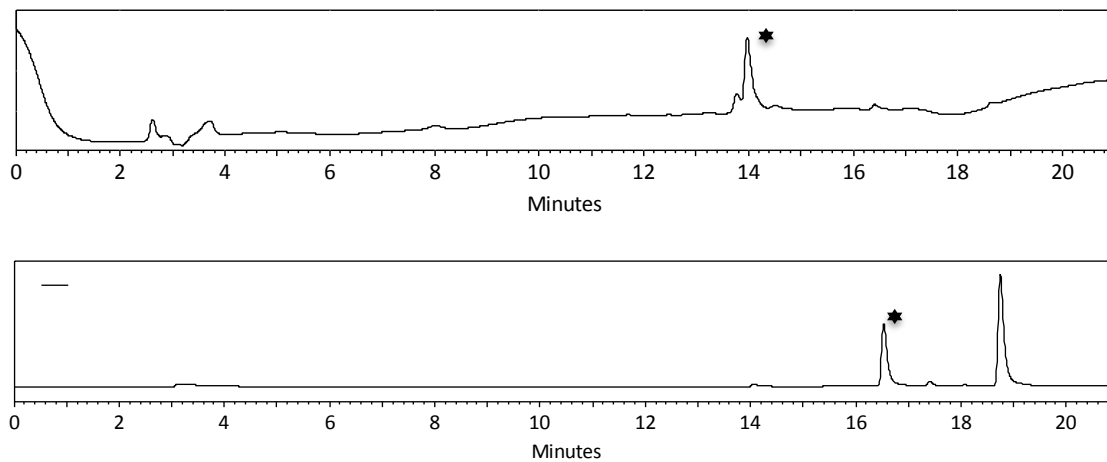


Figure 7-19. HPLC trace of crudes of metalation reaction (top) and fluorescein labeling with FITC (bottom) for **P6**-Rh₂(OAc)₂ metalloprotein synthesis.

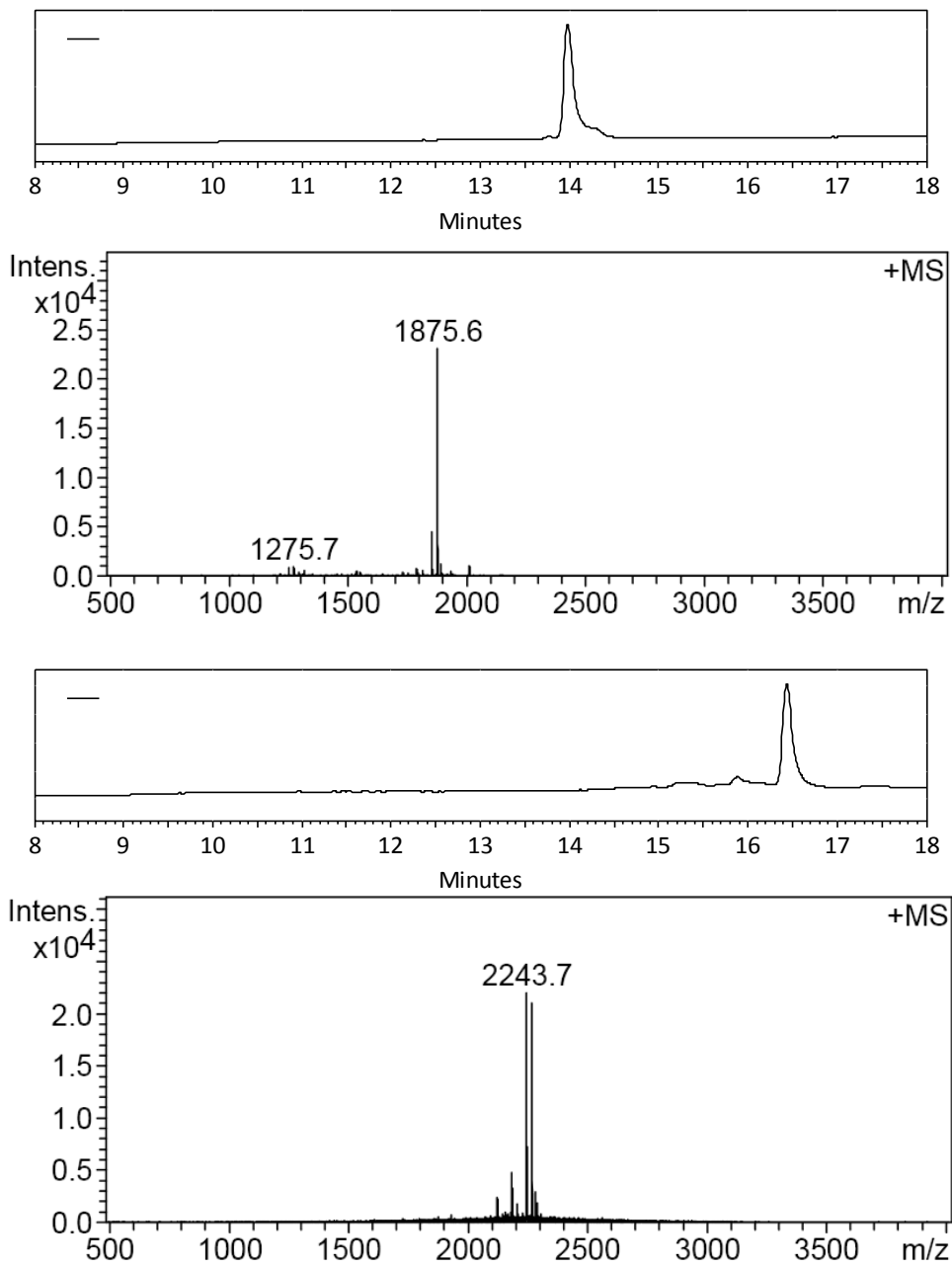


Figure 7-20. HPLC trace and MS data of purified product for **P6-Rh₂(OAc)₂** metallopeptide synthesis before (top) and after (bottom) fluorescein labeling with FITC.

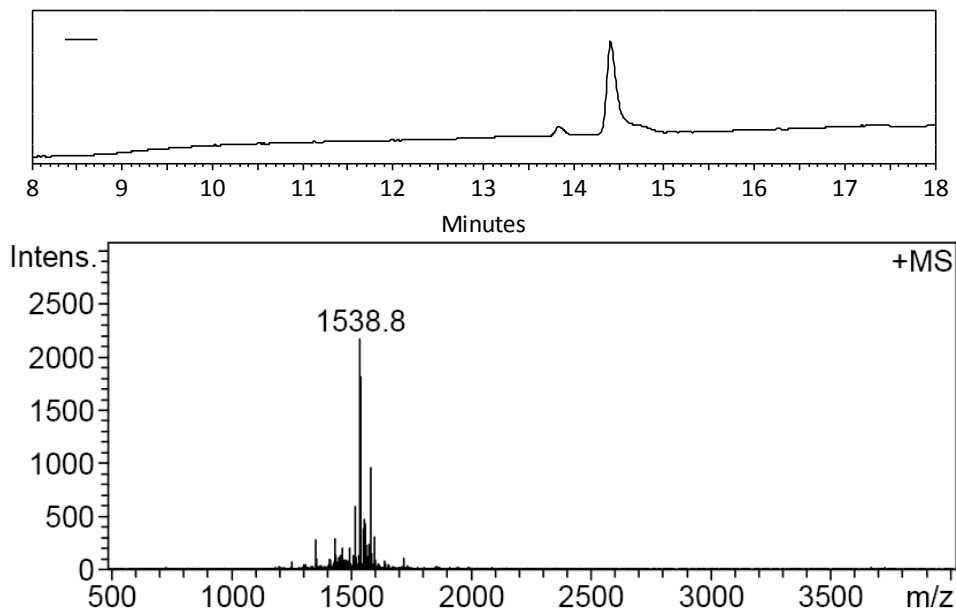


Figure 7-21. HPLC trace and MS data for isolated **P7** peptide.

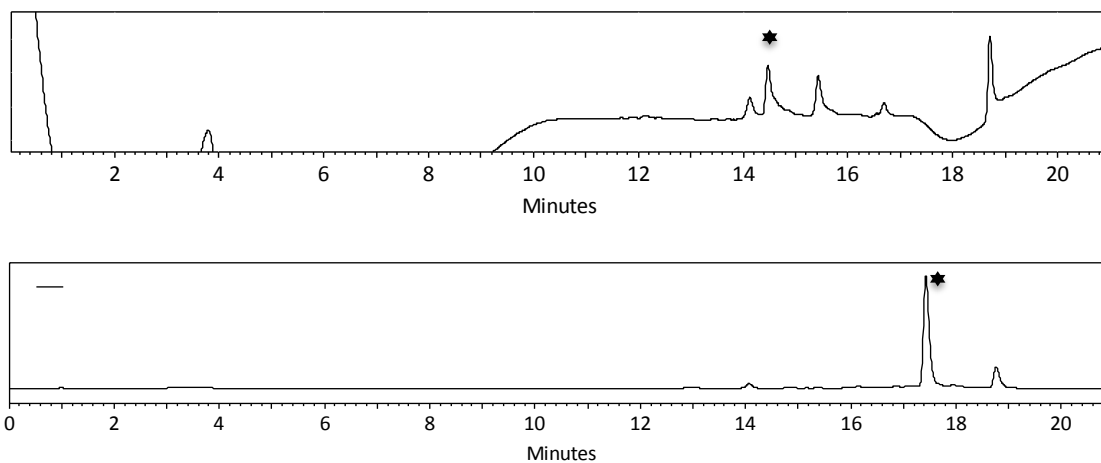


Figure 7-22. HPLC trace of crudes of metalation reaction (top) and fluorescein labeling with FITC (bottom) for **P7-Rh₂(OAc)₂** metallopeptide synthesis.

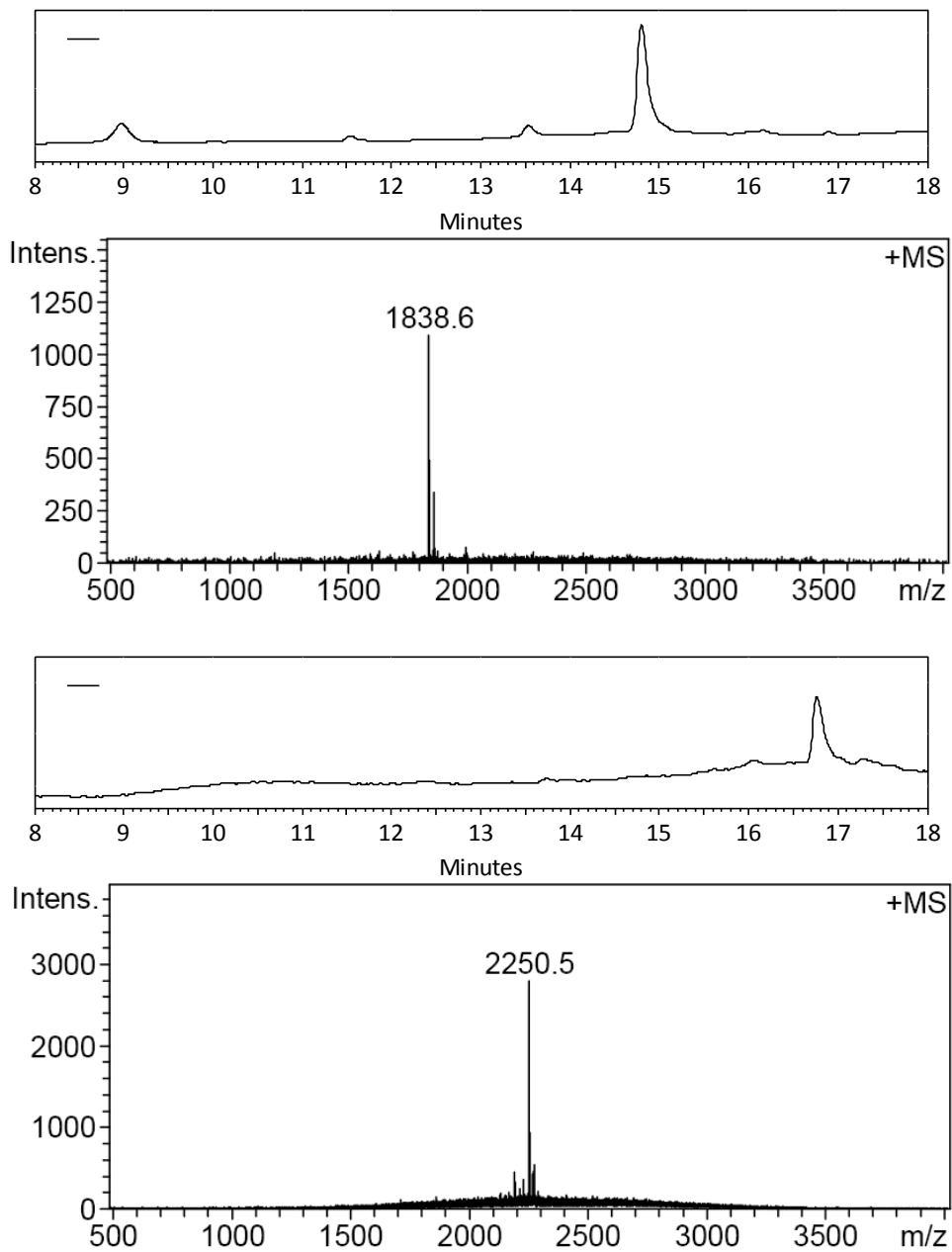


Figure 7-23. HPLC trace and MS data of purified product for **P7-Rh₂(OAc)₂** metallopeptide synthesis before (top) and after (bottom) fluorescein labeling with FITC.

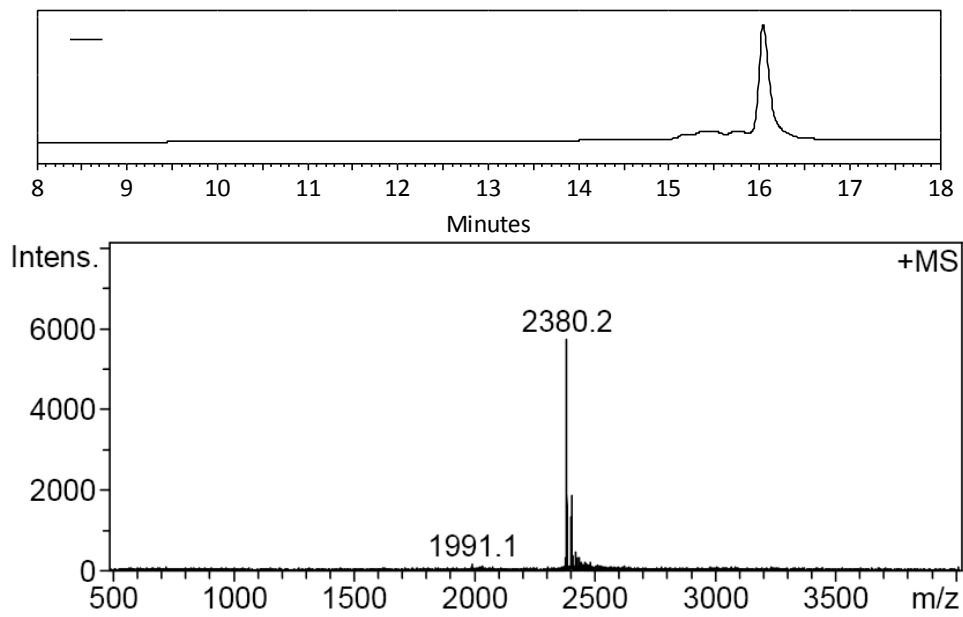


Figure 7-24. HPLC trace and MS data for isolated fluorescein-p53-WT peptide.

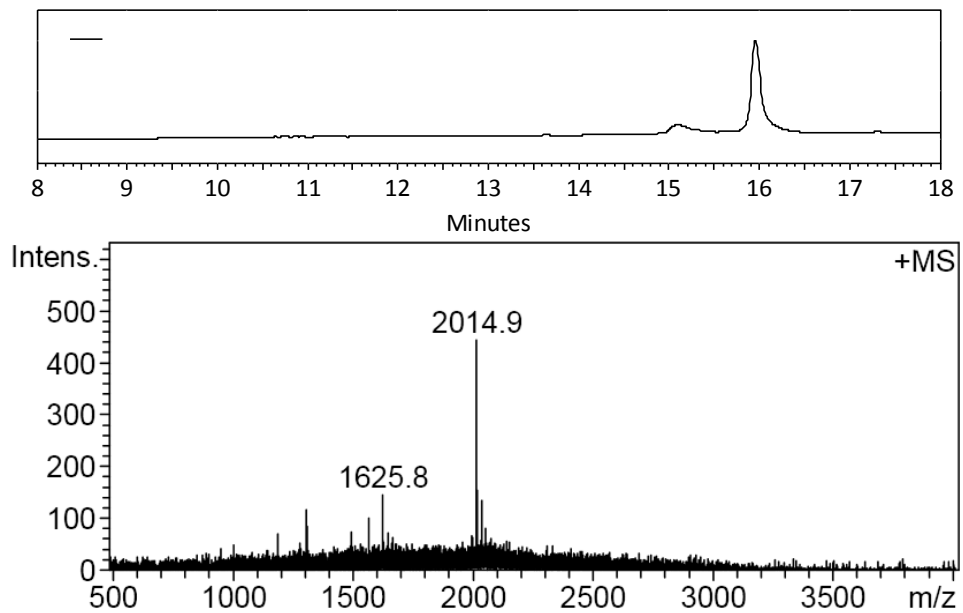


Figure 7-25. HPLC trace and MS data for isolated fluorescein-P5 peptide.

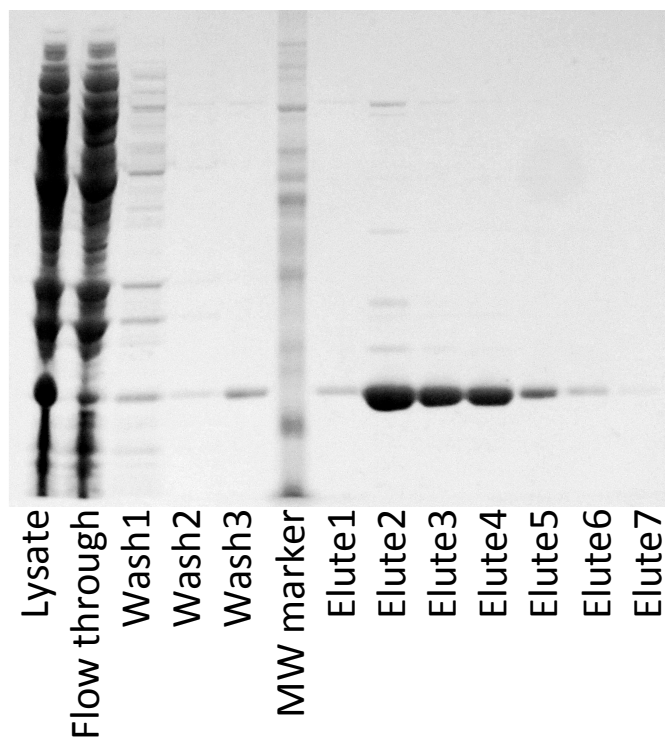


Figure 7-26. SDS-page gel of MDM2 protein purification by Ni-NTA affinity column with gradient concentration of imidazole (wash 2 and 3 – 20 mM, elute 1 – 50 nM, elute 2 and 3 – 100 mM, elute 4-7 – 300 mM).

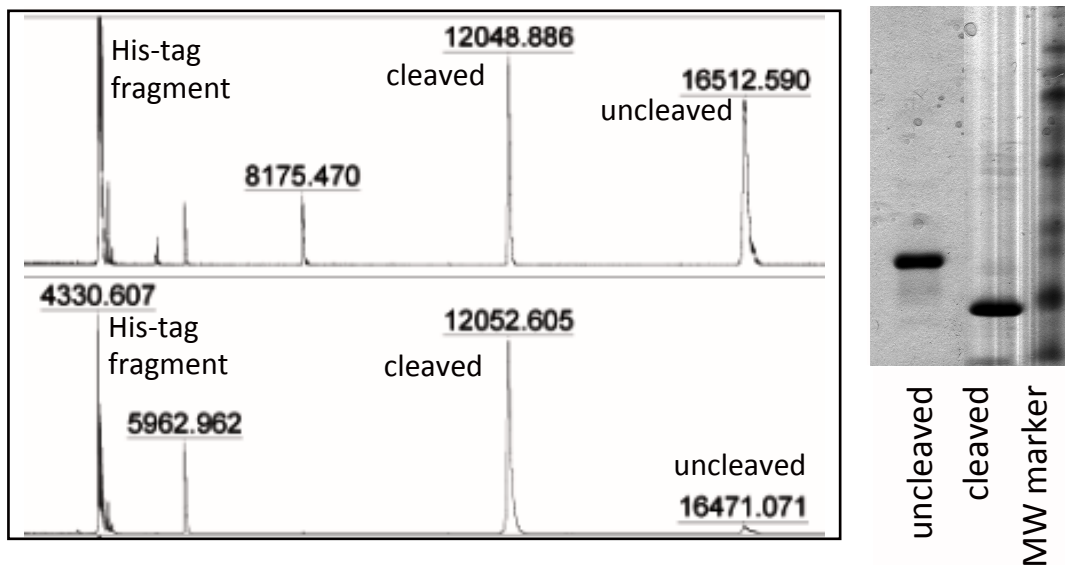


Figure 7-27. MALDI (at 4 °C (top) and rt (bottom) after 12 h rxn) and SDS-page gel for TEV protease cleavage of the His-tag and auxiliary peptide from the MDM2 protein.

7.7. References

- (1) Hajduk, P. J.; Greer, J. *Nat Rev Drug Discov* **2007**, *6*, 211.
- (2) O'Hare, H. M.; Johnsson, K.; Gautier, A. *Curr. Opin. Struct. Biol.* **2007**, *17*, 488.
- (3) Zaykov, A. N.; MacKenzie, K. R.; Ball, Z. T. *Chem. Eur. J.* **2009**, *15*, 8961.
- (4) Ghadiri, M. R.; Fernholz, A. K. *J. Am. Chem. Soc.* **1990**, *112*, 9633.
- (5) Hoang, H. N.; Bryant, G. K.; Kelso, M. J.; Beyer, R. L.; Appleton, T. G.; Fairlie, D. P. *Inorg. Chem.* **2008**, *47*, 9439.
- (6) Banci, L.; Bertini, I.; Calderone, V.; Della-Malva, N.; Felli, I. C.; Neri, S.; Pavelkova, A.; Rosato, A. *Biochem. J.* **2009**, *422*, 37.
- (7) Ferro-Flores, G.; Ramírez, F. M.; Meléndez-Alafort, L.; Santos-Cuevas, C. L. *Mini-Rev. Med. Chem.* **2010**, *10*, 87.
- (8) Kise, K. J.; Bowler, B. E. *Inorg. Chem.* **2003**, *42*, 3891.
- (9) Case, M. A.; McLendon, G. L. *Acc. Chem. Res.* **2004**, *37*, 754.
- (10) Kennedy, M. L.; Gibney, B. R. *Curr. Opin. Struct. Biol.* **2001**, *11*, 485.
- (11) Gilbertson, S. R.; Collibee, S. E.; Agarkov, A. *J. Am. Chem. Soc.* **2000**, *122*, 6522.
- (12) Agarkov, A.; Greenfield, S. J.; Ohishi, T.; Collibee, S. E.; Gilbertson, S. R. *J. Org. Chem.* **2004**, *69*, 8077.
- (13) Fang, Y. Y.; Ray, B. D.; Claussen, C. A.; Lipkowitz, K. B.; Long, E. C. *J. Am. Chem. Soc.* **2004**, *126*, 5403.
- (14) Estieu-Gionnet, K.; Guichard, G. *Expert Opin. Drug Dis.* **2011**, *6*, 937.

- (15) Guarracino, D. A.; Bullock, B. N.; Arora, P. S. *Biopolymers* **2011**, *95*, 1.
- (16) Haridas, V. *Eur. J. Org. Chem.* **2009**, 5112.
- (17) Mustata, G. *Curr. Top. Med. Chem.* **2011**, *11*, 247.
- (18) Verdine, G. L.; Walensky, L. D. *Clin. Canc. Res.* **2007**, *13*, 7264.
- (19) Kim, Y.-W.; Grossmann, T. N.; Verdine, G. L. *Nat. Protocols* **2011**, *6*, 761.
- (20) Stewart, M. L.; Fire, E.; Keating, A. E.; Walensky, L. D. *Nat. Chem. Biol.* **2010**, *6*, 595.
- (21) Bernal, F.; Wade, M.; Godes, M.; Davis, T. N.; Whitehead, D. G.; Kung, A. L.; Wahl, G. M.; Walensky, L. D. *Cancer Cell* **2010**, *18*, 411.
- (22) Bernal, F.; Tyler, A. F.; Korsmeyer, S. J.; Walensky, L. D.; Verdine, G. L. *J. Am. Chem. Soc.* **2007**, *129*, 2456.
- (23) Ma, M. T.; Hoang, H. N.; Scully, C. C. G.; Appleton, T. G.; Fairlie, D. P. *J. Am. Chem. Soc.* **2009**, *131*, 4505.
- (24) Kelso, M. J.; Beyer, R. L.; Hoang, H. N.; Lakdawala, A. S.; Snyder, J. P.; Oliver, W. V.; Robertson, T. A.; Appleton, T. G.; Fairlie, D. P. *J. Am. Chem. Soc.* **2004**, *126*, 4828.
- (25) Catino, A. J.; Forslund, R. E.; Doyle, M. P. *J. Am. Chem. Soc.* **2004**, *126*, 13622.
- (26) Choi, H.; Doyle, M. P. *Org. Lett.* **2007**, *9*, 5349.
- (27) Aguirre, J. D.; Angeles-Boza, A. M.; Chouai, A.; Pellois, J.-P.; Turro, C.; Dunbar, K. R. *J. Am. Chem. Soc.* **2009**, *131*, 11353.
- (28) Joyce, L. E.; Aguirre, J. D.; Angeles-Boza, A. M.; Chouai, A.; Fu, P. K. L.; Dunbar, K. R.; Turro, C. *Inorg. Chem.* **2010**, *49*, 5371.
- (29) Chen, Z.; Popp, B. V.; Bovet, C. L.; Ball, Z. T. *ACS Chem. Biol.* **2011**, *6*, 920.

- (30) Popp, B. V.; Ball, Z. T. *J. Am. Chem. Soc.* **2010**, *132*, 6660.
- (31) Popp, B. V.; Ball, Z. T. *Chem. Sci.* **2011**, *2*, 690.
- (32) Hilderbrand, S. A.; Lim, M. H.; Lippard, S. J. *J. Am. Chem. Soc.* **2004**, *126*, 4972.
- (33) Dunham, S. U.; Chifotides, H. T.; Mikulski, S.; Burr, A. E.; Dunbar, K. R. *Biochemistry* **2004**, *44*, 996.
- (34) Momand, J.; Wu, H.-H.; Dasgupta, G. *Gene* **2000**, *242*, 15.
- (35) Lyubomir T, V. *Trends Mol. Med.* **2007**, *13*, 23.
- (36) Chene, P. *Nat. Rev. Cancer* **2003**, *3*, 102.
- (37) Brown, C. J.; Cheok, C. F.; Verma, C. S.; Lane, D. P. *Trends Pharmacol. Sci.* **2011**, *32*, 53.
- (38) Fischer, P. *Int. J. Pept. Res. Ther.* **2006**, *12*, 3.
- (39) Kussie, P. H.; Gorina, S.; Marechal, V.; Elenbaas, B.; Moreau, J.; Levine, A. J.; Pavletich, N. P. *Science* **1996**, *274*, 948.
- (40) Sakurai, K.; Chung, H. S.; Kahne, D. *J. Am. Chem. Soc.* **2004**, *126*, 16288.
- (41) García-Echeverría, C.; Chène, P.; Blommers, M. J. J.; Furet, P. *J. Med. Chem.* **2000**, *43*, 3205.
- (42) Vassilev, L. T.; Vu, B. T.; Graves, B.; Carvajal, D.; Podlaski, F.; Filipovic, Z.; Kong, N.; Kammlott, U.; Lukacs, C.; Klein, C.; Fotouhi, N.; Liu, E. A. *Science* **2004**, *303*, 844.
- (43) Grasberger, B. L.; Lu, T.; Schubert, C.; Parks, D. J.; Carver, T. E.; Koblisch, H. K.; Cummings, M. D.; LaFrance, L. V.; Milkiewicz, K. L.; Calvo, R. R.; Maguire, D.; Lattanze, J.; Franks, C. F.; Zhao, S.; Ramachandren, K.; Bylebyl, G. R.; Zhang, M.; Manthey, C. L.; Petrella, E. C.; Pantoliano, M. W.; Deckman, I. C.; Spurlino, J. C.; Maroney, A. C.; Tomczuk, B. E.; Molloy, C. J.; Bone, R. F. *J. Med. Chem.* **2005**, *48*, 909.

- (44) Madden, M. M.; Muppidi, A.; Li, Z.; Li, X.; Chen, J.; Lin, Q. *Bioorg. Med. Chem. Lett.* **2011**, *21*, 1472.
- (45) Lessene, G.; Czabotar, P. E.; Colman, P. M. *Nat. Rev. Drug Discovery* **2008**, *7*, 989.
- (46) Czarna, A.; Popowicz, G. M.; Pecak, A.; Wolf, S.; Dubin, G.; Holak, T. A. *Cell Cycle* **2009**, *8*, 1176.
- (47) Knight, S. M. G.; Umezawa, N.; Lee, H.-S.; Gellman, S. H.; Kay, B. K. *Anal. Biochem.* **2002**, *300*, 230.
- (48) Liu, Z.; Olejniczak, E. T.; Fesik, S. W. *Protein Expression Purif.* **2004**, *37*, 493.
- (49) Increased affinity has been reported (Refs 22, 50, 54) for N-terminally truncated MDM2 [18–125]. See references 48 and 54 for a discussion. The binding constants reported here are internally consistent and reproducible.
- (50) Zondlo, S. C.; Lee, A. E.; Zondlo, N. J. *Biochemistry* **2006**, *45*, 11945.
- (51) Harrison, R. S.; Ruiz-Gomez, G.; Hill, T. A.; Chow, S. Y.; Shepherd, N. E.; Lohman, R.-J.; Abbenante, G.; Hoang, H. N.; Fairlie, D. P. *J. Med. Chem.* **2010**, *53*, 8400.
- (52) Ohmori, K.; Ogawa, Y.; Obitsu, T.; Ishikawa, Y.; Nishiyama, S.; Yamamura, S. *Angew. Chem. Int. Ed.* **2000**, *39*, 2290.
- (53) Kemmer, G.; Keller, S. *Nat. Protocols* **2010**, *5*, 267.
- (54) Dastidar, S. G.; Raghunathan, D.; Nicholson, J.; Hupp, T. R.; Lane, D. P.; Verma, C. S. *Cell Cycle* **2011**, *10*, 82.